THERAPEUTIC RNAI-BASED GENE THERAPY FOR NEURODEGENERATIVE DISORDERS

Slowing down the ticking clock

RAYGENE MARTIER

THERAPEUTIC RNAI-BASED GENE THERAPY FOR NEURODEGENERATIVE DISORDERS

Slowing down the ticking clock

Raygene Martier

PhD Thesis, Leiden University, May 2020

Therapeutic RNAi-based gene therapy for neurodegenerative disorders – slowing down the ticking clock

ISBN: 978-94-6182-987-0

Layout and printing production: Off Page, Amsterdam

The printing of this thesis and graduation was financially supported by uniQure

THERAPEUTIC RNAI-BASED GENE THERAPY FOR NEURODEGENERATIVE DISORDERS

Slowing down the ticking clock

Proefschrift

ter verkrijging van
de graad van Doctor aan de Universiteit Leiden,
op gezag van Rector Magnificus prof.mr. C.J.J.M. Stolker,
volgens besluit van het College voor Promoties
te verdedigen op 27 mei 2020
klokke 15.00 uur

door

Raygene Michaël Martier
geboren te Willemstad, Curaçao
in 1987

Promotor:	Prof. Dr. S. J. Van Deventer
Co-promotor:	Dr. P. Konstantinova (uniQure, Amsterdam, The Netherlands)
Leden promotiecommissie:	Dr. W.M.C. van Roon-Mom Prof. Dr. S. van der Maarel Prof. Dr. R. Hoeben Prof. Dr. C. Sampaio[1] Prof. Dr. med. Huu Phuc Nguyen[2] Prof. Dr. R.J. Pasterkamp[3]

[1]CHDI Foundation, Princeton, New Jersey, USA
[2]Department of Human Genetics, Medical Faculty, Ruhr University Bochum, Bochum, Germany
[3]Department of Translational Neuroscience, UMC Utrecht Brain Center, University Medical Center Utrecht

Table of Contents

Chapter 1

General introduction

Concept of gene therapy

Gene therapy is an emerging therapeutic tool to deliver functional genetic material to cells in order to correct a defective gene. By delivering a copy of a therapeutic gene to affected cells, the messenger RNA (mRNA) and/or proteins will be continuously synthesized within the cell, utilizing the cell's own transcriptional and translational machinery[1]. The main advantage of this technology is that it offers a potentially life-long therapeutic effect without the need for repeated administration. Gene therapy can be used to correct defective genes by introducing a functional copy of a defective gene, by silencing a mutant allele using RNA interference (RNAi), by introducing a disease-modifying gene, or by using gene-editing technology.[2–4]

Gene therapy vectors can be either viral or non-viral. Different physical and chemical systems can be applied to deliver therapeutic genes to cells without the need of a viral vector. Non-viral vectors have no size limitation for the therapeutic gene, generally have a low immunogenicity risk and can be produced at relatively low costs.[5] However, because high therapeutic doses are required when using non-viral technologies, and the resulting gene expression is generally transient, most gene therapies now rely on viral vectors. Numerous viral vector types have been tested in clinic, including vaccinia, measles, vesicular stomatitis virus (VSV), polio, reovirus, adenovirus, lentivirus, γ-retrovirus, herpes simplex virus (HSV) and adeno-associated virus (AAV).[6] Vaccinia, measles, VSV, polio, reovirus, adenovirus and HSV vectors are currently mainly used in either vaccines or cancer therapeutics while lenti- and γ-retroviral vectors are predominantly used for transduction of transplantable cells.[7] For *in vivo* gene delivery, AAV is currently the preferred vector. AAV belongs to the Parvoviridae family and is preferred for gene therapy because it is non-replicating (AAV requires a helper virus for replication), has a low immunogenicity profile and is not known to cause disease.[8,9] In the absence of a helper virus, AAV may stably integrate into the host genome, but at relatively low frequency. The genome of wildtype AAV is about 4.7 kb and is flanked between two inverted terminal repeats (ITRs) (Figure 1a).[10] The open reading frame between the ITRs contains a replication (Rep) gene and a capsid (Cap) gene. The ITRs are cis-acting elements and are required for genome replication, integration, and packaging into the capsid. The Rep gene encodes 4 proteins (Rep78, Rep68, Rep52, and Rep40) that have important roles in replication and encapsidation of the viral DNA.[11] The Cap gene encodes three capsid proteins (VP1, VP2, and VP3) and an assembly activating protein that promotes capsid formation.[12] There is a growing number of naturally occurring and engineered AAV serotypes with different viral capsids that have altered tissue tropism, transduction rate, or other features such as the ability to cross the blood-brain barrier[13,14] Recombinant AAV (rAAV) can be produced by replacing the rep and cap genes with an expression cassette containing a therapeutic gene of interest (Figure 1b). Formation of wild type AAV is prevented by expressing the rep and cap genes on a separate plasmid (AAV packaging plasmid or AAV helper plasmid). The ITRs are the minimal region required to be retained in rAAV to allow

packaging of its genome. rAAV might still integrate randomly in the human genome at very low frequencies but most of its genome is maintained as episomal circular structures known as concatamers. rAAVs have been widely used in over 200 human clinical studies and have demonstrated to be safe.[15] AAV-based gene therapies are highly attractive for the treatment of neurogenerative diseases due to the neuronal tropism and good safety profile demonstrated in clinical studies. In addition, a single administration results in long-term, potentially life-long gene expression, which is a main advantage when *in vivo* AAV administration require invasive procedures.

Neurodegenerative diseases

Neurodegenerative diseases are a heterogeneous group of multi-system disorders affecting the central nervous system, ultimately leading to neurodegeneration[16]. Examples of the most common neurodegenerative diseases are amyotrophic lateral sclerosis (ALS), frontotemporal dementia (FTD), spinocerebellar ataxias (SCAs), Huntington's disease (HD), Alzheimer's disease (AD) and Parkinson's disease (PD).[17] The prevalence of these age-dependent disorders is increasing, partly due to the aging population, placing a major economic burden on health care services. Some neurogenerative diseases are caused by genetic mutations and/or cellular and circuit dysregulation. In some cases, different neurodegenerative diseases are linked to the same polymorphisms or mutations, thereby sharing similar pathological mechanisms. It seems that certain environmental or lifestyle factors combined with genetic factors increase the risk for certain neurodegenerative disease but aging is considered to be the most important risk factor for the sporadic cases.[18] Although each neurodegenerative disease have a different pathophysiology, they all lead to damage to the nervous system due to features such as cell death, impaired/failure of axonal regeneration, demyelination and/or neuronal structural/functional deficits.[19] These pathological features occur in different combinations and their causes can be either genetic or unknown.[19] Common underlying causes leading to these conditions can be due to abnormal accumulation of proteins such as amyloid in AD, misfolded proteins (typical for PolyQ diseases), aggregation of proteins such as Tau (AD and traumatic brain injuries), synuclein (PD) or TDP-43 (ALS), RNA toxicity or translational products from repeats expansion within genes.[19,20] Each of these features has unique mechanisms of toxicity which in large part are currently not well understood. Some mechanisms of pathogenesis in neurodegenerative diseases share key characteristics with prions suggesting that progression of certain neurodegenerative diseases may share similar mechanisms involved in prion diseases.[21] For example, misfolded protein aggregates (such as Tau, α-synuclein, amyloid-ß, huntingtin) can spread via cell to cell interaction and invade healthy tissues. The misfolded proteins can induce secondary misfolding of other unrelated aggregation -prone proteins, impairing the entire proteostatic network.[22] Ultimately, they lead to a decline or even complete loss of sensory, motor, and cognitive functions. Symptoms commonly associated with neurodegenerative

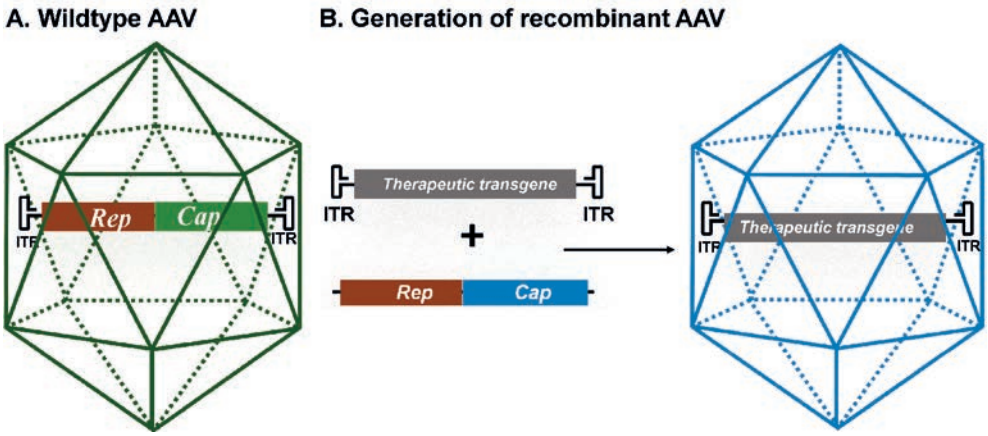

Figure 1. a) Schematic of wild type AAV. Its genome consists of the viral rep and cap genes flanked by two inverted terminal repeats (ITRs). b) Schematic of recombinant AAV (rAAV) generated by replacing the viral genes for a therapeutic gene, flanked by the ITRs. The rep and cap genes are expressed from a different plasmid or viral vector. The rAAV is generated by co-transfecting cells with the transgene cassette flanked by AAV ITRs, the rep and cap genes of a specific AAV serotype, and the adenovirus helper plasmid.

diseases include cognitive impairment, memory loss, apathy, anxiety, muscle weakness, paralyses, difficulties with speech or breath and death.

One great mystery for most neurodegenerative diseases is the onset of clinically manifest symptoms, as pathological alterations usually occur long before symptoms start to develop. Progressive accumulation of neuronal cell damage and the effects of aging are two common explanations and more recently, the role of neuroplasticity in the development and progression of neurodegeneration has also been implicated.[23] The adult brain generally shows less neuroplasticity in response to insults than the developing nervous system.[23] However early-life events and insults such as perinatal infections, an unstructured/abusive environment, social isolation, stress, poor nutrition, exposure to chemicals or metals could possibly interfere with the neuroplastic development in children and adolescents.[24–26] These may place an additional burden on the plastic capacity of the developing neuronal system leading to the disturbance of the structural brain self-organization. A second challenge later in life could trigger the final onset of neurodegeneration and this may be a critical factor determining the onset and course of neurodegeneration.[23]

A major clinical challenge is early diagnosis of neurodegenerative diseases and due to overlapping symptoms, discrimination between the different diseases is difficult. Moreover, early symptoms are often dismissed or interpreted as normal consequences of aging. Apart from diagnostic delay, additional challenges for new therapeutic approaches reaching the stage of clinical development are the lack of druggable targets, the limited choice of delivery methods, and a lack of reliable biomarkers and clinical parameters that

predict therapeutic efficacy or the rate of disease progression. To date neurodegenerative diseases cannot be cured, and only palliative treatments are available. Because these diseases are devastating for patients and their families, and cause a vast burden on society, there is an enormous need to better understand their causes, pathology and clinical progression and to develop early detection methods and new therapeutic interventions. The current thesis presents the development of RNAi-based gene therapies for ALS and SCA3 and discusses the currently available options for delivery to the target cells. Additionally, the preclinical validation of an AAV-based mifepristone-inducible GeneSwitch system is reported as one of the first steps in the development of a small molecule-regulated gene therapy approach.

Amyotrophic lateral sclerosis

ALS (or Lou Gehrig's disease) is the most common adult onset motor neuron disease affecting the upper- and the lower motor neurons in the brain and spinal cord, but other neuroanatomical regions may also be affected.[27,28] The upper motor neurons are found in the motor cortex of the brain, while the lower motor neurons are located along the brainstem, spinal cord and extend to the muscles.[29] Degeneration of the upper motor neurons causes symptoms such as spasticity and hyperreflexia while the loss of lower motor neurons results in progressive muscle weakness, cramps, fasciculations, muscle wasting and paralysis.[29,30] The prevalence of ALS is currently estimated at 5 in 100.000 but the estimated lifetime risk to develop the disease is about 1:400-800.[31,32] The discordance between the low prevalence but high lifetime risk is explained by the fact that ALS patients have a very limited life span with a median survival ranging from two to five years from symptom onset.[28] The understanding of the genetic causes of ALS is continually expanding, but our knowledge of other risk factors such as environmental factors, lifestyle or aging remains poor. Only ten percent of ALS cases are familial, and the causal genetic mutations are usually inherited in a mendelian autosomal dominant manner. Thus, most ALS cases are assumed to occur sporadically, and the main causes are still unknown.

Two drugs have been approved by the Food and Drug Administration for the treatment of ALS, but the efficacy of both drugs is modest. Riluzole, first approved in 1995, is a glutamate receptor antagonist which may increase survival by 2 to 3 months. More than two decades later in 2017, Edaravone, a free radical scavenger was approved but its efficacy is still unclear, and at best the drug has a moderate effect on disease progression.[33] More than 30 genes have been linked to ALS and mutations in chromosome 9 open reading frame 72 *(C9orf72),* superoxide dismutase1 (SOD1), transactive response DNA-binding protein 43 (TDP-43), or fused in sarcoma (FUS) are responsible for most of the familial ALS cases. A hexanucleotide expansion consisting of GGGGCC (G_4C_2) nucleotides in the first intron of the *C9orf72* gene is the most frequent genetic cause of ALS and is found in about 40-50% of familial ALS cases and 5-10% of sporadic ALS cases.[34] The G_4C_2 repeat

is transcribed bidirectionally and affected patients usually carry more than 30 G_4C_2 copies. Interestingly, the same mutation also causes FTD, the second most common form of dementia after AD. *C9orf72* is responsible for 25% of familial FTD cases and 5-7% of sporadic FTD cases. ALS and FTD are considered overlapping diseases as about 15% of ALS patients develop FTD and up to 50% of ALS patients show some degree of functional loss in the frontal lobe of the brain.[32] The function of the *C9orf72* encoded protein is poorly understood, but it may be a regulator of the autophagy-lysosome pathway during nutrient stress responses. [35] There are at least three proposed pathogenic mechanisms in *C9orf72* related ALS and/or FTD patients; 1) RNA-mediated toxicity, 2) RAN translation and 3) haploinsufficiency. It is also possible that a combination of the three mechanisms contributes to the disease pathogenesis (Figure 2).[36,37]

RNA-mediated toxicity

RNA-mediated toxicity was first described in myotonic dystrophy type 1 (DM1), which is caused by a CTG repeat expansion in the 3'UTR of the myotonic dystrophy protein kinase gene.[38,39] It was shown that RNA consisting of CUG repeats folds into stable structures that colocalize with RNA-binding proteins and sequester their function. For example, an important protein that is sequestered by CUG-containing RNA foci is the splicing factor muscleblind-like 1 (MBNL1).[40] The sequestration of MBNL1 leads to its inactivation which subsequently cause mis-splicing of several pre-mRNAs, such as muscle-specific chloride ion channel and insulin receptor.[41,42] RNA foci are observed in several other neurodegenerative diseases caused by repeat expansions including ALS and SCA3.[43] In *C9orf72*-related ALS and FTD, accumulation of sense and antisense G_4C_2-containing RNA foci is detected in several brain-, spinal cord tissues, lymphocytes and fibroblasts. RNA foci are also detected in patient-derived Induced-pluripotent stem cell (iPSC) -neurons. Although RNA foci mainly accumulate in the nucleus of cells they are also observed at lower concentrations in the cytoplasm. Several RNA binding proteins interact with G_4C_2 RNA repeats, such as ADARB2, hnRNPA1, hnRNPA1B2, Pur-α, FUS, Nucleolin and TDP-43.[36,44,45] However the contribution of these proteins to the neurodegeneration is only partially understood.

RAN translation

Another proposed mechanism of toxicity in *C9orf72* related ALS and/or FTD is by repeat-associated non-ATG (RAN) translation.[36,46,47] It has been shown that the repeat-containing transcripts can be translated into dipeptide repeat proteins (DPRs) even in the absence of an ATG start codon and even though the mutation is in a non-coding region of *C9orf72*. These DPR proteins are toxic and they can form aggregates that accumulate in the brain and spinal cord of patients.[48,49] Six DPR proteins can be produced via unconventional translation in all reading frames. Glycine-alanine (GA) and glycine-arginine (GR) are

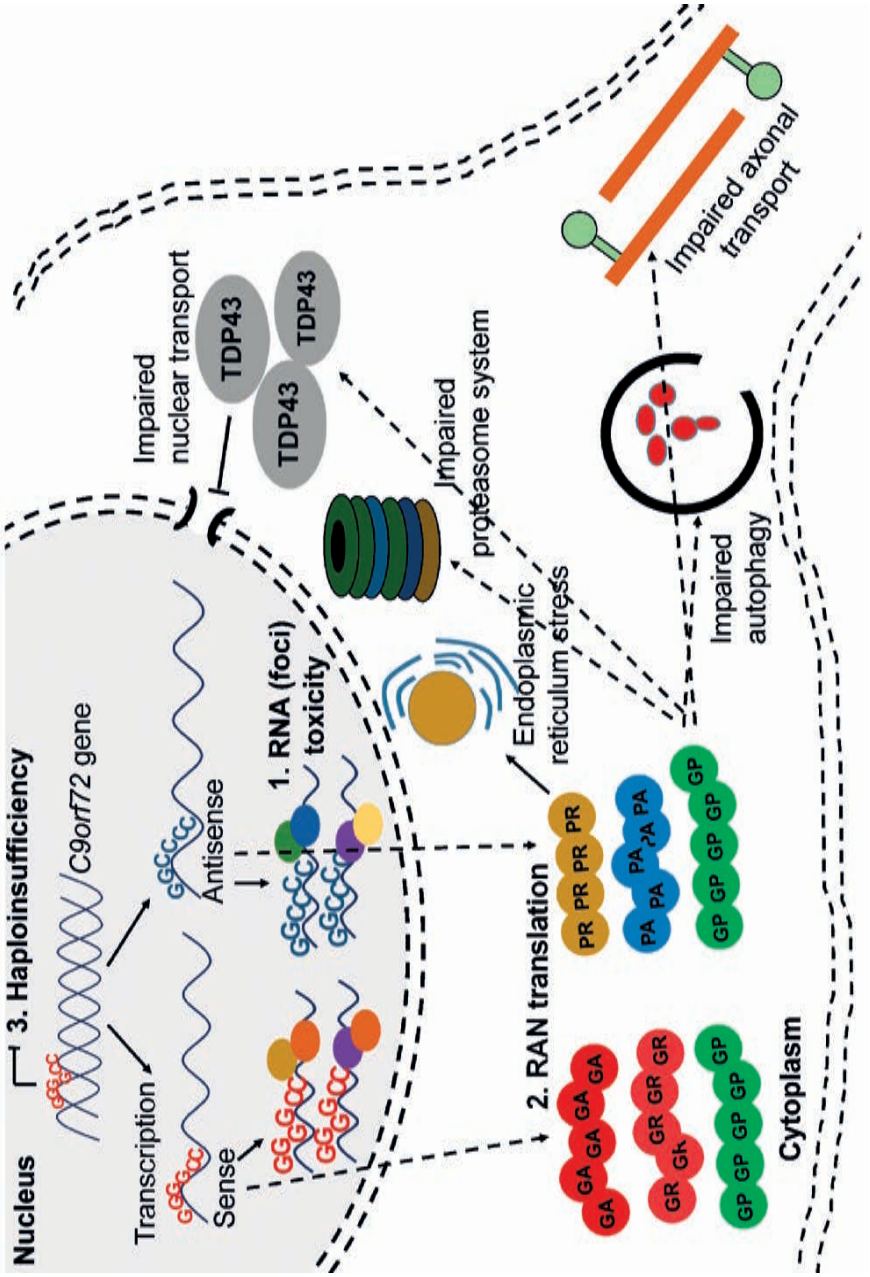

Figure 2. Mechanisms of toxicity associated with *C9orf72* G_4C_2 repeat. a) RNA-mediated toxicity. Repeat-containing sense and antisense RNA transcripts accumulate and sequester RNA binding proteins (1) b) RAN translation. The sense and antisense repeat-containing transcripts undergo RAN translation into five, potentially toxic DPRs (2) b) Haploinsufficiency. Hypermethylation of the expansion leads to reduced transcription of *C9orf72* (3).

produced from the sense repeat-containing transcripts, while proline-arginine (PR) and proline-alanine (PA) are produced from the antisense repeat-containing transcripts. Glycine-proline (GP) is produced from both sense and antisense repeat-containing transcripts.[50] Ample evidence indicates that DPR proteins are toxic and cause neurodegeneration. For example, neurotoxicity, proteasome activity and endoplasmic reticulum stress was observed in primary neurons expressing GA proteins.[51] Addition of recombinant GR and PR proteins to Hela cells and human astrocytes was toxic and caused alterations in RNA processing.[50] Expressing GR and PR proteins in Drosophila caused toxicity and early lethality.[52] Several recent publications demonstrated that DPR proteins can lead to impairment of nuclear transport, causing accumulation of several RNA-binding proteins including TDP-43 in the cytoplasm.[53–55] Cytoplasmic TDP-43 aggregation is observed in ~97% of cases of ALS, including those associated with *C9orf72* mutations. TDP-43 protein is predominantly found in the nucleus but can shuttle between the nucleus and cytoplasm to regulate processes such as RNA processing, transcription, pre-mRNA splicing, transport and stabilization of mRNA.[56–58] In patients, TDP-43 accumulates as cytosolic inclusions with a C-terminal fragment of 25 or 35 kDa. The aggregated TDP-43 is also post-translationally modified, being heavily ubiquitinated, and phosphorylated at the C-terminal region.[56] Notably, mutations in TARDBP, the gene that encodes the TDP-43 protein, have also been linked to ALS, but it remains unclear whether it is depletion of nuclear TDP-43, gain of a toxic function of cytoplasmic TDP-43, or a combination of these processes that are neurotoxic. Recently it was demonstrated that expressing PR in mice also resulted in neurodegeneration and premature death.[59] PR proteins localized to the heterochromatin caused abnormal histone H3 methylation and aberrations in nuclear lamins and heterochromatin protein 1α (HP1α). This resulted in down-regulation of numerous differentially expressed genes and upregulation of many repetitive elements which was accompanied by the accumulation of double-stranded RNA, ultimately leading to neuronal death. Thus, as RNA foci and DPRs both contribute to the pathogenesis of ALS, their inhibition could potentially reduce the disease burden in patients.

Haploinsufficiency

The thought that haploinsufficiency may contribute to *C9orf72*-related ALS originates from the finding that reduced *C9orf72* RNA and protein levels have been reported in brain and spinal cord tissues and in iPSC-neurons derived from ALS patients. Several mechanisms may lead to reduced levels of *C9orf72*, including abortive transcription caused by G-quadruplexes and R-loop structures of the repeat-containing transcripts. In addition, the *C9orf72* locus is hypermethylated in several mutation carriers, which can lead to epigenetic silencing and similar mechanisms of gene silencing are observed in other repeat expansion diseases such as Friedrich ataxia and fragile X mental retardation syndrome. However, haploinsufficiency alone does not explain the observed ALS pathology in patients. Several loss-of-function mutations in *C9orf72* have been identified

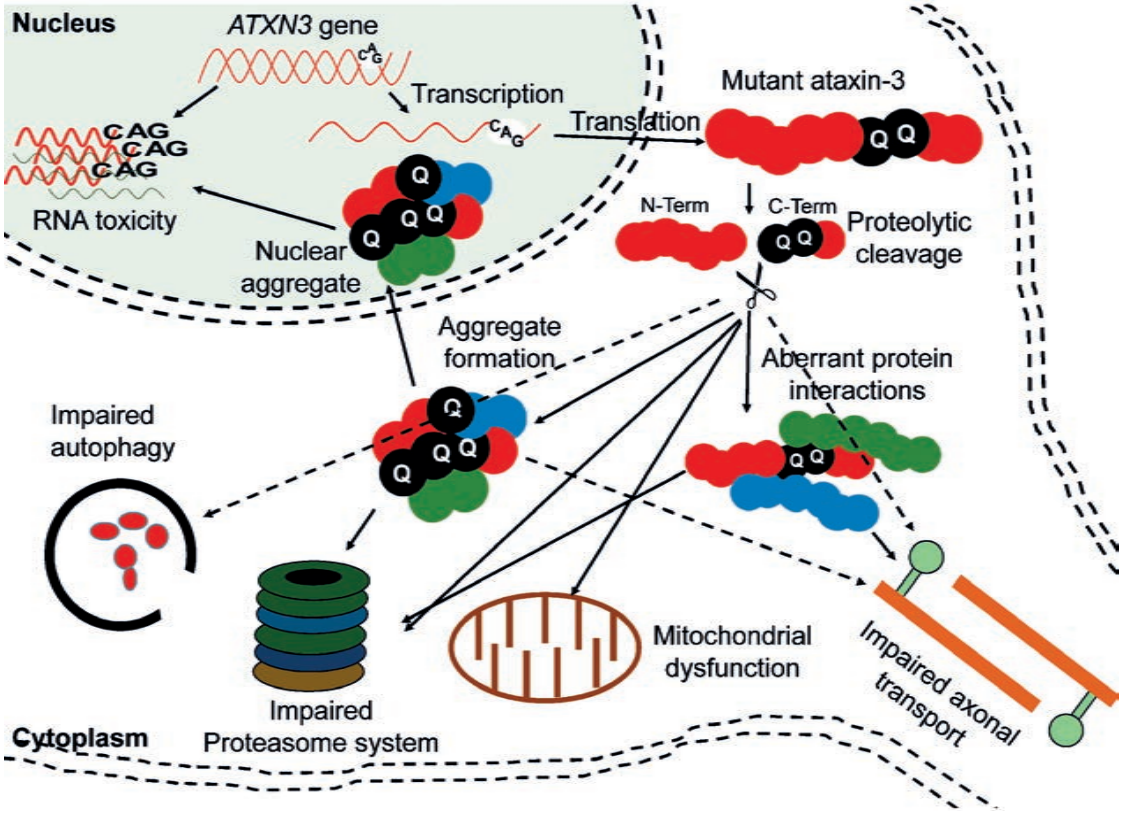

Figure 3. Ataxin-3 mediated mechanisms of toxicity. 1) RNA toxicity. RNA containing the CUG repeats can sequester function of transcription factor 2) Mutant ataxin-3 toxicity. The CAG repeat-containing *ATXN3* transcript is translated into a protein with a polyQ expansion. Proteolytic cleavage of mutant ataxin-3 can generate C-terminal protein fragments containing the polyQ repeat. The mutant ataxin-3 and C-terminal protein fragments can both cause several cellular disturbances such as transcriptional deregulation, impaired autophagy, mitochondrial dysfunction, proteasomal impairment, compromised axonal transport and DNA damage.

and seemed to be non-pathogenic.[60] Furthermore, complete *C9orf72* knockout mice showed no neurodegeneration but rather splenomegaly, enlarged cervical lymph nodes, and autoimmune related premature death.[61,62] Interestingly, this phenotype was rescued in mice hemizygous for *C9orf72,* suggesting that a partial knockdown of the gene would be well tolerated.[62] A recent publication suggest a cooperative pathogenesis between gain- and loss-of function mechanisms.[37] Reduced *C9orf72* protein in cultured motor neurons caused accumulation of glutamate receptors and excitotoxicity in response to glutamate. In addition, these motor neurons showed impaired clearance of DPRs and were hypersensitive for these proteins.

As most evidence points towards a toxic gain of function resulting from this mutation, an RNAi-based gene therapy would be an attractive therapeutic approach to silence the mutated gene.

Spinocerebellar ataxia type 3

The spinocerebellar ataxias (SCAs) are a large group of neurodegenerative diseases that are characterized by progressive ataxia due to degeneration of the cerebellum and often adjacent regions. SCAs are inherited in an autosomal-dominant manner and have a prevalence of about 1-3 in 100.000, although this highly vary between geography and ethnicity.[63,64] More than 40 different types of SCA have been identified and the most common ones (SCA1, SCA2, SCA3, SCA6, SCA7 and SCA17) are caused by a CAG nucleotide repeat expansion encoding polyglutamine (polyQ).[65] SCA3 (also known as Machado-Joseph disease or MJD) is the second most common PolyQ disorder after HD and the most common among the SCAs. SCA3 patients experience progressive ataxia, affecting balance, gait and speech and frequently symptoms are pyramidal signs, progressive external ophthalmoplegia, dysarthria, dysphagia, rigidity, distal muscle atrophies and double vision.[66] The pathogenic CAG repeat is in the penultimate exon of *ATXN3* gene on chromosome 14q32.1 and the disease severity is related to the number of CAG repeats:[67] Up to 44 CAG repeats are considered normal, between 45 to 51 repeats are associated with intermediate or low penetrance of the disease, while SCA3 patients usually have more than 51 repeats. The survival rate is variable and usually between 10 to 21 years after symptom onset.[68] Similar to ALS, there is no cure for SCA3 and current treatments are based on antispasmodic drugs to help reduce spasticity, speech therapy and physiotherapy. Several molecules such as sulfamethoxazole-trimethoprim, varenicline and lithium carbonate have been tested in clinical trials, but all failed to show clinical improvement.

The *ATXN3* gene encodes a 42-kDa protein called ataxin-3 which consists of a N-terminal catalytic Josephin domain and two to three (dependent on the splice variant) C-terminal ubiquitin (Ub)-interacting motifs flanking the polyQ tract.[65,66,69] The ataxin-3 protein is widely expressed in different cell types of peripheral and neuronal tissues and present in both nucleus and cytoplasm.[70] Ataxin-3 is believed to interact with up to 100

proteins involved in ubiquitin-dependent pathways and quality control. The protein has a role in various ubiquitin-dependent pathways that maintain protein homeostasis. By partnering with ubiquitin ligases, ataxin-3 may be able to regulate, or edit, the lengths and linkage types of ubiquitin chains on proteins and in this manner either rescue proteins from being degraded, or stimulate protein breakdown. [71,72] Additional roles in endoplasmic reticulum-associated degradation, aggresome (aggregates of misfolded proteins) production and DNA repair have also been implicated.[73–77]

Mechanisms of toxicity

The mutant ataxin-3 protein is neurotoxic but the exact pathways leading to neurodegeneration are not completely understood. Two attractive hypotheses postulate a gain of toxicity and RNA-mediated toxicity (Figure 3). The expanded CAG repeat in the *ATXN3* gene leads to formation of an ataxin-3 protein with an expanded polyQ tract at its C-terminal region with toxic gain of function properties. In addition, the mutated protein causes aggregate formation in neurons which is typical for polyQ diseases. Aggregates are found in different types of neurons in the brain stem (ventral pons), substantia nigra, globus pallidus, dorsal medulla and dentate nucleus.[66,69] Although the aggregates are mainly detected in the nucleus, they are also found at low levels in cytoplasm of neurons in affected areas and in axons within fiber tracts known to undergo neurodegeneration in the disease.[78] The aggregates consist of different types of proteins such as ataxin-3 (wildtype and mutant), heat-shock proteins, transcription factors and other polyQ disease-associated proteins. It is believed that sequestering of these functional proteins contributes to cellular dysfunction and neurodegeneration. Furthermore, proteolytic cleavage of the mutant ataxin-3 may lead to generation of shorter soluble PolyQ fragments that are also toxic. Another hypothesis is that the polyQ expansion induces conformational changes in ataxin-3 and alters its function in multiple ubiquitin-dependent pathways that can lead to altered binding properties, loss of protein function, disorganized subcellular localization, aggregation, and altered proteolytic cleavage.[66,79]

In addition to the mechanisms described above, which are based on protein toxicity, RNA toxicity could also contribute to the disease. As mentioned before, RNA containing CUG repeats can sequester various transcription factors and undergo RAN translation. A crucial evidence for RNA toxicity was observed in nematodes. CAG repeats cloned into the 3' UTR of a marker protein showed severe toxicity in a length-dependent manner in Caenorhabditis elegans (C. elegans). The CUG RNAs formed RNA foci and colocalized with C. elegans muscleblind protein. The highest CAG repeats were embryonically lethal while the shorter CAG repeats were tolerated.[80,81] Since the mutated *ATXN3* gene produces a protein with a toxic gain of function, it is an ideal target for an RNAi-based gene therapy approach.

In vivo and *in vitro* models for ALS and SCA3

Model systems that recapitulate the different aspects of the diseases are essential to understand the pathology, and to predict clinical efficacy during early development of new therapeutic approaches. Development of animal models for neurodegenerative diseases is a major challenge as the diseases have complex pathologies and symptoms can take decades to unfold. As a result, most of the currently available animal models for neurodegenerative diseases are not exact phenotypes of the human diseases and therefore lack the ability to forecast clinical success of new therapeutic approaches. Moreover, studies performed *in vitro* and *in vivo* on cells and small animals are difficult to translate to larger animals, because factors such as delivery route, dosing, distribution and toxicity vary between the different model systems.[82]

Animal models for *C9orf72* ALS/FTD

Various mouse models have been generated for *C9orf72* ALS/FTD that recapitulate distinct disease-related pathological, functional, and behavioral phenotypes. An overview of the currently available models is shown in Table 1. The first mouse model for *C9orf72* ALS was created in 2015 by somatic transduction of the C57BL/6J mouse CNS using an AAV carrying 66 G_4C_2 repeat.[83] Although this model did not develop the severe ALS/FTD

Table 1. Overview of the currently available mouse models for *C9orf72* related ALS and/or FTD.

ALS mouse model	Mutation	phenotype
AAV-$G_4C_2$66 (Chew et al. 2015)	$(G_4C_2)_{66}$ + 119 bp 5′ + 100 bp 3′ region (expressed by CBA promotor)	Mild: Histopathological features, Anxiety, decreased sociability, reduced motor function, weight loss, loss of NeuN positive neurons in cortex, motor cortex, Purkinje cells.[83]
BAC-C9-500/300 (Peters et al. 2015)	Human *C9orf72* (exon 1-6) + ~500 G_4C_2 repeats + 141 Kb 5′ region	Only histopathological features (no TDP-43 pathology), no behavioural.[86]
Tg(*C9orf72*_3) Line 112 (BAC-C9-(100-1000)) (O'Rourke et al. 2015)	Human *C9orf72* (1-11) + mix of 100-1000 G_4C_2 repeats + 110 Kb 5′ + 20 Kb 3′ region	Only histopathological features (no TDP-43 pathology), no behavioural.[84]
BAC-C9-450 (Jiang et al. 2016)	Human *C9orf72* (exon 1-5) + ~450 G_4C_2 repeats + 140 Kb 5′region	Mild: Histopathological features, spatial learning deficit, anxiety, ~ 10% loss of hippocampal neurons.[62]
BAC-C9-500 (Liu et al. 2016)	Human *C9orf72* (1-11) + ~500 G_4C_2 repeats + 52 Kb 5′ + 19 Kb 3′ region	Severe: Histopathological features, impaired motor function, reduced grip strength, hindlimb paralysis, decreased survival, loss of Purkinje cells, interneurons, upper and lower motor neurons.[85]

symptoms, some important features were observed that correlate with the pathology in patients. For example, sense RNA foci and DPRs produced from RAN translation were observed and TDP-43 inclusions were found in ~7-8% of neurons in the cortex and hippocampus.[83] In addition, mild neurodegeneration but no motor neuron loss was observed.[83] Four other transgenic mouse models were created expressing either full length or truncated human *C9orf72* with the G_4C_2 expansion. The *C9orf72* Exon 1–6 BAC (G_4C_2)500 SJL/B6 mice expressed sense and antisense RNA foci and poly GP proteins but no motor and/or behavioral impairment was observed.[47] The Tg(*C9orf72*_3) line 112 mouse was created containing the full length human *C9orf72* with multiple G_4C_2-repeat sizes ranging from 100 to 1000 repeats.[84] This model showed sense and antisense RNA foci and mild accumulation of poly GP but despite some evidence for nuclear stress there was no neuronal loss observed. Similarly, the BAC-C9-450 model also produced sense and antisense RNA foci in some brain regions and in the spinal cord as well as DPR proteins with an age dependent increase of poly(GA).[62] Despite a partial learning deficit and increased anxiety, no other motor or behavioral changes were observed. In contrast, the FVB/NJ-Tg(*C9orf72*)500Lpwr/J mouse model expressing the full length mutated human *C9orf72* gene including the 52 Kb 5'upstream region and the 19 Kb 3' downstream region of the gene did show progressive neurodegeneration and decreased survival which is also seen in ALS patients.[85] Sense RNA foci were observed in almost all NeuN positive neurons in the cortex, hippocampus and cerebellum. Antisense RNA foci were predominantly found in the motor cortex, hippocampus, cerebellar Purkinje layer and interneurons in the lateral and posterior horn of the spinal cord. DPR proteins in this mouse model increased with age throughout the brain, and nuclear and cytoplasmic TDP-43 aggregates were mainly observed in degenerating brain regions. The severe phenotype was exclusively observed in about one third of the females, while most of the males and females developed a mild phenotype. Nevertheless, the observations made in this model strongly support the involvement of the G_4C_2 repeat-mediated gain of toxicity in the disease pathology.

Despite the variable penetrance, these models could still be valuable tools for research as they all displayed some specific features such as RNA foci and DPR proteins that are key characteristics of *C9orf72* related ALS/FTD patients.

Animal models for SCA3

More than ten transgenic models for SCA3 have been published, all with variable differences in pathology and phenotype and most of them showing a mild form of neurodegeneration.[87] A summary of the most commonly used mouse models and their key characteristics is shown in Table 2. Three models showed a severe phenotype and will be discussed here in more detail. The first transgenic mouse model for SCA3 was created more than two decades ago expressing either full length or truncated ataxin-3 with 79 CAG repeat (Q79). Surprisingly, a severe ataxic phenotype was observed only in

Table 2. Overview of the currently available mouse models for SCA3.

SCA3 mouse model	Mutation	phenotype
Q79 (Ikeda et al. 1998)	L7 promotor + Human Ataxin 3 +79 CAG L7 promotor + truncated Human Ataxin 3 +79 CAG	Severe when 79 CAG is expressed by itself: severe ataxia, gait disturbances, motor deficits.[88]
MJD84.2 (Cemal et al. 2002)	Human ataxin-3 (YAC) + 84 CAG + 35 Kb 5′ + 150 kb 3′	Intermediate: gait abnormalities, hypoactivity, Limb clasping, atrophy of the cerebellar Purkinje and molecular cell layers.[95]
Homozygous Q71C (Goti et al. 2004)	Mouse prion promotor + human ataxin-3 + 71 CAG	Severe: progressive postural instability, gait and limb ataxia, weight loss, premature death, neuronal intranuclear inclusions, decreased TH-positive neurons in the substantia nigra. [92]
70.61 (Bichelmeier et al. 2007)	Mouse prion promotor + Ataxin-3 + 70 or 184 CAG	Severe: intranuclear inclusions in cortex and cerebellum, Shrinkage of ~ 50-80% of Purkinje cells, premature death[96]
Ataxin-3-Q79HA (Chou et al. 2008)	Mouse prion promotor + Ataxin-3 + 79 CAG	Intermediate: neuronal dysfunction, ataxia, downregulation and upregulation of several genes.[97]
PrP/MJD77-het/hom (Boy et al. 2009)	Ataxin-3 + 77 CAG	Mild: Cerebellar dysfunction, reduced anxiety, hyperactivity, impaired rotarod performance, weight loss.[98]
HDProm-MJD148 (Boy et al. 2010)	ataxin-3 +148 CAG (expressed by Huntingtin promotor)	Mild: Late onset symptoms, declined motor coordination after one year.[99]
Hemi-CMVMJD94 (Silva-Fernandes et al. 2010)	ataxin-3 + 94 CAG (expressed by CMV promotor)	Mild: represents early disease symptoms, neuronal atrophy and astrogliosis in several brain regions.[100]
Lentiviral Atx3-72Q (Nóbrega et al. 2013)	Ataxin-3 + CAG (expressed by PGK promotor)	Mild: reduced motor coordination, wide-based ataxic gait, and hyperactivity. accumulation of intranuclear inclusions, neurodegeneration.[101]
Humanized SCA3 knockin (Ki91) (Switonski et al. 2015)	Ataxin-3+91 CAG	Mild: deficits in coordination, transcriptional changes in the brain, amyloid depositions, mild degeneration of Purkinje cells in older mice, increased GFAP-positive glia in cerebellar white matter.[102]

the truncated model, with degeneration of the cerebellum and loss of Purkinje cells.[88] Due to this observation, it was strongly suggested that the C-terminal fragment of ataxin-3 containing the expanded polyQ could be more toxic by itself than when expressed as part of full length ataxin-3. Consistently, putative cleavage fragments of expanded ataxin-3 were identified in cell models, in post-mortem brains tissues of a SCA3 mouse model, in a drosophila model and in patients.[89-93] It is now well-accepted that the gain of toxicity is directly caused by the CAG repeat and that the affected neurons express a protease that cleaves the mutant ataxin-3 protein, releasing short soluble polyQ fragments that are highly neurotoxic and more prone to form aggregates.[80,81] Besides proteolytic cleavage of the C-terminal of the mutant ataxin-3 protein, mis-splicing could also play a role. A crucial evidence of mis-splicing leading to production of toxic short polyQ proteins was observed in HD. It was shown that exon 1 of the huntingtin, gene which contains the CAG repeat does not always splice to exon 2 but generates small polyadenylated HTTexon1 mRNA that encodes a small, highly pathogenic exon 1-polyQ HTT protein (also known as "exon-1 protein").[94]

The two other SCA3 mouse models (Q71C and 70.61) with a severe phenotype both express mutant ataxin-3 under control of the prion protein promotor. Within 1 to 8 months, both models showed early onset and a rapidly progressive type of SCA3 with several abnormalities such as progressive neurodegeneration, weight loss, behavioral problems, neuronal inclusions and premature death. Taken together, all these models could be useful to further study the disease mechanism in SCA3 and serve as tools for preclinical studies targeting mutant ataxin-3. It should be noted that the models with a severe phenotype all use non-native promoters to drive expression of mutant ataxin-3, lack regulatory flanking sequences, and often contain an excessive number of transgene copies. Thus, these models do not exactly mimic the expression pattern of mutant ataxin-3 in patients.

In vitro models for ALS and SCA3

Induced-pluripotent stem cell (iPSC) technology is revolutionizing the study of genetic diseases and is now pivotal for the development of targeted therapies. The use of iPSC technology was made possible when Professor Shinya Yamanaka showed that expression of four transcription factors (Myc, Oct3/4, Sox2 and Klf4) in fibroblasts reprograms the cells into pluripotent stem cells with the capability for indefinite self-renewal. For this discovery he was awarded the Noble prize in 2012.[103] It was subsequently demonstrated that iPSCs can be generated from different human somatic cell types that can be easily obtained such as fibroblasts, white blood cells, renal epithelial cells, keratinocytes etc. What made this technology widely accepted was the fact that it bypasses the ethical concerns associated with the use of embryonic stem cells and depending on the type of study, it may even replace animal models. iPSC lines can be generated from patients and differentiated back toward the disease-specific cells. For ALS, iPSC- derived motor neurons

have been of particular interest to study toxicity caused by the G_4C_2 repeat and to test therapeutic compounds. Cortical neurons can also be generated from iPSCs representing the cells primarily affected in FTD. For SCA3, it is currently still challenging to model cerebellar diseases with iPSC technology and although generation of cerebellar neurons such as Purkinje cells from iPSCs has been reported, this seems difficult to reproduce.[104] Hence, modeling cerebellar neurons with iPSC technology is less commonly reported as compared to other neuronal cell types in the frontal brain, midbrain and spinal cord. iPSC technology makes it possible to generate cell models for an individual or a specific group of patients which is a big advantage when compared to the different types of animal models, that always display species-related differences. Human-derived iPSCs with a wide variety of genetic backgrounds can be differentiated into different types of cells. This makes iPSC technology a very useful tool to study disease mechanisms, to use in early drug discovery (e.g screening of new therapeutic compounds), for toxicology testing and for prediction of off-target effects of gene modulating compounds (e.g. RNAi) in humans.

A limitation of iPSC systems is that *in vitro* two-dimension (2D) monocultures fail to represent physiological cellular functions and signaling pathways due to the lack of cell-cell and cell-matrix interactions. Recently, it was discovered that iPSCs can also be cultured in three dimensions (3D) to generate organoids that could represent different types of tissues, including different brain regions.[105,106] These 3D brain organoids allow cell-cell interactions and complex cyto-architectures to be modeled and studied in greater detail and in more physiological contexts. It is currently difficult to control the cell type organization and cell-cell or cell-matrix interactions and most organoid only represent single or partial components of a tissue. Efforts are being made to make organoids with multiple cell types in a more controlled fashion which may be promising in the future to replace animal models. While the use of animal models may be significantly reduced with the current advances on iPSC technology, at present, drug development and study of disease mechanisms still rely on a combination of different in vitro and *in vivo* model systems.

RNAi-based therapeutic strategies for neurogenerative diseases

As discussed, several neurodegenerative diseases are caused by mutations that lead to gain of toxic functions, and gene silencing technologies are attractive to lower the expression of disease-causing genes. A specific technology that can be applied for gene silencing is RNA interference (RNAi).

The discovery of RNAi dates almost three decades (1990) back, when Napoli and Jorgensen reported that injection of an extra chimeric copy of chalcone synthase, a gene responsible for the purple pigment anthocyanin in petunias, unexpectedly resulted in white petunias.[107] Thus, instead of complementing each other and producing extra purple flowers, the two copies of chalcone synthase seemed to interact with each other and

turned themselves off. The mechanism underlying this observation remained unclear until 1998, when Andrew Fire and Craig C. Mello provided an explanation of the RNAi mechanism. They discovered that a small non-coding RNA, miRNA (lin-4), binds to the 3'-UTR of the lin-14 mRNA in C. elegans, silencing its expression. For this work they were awarded the Nobel prize in Physiology or Medicine in 2006.[108] It was subsequently demonstrated that miRNA-mediated silencing also occurs in mammalian cells and this mechanism became a popular new tool to study gene function.[109]

It is now known that RNAi is a naturally occurring process in eukaryotic cells where double stranded RNA molecules can knock down or suppress the expression of genes that contain a homologous RNAi target sequence. RNAi plays an important physiological role in gene regulation and also has a function in the innate immune response of cells by providing protection against foreign nucleic acids from pathogens such as viruses and bacteria.[110] One of the first discovered mediators of RNAi is the RNAi-induced silencing complex (RISC), which has a nuclease activity that can cleave mRNA and knock down its expression. RNAi can be triggered by both endogenous and exogeneous double stranded RNAs.[111–113] Three types of small non-coding RNAs use the RNAi pathway; microRNA (miRNAs), small interfering RNA (siRNA) and piwi-interacting RNAs (piRNAs). miRNAs and siRNAs have a role as negative regulators of gene expression, while the piRNAs defend organisms against transposable elements.[114] miRNAs and siRNA are both widely being used as therapeutics in clinical trials and each system has its own merits. The focus of this thesis will be on miRNAs

miRNAs and their processing

miRNAs are small non-coding RNAs that are thought to regulate about 30% of genes in humans. More than 2000 miRNAs (www.mirbase.org) have been identified in humans and these are known to regulate several important cellular processes. Dysregulation of miRNAs is associated with several types of metabolic and CNS diseases, and with cancer. Apart from regulating gene expression, miRNAs can act as signaling molecules for intercellular communication. For example, it has been shown that miRNAs can be packaged into exosomes or microvesicles that following secretion, can be endocytosed by secondary cells, and re-establish their function.[115]

The biogenesis of a miRNA is tightly regulated in humans and involves 4 key enzymes; Drosha, exportin 5, Dicer and argonaute (AGO) proteins (Figure 4). The precursor of a miRNA is naturally encoded in the genome and is transcribed by RNA polymerase II or III into a long primary miRNA (pri-miRNA) with a cap and poly-A tail. The pri-miRNA transcript folds into a complex hairpin structure consisting of a double-stranded stem of about 30 base pairs, a terminal loop and two flanking unstructured single-stranded tails. The pri-miRNA is further processed in the cell nucleus by a ribonuclease called Drosha, resulting in a short 70-nt stem-loop structured precursor miRNA (pre-miRNA). The pre-miRNA is then transported to the cytoplasm by exportin 5 and is cleaved into

a short double stranded miRNA by a RNAse III enzyme called Dicer. The double stranded miRNA is recognized by AGO proteins and is loaded on RISC, usually preserving the guide strand and degrading the passenger strand. The RISC-AGO complex guides the miRNA guide strand to its target mRNA and induce its degradation and/or inhibit its translation. The first seven nucleotides near the 5'end of the guide strand form the seed sequence and are critical for the target recognition. It is also worth to mention that not all miRNAs are processed as described above and miRNA processing in plants differs at several points from the above described pathway. Furthermore, several mammalian miRNAs can bypass Drosha and currently one miRNA is known to bypass Dicer processing.[116] This Dicer-independent miRNA is microRNA-451a (miR-451a or miR-451), which has a role in the regulation of erythroid development.[117] Its recognition by Dicer seems to be perturbed due to its unusually short base paired stem and as a result, an active strand derived from the stem is produced, consisting of the single-stranded loop and part of the complementary stem region (figure 4). The ability to design artificial miRNAs that specifically silence disease-related genes is the basis for therapeutics such as miRNA mimics, anti-miRs and artificial miRNAs. miRNA mimics are double stranded miRNAs made synthetically to match a corresponding miRNA, aiming to compensate the loss of miRNAs that are downregulated in diseases. Anti-miRs are artificially made single stranded miRNA to bind target miRNAs and inhibit their function. Artificial miRNAs are made by replacing the guide strand sequence of an endogenous miRNA precursor with the sequence of an mRNA of interest, enabling silencing of genes that are upregulated in diseases (figure 5). Recently, the miQURE™ Gene Silencing platform was introduced by uniQure. miQURE uses the advantages of the non-canonical processing of miR-451 to silence genes involved in diseases. miR-451 produces no passenger strand as the pre-miR-451 escapes Dicer cleavage and only a 5' arm strand is active on the targets. Thus, there is no miRNA duplex formation that requires strand separation and selection for the RISC. Because of this efficient processing, off-target effects due to a passenger strand activity can be neglected. This technology was first applied in uniQure's Huntington's disease program and is now being investigated for application in other neurodegenerative diseases such as ALS and SCA3 and for liver indications.

Clinical applications for Therapeutic RNAi

Several RNAi-targeted therapeutics have reached clinical development. For example, MRX34 (synthetic miR-34), a miRNA developed by Mirna Therapeutics was the first to enter a clinical trial to treat different types of cancer.[118,119] Its mode of action was to decrease the expression of collagen and other proteins that are involved in fibrous scar formation. However, clinical development was terminated in 2016 due to several immune-related severe adverse events. An example of a successful anti-miR clinical trial is Miravirsen, an Locked Nucleic Acid (LNA) anti-miR-122 oligo developed by Santaris Pharma to treat Hepatitis C.[120] The phase II trials demonstrated reduced Hepatitis C viral load, even at low

therapeutic concentrations and no adverse events was observed.[121–123] Another phase I/II clinical trial to treat patients with Hepatitis C infection was based on shRNAs and was conducted by Benitec Biopharma. Their lead product was TT-034 which is based on intravenous AAV8 delivery of three independent shRNAs targeting three well-conserved

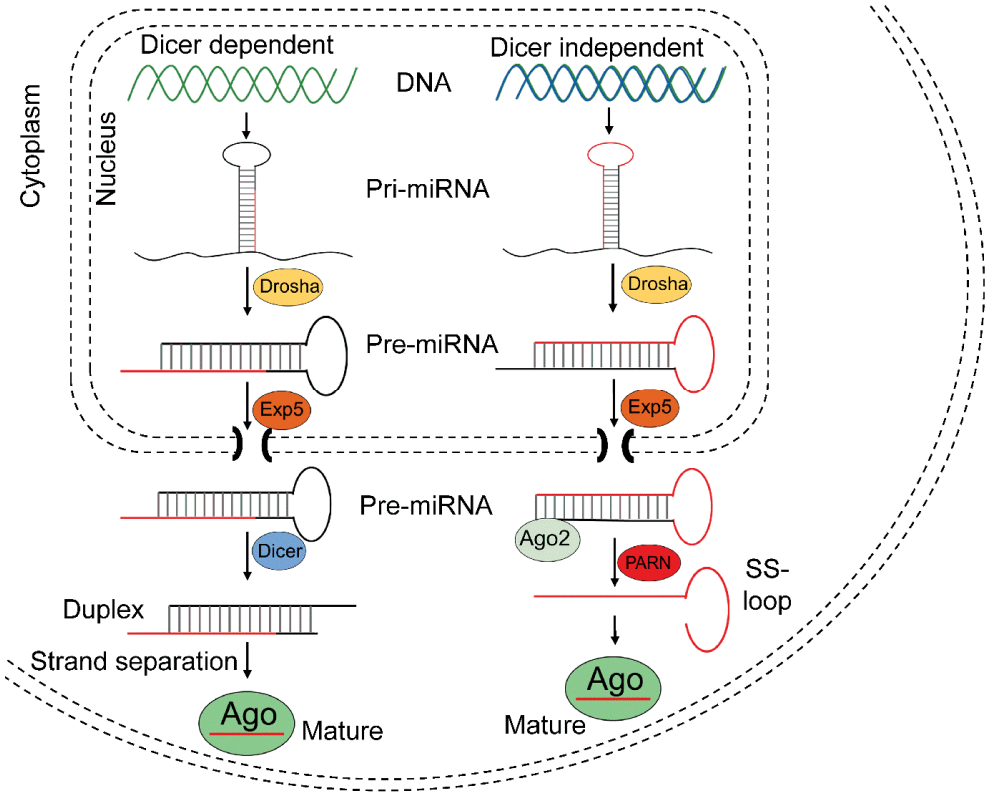

Figure 4. Schematic of miRNA processing pathway. Most miRNAs are processed in the Dicer dependent (canonical) pathway shown in the left part of the figure. After being transcribed, the pri-miRNA transcripts are cropped by Drosha in the nucleus, resulting in a 60–70 nt pre-miRNA. The pre-miRNA is exported to the cytoplasm by Exportin 5 and the hairpin is then diced by Dicer into ~22-nt miRNA duplex, after which it is separated into a guide and passenger strand. The guide strand is usually loaded into Ago proteins to form RISC. There are four Ago proteins and all are capable to repress translation or promote mRNA degradation. Ago2 is the only Ago protein with a slicer activity which plays a critical role in Dicer independent processing of miR451 (right part of the figure). miR451 is also processed in the nucleus by Drosha, but results in a unusually short, 41–42-nt pre-miRNA which is not recognized by Dicer and do not form a miRNA duplex. However, the further processing of miR-451 requires the slicer activity of Ago2. Ago2 cleaves the 3' arm of pre-miRNA by its slicer activity and yields a 30-nt intermediate whose 3' end is further trimmed by PARN to generate a mature, ~23-nt miRNA. This mature miRNA is loaded into Ago proteins to form the RISC.

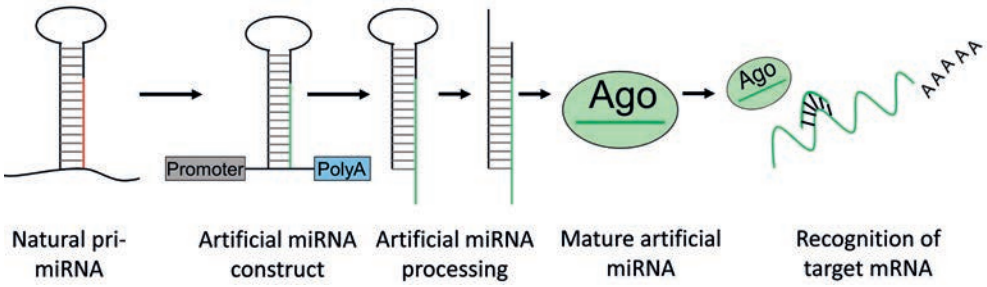

Figure 5. Artificial miRNA design. Artificial miRNAs can be made by replacing the mature miRNA sequence of a natural pri-miRNA for a complementary sequence of a target mRNA of interest. The artificial pri-miRNA sequence can be cloned in an expression construct. Upon transfection with the artificial miRNA construct, the artificial miRNA is processed in the cell into a mature artificial miRNA which can bind and knockdown expression of a mRNA of interest.

sequences located in the 5' UTR and NS5B regions of the HCV genome.[124] Overall, TT-034 was well tolerated and safe in patients. Furthermore, liver biopsies revealed sustained transduction of hepatocytes and expression of the three anti-HCV shRNAs. However, Benitec Biopharma decided to discontinue this program due to decrease in commercial opportunities for TT-034 following the introduction of highly effective viral eradication strategies based on (combinations of) small molecules. Compared to miRNAs, siRNAs have been more widely tested in clinical trials for treatment of different types of diseases such as cancer, viral infections, age-related macular degeneration, diabetic macular, hypercholesterolemia and ocular hypertension.[125] DNA constructs encoding therapeutic RNAi following delivery by lentiviral vectors have also been clinically tested. Benitec, Inc in collaboration with the City of Hope National Medical Center conducted a trial to treat HIV-1 infection in AIDS/lymphoma patients.[126] This was executed by genetically modifying hematopoietic stem cells (hSC) *ex vivo* by transduction with a lentiviral vector expressing three small RNAs targeting HIV: An shRNA targeting an exon in HIV-1 tat/rev , a RNA decoy for the HIV TAT-reactive element, and a ribozyme targeting the host cell CCR5 chemokine receptor. The transduced hSC were then infused into patients whose bone marrow has been ablated to treat their AIDS related lymphoma. Sustained expression of the anti-tat/rev shRNA and ribozyme was observed for up to 24 months post-infusion.[123] Although this study demonstrated feasibility and safety of this approach, it failed to demonstrate clinical benefit because an insufficient number of hSCs was transduced.

In the neurodegenerative field, uniQure recently obtained Food and Drug Administration (FDA) clearance for AMT-130 and this will be the first AAV-miRNA-based gene therapy for a neurodegenerative disease to start a Phase I/II clinical trial. AMT-130 is based on a miRNA designed to target both wild-type and mutant Huntingtin allele (AAV5-miHTT).[127,128] Significant lowering of human mutant huntingtin mRNA and protein was achieved in the brain of a transgenic HD (tgHD) minipig model after a single

administration into the brain. [128] uniQure plans to start the first PhaseI/II clinical trial in early HD patients in the second half of 2019. A similar approach is being pursued by Voyager Therapeutics and promising results have been obtained with their lead candidate VY-HTT01 in preclinical models. miRNA mediated silencing is thought to be an attractive therapeutic modality in many other neurodegenerative diseases, including the SCAs, ALS, FTD, synucleopathies including Parkinson's disease, tauopathies and AD.[129–132] miRNAs may cause toxicity related to (passenger strand) off-target toxicity. Hence, during development these effects should be closely investigated and minimized, by selecting scaffolds with little to no passenger strand activity and by predicting the chances of binding to off-target genes using computer-based bioinformatic tools. Another important limitation of miRNA-based therapeutics is the required efficacy in the nucleus of cells, because active mature miRNAs resulting from canonical Dicer processing in the cytoplasm are thought not to re-enter the nucleus. However, as many of these hurdles are being tackled, more miRNA therapeutics are expected to reach the clinic.

Common alternative silencing strategies

Antisense oligonucleotides

Antisense oligonucleotides (ASOs) are short, synthetic, single-stranded nucleic acids of about 20-25 bases long that bind cellular RNA and reduce, restore, or modify protein expression via several distinct mechanisms. The silencing pathway of ASOs differs from siRNA and miRNAs and there is no known cellular mechanism to facilitate strand recognition. ASOs classically bind to complementary mRNA through Watson Crick base-pairing leading to endonuclease-mediated transcriptional knockdown.[133] Once bound to the mRNA, ASOs can form an RNA–DNA hybrid that becomes a substrate for the enzyme RNase H, which hydrolyzes the mRNA resulting in its degradation.[134] The cleaved mRNA products are then processed by the normal cellular degradation pathways in the nucleus and cytoplasm.[135] ASOs can be engineered to have enhanced pharmacological properties by introducing backbone modifications. For example, modified ASOs can knockdown gene expression by sterically blocking splicing factors and altering pre-mRNA splicing, or by preventing ribosome recruitment to block mRNA translation.[136] Interestingly, ASOs can destabilize splicing sites and displace or recruit splicing factors when designed

Table 3. clinical trials using ASOs for ALS by Ionis Pharmaceuticals

Disease	Trial code	Vector	Delivery route	Status (completion year)	Sponsor
ALS[137,138]	NCT01041222	ASO (SOD1)	Intrathecal	Phase I (2012)	Ionis Pharmaceuticals
ALS	NCT02623699	ASO (SOD1)	Intrathecal	Phase I/II (2019)	Biogen & Ionis Pharmaceuticals
ALS	NCT03626012	*ASO (C9orf72)*	Intrathecal	Phase I (2022)	Biogen & Ionis

to bind within intron–exon junctions. This makes it possible to exclude ("skip") or include exons of interest, which can be beneficial in genetic diseases.[136] Through this mechanism normal gene function can be restored by re-establishing a normal reading frame following a pathogenic frame shift, or by excluding mutated segments of DNA.[133] ASOs have been used in preclinical studies since the 1970s and several programs have made it into clinical development. A phase I ALS trial using intrathecal administration of ASOs targeting SOD1 was completed in 2012 by Ionis Pharmaceuticals (Table 3).[137,138] Unfortunately this study failed to show a reduction of SOD1 protein which was explained by the low target tissue ASO concentration but the treatment proved to be safe, and a follow up phaseI/II trial study is ongoing (BIIB067; IONIS-SOD1). Ionis Pharmaceuticals also initiated a phase I clinical trial in 2019 with ASOs targeting *C9orf72*-ALS patients (BIIB078). BIIB078 targets specifically the intronic region of *C9orf72* to cause reduction of only the repeat-containing *C9orf72* transcripts and is administered intrathecally to adult patients. Ionis Pharmaceuticals has developed ASOs for many other diseases and have ongoing clinical trials for HD, DM1 and SMA. Furthermore, several preclinical studies have shown efficacy of ASOs in *C9orf72*-related ALS and SCA3 in vitro and in vivo but these programs have not yet reached clinical development. A clinical study (NCT03508947) with ASOs that has raised some concerns regarding toxicity was performed by WAVE life Sciences to treat patients with Duchenne muscular dystrophy (DMD). DMD is a fatal genetic disorder characterized by progressive muscle wasting and is caused by mutations in the DMD gene which encodes for dystrophin, an essential protein to maintain muscle integrity. The ASO was administered intravenously and was designed to skip the mutated exon 51 in the DMD gene to restore normal function of dystophin.[139] Adverse events such as headache, fever, vomiting and tachycardia occurred in the low and mid dose groups and these adverse events were even more severe in the high-dosed groups. WAVE life sciences reported to continue with the lower doses for Phase II/III trial which is expected to be initiated in 2019 but it is unclear if these adverse events will re-occur during re-administration and whether or not the lower doses are therapeutically effective. A major limitation of ASOs for clinical application is that they are degraded by endo- and exonucleases and re-administration is required.[140] This is especially problematic in CNS disorders that require invasive delivery methods. However, the pharmacological profiles of ASOs can be enhanced by introducing chemical modifications and efforts are being made to improve ASOs delivery to for example cross the blood brain barrier (BBB) and to improve target engagement.[141]

Gene Editing (CRISPR)

Gene editing is a relatively novel approach to remove, add or alter DNA in a sequence-specific manner. The pivotal discovery that made gene editing possible was the discovery that the endogenous cellular repair machinery can be triggered by targeted DNA double strand breaks (DSBs) through homology-directed repair (HDR) or nonhomologous end-

joining (NHEJ). DNA DSBs can be introduced at a precise location by using engineered nucleases harboring a sequence-specific DNA-binding domain, fused to a DNA cleavage module. The most popular nucleases are zinc-finger nucleases (ZFNs), transcription activator-like effector nucleases (TALENs), and the RNA-guided clustered regulatory interspaced short palindromic repeats (CRISPR) and CRISPR-associated system 9 (Cas9) (CRISPR/Cas9). ZFNs are currently the only gene editing technology that have made it to clinical trials. In 2018 Sangamo Therapeutics started a clinical trial using this technology in mucopolysaccharidosis II (MPS II). ZFNs consist of ~30 amino acids which folds into ββα "fingers" structures that recognize and bind a trinucleotide sequence of DNA.[142–144] The nuclease domain is based on a restriction endonuclease (FokI) that can cut DNA when following dimerization.[142] Binding to DNA sequences longer than 3 and up to 18 base pairs (in multiples of 3 base pairs) is possible by arranging a series of linked zinc-fingers. However, this requires recoding of proteins for each new target site which is a very challenging and time-consuming process. Another limitation is the restricted target site selection as zinc-fingers can only target binding sites every ~50-200 base pairs in a random DNA sequence [142] Furthermore, all gene editing technologies including zinc-fingers may have off-target effects, resulting in unwanted induction of DNA mutations or deletions. Like ZFNs, TALENs are based on a DNA-protein association but they use a different DNA binding domain termed (transcription activator-like effectors) TALE repeats.[142] A TALE motif can recognize a single nucleotide and an array of TALEs can recognize and bind to a longer DNA sequence. Unlike ZFNs, the design of TALENs are less complicated and the TALE repeat array can be easily extended to whatever length is desired.[142] Furthermore, as compared to ZFNs, site-specific targeting is easier because multiple TALEN pairs are available for each base pair of a random DNA sequence. Some major limitations for TALENs are off-target effects and compared to ZFNs, they are about 3x larger in size (~3 Kb) which makes delivery by viral vectors more challenging.

CRISPR/Cas9 is the latest of the above-mentioned nuclease systems and is based on a naturally occurring process in the adaptive immune system of the bacteria Streptococcus pyogenes. CRISPR/Cas9 is distinct from ZFN and TALEN endonucleases in that it does not use a protein but an RNA-guided system to perform genome editing. Unlike the other nuclease systems, CRISPR/Cas9 does not require custom design of novel proteins for each DNA target site. Thus, the design of constructs is relatively easy and cost-effective. Bacteria use the RNA-guided Cas proteins to create DSBs in exogenous DNA derived from invading viruses (bacteriophages).It does so by creating CRISPR arrays from exogenous DNA by insertion of these DNA sequences between short palindromic repeats in the CRISPR locus of its own DNA. Upon a repeated viral attack, these "foreign" inserts can be transcribed from the virus specific CRISPR locus into CRISPR RNA fragments that match the invading viral DNA. CRISPR RNAs contain a tail transcribed from the CRISPR locus which facilitates incorporation into complexes to form hairpins-like structures that allow them to dock on a Cas protein. The Cas protein is then guided by the CRISPR RNA to hybridize to its parental exogeneous DNA and induce a DSB.[145] This CRISPR/Cas9

system can be implemented in eukaryotes by designing sequences that target a specific DNA sequence and co-expressing Cas9. The Cas9 protein cuts the DNA at the target site, which is repaired by HDR or NHEJ. Several animal models have been created using the CRISPR/Cas9 system and a rapidly increasing number of preclinical studies show the promises of this technology in combination with gene therapy for the treatment of neurodegenerative diseases. For example, in AD, the defective (amyloid precursor protein) APP gene was successfully edited in human fibroblasts using a CRISPR/cas9 construct and this resulted in reduction of Amyloid beta, a main component of plaques found in brain of AD patients.[146] In ALS, the G_4C_2 repeat in the non-coding region of the *C9orf72* gene was successfully deleted in transfected patient-derived iPSCs and this prevented RNA foci formation as well as the promoter hypermethylation that is typical for ALS.[147] For HD, permanent suppression of mutant Huntingtin and it's aggregates was achieved in the striatum of the HD140Q-knock-in mice by CRISPR/Cas9.[148] For SCA3, CRISPR/Cas9-mediated deletion CAG repeat in *ATXN3* gene was successfully performed in patient-derived iPSCs.[149] Following the CAG deletion, the iPSCs retained pluripotency and neurons differentiated from these cells retained a normal ubiquitin-binding capacity of *ATXN3*.

The CRISPR/Cas9 system has great potential for targeting pathogenic genes, but a major hurdle is the occurrence of off-target effects, Cas9 specificity, and potential mutagenesis. Not unexpectedly, continuous expression of Cas9 proteins at high concentrations has been linked to toxicity.[150] The chances for off-target binding in the host genome using current systems are estimated to be relatively high (≥50%).[151] Another limitation is the delivery method as the CRISPR/Cas9 components are about 8-10 kb long whereas AAV vectors have a packaging capacity limited to 4.8 kb. Thus, the CRISPR/Cas9 system has a huge potential to be developed in therapeutic approaches but major challenges need to be overcome to make this technology suitable to treat human diseases.

AAVs for gene transfer to the nervous system

A major difficulty to treat neurodegenerative diseases remains the method of administration. Due to existence of the BBB, many small molecules and most therapeutic nucleotides or gene therapy vectors that are administered systemically or orally fail to reach the brain or spinal cord at a therapeutically relevant dose. Different alternative routes of administration are being investigated for delivery to the CNS and their application is highly depended on the disease pathology. While some diseases require local targeting or transduction, others require widespread distribution throughout the CNS. Intracerebral administration, directly injected in the parenchyma of the brain can be safely and effectively done using convection-enhanced delivery (CED) in combination with precise positioning using magnetic resonance imaging-based guidance technologies (MRI).[152] CED uses a pressure gradient to generate bulk flow within the brain parenchyma. Due to the low velocity of injection, potential structural damage is minimized, and a uniform distribution can be

obtained.[153,154] The advantage of this injection route is that it bypasses the BBB and high local transduction can be obtained with a relatively low dose of AAV, with limited leakage to periphery organs. Further spread of AAV may occur via anterograde or retrograde transport along axons but this is highly dependent on the AAV serotype.[9,155] A drawback of this delivery route is that the procedure itself is invasive and may lead to complications such as bleeding or leakage of the administered vector into the CSF. In addition, intracerebral administration is only suitable for diseases with pathology limited to specific brain areas. Alternative routes to cover larger areas of the CNS are systemic or intrathecal delivery. Systemic delivery by intravenous injection is a relatively simple procedure, less invasive and avoids costly neurosurgical procedures. However, systemic delivery of AAV gene therapy is currently less suitable for neurodegenerative disorders because the bulk of such vectors is taken up by peripheral organs and can cause systemic immunogenicity. Even though some vectors can cross the BBB, the target tissue concentration after systemic delivery is often not therapeutically relevant. Nevertheless, a successful clinical trial with systemic administration was performed by AveXis to treat children with SMA.[156] The vector used was a self-complementary AAV9 and following systemic administration a therapeutic effect in motor neurons of the spinal cord was observed. It remains questionable whether similar effects can be obtained in adults as the integrity of the BBB is known to be different. Despite the initial promising results, AveXis changed the delivery method in children to an intrathecal administration route in the follow up study. This amendment was based on a study in NHP showing improved transduction of the CNS with up to 10 times lower intrathecal dose as compared to intravenous administration.[157] Intrathecal administration can be done through lumbar puncture, direct administration into the cisterna magna or in the cerebral ventricle.[158,159] Thus, the vector is delivered directly into the CNS bypassing the BBB. This approach is less invasive than intracerebral administration and usually show less leakage to the periphery organs as compared to systemic administration. One limitation of intrathecal administration is dilution of vector and the consequent transduction is usually lower when compared to intracerebral administration. Furthermore, transduction of the deeper brain structures is poor, possibly because the vector needs to pass the ependymal cell layer or the pia mater.[160,161]

Gene therapy clinical trials for neurogenerative diseases

Several gene therapies for different types of neurodegenerative diseases have progressed into clinical development. For *C9orf72* related ALS and SCA3, no gene therapy has been clinically investigated yet. An overview of the currently ongoing clinical trials published on https://clinicaltrials.gov is depicted in table 4 and will be further discussed in this paragraph.

Parkinson's disease

PD is a neurodegenerative disorder caused by loss of dopaminergic neurons in the substantia nigra, leading to bradykinesia, rigidity, tremor, and gait dysfunction.

Expressing neurotrophic factors such as GDNF delivered by AAV was tested in a single clinical trial and AAV-delivered neurturin (NTN) was investigated in three clinical trials for PD. The rationale for delivering these neurotrophic factors was not to target a causative pathological molecular pathway but to provide neurotrophic support to the degenerating neuronal population. Although these studies were well tolerated, their efficacies are unclear. However, these studies were important to demonstrate the feasibility and tolerability of intraparenchymal AAV delivery of gene therapy directly in the human brain.

Most gene therapy approaches for PD aim to restore dopamine production in neurons. Deliveryof 1-amino acid decarboxylase (AADC), a key enzyme for dopamine production showed to be more promising than neurotrophic factors. Proof of concept studies in NHP showed an increase in levels of dopamine which was sustained for up 7 years.[154,162] The first AAV delivered AADC study in humans (NCT00229736) was in general well tolerated with some minor side effects.[163,164] A significant improvement of Parkinson's Disease Rating Scale (UPDRS) scores was reported at 6 months post-surgery which was sustained for up to 2 years. These promising results have triggered other AAV-based trials on AADC delivery and several studies are currently ongoing with higher doses and larger cohorts of patients. A clinical trial using a intrastriatal delivered lentivirus (ProSavin) expressing the three key tyrosine hydrolase, AADC, and GTP cyclohydrolase-1, with the aim of providing a continuous source of dopamine in the striatum has also demonstrated to be safe and well tolerated with no surgical complications (CT01856439).[165,166] A significant improvement of motor function was observed, and a long-term analysis is ongoing. Another lentiviral gene therapy that is currently being tested in clinic and very similar to ProSavin also expresses tyrosine hydroxylase, AADC and GTP-cyclohydrolase. While there is no data available yet from this study, the preclinical results in human primary neuronal cultures and NHP showed higher dopamine production compared to ProSavin.[167]

Alzheimer's disease

AD is the most common cause of age-related dementia affecting more than 40% of individuals of 85 years and older. More than 100 therapeutic compounds have been tested to date, but all failed to positively modify the course of the disease. Most gene therapy clinical trials for AD are based on intracerebral delivery of AAV-NGF. NGF encodes nerve growth factor and similar to GDNF and NTN, could provide neurotrophic support to neurons. Preclinical studies have shown that NGF can prevent degeneration of adult cholinergic neurons in the fore brain after injury.[168,169] Although the surgical procedures and the treatments proved to be safe in humans, the efficacy of the studies was inconclusive. A more recent study for AD is based on intracisternal delivery of AAVrh.10hAPOE2 (NCT03634007). It was shown that inherence of an extra allele of *APOE4* gene, a variant

Table I. Gene therapy clinical trials for neurogenerative diseases

Disease	Trial code	Vector
Parkinson[184]	NCT00252850	AAV2- Neurturin
Parkinson[155]	NCT00400634	AAV2-Neurturin
Parkinson[185]	NCT00985517	AAV2-Neurturin
Parkinson[186–188]	NCT01621581	AAV2-GDNF
Parkinson[163]	NCT00229736	AAV-hAADC-2
Parkinson	NCT01973543	AAV2-hAADC
Parkinson	NCT03562494	AAV2-hAADC
Parkinson	NCT02418598	AAV-hAADC-2
Parkinson[166]	NCT01856439	ProSavin (LV-TH-GCH-AADC)
Parkinson	NCT03720418	AXO-Lenti-PD(OXB-102-01)
Parkinson[189,190]	NCT00643890	AAV-GAD
Alzeimer	NCT00087789	AAV2-NGF
Alzeimer[191]	NCT00876863	AAV2-NGF
Alzeimer	NCT03634007	AAVrh.10hAPOE2
Batten[192–194]	NCT03770572	AAV9-CLN3
Batten[195]	NCT00151216	AAV2CUhCLN2
Batten	NCT01161576	AVRh.10CUhCLN2
Batten	NCT02725580	scAAV9.CB.CLN6
Mucopolysaccharidosis Type IIIA[173]	NCT03612869	AAVrh10-h.SGSH
X-Linked Myotubular Myopathy	NCT03199469	AAV8-hMTM1
spinal muscular atrophy Type 1	NCT02122952	AAV9-SMN
spinal muscular atrophy[157,196]	NCT03505099	AAV9-SMN
spinal muscular atrophy[157,196]	NCT03306277	AAV9-SMN
spinal muscular atrophy[156,197]	NCT03461289	AAV9-SMN
spinal muscular atrophy[156,197]	NCT03381729	AAV9-SMN
Pompe disease[198]	NCT03533673	AAV2/8LSPhGAA
Pompe disease	NCT02240407	rAAV9-DES-hGAA
Pompe disease[199]	NCT00976352	rAAV1-CMV-GAA
Canavan disease[200]	NA	AAV2- hASPA
AADC deficiency	NCT01395641	AAV2- hAADC
AADC deficiency	NCT02926066	AAV2- hAADC
AADC deficiency	NCT02852213	AAV2- hAADC
MPS I[201]	NCT02702115	AAV6-ZFN
MPS II[202]	NTC03041324	AAV6-ZFN
MPS IIIA	NCT02716246	AAV9-hSGSH
MPS IIIA[173]	NCT03612869	AAVrh.10- hSGSH
Sanfilippo Disease Type A	NCT02053064	AAVrh10- SGSH
MPSIIIB[174]	NCT03300453	AAV5- hNAGLU
MPSIIIB	NCT03315182	AAV9- hNAGLU
Huntington's disease	NA	AAV5-miHTT

Delivery route	Status (completion year)	Sponsor
Intrastriatal	Phase I (2007)	Ceregene
Putamen	Phase II (2008)	Ceregene
Substantia nigra	Phase II (2018)	Sangamo Therapeutics
Putamen	Phase I (2027)	National Institute of Neurological Disorders and Stroke (NINDS)
Intrastriatal	Phase I (2013)	Genzyme
Intrastriatal	Phase I (2019)	Voyager Therapeutics
Intrastriatal	Phase II (2020)	Voyager Therapeutics
Putamen	Phase II (2022)	Jichi Medical University
Intrastriatal	Phase I/II (2021)	Oxford BioMedica
Intrastriatal	Phase I/II (2020)	Axovant Sciences Ltd
Subthalamic nucleus	Phase II (terminated)	Neurologix, Inc
Basal forebrain	Phase 1 (2010)	Ceregene
Basal forebrain	Phase II (2020)	Sangamo Therapeutics
Intracisternal	Phase I (2020)	Weill Medical College of Cornell University
Intrathecal	Phase II (2022)	Nationwide Children's Hospital & Amicus Therapeutics
Intracranial	Phase I (2019)	Weill Medical College of Cornell University
Intracranial	Phase I (2020)	Weill Medical College of Cornell University
Intrathecal	Phase II (2019)	Nationwide Children's Hospital
Intracerebral	Phase III (2022)	LYSOGENE
Intravenous	Phase II (2025)	Audentes Therapeutics
Intravenous	Phase I (2019)	AveXis, Inc
Intravenous	Phase I (2020)	AveXis, Inc
Intravenous	Phase I (2020)	AveXis, Inc
Intravenous	Phase III (2020)	AveXis, Inc.
Intrathecal	Phase I (2020)	AveXis, Inc.
Intravenous	Phase II (2020)	Actus Therapeutics, Inc
intramuscular	Phase I (2019)	University of Florida
intradiaphragmatic	Phase II (2015)	University of Florida
Intraparenchymal	Phase I (2002)	National Institute of Neurological Disorders and Stroke
Intraparenchymal (Putamen)	Phase I/II (2020)	National Taiwan University Hospital
Intraparenchymal (Putamen)	Phase II (2018)	National Taiwan University Hospital
Intraparenchymal	Phase I (2020)	National Taiwan University Hospital
Intravenous	Phase I (2020)	Sangamo Therapeutics
Intravenous	Phase I (N.A)	Sangamo Therapeutics
Intravenous	Phase I/II (2019)	Abeona Therapeutics
Intracerebral	Phase II/III (2022)	LYSOGENE
Intracerebral	Phase II (2017)	LYSOGENE
Intracerebral	Phase I/II (2019)	UniQure Biopharma B.V.
Intravenous	Phase I/II (2020)	Nationwide Children's Hospital
Intrastriatal	Phase I/II (N.A)	UniQure Biopharma B.V.

of apolipoprotein E (*APOE*) can significantly increase the risk for developing sporadic AD, while *APOE2* homozygotes are protected against the disease. Thus, APOE2 delivery could potentially be beneficial in *APOE4* homozygous patients.[170] Whether this approach indeed modifies the course of the disease is yet to be demonstrated.

Batten disease

Batten disease or neuronal ceroid lipofuscinosis (NCLs) is a rare group of neurodegenerative disorders that can manifest in infants, children and adults. Symptoms include epilepsy, loss of cognitive and motor function, degeneration of the retina leading to blindness, and early death. More than a dozen CLN genes and more than 430 loss of function mutations have been linked to the diseases.[171] AAV-based clinical trials for Batten disease have mainly focused on delivery of AAV-CLN2 and AAV-CLN3. The first study (NCT00151216), using intracranial delivery of AAV2CUhCLN2 showed little therapeutic benefit. A follow up study is still ongoing and used a different vector (AAVRh.10CUhCLN2) but abnormal T2 hyperintensities was observed in first dosed patient and led to a lowering of the dose for the following patient. For CLN3, one study (NCT03770572) is still recruiting and is based on AAV9-CLN3 delivery. For CLN6, an study with intrathecally delivered scAAV9. CB.CLN6 is ongoing. A press release announcement from the preliminary data from the first two dosed patients stated no further progression of the disease (according to the Hamburg motor and language score) during the first two years after dosing.

Mucopolysaccharidoses (MPSs)

Mucopolysaccharidoses (MPSs) are rare metabolic diseases that are caused by impaired degradation of mucopolysaccharides, leading to accumulation of glycosaminoglycans in the lysosome. Symptoms can be detected as early as during the prenatal period but can also occur in adulthood. The symptoms in adults include difficulty of speech, ataxia, weakness, and dyskinesia, while children usually show neurological impairment, developmental delay and premature death.[172] Several gene therapy clinical trials are currently in progress for the treatment of MPS I (Hurler infantile syndrome or Hurler-Scheie and Scheie for the juvenile and adult forms), MPS II (Hunter syndrome), MPS IIIA and MPS IIIB (Sanfilippo syndromes A and B). For MPS I and MPS II, the trials are based on intravenous AAV delivery of ZFN therapeutic agents to insert a functional copy of alpha- L-Iduronidase (IDUA) or iduronate 2-sulfatase (IDS) into the albumin locus of patient hepatocytes. These trials are currently being tested in adult patients aiming to improve the peripheral symptoms of these diseases. For MPS IIIA, the main goal is to deliver a functional copy of the human N-sulfoglucosamine sulfohydrolase (h.SGSH) directly into the brain of young children. Thus far, h.SGSH delivery seems to be safe, but the therapeutic benefit was limited with cognitive improvement observed in only one patient.[173] For the treatment of MPS IIIB, the goal is to deliver N-sulfoglucosamine sulfohydrolase (NAGLU) to restore its expression in patients. Both intracerebral and intravenous delivery of AAV-NAGLU have shown to be

promising in preclinical studies in rodent and dog models but whether this translates to therapeutic benefit in patients is yet to be demonstrated.[174,175]

Pompe disease

Pompe disease is a progressive neuromuscular disorder and is caused by a mutation in the acid alpha-glucosidase (GAA) gene, which encodes an enzyme required to degrade lysosomal glycogen.[176] Accumulation of glycogen in multiple tissues results in cardiac, respiratory, and skeletal muscle dysfunction. Preclinical studies in GAA knockout mouse models showed rescue of glycogen accumulation in muscle and the central nervous system and increased survival upon delivery of GAA by AAV.[177] Delivery of GAA by AAV is currently being tested in three different clinical trials.

Spinal muscular atrophy

SMA is caused by the loss of function of the gene encoding the survival motor neuron 1 (SMN1) protein and is characterized by progressive loss of the lower motor neurons. The most severe form is type 1 SMA which affect infants. The patients usually die before the age of 20 months. Several clinical trials are run by AveXis based on AAV9-SMN delivery. Thus far, remarkable clinical benefit was observed including increased motor functions, head control, sitting, rolling over and speaking. The high dose of intravenous injected AAV9-SMN led to an increase in serum aminotransferase, a sign of liver toxicity, which was managed by oral prednisolone. Intrathecal delivery of AAV9-SMN is also being investigated by AveXis as improved transduction of the CNS was observed in lower dose as compared to intravenous administration in NHP. This program is currently also being investigated in clinic for other types of SMA (NCT03306277, NCT03505099, NCT03461289, and NCT03381729), results of which are pending (Table 1). A Biological License Application was submitted to the US FDA in November 2018 by Novartis, which acquired AveXis. In March 2019, Novartis announced the FDA approval of AAV9-SMN (Zolgensma®) for the treatment of pediatric SMA type 1 patients.

Huntington's disease

HD is the most common autosomal dominant neurodegenerative disorder worldwide.[178,179] The genetic cause is an expansion of 39 CAG triplets or more in first exon of the huntingtin (HTT) gene.[180] The mutated gene produces a mutant HTT protein that contain a long polyglutamine (polyQ) tract and results in a toxic gain of function. The mutant HTT protein causes neuropathology affecting the entire brain, with medium spiny neurons of the striatum being particularly vulnerable at early stages.[181,182] The clinical symptoms include progressive motor, cognitive, and psychiatric disturbances. Currently there is no treatment available that would halt or delay disease progression. Artificial DNA or RNA molecules to achieve lowering of HTT translation as a potential therapy for HD have been

broadly investigated in preclinical studies but few have made it to clinical trials. IONIS was the first to initiate a Phase I/II clinical trial (NCT02519036) in 2015 based on HTT lowering with an intrathecally administered antisense oligonucleotide targeting both wildtype and mutant HTT. This trial was safe and a reduction of HTT protein was detected in the CSF.[183] Roche is continuing this study with a large phase III trial (NCT03761849) that was launch in 2018 and will be conducted at around 80-90 sites in about 15 countries. It remains unknown whether this intrathecally delivered ASO will reach the deeper brain structures to achieve sufficient lowering of the mutant HTT in the striatum. Concerningly, the latest published data using this approach showed a dose- and time-dependent increase of the ventricular volume, which suggests that the treatment cause more CNS atrophy, instead of the desired prevention of CNS atrophy.

UniQure will launch the first AAV-based RNAi therapy for HD in the second half of 2019. The therapeutic candidate is AAV5-miHTT (AMT-130), which is based on an anti-HTT miRNA targeting a region close to the repeat in exon 1 of the HTT gene to silence both wildtype and mutant HTT. AMT-130 will be injected directly in the striatum and should provide a long-lasting production of miHTT with no re-administration required. Due to the close proximity of the miHTT target site to the CAG repeat, it is expected that AMT-130 also targets the short HTTexon1 fragments which are highly toxic.

Controlled gene therapy using inducible systems

One potential issue with current gene therapies is the irreversible state as transgene expression cannot be stopped. Thus, if continued expression of a therapeutic gene causes unwanted effects, these side effects would most likely persist in the patient without the possibility to terminate the treatment or control the dose. For example, the expression of recombinant GDNF showed side effects associated with cerebellar Purkinje cell loss in non-human primate models.[203] In this case, inducible systems that could provide a more controlled expression of the transgene would be highly beneficial and would add considerably to the safety profile of the gene therapy.

Most classical inducible systems are based on two elements: the first is a chimeric transactivator protein capable of modulating gene expression in a drug-dependent (inducer) manner and the second is an inducible promoter which is often a minimal pol II promoter linked to sequences recognized by the chimeric transactivator protein.[204] These two elements can also be combined in a single expression system to express both transgene and the transactivator protein in a single plasmid or expression vector.[205] Additionally, two mechanisms of gene regulation can be distinguished, called On-switch and Off-switch. In the On-switch mechanism, the chimeric transactivator protein binds specifically to its DNA recognition sequence within the inducible promoter in the presence of the inducer, which in consequence activates gene expression. In the Off-switch mechanism, the chimeric protein-repressor is constantly bound to its recognition sequences and dissociates upon induction allowing transcription. An inducible gene

expression system should fulfil several requirements for safe and long-term gene therapy application, including low basal expression in absence of the inducer and a high induction ratio. Another important safety requirement is that the chimeric proteins used in inducible systems, in active or inactive form, do not interfere with endogenous gene expression, because chimeric proteins are formed from potent transcription factors that can lead to unspecific activation of endogenous promoters and thus interfere with cellular processes. The safety aspects should also be determined for all inducible system components within the context of immune system activation.

Regulated gene expression should ideally exhibit a wide dynamic range of induction with dose-response over a broad range of inducer concentrations, as opposed to acting merely as an on-off switch. For therapeutic applications, additional safety measures are required to minimize potential immune responses or other unwanted effects. For example, the regulatory proteins should be built from human proteins and should respond to an inducer that is safe, physiologically inert at the doses used, and with pharmacokinetics that permit a clinically tractable dosing regimen.

Several inducible gene expression systems have been developed including tetracycline, rapamycine, Isopropyl β-D-1-thiogalactopyranoside (IPTG), ecdysone and mifepristone dependent technologies.[206–208] In this paragraph the GeneSwitch and tetracycline-dependent (tet) system are discussed as they are currently the most widely used inducible systems.

GeneSwitch

GeneSwitch is one of the best characterized inducible systems for regulation of gene expression.[207,209] It exploits a chimeric transactivator GeneSwitch protein which consists of a DNA binding domain from the yeast Gal4 protein (Gal4 BD), a truncated ligand binding domain from human progesterone receptor (PR) and a p65 transcriptional activation domain of the human NF-kappa B transcription factor (p65) (Figure 6). The second component is the GeneSwitch inducible promoter, which consists of a minimal pol II promoter with upstream activation sequences (Gal4) that can be recognized by Gal4 BD of the GeneSwitch protein. This hybrid system can be activated by the antiprogestin mifepristone (MFP), a clinically approved synthetic steroid that binds to the PR domain of the GeneSwitch protein. MFP induces GeneSwitch conformational changes and dimerization, resulting in binding of the GeneSwitch dimer to the Gal4 sites placed upstream of a promoter to activate transcription of a transgene. In absence of mifepristone, the transgene will remain silent. The GeneSwitch system is highly attractive for clinical application as it does not contain any bacterial or viral components and is considered to be less immunogenic than most other inducible systems. The classical GeneSwitch system has been optimized to be delivered in a single vector, with low background levels and a high transgene expression after induction. Furthermore, GeneSwitch proved promising in combination with AAV-based gene therapy in preclinical studies for neurodegenerative

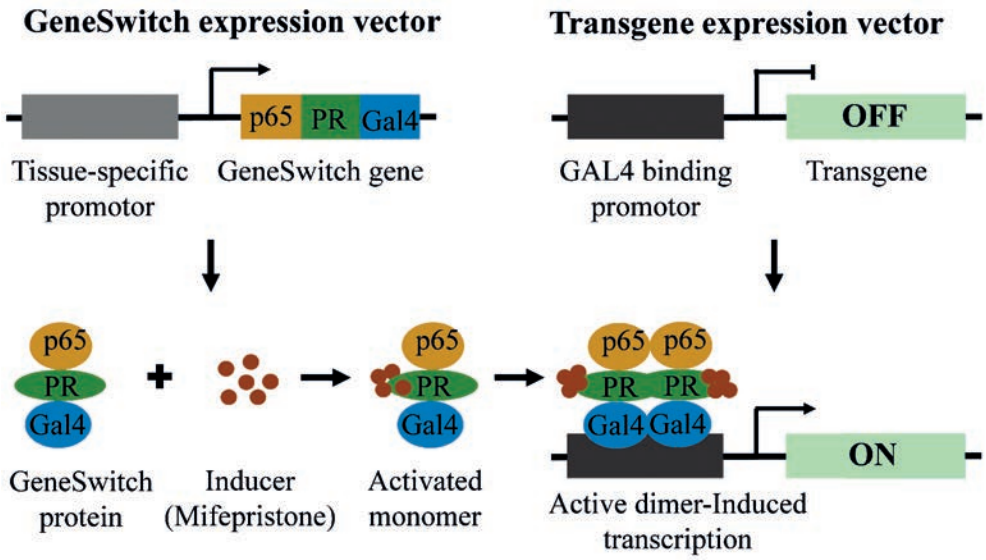

Figure 6. A schematic of the GeneSwitch system and its mechanism of action. The classical GeneSwitch system consists of two expression cassettes on two separate vectors; one containing the GeneSwitch gene and one containing the transgene. The expression of GeneSwitch is driven by a promoter, which can be tissue specific. Expression of the transgene is driven by a minimal pol II promoter with Gal4 binding sites. The GeneSwitch protein comprises yeast Gal4 DNA-binding domain, a human p65 activation domain and a Mifepristone (MFP) controlled domain derived from the human progesterone receptor. The GeneSwitch protein (monomer) can be activated by the steroid inducer MFP. And active dimer is formed that can attach to the Gal4-binding sites in the inducible promoter of the transgene. Hence only in the presence of MFP the transgene is transcribed.

diseases.[205] For example, GDNF expression was successfully induced up to three hundred-fold in rat brains and the expression was reversible with no background expression. It was also possible to re-activate GDNF expression after long-term off-status, and therapeutic benefits of induced GDNF was demonstrated in a PD rat model by restoring motor pathology.[205,210] The major advantage of the GeneSwitch system is that it lacks virally- or bacterially derived components thus limiting a potential immune reaction to GeneSwitch expression. Another advantage of the system is its inducer MFP, which is a marketed drug with well characterized pharmacokinetics and the induction occurs at sub-therapeutic MFP concentrations.[211] One concern is that expression of GeneSwitch for one month resulted in transcriptional changes in the murine liver.[209] Although these alterations were not associated with any biochemical or morphological changes, this aspect needs more attention.

(tet) system

Another inducible system is the tetracycline-dependent (tet) system which is currently the most widely used regulatable system.[212] There are two versions, namely a tetOFF and a tetON system. TetOFF is based on a fusion between the wild-type tet repressor and the activation domain of the HSV VP16 transcription factor.[213] In the tetON system, the tet repressor sequence has been replaced by a mutant which reverses the tet-repressor to a tet-inducer system.[214] Compared to tetOFF, tetON seems more suitable for further development to use in clinic as repeated punctual treatments using an inducible system is more favorable than a repressible system.[214] TetON consists of a transactivator-protein (rtTA) that can be activated by the antibiotic doxycycline and bind to a Tet promoter upstream of a transgene of interest. The TetON system was also successfully used in combination with AAV gene therapy in rodents and showed controlled expression of GDNF in brain of rats.[213] However, some major concerns are the side effects that may be caused by the inducer (an antibiotic) and the immunogenicity caused by the rtTA protein. Long-term exposure to antibiotics is undesirable and the rtTA protein of this system which is derived from bacteria showed to be highly immunogenic in non-human primates.[215,216] Therefore, the GeneSwitch system is currently preferable for further development into an applicable system in humans.

1

References

1. Porada, CD, Stem, C and Almeida-porada, G (2013). Gene therapy: the promise of a permanent cure. *N C Med J* 74: 526–529.
2. Saraiva, J, Nobre, RJ and Pereira de Almeida, L (2016). Gene therapy for the CNS using AAVs: The impact of systemic delivery by AAV9. *J. Control. Release* 241: 94–109.
3. Grimm, D and Kay, MA (2007). RNAi and gene therapy: a mutual attraction. *Hematology Am. Soc. Hematol. Educ. Program*doi:10.1182/asheducation-2007.1.473.
4. Dow, LE, Fisher, J, O'Rourke, KP, Muley, A, Kastenhuber, ER, Livshits, G, *et al.* (2015). Inducible in vivo genome editing with CRISPR-Cas9. *Nat. Biotechnol.* doi:10.1038/nbt.3155.
5. Nayerossadat, N, Ali, P and Maedeh, T (2012). Viral and nonviral delivery systems for gene delivery. *Adv. Biomed. Res.* doi:10.4103/2277-9175.98152.
6. Lundstrom, K (2018). Viral Vectors in Gene Therapy. *Dis. (Basel, Switzerland)* 6.
7. Finer, M and Glorioso, J (2017). A brief account of viral vectors and their promise for gene therapy. *Gene Ther.*doi:10.1038/gt.2016.71.
8. Naso, MF, Tomkowicz, B, Perry, WL and Strohl, WR (2017). Adeno-Associated Virus (AAV) as a Vector for Gene Therapy. *BioDrugs*doi:10.1007/s40259-017-0234-5.
9. Aschauer, DF, Kreuz, S and Rumpel, S (2013). Analysis of Transduction Efficiency, Tropism and Axonal Transport of AAV Serotypes 1, 2, 5, 6, 8 and 9 in the Mouse Brain. *PLoS One* 8.
10. Ojala, DS, Amara, DP and Schaffer, D V. (2015). Adeno-associated virus vectors and neurological gene therapy. *Neuroscientist* 21: 84–98.
11. Collaco, RF, Kalman-Maltese, V, Smith, AD, Dignam, JD and Trempe, JP (2003). A Biochemical Characterization of the Adeno-associated Virus Rep40 Helicase. *J. Biol. Chem.*doi:10.1074/jbc.M301537200.
12. Sonntag, F, Schmidt, K and Kleinschmidt, JA (2010). A viral assembly factor promotes AAV2 capsid formation in the nucleolus. *Proc. Natl. Acad. Sci.*doi:10.1073/pnas.1001673107.
13. Zincarelli, C, Soltys, S, Rengo, G and Rabinowitz, JE (2008). Analysis of AAV serotypes 1-9 mediated gene expression and tropism in mice after systemic injection. *Mol. Ther.* 16: 1073–1080.
14. Deverman, BE, Pravdo, PL, Simpson, BP, Kumar, SR, Chan, KY, Banerjee, A, *et al.* (2016). Cre-dependent selection yields AAV variants for widespread gene transfer to the adult brain. *Nat. Biotechnol.* advance on: 1–7.
15. Hudry, E and Vandenberghe, LH (2019). Therapeutic AAV Gene Transfer to the Nervous System: A Clinical Reality. *Neuron*doi:10.1016/j.neuron.2019.02.017.
16. Gitler, AD, Dhillon, P and Shorter, J (2017). Neurodegenerative disease: models, mechanisms, and a new hope. *Dis. Model. Mech.*doi:10.1242/dmm.030205.
17. Bertram, L and Tanzi, RE (2005). The genetic epidemiology of neurodegenerative disease. *J. Clin. Invest.*doi:10.1172/JCI24761.
18. Brown, RC, Lockwood, AH and Sonawane, BR (2005). Neurodegenerative diseases: An overview of environmental risk factors. *Environ. Health Perspect.*doi:10.1289/ehp.7567.
19. Hussain, R, Zubair, H, Pursell, S and Shahab, M (2018). Neurodegenerative Diseases: Regenerative Mechanisms and Novel Therapeutic Approaches. *Brain Sci.* 8.
20. Blokhuis, AM, Groen, EJN, Koppers, M, van den Berg, LH and Pasterkamp, RJ (2013). Protein aggregation in amyotrophic lateral sclerosis. *Acta Neuropathol.* 125: 777–794.
21. Frost, B and Diamond, MI (2010). Prion-like mechanisms in neurodegenerative diseases. *Nat. Rev. Neurosci.*doi:10.1038/nrn2786.
22. Sweeney, P, Park, H, Baumann, M, Dunlop, J, Frydman, J, Kopito, R, *et al.* (2017). Protein misfolding in neurodegenerative diseases: Implications and strategies. *Transl. Neurodegener.*doi:10.1186/s40035-017-0077-5.

23. Schaefers, ATU and Teuchert-Noodt, G (2016). Developmental neuroplasticity and the origin of neurodegenerative diseases. *World J. Biol. Psychiatry* doi:10.3109/15622975.2013.797104.
24. Miller, DB and O'Callaghan, JP (2008). Do early-life insults contribute to the late-life development of Parkinson and Alzheimer diseases? *Metabolism.*doi:10.1016/j.metabol.2008.07.011.
25. Logroscino, G (2005). The role of early life environmental risk factors in Parkinson disease: What is the evidence? *Environ. Health Perspect.*doi:10.1289/ehp.7573.
26. Mortimer, JA and Borenstein, AR (2007). Early-life risk factors for Alzheimer's disease. *Res. Pract. Alzheimers. Dis.*
27. Geser, F, Lee, VMY and Trojanowski, JQ (2010). Amyotrophic lateral sclerosis and frontotemporal lobar degeneration: A spectrum of TDP-43 proteinopathies. *Neuropathology* 30: 103–112.
28. Oskarsson, B, Gendron, TF and Staff, NP (2018). Amyotrophic Lateral Sclerosis: An Update for 2018. *Mayo Clin. Proc.* doi:10.1016/j.mayocp.2018.04.007.
29. Ravits, JM and La Spada, AR (2009). Als motor phenotype heterogeneity, focality, and spread: Deconstructing motor neuron degenerationsymbol. *Neurology*doi:10.1212/WNL.0b013e3181b6bbbd.
30. Ferrari, R, Kapogiannis, D, Huey, ED and Momeni, P (2011). FTD and ALS: a tale of two diseases. *Curr. Alzheimer Res.* 8: 273–94.
31. Ingre Caroline, PMR, Fredrik Piehl, FK and Fang., F (2015). Risk factors for amyotrophic lateral sclerosis. *Clin. Epidemiol.*: 181–193.
32. Bennion Callister, J and Pickering-Brown, SM (2014). Pathogenesis/genetics of frontotemporal dementia and how it relates to ALS. *Exp. Neurol.*doi:10.1016/j.expneurol.2014.06.001.
33. Cruz, MP (2018). Edaravone (Radicava): A Novel Neuroprotective Agent for the Treatment of Amyotrophic Lateral Sclerosis. *P T*.
34. Umoh, ME, Fournier, C, Li, Y, Polak, M, Shaw, L, Landers, JE, *et al.* (2016). Comparative analysis of *C9orf72* and sporadic disease in an ALS clinic population. *Neurology*doi:10.1212/WNL.0000000000003067.
35. Liu, Y and Wang, J (2019). C9orf72-dependent lysosomal functions regulate epigenetic control of autophagy and lipid metabolism. *Autophagy*: 1–2 doi:10.1080/15548627.2019.1580106.
36. Kumar, V, Hasan, GM and Hassan, MI (2017). Unraveling the role of RNA mediated toxicity of *C9orf72* repeats in C9-FTD/ALS. *Front. Neurosci.*doi:10.3389/fnins.2017.00711.
37. Shi, Y, Lin, S, Staats, KA, Li, Y, Chang, W-HH, Hung, S-TT, *et al.* (2018). Haploinsufficiency leads to neurodegeneration in *C9orf72* ALS/FTD human induced motor neurons. *Nat. Med.* 24: 313–325.
38. Mahadevan, M, Tsilfidis, C, Sabourin, L, Shutler, G, Amemiya, C, Jansen, G, *et al.* (1992). Myotonic dystrophy mutation: An unstable CTG repeat in the 3' untranslated region of the gene. *Science (80-.).*doi:10.1126/science.1546325.
39. Taneja, KL, McCurrach, M, Schalling, M, Housman, D and Singer, RH (1995). Foci of trinucleotide repeat transcripts in nuclei of myotonic dystrophy cells and tissues. *J. Cell Biol.*doi:10.1083/jcb.128.6.995.
40. Mankodi, A, Logigian, E, Callahan, L, McClain, C, White, R, Henderson, D, *et al.* (2000). Myotonic dystrophy in transgenic mice expressing an expanded CUG repeat. *Science (80-.).*doi:10.1126/science.289.5485.1769.
41. Dansithong, W, Paul, S, Comai, L and Reddy, S (2005). MBNL1 is the primary determinant of focus formation and aberrant insulin receptor splicing in DM1. *J. Biol. Chem.*doi:10.1074/jbc.M410781200.
42. Mankodi, A, Takahashi, MP, Jiang, H, Beck, CL, Bowers, WJ, Moxley, RT, *et al.* (2002). Expanded CUG repeats trigger aberrant splicing of ClC-1 chloride channel pre-mRNA and hyperexcitability of skeletal muscle in myotonic dystrophy. *Mol. Cell*doi:10.1016/S1097-2765(02)00563-4.

43. Belzil, V V., Gendron, TF and Petrucelli, L (2013). RNA-mediated toxicity in neurodegenerative disease. *Mol. Cell. Neurosci.*doi:10.1016/j.mcn.2012.12.006.
44. Donnelly, CJ, Zhang, PW, Pham, JT, Heusler, AR, Mistry, NA, Vidensky, S, *et al.* (2013). RNA Toxicity from the ALS/FTD *C9orf72* Expansion Is Mitigated by Antisense Intervention. *Neuron* 80: 415–428.
45. Sareen, D, O'Rourke, JG, Meera, P, Muhammad, AKMG, Grant, S, Simpkinson, M, *et al.* (2013). Targeting RNA foci in iPSC-derived motor neurons from ALS patients with a *C9orf72* repeat expansion. *Sci. Transl. Med.*doi:10.1126/scitranslmed.3007529.
46. Stepto, A, Gallo, JM, Shaw, CE and Hirth, F (2014). Modelling *C9orf72* hexanucleotide repeat expansion in amyotrophic lateral sclerosis and frontotemporal dementia. *Acta Neuropathol.* 127: 377–389.
47. Peters, OM, Cabrera, GT, Tran, H, Gendron, TF, McKeon, JE, Metterville, J, *et al.* (2015). Human *C9orf72* Hexanucleotide Expansion Reproduces RNA Foci and Dipeptide Repeat Proteins but Not Neurodegeneration in BAC Transgenic Mice. *Neuron* 88: 902–909.
48. Zu, T, Gibbens, B, Doty, NS, Gomes-pereira, M, Huguet, A and Stone, MD (2011). Non-ATG– initiated translation directed by microsatellite expansions. *Proc. Natl. Acad. Sci.*doi:10.1073/pnas.1013343108/-/DCSupplemental.www.pnas.org/cgi/doi/10.1073/pnas.1013343108.
49. Zu, T, Liu, Y, Banez-Coronel, M, Reid, T, Pletnikova, O, Lewis, J, *et al.* (2013). RAN proteins and RNA foci from antisense transcripts in *C9orf72* ALS and frontotemporal dementia. *Proc. Natl. Acad. Sci.* 110: E4968–E4977.
50. Gitler, AD and Tsuiji, H (2016). There has been an awakening: Emerging mechanisms of *C9orf72* mutations in FTD/ALS. *Brain Res.*doi:10.1016/j.brainres.2016.04.004.
51. Zhang, YJ, Jansen-West, K, Xu, YF, Gendron, TF, Bieniek, KF, Lin, WL, *et al.* (2014). Aggregation-prone c9FTD/ALS poly(GA) RAN-translated proteins cause neurotoxicity by inducing ER stress. *Acta Neuropathol.* doi:10.1007/s00401-014-1336-5.
52. Mizielinska, S, Gronke, S, Niccoli, T, Ridler, CE, Clayton, EL, Devoy, A, *et al.* (2014). *C9orf72* repeat expansions cause neurodegeneration in Drosophila through arginine-rich proteins. *Science (80-.).* 345: 1192–1194.
53. Zhang, K, Donnelly, CJ, Haeusler, AR, Grima, JC, Machamer, JB, Steinwald, P, *et al.* (2015). The *C9orf72* repeat expansion disrupts nucleocytoplasmic transport. *Nature* 525: 56–61.
54. Jovičič, A, Mertens, J, Boeynaems, S, Bogaert, E, Chai, N, Yamada, SB, *et al.* (2015). Modifiers of *C9orf72* dipeptide repeat toxicity connect nucleocytoplasmic transport defects to FTD/ALS. *Nat. Neurosci.* 19: 1226–1229.
55. Freibaum, BD, Lu, Y, Lopez-Gonzalez, R, Kim, NC, Almeida, S, Lee, K-HH, *et al.* (2015). GGGGCC repeat expansion in *C9orf72* compromises nucleocytoplasmic transport. *Nature* 525: 129–133.
56. Moujalled, D, Grubman, A, Acevedo, K, Yang, S, Ke, YD, Moujalled, DM, *et al.* (2017). TDP-43 mutations causing amyotrophic lateral sclerosis are associated with altered expression of RNA-binding protein hnRNP K and affect the Nrf2 antioxidant pathway. *Hum. Mol. Genet.* 26: 1732–1746.
57. Chen-Plotkin, AS, Lee, VMY and Trojanowski, JQ (2010). TAR DNA-binding protein 43 in neurodegenerative disease. *Nat. Rev. Neurol.*doi:10.1038/nrneurol.2010.18.
58. Warraich, ST, Yang, S, Nicholson, GA and Blair, IP (2010). TDP-43: A DNA and RNA binding protein with roles in neurodegenerative diseases. *Int. J. Biochem. Cell Biol.*doi:10.1016/j.biocel.2010.06.016.
59. Zhang, Y-J, Guo, L, Gonzales, PK, Gendron, TF, Wu, Y, Jansen-West, K, *et al.* (2019). Heterochromatin anomalies and double-stranded RNA accumulation underlie *C9orf72* poly(PR) toxicity. *Science (80-.).* 363: eaav2606.
60. Harms, MB, Cady, J, Zaidman, C, Cooper, P, Bali, T, Allred, P, *et al.* (2013). Lack of *C9orf72* coding mutations supports

a gain of function for repeat expansions in amyotrophic lateral sclerosis. *Neurobiol. Aging* 34.

61. Koppers, M, Blokhuis, AM, Westeneng, HJ, Terpstra, ML, Zundel, CAC, Vieira De Sá, R, *et al.* (2015). *C9orf72* ablation in mice does not cause motor neuron degeneration or motor deficits. *Ann. Neurol.* 78: 426–438.
62. Jiang, J, Zhu, Q, Gendron, TF, Saberi, S, McAlonis-Downes, M, Seelman, A, *et al.* (2016). Gain of Toxicity from ALS/FTD-Linked Repeat Expansions in *C9orf72* Is Alleviated by Antisense Oligonucleotides Targeting GGGGCC-Containing RNAs. *Neuron* 90: 535–550.
63. Rosenberg, RN (1992). Machado-Joseph disease: An autosomal dominant motor system degeneration. *Mov. Disord.* 7: 193–203.
64. Rüb, U, Brunt, ER and Deller, T (2008). New insights into the pathoanatomy of spinocerebellar ataxia type 3 (Machado-Joseph disease). *Curr. Opin. Neurol.* 21: 111–116.
65. Paulson, HL, Shakkottai, VG, Clark, HB and Orr, HT (2017). Polyglutamine spinocerebellar ataxias-from genes to potential treatments. *Nat. Rev. Neurosci.* doi:10.1038/nrn.2017.92.
66. Evers, MM, Toonen, LJA and Van Roon-Mom, WMC (2014). Ataxin-3 protein and RNA toxicity in spinocerebellar ataxia type 3: Current insights and emerging therapeutic strategies. *Mol. Neurobiol.* 49: 1513–1531.
67. Kawaguchi, Y, Okamoto, T, Taniwaki, M, Aizawa, M, Inoue, M, Katayama, S, *et al.* (1994). CAG expansions in a novel gene for Machado-Joseph disease at chromosome 14q32.1. *Nat. Genet.* 8: 221–228.
68. Kieling, C, Prestes, PR, Saraiva-Pereira, ML and Jardim, LB (2007). Survival estimates for patients with Machado-Joseph disease (SCA3). *Clin. Genet.* doi:10.1111/j.1399-0004.2007.00910.x.
69. Paulson, HL, Perez, MK, Trottier, Y, Trojanowski, JQ, Subramony, SH, Das, SS, *et al.* (1997). Intranuclear inclusions of expanded polyglutamine protein in spinocerebellar ataxia type 3. *Neuron* 19: 333–344.
70. Macedo-Ribeiro, S, Cortes, L, Maciel, P and Carvalho, AL (2009). Nucleocytoplasmic shuttling activity of ataxin-3. *PLoS One* 4.
71. Burnett, B, Li, F and Pittman, RN (2003). The polyglutamine neurodegenerative protein ataxin-3 binds polyubiquitylated proteins and has ubiquitin protease activity. *Hum. Mol. Genet.*doi:10.1093/hmg/ddg344.
72. Todi, S V., Winborn, BJ, Scaglione, KM, Blount, JR, Travis, SM and Paulson, HL (2009). Ubiquitination directly enhances activity of the deubiquitinating enzyme ataxin-3. *EMBO J.*doi:10.1038/emboj.2008.289.
73. Wang, H, Ying, Z and Wang, G (2012). Ataxin-3 regulates aggresome formation of copper-zinc superoxide dismutase (SOD1) by editing K63-linked polyubiquitin chains. *J. Biol. Chem.*doi:10.1074/jbc.M111.299990.
74. Chatterjee, A, Saha, S, Chakraborty, A, Silva-Fernandes, A, Mandal, SM, Neves-Carvalho, A, *et al.* (2015). The Role of the Mammalian DNA End-processing Enzyme Polynucleotide Kinase 3'-Phosphatase in Spinocerebellar Ataxia Type 3 Pathogenesis. *PLoS Genet.* doi:10.1371/journal.pgen.1004749.
75. Gao, R, Liu, Y, Silva-Fernandes, A, Fang, X, Paulucci-Holthauzen, A, Chatterjee, A, *et al.* (2015). Inactivation of PNKP by Mutant *ATXN3* Triggers Apoptosis by Activating the DNA Damage-Response Pathway in SCA3. *PLoS Genet.*doi:10.1371/journal.pgen.1004834.
76. Minoia, M, Pfeiffer, A, Acs, K, Wiegant, WW, Luijsterburg, MS, van Attikum, H, *et al.* (2017). Ataxin-3 consolidates the MDC1-dependent DNA double-strand break response by counteracting the SUMO-targeted ubiquitin ligase RNF4. *EMBO J.*doi:10.15252/embj.201695151.
77. Ashkenazi, A, Bento, CF, Ricketts, T, Vicinanza, M, Siddiqi, F, Pavel, M, *et al.* (2017). Polyglutamine tracts regulate beclin 1-dependent autophagy. *Nature*doi:10.1038/nature22078.
78. Matos, C, Pereira de Almeida, L and Nóbrega, C (2018). Machado-Joseph

disease / Spinocerebellar ataxia type 3:lessons from disease pathogenesis and clues into therapy. *J. Neurochem.* doi:10.1111/jnc.14541.

79. Jana, NR and Nukina, N (2004). Misfolding promotes the ubiquitination of polyglutamine-expanded ataxin-3, the defective gene product in SCA3/MJD. *Neurotox. Res.*doi:10.1007/BF03033448.
80. Nalavade, R, Griesche, N, Ryan, DP, Hildebrand, S and Krauß, S (2013). Mechanisms of RNA-induced toxicity in CAG repeat disorders. *Cell Death Dis.* doi:10.1038/cddis.2013.276.
81. Wang, LC, Chen, KY, Pan, H, Wu, CC, Chen, PH, Liao, YT, *et al.* (2011). Muscleblind participates in RNA toxicity of expanded CAG and CUG repeats in Caenorhabditis elegans. *Cell. Mol. Life Sci.* 68: 1255–1267.
82. Joshi, CR, Labhasetwar, V and Ghorpade, A (2017). Destination Brain: the Past, Present, and Future of Therapeutic Gene Delivery. *J. Neuroimmune Pharmacol.* doi:10.1007/s11481-016-9724-3.
83. Chew, J, Gendron, TF, Prudencio, M, Sasaguri, H, Zhang, Y-JYJ, Castanedes-Casey, M, *et al.* (2015). *C9orf72* repeat expansions in mice cause TDP-43 pathology, neuronal loss, and behavioral deficits. *Science (80-.).* 348: 1151–1154.
84. O'Rourke, JG, Bogdanik, L, Muhammad, AKMG, Gendron, TF, Kim, KJ, Austin, A, *et al.* (2015). *C9orf72* BAC Transgenic Mice Display Typical Pathologic Features of ALS/FTD. *Neuron* 88: 892–901.
85. Liu, Y, Pattamatta, A, Zu, T, Reid, T, Bardhi, O, Borchelt, DR, *et al.* (2016). *C9orf72* BAC Mouse Model with Motor Deficits and Neurodegenerative Features of ALS/FTD. *Neuron* 90: 521–534.
86. Xu, Z, Poidevin, M, Li, X, Li, Y, Shu, L, Nelson, DL, *et al.* (2013). Expanded GGGGCC repeat RNA associated with amyotrophic lateral sclerosis and frontotemporal dementia causes neurodegeneration. *Proc. …* 110: pp 7778–7783.
87. Gould, VFC (2012). Mouse Models of Spinocerebellar Ataxia Type 3 (Machado-Joseph Disease). *Neurotherapeutics* doi:10.1007/s13311-012-0117-x.
88. Ikeda, H, Yamaguchi, M, Sugai, S, Aze, Y, Narumiya, S and Kakizuka, A (1996). Expanded polyglutamine in the machado-joseph disease protein induces cell death in vitro and in vivo. *Nat. Genet.*doi:10.1038/ng0696-196.
89. Jung, J, Xu, K, Lessing, D and Bonini, NM (2009). Preventing Ataxin-3 protein cleavage mitigates degeneration in a Drosophila model of SCA3. *Hum. Mol. Genet.*doi:10.1093/hmg/ddp456.
90. Yamamoto, Y, Hasegawa, H, Tanaka, K and Kakizuka, A (2001). Isolation of neuronal cells with high processing activity for the Machado-Joseph disease protein. *Cell Death Differ.* 8: 871–873.
91. Berke, SJS, Schmied, FAF, Brunt, ER, Ellerby, LM and Paulson, HL (2004). Caspase-mediated proteolysis of the polyglutamine disease protein ataxin-3. *J. Neurochem.* 89: 908–918.
92. Goti, D (2004). A Mutant Ataxin-3 Putative-Cleavage Fragment in Brains of Machado-Joseph Disease Patients and Transgenic Mice Is Cytotoxic above a Critical Concentration. *J. Neurosci.* doi:10.1523/jneurosci.2734-04.2004.
93. Colomer Gould, VF, Goti, D and Kiluk, J (2006). A neuroendocrine dysfunction, not testicular mutant ataxin-3 cleavage fragment or aggregate, causes cell death in testes of transgenic mice. *Cell Death Differ.* 13: 524–526.
94. Neueder, A, Landles, C, Ghosh, R, Howland, D, Myers, RH, Faull, RLM, *et al.* (2017). The pathogenic exon 1 HTT protein is produced by incomplete splicing in Huntington's disease patients. *Sci. Rep.* doi:10.1038/s41598-017-01510-z.
95. Cemal, CK (2002). YAC transgenic mice carrying pathological alleles of the MJD1 locus exhibit a mild and slowly progressive cerebellar deficit. *Hum. Mol. Genet.* doi:10.1093/hmg/11.9.1075.
96. Habig, K, Hubener, J, Schmidt, T, Riess, O, Boy, J, Wolburg, H, *et al.* (2007). Nuclear Localization of Ataxin-3 Is Required for the Manifestation of Symptoms in SCA3:

In Vivo Evidence. *J. Neurosci.*doi:10.1523/jneurosci.4540-06.2007.
97. Chou, AH, Yeh, TH, Ouyang, P, Chen, YL, Chen, SY and Wang, HL (2008). Polyglutamine-expanded ataxin-3 causes cerebellar dysfunction of SCA3 transgenic mice by inducing transcriptional dysregulation. *Neurobiol. Dis.*doi:10.1016/j.nbd.2008.03.011.
98. Boy, J, Schmidt, T, Wolburg, H, Mack, A, Nuber, S, Böttcher, M, *et al.* (2009). Reversibility of symptoms in a conditional mouse model of spinocerebellar ataxia type 3. *Hum. Mol. Genet.*doi:10.1093/hmg/ddp381.
99. Boy, J, Schmidt, T, Schumann, U, Grasshoff, U, Unser, S, Holzmann, C, *et al.* (2010). A transgenic mouse model of spinocerebellar ataxia type 3 resembling late disease onset and gender-specific instability of CAG repeats. *Neurobiol. Dis.* doi:10.1016/j.nbd.2009.08.002.
100. Silva-Fernandes, A, Costa, M do C, Duarte-Silva, S, Oliveira, P, Botelho, CM, Martins, L, *et al.* (2010). Motor uncoordination and neuropathology in a transgenic mouse model of Machado-Joseph disease lacking intranuclear inclusions and ataxin-3 cleavage products. *Neurobiol. Dis.* doi:10.1016/j.nbd.2010.05.021.
101. Nóbrega, C, Nascimento-Ferreira, I, Onofre, I, Albuquerque, D, Conceição, M, Déglon, N, *et al.* (2013). Overexpression of mutant ataxin-3 in mouse cerebellum induces ataxia and cerebellar neuropathology. *Cerebellum*doi:10.1007/s12311-012-0432-0.
102. Switonski, PM, Szlachcic, WJ, Krzyzosiak, WJ and Figiel, M (2015). A new humanized ataxin-3 knock-in mouse model combines the genetic features, pathogenesis of neurons and glia and late disease onset of SCA3/MJD. *Neurobiol. Dis.*doi:10.1016/j.nbd.2014.09.020.
103. Takahashi, K and Yamanaka, S (2006). Induction of Pluripotent Stem Cells from Mouse Embryonic and Adult Fibroblast Cultures by Defined Factors. *Cell*doi:10.1016/j.cell.2006.07.024.
104. Watson, LM, Wong, MMK, Vowles, J, Cowley, SA and Becker, EBE (2018). A Simplified Method for Generating Purkinje Cells from Human-Induced Pluripotent Stem Cells. *Cerebellum*doi:10.1007/s12311-017-0913-2.
105. Marton, RM and Paşca, SP (2016). Neural Differentiation in the Third Dimension: Generating a Human Midbrain. *Cell Stem Cell*doi:10.1016/j.stem.2016.07.017.
106. Pasca, AM, Sloan, SA, Clarke, LE, Tian, Y, Makinson, CD, Huber, N, *et al.* (2015). Functional cortical neurons and astrocytes from human pluripotent stem cells in 3D culture. *Nat. Methods*doi:10.1038/nmeth.3415.
107. Napoli, C (1990). Introduction of a Chimeric Chalcone Synthase Gene into Petunia Results in Reversible Co-Suppression of Homologous Genes in trans. *PLANT CELL ONLINE*doi:10.1105/tpc.2.4.279.
108. Fire, A, Xu, S, Montgomery, MK, Kostas, SA, Driver, SE and Mello, CC (1998). Potent and specific genetic interference by double-stranded RNA in caenorhabditis elegans. *Nature*doi:10.1038/35888.
109. Elbashir, SM, Harborth, J, Lendeckel, W, Yalcin, A, Weber, K and Tuschl, T (2001). Duplexes of 21-nucleotide RNAs mediate RNA interference in cultured mammalian cells. *Nature*doi:10.1038/35078107.
110. Ozcan, G, Ozpolat, B, Coleman, RL, Sood, AK and Medicine, R (2016). Preclinical and clinical development of siRNA-based therapeutics. *Adv Drug Deliv Rev.* doi:10.1016/j.addr.2015.01.007.Preclinical.
111. Baulcombe, DC (1996). RNA as a target and an initiator of post-transcriptional gene silencing in trangenic plants. *Plant Mol. Biol.*doi:10.1007/BF00039378.
112. Montgomery, MK and Fire, A (1998). Double-stranded RNA as a mediator in sequence-specific genetic silencing and co-suppression. *Trends Genet.*doi:10.1016/S0168-9525(98)01510-8.
113. Saito, T, Saetrom, P, Lee, RC, Zamore, PD, Tuschl, T, Sharp, P a, *et al.* (2015). RNAi: double-stranded RNA directs the ATP-dependent cleavage of mRNA at 21 to 23 nucleotide intervals. *Cell*doi:10.1016/S0092-8674(00)80620-0.
114. Aravin, AA, Hannon, GJ and Brennecke, J (2007). The Piwi-piRNA pathway provides

an adaptive defense in the transposon arms race. *Science (80-.).*doi:10.1126/science.1146484.

115. Kreth, S, Hübner, M and Hinske, LC (2018). MicroRNAs as clinical biomarkers and therapeutic tools in perioperative medicine. *Anesth. Analg.* 126: 670–681.
116. Yang, JS and Lai, EC (2011). Alternative miRNA Biogenesis Pathways and the Interpretation of Core miRNA Pathway Mutants. *Mol. Cell*doi:10.1016/j.molcel.2011.07.024.
117. Herrera-Carrillo, E and Berkhout, B (2017). Dicer-independent processing of small RNA duplexes: mechanistic insights and applications. *Nucleic Acids Res.* 45: 10369–10379.
118. Beg, MS, Brenner, AJ, Sachdev, J, Borad, M, Kang, YK, Stoudemire, J, *et al.* (2017). Phase I study of MRX34, a liposomal miR-34a mimic, administered twice weekly in patients with advanced solid tumors. *Invest. New Drugs*doi:10.1007/s10637-016-0407-y.
119. M.S., B, D.S., H, J.C., S, A.J., B, M.J., B, H.Y., L, *et al.* (2016). First-in-human trial of microRNA cancer therapy with MRX34, a liposomal miR-34 mimic: Phase Ia expansion in patients with advanced solid tumors. *J. Clin. Oncol.*
120. Gebert, LFR, Rebhan, MAE, Crivelli, SEM, Denzler, R, Stoffel, M and Hall, J (2014). Miravirsen (SPC3649) can inhibit the biogenesis of miR-122. *Nucleic Acids Res.*doi:10.1093/nar/gkt852.
121. Chang, J, Guo, J-T, Jiang, D, Guo, H, Taylor, JM and Block, TM (2008). Liver-specific microRNA miR-122 enhances the replication of hepatitis C virus in nonhepatic cells. *J. Virol.*doi:10.1128/JVI.02575-07.
122. Henke, JI, Goergen, D, Zheng, J, Song, Y, Schüttler, CG, Fehr, C, *et al.* (2008). microRNA-122 stimulates translation of hepatitis C virus RNA. *EMBO J.*doi:10.1038/emboj.2008.244.
123. Tiemann, K and Rossi, JJ (2009). RNAi-based therapeutics-current status, challenges and prospects. *EMBO Mol. Med.*doi:10.1002/emmm.200900023.
124. Patel, K, Kilfoil, G, Wyles, DL, Naggie, S, Lawitz, E, Bradley, S, *et al.* (2016). 258. Phase I/IIa Study of TT-034, a DNA-Directed RNA Interference (ddRNAi) Agent Delivered as a Single Administration for the Treatment of Subjects with Chronic Hepatitis C Virus (HCV). *Mol. Ther.* doi:10.1016/s1525-0016(16)33067-2.
125. Chakraborty, C, Sharma, AR, Sharma, G, Doss, CGP and Lee, S-S (2017). Therapeutic miRNA and siRNA: Moving from Bench to Clinic as Next Generation Medicine. *Mol. Ther. Nucleic Acids*doi:10.1016/j.omtn.2017.06.005.
126. DiGiusto, DL, Krishnan, A, Li, L, Li, H, Li, S, Rao, A, *et al.* (2010). RNA-based gene therapy for HIV with lentiviral vector-modified CD34 + cells in patients undergoing transplantation for AIDS-related lymphoma. *Sci. Transl. Med.* doi:10.1126/scitranslmed.3000931.
127. Miniarikova, J, Zanella, I, Huseinovic, A, van der Zon, T, Hanemaaijer, E, Martier, R, *et al.* (2016). Design, Characterization, and Lead Selection of Therapeutic miRNAs Targeting Huntingtin for Development of Gene Therapy for Huntington's Disease. *Mol. Ther. Nucleic Acids* 5: e297.
128. Evers, MM, Miniarikova, J, Juhas, S, Vallès, A, Bohuslavova, B, Juhasova, J, *et al.* (2018). AAV5-miHTT Gene Therapy Demonstrates Broad Distribution and Strong Human Mutant Huntingtin Lowering in a Huntington's Disease Minipig Model. *Mol. Ther.* 26: 2163–2177.
129. Xu, GX, Zhou, H, Zhou, S, Yu, Y, Wu, R and Xu, Z (2005). An RNAi strategy for treatment of amyotrophic lateral sclerosis caused by mutant Cu,Zn superoxide dismutase. *J. Neurochem.* doi:10.1111/j.1471-4159.2004.02860.x.
130. Liu, ZH, Li, SL, Liang, Z Bin, Zhao, Y, Zhang, YL, Yang, YQ, *et al.* (2013). Targeting β-secretase with RNAi in neural stem cells for Alzheimer's disease therapy. *Neural Regen. Res.* doi:10.3969/j.issn.1673-5374.2013.33.003.
131. Nóbrega, C, Nascimento-Ferreira, I, Onofre, I, Albuquerque, D, Hirai, H, Déglon, N, *et al.* (2013). Silencing Mutant Ataxin-3 Rescues Motor Deficits and

Neuropathology in Machado-Joseph Disease Transgenic Mice. *PLoS One* 8.

132. Do Carmo Costa, M, Luna-Cancalon, K, Fischer, S, Ashraf, NS, Ouyang, M, Dharia, RM, *et al.* (2013). Toward RNAi therapy for the polyglutamine disease Machado-Joseph disease. *Mol. Ther.* 21: 1898–1908.
133. Rinaldi, C and Wood, MJA (2018). Antisense oligonucleotides: The next frontier for treatment of neurological disorders. *Nat. Rev. Neurol.*doi:10.1038/nrneurol.2017.148.
134. Wu, H, Lima, WF, Zhang, H, Fan, A, Sun, H and Crooke, ST (2004). Determination of the Role of the Human RNase H1 in the Pharmacology of DNA-like Antisense Drugs. *J. Biol. Chem.* doi:10.1074/jbc.M311683200.
135. Lima, WF, De Hoyos, CL, Liang, XH and Crooke, ST (2016). RNA cleavage products generated by antisense oligonucleotides and siRNAs are processed by the RNA surveillance machinery. *Nucleic Acids Res.* doi:10.1093/nar/gkw065.
136. Havens, MA and Hastings, ML (2016). Splice-switching antisense oligonucleotides as therapeutic drugs. *Nucleic Acids Res.* doi:10.1093/nar/gkw533.
137. Miller, TM, Pestronk, A, David, W, Rothstein, J, Simpson, E, Appel, SH, *et al.* (2013). An antisense oligonucleotide against SOD1 delivered intrathecally for patients with SOD1 familial amyotrophic lateral sclerosis: A phase 1, randomised, first-in-man study. *Lancet Neurol.* doi:10.1016/S1474-4422(13)70061-9.
138. Miller, T, Pestronk, A, David, W, Rothstein, J, Simpson, E, Appel, SH, *et al.* (2013). A Phase I, Randomised, First-in-Human Study of an Antisense Oligonucleotide Directed Against SOD1 Delivered Intrathecally in SOD1-Familial ALS Patients. *Lancet Neurol*doi:10.1016/S1474-4422(13)70061-9.
139. Echevarría, L, Aupy, P and Goyenvalle, A (2018). Exon-skipping advances for Duchenne muscular dystrophy. *Hum. Mol. Genet.* 27: R163–R172.
140. Evers, MM, Toonen, LJA and van Roon-Mom, WMC (2015). Antisense oligonucleotides in therapy for neurodegenerative disorders. *Adv. Drug Deliv. Rev.*doi:10.1016/j.addr.2015.03.008.
141. Juliano, RL (2016). The delivery of therapeutic oligonucleotides. *Nucleic Acids Res.*doi:10.1093/nar/gkw236.
142. Gupta, RM and Musunuru, K (2014). Expanding the genetic editing tool kit: ZFNs, TALENs, and CRISPR-Cas9. *J. Clin. Invest.*doi:10.1172/JCI72992.
143. Corrigan-Curay, J, O'Reilly, M, Kohn, DB, Cannon, PM, Bao, G, Bushman, FD, *et al.* (2015). Genome Editing Technologies: Defining a Path to Clinic. *Mol. Ther.* doi:10.1038/mt.2015.54.
144. (2018). First in vivo human genome editing trial. *Nat. Biotechnol.*doi:10.1038/nbt0118-5b.
145. Cong, L and Zhang, F (2014). Genome engineering using crispr-cas9 system. *Chromosom. Mutagen. Second Ed.*doi:10.1007/978-1-4939-1862-1_10.
146. Gyorgy, B., Ingelsson, M., Loov, C., Takeda, S., Lannfelt, L., Hyman, B.T., et al. (2016). CRISPR-Cas9 mediated gene editing in a monogenic form of Alzheimer's disease. *Mol Ther* 24: S226–S227.
147. Pribadi, M, Yang, Z, Kim, TS, Swartz, EW, Huang, AY, Chen, JA, *et al.* (2016). CRISPR-Cas9 targeted deletion of the *C9orf72* repeat expansion mutation corrects cellular phenotypes in patient-derived iPS cells. *BioRxiv*.
148. Yang, S, Chang, R, Yang, H, Zhao, T, Hong, Y, Kong, HE, *et al.* (2017). CRISPR/Cas9-mediated gene editing ameliorates neurotoxicity in mouse model of Huntington's disease. *J. Clin. Invest.* doi:10.1172/JCI92087.
149. Ouyang, S, Xie, Y, Xiong, Z, Yang, Y, Xian, Y, Ou, Z, *et al.* (2018). CRISPR/Cas9-Targeted Deletion of Polyglutamine in Spinocerebellar Ataxia Type 3-Derived Induced Pluripotent Stem Cells. *Stem Cells Dev.*doi:10.1089/scd.2017.0209.
150. Morgens, DW, Wainberg, M, Boyle, EA, Ursu, O, Araya, CL, Kimberly Tsui, C, *et al.* (2017). Genome-scale measurement of off-target activity using Cas9 toxicity in

high-throughput screens. *Nat. Commun.* doi:10.1038/ncomms15178.
151. Zhang, XH, Tee, LY, Wang, XG, Huang, QS and Yang, SH (2015). Off-target effects in CRISPR/Cas9-mediated genome engineering. *Mol. Ther. - Nucleic Acids*doi:10.1038/mtna.2015.37.
152. Salegio, EA, Samaranch, L, Kells, AP, Forsayeth, J and Bankiewicz, K (2012). Guided delivery of adeno-associated viral vectors into the primate brain. *Adv. Drug Deliv. Rev.*doi:10.1016/j.addr.2011.10.005.
153. Richardson, RM, Kells, AP, Martin, AJ, Larson, PS, Starr, PA, Piferi, PG, *et al.* (2011). Novel platform for MRI-guided convection-enhanced delivery of therapeutics: Preclinical validation in nonhuman primate brain. *Stereotact. Funct. Neurosurg.* doi:10.1159/000323544.
154. Bankiewicz, KS, Eberling, JL, Kohutnicka, M, Jagust, W, Pivirotto, P, Bringas, J, *et al.* (2000). Convection-enhanced delivery of AAV vector in Parkinsonian monkeys; in vivo detection of gene expression and restoration of dopaminergic function using pro-drug approach. *Exp. Neurol.* doi:10.1006/exnr.2000.7408.
155. Warren Olanow, C, Bartus, RT, Baumann, TL, Factor, S, Boulis, N, Stacy, M, *et al.* (2015). Gene delivery of neurturin to putamen and substantia nigra in Parkinson disease: A double-blind, randomized, controlled trial. *Ann. Neurol.*doi:10.1002/ana.24436.
156. Sproule, D, Kissel, J, Burghes, A, Al-Zaidy, S, Kaspar, B, Alfano, L, *et al.* (2017). AVXS-101 phase 1 gene therapy clinical trial in SMA Type 1: end-of-Study event free survival and achievement of developmental milestones. *Neuromuscul. Disord.*doi:10.1016/j.nmd.2017.06.412.
157. Meyer, K, Ferraiuolo, L, Schmelzer, L, Braun, L, McGovern, V, Likhite, S, *et al.* (2015). Improving single injection CSF delivery of AAV9-mediated gene therapy for SMA: A dose-response study in mice and nonhuman primates. *Mol. Ther.* doi:10.1038/mt.2014.210.
158. Hocquemiller, MM, Giersch, L, Audrain, M, Parker, S and Cartier, N (2016). Adeno-Associated Virus-Based Gene Therapy for CNS Diseases. *Hum. Gene Ther.* 27: 478–496.
159. Hinderer, C, Bell, P, Katz, N, Vite, C, Louboutin, J-P, Bote, E, *et al.* (2017). Evaluation of intrathecal routes of administration for adeno-associated virus vectors in large animals. *Hum. Gene Ther.* doi:10.1089/hum.2017.026.
160. Mittermeyer, G, Christine, CW, Rosenbluth, KH, Baker, SL, Starr, P, Larson, P, *et al.* (2012). Long-term evaluation of a phase I study of AADC gene therapy for Parkinson's Disease. *Hum. Gene Ther.* doi:10.1089/hum.2011.220.
161. Dindot, S, Piccolo, P, Grove, N, Palmer, D and Brunetti-Pierri, N (2011). Intrathecal injection of helper-dependent adenoviral vectors results in long-term transgene expression in neuroependymal cells and neurons. *Hum. Gene Ther.*doi:10.1089/hum.2010.147 [doi].
162. Bankiewicz, KS, Forsayeth, J, Eberling, JL, Sanchez-Pernaute, R, Pivirotto, P, Bringas, J, *et al.* (2006). Long-Term Clinical Improvement in MPTP-Lesioned Primates after Gene Therapy with AAV-hAADC. *Mol. Ther.*doi:10.1016/j.ymthe.2006.05.005.
163. Christine, CW, Starr, PA, Larson, PS, Eberling, JL, Jagust, WJ, Hawkins, RA, *et al.* (2009). Safety and tolerability of putaminal AADC gene therapy for Parkinson disease. *Neurology* doi:10.1212/WNL.0b013e3181c29356.
164. Eberling, JL, Jagust, WJ, Christine, CW, Starr, P, Larson, P, Bankiewicz, KS, *et al.* (2008). Results from a phase I safety trial of hAADC gene therapy for Parkinson disease. *Neurology*doi:10.1212/01.wnl.0000312381.29287.ff.
165. Piguet, F, Alves, S and Cartier, N (2017). Clinical Gene Therapy for Neurodegenerative Diseases: Past, Present, and Future. *Hum. Gene Ther.*doi:10.1089/hum.2017.160.
166. Palfi, S, Gurruchaga, JM, Scott Ralph, G, Lepetit, H, Lavisse, S, Buttery, PC, *et al.* (2014). Long-term safety and tolerability of ProSavin, a lentiviral vector-based gene therapy for Parkinson's disease: A dose

escalation, open-label, phase 1/2 trial. *Lancet* doi:10.1016/S0140-6736(13)61939-X.

167. Romina A. Badin, 1 Katie M. Binley, 2 Nadja VanCamp, Caroline Jan, Jeanne Gourlay, Hannah Stewart, Scott Ralph, Yatish Lad, Koichi Hosomi, Stephane Palfi, Phillippe Hantraye, KM. 395. OXB-102: An Enhanced Gene Therapy for Parkinson's Disease. *DOI: https://doi.org/10.1016/S1525-0016(16)35408-9*.
168. Hefti, F (2018). Nerve growth factor promotes survival of septal cholinergic neurons after fimbrial transections. *J. Neurosci.* doi:10.1523/jneurosci.06-08-02155.1986.
169. Kromer, LF (1987). Nerve growth factor treatment after brain injury prevents neuronal death. *Science (80-.).* doi:10.1126/science.3798108.
170. Rosenberg, JB, Kaplitt, MG, De, BP, Chen, A, Flagiello, T, Salami, C, *et al.* (2018). AAVrh.10-Mediated APOE2 Central Nervous System Gene Therapy for APOE4-Associated Alzheimer's Disease. *Hum. Gene Ther. Clin. Dev.* doi:10.1089/humc.2017.231.
171. Mole, SE and Cotman, SL (2015). Genetics of the neuronal ceroid lipofuscinoses (Batten disease). *Biochim. Biophys. Acta - Mol. Basis Dis.* doi:10.1016/j.bbadis.2015.05.011.
172. Platt, FM (2018). Emptying the stores: Lysosomal diseases and therapeutic strategies. *Nat. Rev. Drug Discov.* doi:10.1038/nrd.2017.214.
173. Vincent, F, Adamsbaum, C, Hocquemiller, M, Crystal, RG, Zérah, M, Fraldi, A, *et al.* (2014). Intracerebral Administration of Adeno-Associated Viral Vector Serotype rh.10 Carrying Human SGSH and SUMF1 cDNAs in Children with Mucopolysaccharidosis Type IIIA Disease: Results of a Phase I/II Trial . *Hum. Gene Ther.* doi:10.1089/hum.2013.238.
174. Ellinwood, NM, Ausseil, J, Desmaris, N, Bigou, S, Liu, S, Jens, JK, *et al.* (2011). Safe, efficient, and reproducible gene therapy of the brain in the dog models of sanfilippo and hurler syndromes. *Mol. Ther.* doi:10.1038/mt.2010.265.
175. Fu, H, Dirosario, J, Killedar, S, Zaraspe, K and McCarty, DM (2011). Correction of neurological disease of mucopolysaccharidosis IIIB in adult mice by rAAV9 trans-blood-brain barrier gene delivery. *Mol. Ther.* doi:10.1038/mt.2011.34.
176. Corti, M, Cleaver, B, Clément, N, Conlon, TJ, Faris, KJ, Wang, G, *et al.* (2015). Evaluation of Readministration of a Recombinant Adeno-Associated Virus Vector Expressing Acid Alpha-Glucosidase in Pompe Disease: Preclinical to Clinical Planning. *Hum. Gene Ther. Clin. Dev.* doi:10.1089/humc.2015.068.
177. Puzzo, F, Colella, P, Biferi, MG, Bali, D, Paulk, NK, Vidal, P, *et al.* (2017). Rescue of Pompe disease in mice by AAV-mediated liver delivery of secretable acid α-glucosidase. *Sci. Transl. Med.* doi:10.1126/scitranslmed.aam6375.
178. Rawlins, MD, Wexler, NS, Wexler, AR, Tabrizi, SJ, Douglas, I, Evans, SJW, *et al.* (2016). The prevalence of huntington's disease. *Neuroepidemiology* doi: 10.1159/000443738.
179. Fisher, ER and Hayden, MR (2014). Multisource ascertainment of Huntington disease in Canada: Prevalence and population at risk. *Mov. Disord.* doi:10.1002/mds.25717.
180. Miniarikova, J, Evers, MM and Konstantinova, P (2018). Translation of MicroRNA-Based Huntingtin-Lowering Therapies from Preclinical Studies to the Clinic. *Mol. Ther.* 26: 947–962.
181. Bates, GP, Dorsey, R, Gusella, JF, Hayden, MR, Kay, C, Leavitt, BR, *et al.* (2015). Huntington disease. *Nat. Rev. Dis. Prim.* 1: 15005.
182. Ross, CA and Tabrizi, SJ (2011). Huntington's disease: From molecular pathogenesis to clinical treatment. *Lancet Neurol.* doi:10.1016/S1474-4422(10)70245-3.
183. Tabrizi, SJ, Leavitt, BR, Landwehrmeyer, GB, Wild, EJ, Saft, C, Barker, RA, *et al.* (2019). Targeting Huntingtin Expression in Patients with Huntington's Disease. *N. Engl. J. Med.* doi:10.1056/NEJMoa1900907.
184. Marks, WJ, Ostrem, JL, Verhagen, L, Starr, PA, Larson, PS, Bakay, RA, *et al.* (2008).

Safety and tolerability of intraputaminal delivery of CERE-120 (adeno-associated virus serotype 2-neurturin) to patients with idiopathic Parkinson's disease: an open-label, phase I trial. *Lancet Neurol.* doi:10.1016/S1474-4422(08)70065-6.

185. Bartus, RT, Baumann, TL, Siffert, J, Herzog, CD, Alterman, R, Boulis, N, *et al.* (2013). Safety/feasibility of targeting the substantia nigra with AAV2-neurturin in Parkinson patients. *Neurology*doi:10.1212/WNL.0b013e3182904faa.
186. Airaksinen, MS and Saarma, M (2002). The GDNF family: Signalling, biological functions and therapeutic value. *Nat. Rev. Neurosci.*doi:10.1038/nrn812.
187. Bäckman, CM, Shan, L, Zhang, YJ, Hoffer, BJ, Leonard, S, Troncoso, JC, *et al.* (2006). Gene expression patterns for GDNF and its receptors in the human putamen affected by Parkinson's disease: A real-time PCR study. *Mol. Cell. Endocrinol.*doi:10.1016/j.mce.2006.03.013.
188. Björklund, A, Kirik, D, Rosenblad, C, Georgievska, B, Lundberg, C and Mandel, RJ (2000). Towards a neuroprotective gene therapy for Parkinson's disease: Use of adenovirus, AAV and lentivirus vectors for gene transfer of GDNF to the nigrostriatal system in the rat Parkinson model. *Brain Res.*doi:10.1016/S0006-8993(00)02915-2.
189. LeWitt, PA, Rezai, AR, Leehey, MA, Ojemann, SG, Flaherty, AW, Eskandar, EN, *et al.* (2011). AAV2-GAD gene therapy for advanced Parkinson's disease: A double-blind, sham-surgery controlled, randomised trial. *Lancet Neurol.* doi:10.1016/S1474-4422(11)70039-4.
190. Kaplitt, MG, Feigin, A, Tang, C, Fitzsimons, HL, Mattis, P, Lawlor, PA, *et al.* (2007). Safety and tolerability of gene therapy with an adeno-associated virus (AAV) borne GAD gene for Parkinson's disease: an open label, phase I trial. *Lancet* doi:10.1016/S0140-6736(07)60982-9.
191. Rafii, MS, Tuszynski, MH, Thomas, RG, Barba, D, Brewer, JB, Rissman, R a., *et al.* (2018). Adeno-Associated Viral Vector (Serotype 2)–Nerve Growth Factor for Patients With Alzheimer Disease. *JAMA Neurol.*doi:10.1001/jamaneurol.2018.0233.
192. Schulz, A, Kohlschütter, A, Mink, J, Simonati, A and Williams, R (2013). NCL diseases - clinical perspectives. *Biochim. Biophys. Acta - Mol. Basis Dis.* doi:10.1016/j.bbadis.2013.04.008.
193. Drack, A V., Mullins, RF, Pfeifer, WL, Augustine, EF, Stasheff, SF and Hong, SD (2015). Immunosuppressive Treatment for Retinal Degeneration in Juvenile Neuronal Ceroid Lipofuscinosis (Juvenile Batten Disease). *Ophthalmic Genet.* doi:10.3109/13816810.2014.886271.
194. Foust, KD, Schuberth, K, Odvody, J, Kielian, T, Bosch, ME, Fitzgerald, JA, *et al.* (2016). Self-Complementary AAV9 Gene Delivery Partially Corrects Pathology Associated with Juvenile Neuronal Ceroid Lipofuscinosis (CLN3). *J. Neurosci.* 36: 9669–9682.
195. Dyke, JP, Worgall, S, Crystal, RG, Neyzi, N, Sondhi, D, Greenwald, BM, *et al.* (2008). Treatment of Late Infantile Neuronal Ceroid Lipofuscinosis by CNS Administration of a Serotype 2 Adeno-Associated Virus Expressing CLN2 cDNA. *Hum. Gene Ther.* doi:10.1089/hum.2008.022.
196. Duque, SI, Arnold, WD, Odermatt, P, Li, X, Porensky, PN, Schmelzer, L, *et al.* (2015). A large animal model of spinal muscular atrophy and correction of phenotype. *Ann. Neurol.*doi:10.1002/ana.24332.
197. S., A-Z, R., S, W.D., A, L., R-K, T., P, L., L, *et al.* (2017). AVXS-101 phase 1 gene replacement therapy clinical trial in SMA type 1: Ventilation support free survival and achievement of developmental milestones. *Ann. Neurol.*
198. Han, S oh, Ronzitti, G, Arnson, B, Leborgne, C, Li, S, Mingozzi, F, *et al.* (2017). Low-Dose Liver-Targeted Gene Therapy for Pompe Disease Enhances Therapeutic Efficacy of ERT via Immune Tolerance Induction. *Mol. Ther. - Methods Clin. Dev.*doi:10.1016/j.omtm.2016.12.010.
199. Cleaver, BD, Byrne, BJ, Clément, N, Islam, S, Smith, BK, Collins, SW, *et al.* (2013). Phase I/II Trial of Adeno-Associated Virus–Mediated Alpha-Glucosidase Gene Therapy to the Diaphragm for Chronic

Respiratory Failure in Pompe Disease: Initial Safety and Ventilatory Outcomes. *Hum. Gene Ther.*doi:10.1089/hum.2012.250.

200. Leone, P, Shera, D, McPhee, SWJ, Francis, JS, Kolodny, EH, Bilaniuk, LT, *et al.* (2012). Long-term follow-up after gene therapy for canavan disease. *Sci. Transl. Med.* doi:10.1126/scitranslmed.3003454.
201. Harmatz, P, Muenzer, J, Burton, BK, Ficicioglu, C, Lau, HA, Leslie, ND, *et al.* (2018). Update on phase 1/2 clinical trials for MPS I and MPS II using ZFN-mediated in vivo genome editing. *Mol. Genet. Metab.* doi:10.1016/j.ymgme.2017.12.143.
202. Laoharawee, K, DeKelver, RC, Podetz-Pedersen, KM, Rohde, M, Sproul, S, Nguyen, HO, *et al.* (2018). Dose-Dependent Prevention of Metabolic and Neurologic Disease in Murine MPS II by ZFN-Mediated In Vivo Genome Editing. *Mol. Ther.* doi:10.1016/j.ymthe.2018.03.002.
203. Luz, M, Mohr, E and Fibiger, HC (2016). GDNF-induced cerebellar toxicity: A brief review. *Neurotoxicology*doi:10.1016/j.neuro.2015.10.011.
204. Akmammedov, A, Geigges, M and Paro, R (2017). Single vector non-leaky gene expression system for Drosophila melanogaster. *Sci. Rep.* doi:10.1038/s41598-017-07282-w.
205. Cheng, S, Tereshchenko, J, Zimmer, V, Vachey, G, Pythoud, C, Rey, M, *et al.* (2018). Therapeutic efficacy of regulable GDNF expression for Huntington's and Parkinson's disease by a high-induction, background-free "GeneSwitch" vector. *Exp. Neurol.* 309: 79–90.
206. Harkins, RN, Szymanski, P, Petry, H, Brooks, A, Qian, HS, Schaefer, C, *et al.* (2008). Regulated expression of the interferon-beta gene in mice. *Gene Ther.* 15: 1–11.
207. Reboredo, M, Kramer, MG, Smerdou, C, Prieto, J and Rivas, JD Las (2008). Transcriptomic Effects of Tet-On and Mifepristone-Inducible Systems in Mouse Liver. *Hum. Gene Ther.*doi:10.1089/hum.2008.057.
208. Xu, ZL, Mizuguchi, H, Mayumi, T and Hayakawa, T (2003). Regulated gene expression from adenovirus vectors: A systematic comparison of various inducible systems. *Gene* 309: 145–151.
209. Harkins, RN, Szymanski, P, Petry, H, Brooks, A, Qian, HS, Schaefer, C, *et al.* (2008). Regulated expression of the interferon-β gene in mice. *Gene Ther.* 15: 1–11.
210. Tereshchenko, J, Maddalena, A, Bähr, M and Kügler, S (2014). Pharmacologically controlled, discontinuous GDNF gene therapy restores motor function in a rat model of Parkinson's disease. *Neurobiol. Dis.* 65: 35–42.
211. Burcin, MM, Schiedner, G, Kochanek, S, Tsai, SY and O'Malley, BW (2002). Adenovirus-mediated regulable target gene expression in vivo. *Proc. Natl. Acad. Sci.*doi:10.1073/pnas.96.2.355.
212. T. Das, A, Tenenbaum, L and Berkhout, B (2016). Tet-On Systems For Doxycycline-inducible Gene Expression. *Curr. Gene Ther.*doi:10.2174/1566523216666160524144041.
213. Gossen, M and Bujard, H (2006). Tight control of gene expression in mammalian cells by tetracycline-responsive promoters. *Proc. Natl. Acad. Sci.*doi:10.1073/pnas.89.12.5547.
214. Chtarto, A, Humbert-Claude, M, Bockstael, O, Das, AT, Boutry, S, Breger, LS, *et al.* (2016). A regulatable AAV vector mediating GDNF biological effects at clinically-approved sub-antimicrobial doxycycline doses. *Mol. Ther. - Methods Clin. Dev.* 3: 16027.
215. Favre, D, Blouin, V, Provost, N, Spisek, R, Porrot, F, Bohl, D, *et al.* (2002). Lack of an immune response against the tetracycline-dependent transactivator correlates with long-term doxycycline-regulated transgene expression in nonhuman primates after intramuscular injection of recombinant adeno-associated virus. *J. Virol.*
216. Le Guiner, C, Stieger, K, Toromanoff, A, Guilbaud, M, Mendes-Madeira, A, Devaux, M, *et al.* (2014). Transgene regulation using the tetracycline-inducible TetR-KRAB system after AAV-mediated gene transfer in rodents and nonhuman primates. *PLoS One*doi:10.1371/journal.pone.0102538.

1

Scope of this thesis

During the past decades, several discoveries have highlighted the potential of AAV-based gene therapy for the treatment of inherited diseases. By means of gene replacement or RNAi, gene therapy has emerged as an attractive and clinically viable option to treat neurodegenerative diseases. In the current thesis we developed and characterized RNAi-based gene therapy for ALS and SCA3 aiming to silence two single genes that are the root cause of the diseases. These diseases have a very high unmet medical need with a progressive decline in the quality of life and no effective treatments available. Additionally, different delivery methods of AAV-based gene therapy were investigated for the CNS, as well as methods to regulate the transgene expression.

Chapter 1 introduces the concept of gene silencing using miRNAs and provides an overview of the pathogenesis of neurodegenerative diseases that are the subject of this thesis. The challenges for developing novel therapies for neurodegenerative diseases are discussed with an emphasis on ALS and SCA3. Chapter 2 describes the design of a novel miRNA-based gene silencing technology for ALS. miRNAs targeting different regions of *C9orf72* were designed and tested *in vitro* for silencing efficacy. For a long time, the functionality of miRNAs was thought to be restricted to the cytoplasm but some diseases, including *C9orf72*-related ALS require intranuclear silencing of the pathogenic repeat-containing transcripts. We demonstrated that nuclear silencing is possible with our miRNAs. We also report on feasibility of different targeting strategies to silence the sense- and/or antisense transcripts. Targeting exons within the *C9orf72* gene resulted in lowering of the healthy and mutated sense transcript, but not the antisense transcripts. Targeting both sense and antisense transcript can be achieved by expressing two miRNAs in a concatenated fashion in a single expression vector. An approach to target only the mutated transcripts is also possible by developing miRNAs close to the repeat region, but targeting the repeat region directly was not successful as this region consisted solely from GC nucleotides and has a highly complicated tertiary structure. In chapter 3, the therapeutic potential of *C9orf72*-targeting miRNAs was tested on patient-derived iPSC-neurons and in an *C9orf72* ALS mouse model. We confirmed the presence and activity of the therapeutic miRNAs in the nucleus of cells and showed reduction of the repeat-containing transcripts as well as nuclear RNA foci formation in the brain of an ALS mouse model. In chapter 4, the miQURE technology was applied to further develop a miRNA gene therapy for SCA3. Several miRNAs were tested *in vitro*, and three lead candidates were incorporated into AAV5. The therapeutic potential of these constructs was tested in human iPSC-neurons and in an SCA3 knock-in mouse model using different routes of delivery. We demonstrated strong reduction of *ATXN3* mRNA in both model systems. Further support for this approach was provided by the finding that mutant ataxin-3 protein was reduced in the brain stem and cerebellum of treated mice. Targeting the affected brain regions is critical for AAV-based silencing technologies. In chapter 5 we studied the biodistribution of AAV5 in the rat brain using different delivery routes. We

found that each delivery route has its own merits and should be carefully investigated for each type of disease. In many cases it may be useful to be able to regulate the expression of therapeutic constructs in the brain following delivery. In chapter 6, a proof on concept study was performed to investigate the ability to regulate expression of a therapeutic transgene using the mifepristone regulated GeneSwitch system. Using a novel design that can fit both the GeneSwitch system and the transgene in a single vector, we showed that this system is safe and that it is possible to regulate expression of the transgene *in vitro* and *in vivo* using. In chapter 7, we discussed our main findings and compare our therapeutic strategies with others. We further discussed the future perspectives for gene therapies for neurodegenerative diseases. Overall, we provided evidence that our RNAi-technology has the potential to be further developed in effective therapies for a group of severe diseases with no medical cure and a high demand for novel treatments.

Chapter 2

Artificial MicroRNAs Targeting *C9orf72* Can Reduce Accumulation of Intra-nuclear Transcripts in ALS and FTD Patients

Raygene Martier[1,2], Jolanda M. Liefhebber, Jana Miniarikova[1,2], Tom van der Zon[1], Jolanda Snapper[1], Iris Kolder[3], Harald Petry[1], Sander J. van Deventer[1,2], Melvin M. Evers[1], Pavlina Konstantinova[1]

[1]Department of Research & Development, uniQure Biopharma B.V., Amsterdam, the Netherlands;
[2]Department of Gastroenterology and Hepatology, Leiden University Medical Center, Leiden, the Netherlands;
[3]BaseClear B.V., Sylviusweg 74, 2333 BE, Leiden, The Netherlands.

Mol. Ther. Nucleic. Acids. (2019); 14: 593-608

Abstract

The most common pathogenic mutation in amyotrophic lateral sclerosis (ALS) and frontotemporal dementia (FTD) is an intronic GGGGCC (G_4C_2) repeat in the chromosome 9 open reading frame 72 (*C9orf72*) gene. Cellular toxicity due to RNA foci and dipeptide repeat (DPR) proteins produced by the sense and antisense repeat-containing transcripts is thought to underlie the pathogenesis of both diseases.

RNA-seq data of *C9orf72*-ALS patients and controls were analyzed to better understand the sequence conservation of *C9orf72* in patients. MicroRNAs were developed in conserved regions to silence *C9orf72* (miC) and the feasibility of different silencing approaches was demonstrated in reporter overexpression systems. In addition, we demonstrated the feasibility of a bidirectional targeting approach by expressing two concatenated miC hairpins.

The efficacy of miC was confirmed by the reduction of endogenously expressed *C9orf72 mRNA* in both nucleus and cytoplasm and ~50% reduction of nuclear RNA foci in $(G_4C_2)_{44}$ expressing cells. Ultimately, two miC candidates were incorporated in adeno-associated viral vector serotype 5 (AAV5) and silencing of *C9orf72* was demonstrated in HEK293T cells and Induced pluripotent stem cell (iPSC)-derived neurons. These data support the feasibility of miRNA-based and AAV-delivered gene therapy that could alleviate the gain of toxicity seen in ALS and FTD patients.

Introduction

Amyotrophic lateral sclerosis (ALS) is a devastating neurodegenerative disease characterized by progressive degeneration of the upper and lower motor neurons leading to muscle atrophy and paralysis. There is no disease-modifying therapy for ALS and most patients die with respiratory failure within 3-5 years after the onset of symptoms.[1–3] An significant number of ALS patients also develop frontotemporal dementia (FTD), a presenile dementia caused by progressive degeneration of the frontal and temporal lobes.[3,4] The most common genetic cause of familial and sporadic ALS and FTD is an expanded GGGGCC (G_4C_2) repeat in the first intron of the chromosome 9 open reading frame 72 (*C9orf72*) gene.[2,5] The G_4C_2 repeat in patients can be several hundred of repeats long and is transcribed bidirectionally.[2,6] Generally, less than 30 repeats are considered nonpathogenic.[2,6,7]

The G_4C_2 repeat is found in approximately 40% of familial ALS cases and 9% of sporadic ALS.[8,9] The mechanisms underlying the involvement of *C9orf72* in neurodegeneration have been a debate for several years, with loss of function, gain of toxicity, or a combination of both being implicated.[10,11] A reduction of *C9orf72* transcripts is detected in a significant number of *C9orf72*-ALS (C9-ALS) patients, supporting loss of function.[9,12] However, complete elimination of *C9orf72* in mice causes immune system related pathology but no motor deficits. These conditions were rescued in mice hemizygous for *C9orf72* that express 50% of *C9orf72* mRNA.[13,14] In humans, a few loss-of-function mutations in *C9orf72* were identified and all seemed to be non-pathogenic, thus *C9orf72* reduction in humans is likely to be tolerable.[15] Most evidences suggest that *C9orf72*-related pathogenicity is a result of gain of toxicity by accumulation of sense and antisense RNA foci in the nucleus, and deposition of dipeptide repeat (DPR) proteins in the cytoplasm.[8,16–21] RNA foci can bind and sequester the function of RNA binding proteins leading to RNA-mediated toxicity.[20,22] DPR proteins are a linked to a variety of toxic effects.[10,20,22] Thus, lowering the accumulation of RNA foci and DPR proteins is an attractive therapeutic strategy in ALS and FTD.

Directly targeting the G_4C_2 repeat to exclusively silence the repeat containing transcripts is preferable, but challenging due to the high GC content, bidirectional transcription, intronic position and nuclear localization.[23] The repeat-containing transcripts are also poorly characterized and sequence variations downstream of the G_4C_2 repeat region suggest that the area close to the repeat may not be well conserved between patients.[24]

Fully complementary anti-GGGGCC or anti-CCCCGG single-stranded silencing RNAs (ss-siRNAs) reduced *C9orf72* sense and antisense foci.[25] Antisense oligonucleotides (ASOs) against *C9orf72* intron 1 near the G_4C_2 repeat also resulted in reduction of sense RNA foci and DPR proteins, while the overall *C9orf72* levels were not affected.[18,26,27] Interestingly, RNA foci and DPR proteins were also reduced by ASOs against exonic regions to target all *C9orf72* transcripts. Thus, both mutant specific or total *C9orf72* silencing approaches can lower RNA foci and DPR proteins.

Administration of synthetic siRNAs and ASOs are promising but require repeated administration. We and others have reported that siRNAs derived from short hairpin RNA (shRNA) or microRNA (miRNA) scaffolds delivered with adeno-associated viral (AAV) vectors have the advantage to provide long lasting therapeutic effects in different disease models of the central nervous system (CNS).[28–31] High concentrations of shRNAs can bypass the nuclear RNase III Drosha processing and overload the cytoplasm with double stranded RNA, leading to toxicity.[32] miRNAs are safer, as their precursors are encoded in the genome, thus mimicking the natural processing pathway. Moreover, the miRNA-expression cassette can be driven by polymerase (pol) II or pol III promoters allowing for tissue- or cell-specific expression.

We here report on the development of therapeutic miRNAs (miC) as proof of concept to silence *C9orf72* mRNA. We used a recently published RNA-seq library from C9-ALS patients to investigate *C9orf72* expression and sequence composition for identification of potential miC target sites in intron 1 and exonic regions.[33] miC constructs were designed to target the sense, antisense or both strands of *C9orf72*. The natural cellular primary (pri)-miR-101-1 and pri-miR-451 scaffold were selected to embed the miC sequences based on our previous findings that both scaffolds produced guide strands that were highly active.[31] Pri-miRNAs are produced by RNA pol I or RNA pol II transcription and fold into hairpin-like scaffold which determine their further processing by the microprocessor complex.[34] The tail of pri-miRNAs is cleaved by Drosha in the nucleus generating a precursor miRNA (pre-miRNA) that is subsequently exported to the cytoplasm for further processing into a mature miRNA.[35–37] The silencing efficacy of the miC-101 and miC-451 candidates were tested on luciferase (luc) reporters and confirmed with knockdown of the endogenously expressed *C9orf72* mRNA. The processing pattern was determined by next generation sequencing (NGS).

One major challenge for an effective RNAi approach is the nuclear localization of the repeat containing transcripts, as the mature miC is produced in the cytoplasm. Therefore, the expression and silencing efficacy of the miC candidates in both nucleus and cytoplasm was investigated, and we studied the ability of these constructs to silence nuclear RNA foci formation caused by G_4C_2 repeats. Finally, two candidates were selected and incorporated into AAV5 vector to test their efficacy *in vitro* on Human embryonic kidney (HEK)293T cells and in frontal brain-like neurons generated from Induced pluripotent stem cells (iPSCs) from an FTD patient. The expression of total *C9orf72 (all C9orf72 sense transcripts)* was significantly reduced in both cell lines. Hence, our data provide evidence on the efficacy of artificial miRNAs against *C9orf72* as a promising AAV-based gene therapy for ALS and FTD.

Results

Reduced *C9orf72* levels detected by RNA-seq in C9-ALS patients

The human *C9orf72* gene consists of 12 exons that can be transcribed in three different transcript variants (V1, V2, V3) (figure 1a). The G_4C_2 repeat in intron 1 is in the promoter region of V2 and the first intron of V1 and V3. We used a publically available RNA-seq library to determine the expression of *C9orf72* in cerebellar and cortical tissues of 8 C9-ALS patients and 7 healthy controls.[33] Notably, we found that *C9orf72* is higher expressed (~ 2-fold) in the cerebellum compared to cortex in both C9-ALS patients and controls (figure 1b). It was also found that *C9orf72* mRNA expression is consistently reduced in both cerebellum and cortex of C9-ALS patients. To determine if the reduction seen in C9-ALS patients is variant specific, we investigated the relative expression of V1, V2 and V3 in patients and controls (figure 1c). Expression of V1, V2 and V3 was determined in percentage, relative to total (100%) *C9orf72* expression. In both cerebellum and cortex, the proportion of the variants in patients and controls were similar, suggesting that the reduction of *C9orf72* mRNA levels in C9-ALS patients is not variant specific.

Intronic inclusions due to G_4C_2 repeat are detected in C9-ALS patients by RNA-seq

C9orf72 Intron 1 should be spliced out and degraded but defective splicing may result in accumulation of repeat containing transcripts in the cell nucleus.[38] These repeat-containing transcripts are poorly characterized and there is little information on the conservation of this region in C9-ALS patients. To address this question, read alignments from C9-ALS patients and controls were compared to investigate the sequence conservation of intronic and exonic regions of *C9orf72* transcripts (figure 1d). The read depth in exon 1a, exon 1b, intron 1, exon 2 and exon 11 was estimated by correcting the total number of reads by the area size. We found a complete coverage of exon 2 to exon 11, though read depth in exon 1a, exon 1b and intronic regions was very low in both C9-ALS and control groups. Exonic regions from exon 2 to exon 11 were less covered in patients while read depth for intron 1 in the patients was comparable with controls. To estimate the relative coverage of the exons and introns, the ratio between the number of reads in C9-ALS patients and controls was determined (figure 1e). All *C9orf72* exonic regions were about twofold lower expressed in C9-ALS patients. Intron 1 had the same number of reads in patient samples compared to controls, while intron 2-4 was 1.4 times higher in C9-ALS patients than controls. Introns 5, 6 and 7 were excluded as these could potentially be 3'UTR of the short *C9orf72* variant and coverage of intron 8, 9 and 10 was not increased in C9-ALS patients. Similarly, in the frontal cortex samples of C9-ALS patients the coverage ratio between intronic and exonic regions were increased (supplementary figure S1). Thus, although exonic regions were expressed twofold lower in C9-ALS patients, this was not the case for intron 1-4, suggesting that intronic *C9orf72* reads are relatively overexpressed

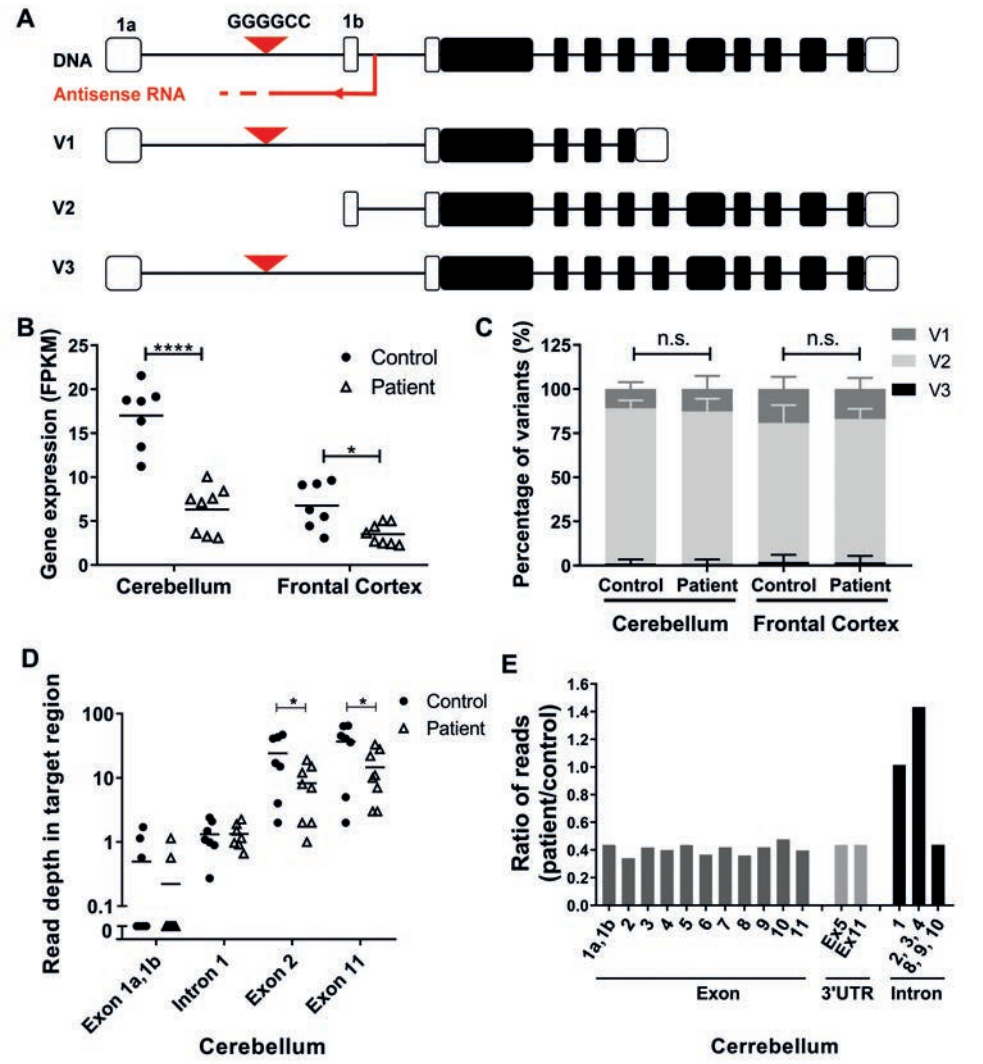

Figure 1. *C9orf72* expression and target regions. a) Schematic of *C9orf72* gene and transcript variants**.** The G_4C_2 repeat is in intron 1 of transcript variants V1 and V3 and in the promotor region of V2. b) *C9orf72* expression in C9-ALS patients and controls. *C9orf72* gene expression was determined from RNA-seq libraries in cerebellum and frontal cortex from 8 C9-ALS patients and 7 control donors. The mean expression values are shown in Fragments Per Kilobase of transcript per Million mapped reads (FPKM). c) Relative expression of predicted *C9orf72* variants. The mRNA variants in C9-ALS and controls were predicted from the mapped and aligned RNA-seq data. Isoform V1 is predicted from reads alignment from exon 1a to exon 5 (1950bp), isoform V2 from exon 1b to exon 11 (3243bp) and isoform V3 from exon 1a to exon 11 (3338bp). Expression of *C9orf72* isoforms is presented in percentage of the total (100%) *C9orf72* expression. T-tests were performed between groups and n.s. indicates no significant differences in the levels of all isoforms. d) Estimation of the read depth per region in *C9orf72*. Read depth was estimated for exon 1a, intron 1, exon 1b, exon 2 and exon 11 in cerebellum from C9-ALS patient and controls. The total amount of reads per region were counted and corrected for the area size. Each dot or triangle represents

a single sample e) Ratio of reads between C9-ALS patients and controls in cerebellum. The total amount of reads counted in different intronic and exonic regions from C9-ALS patients were divided by the total amount of reads from the same region of control donors. Data were evaluated using two-way ANOVA with Tukey's multiple comparison: *p < 0.05; **p < 0.01; ***p < 0.001; ****p < 0.0001.

in C9-ALS patients. Our data confirm previous findings that the higher amount of intronic sequences in the *C9orf72* mRNA could be due to aberrant splicing.[38,39]

Design of miRNAs targeting conserved *C9orf72* regions

We selected the well conserved exon 2 and exon 11 as target sites for a total silencing approach. Due to the poor coverage of intron 1, we selected regions that have been successfully targeted before by ASOs.[26] For the antisense strand, a region that has been identified before by PCR was selected.[40] We designed miC expression constructs miC1-miC11 and miC22-miC31 in intron 1 to target only the sense intronic transcripts (figure 2a). miC32-miC50 were designed in exon 2 and exon 11 to target all sense *C9orf72* transcripts. miC12*- miC22* were designed on the antisense strand to target only the antisense transcripts and are indicated with an asterisk (*). The miC sequences were embedded in the pri-miR-101 and pri-miR-451 scaffold because of previous findings by us that both scaffolds produce high amount of active guide strands.[31] The pri-miC-101 and pri-miC-451 structures were predicted to produce mature miC lengths of 21nt and 22nt respectively (figure 2b). The miC constructs were expressed by the synthetic CMV early enhancer and chicken β actin (CAG) promotor (figure 2c). This promoter is known to drive stable and high expression of a transgene and is highly active in the CNS.[41]

In vitro testing of miC-101 and miC-451 constructs on reporter systems

To test the efficacy of the miC candidates, we designed Luc reporters bearing complementary *C9orf72* target regions fused to the renilla luciferase (RL) gene (figure 2d). As targets, intron 1, exon 2, exon 11 and the antisense strand sequences were used. Independently from RL, firefly luciferase (FL) was expressed from the reporter vector to correct for transfection efficiency.

We first performed a prescreening for all the miC expression constructs by co-transfection with the corresponding Luc reporters in a 1:1 ratio. Of the miC variants designed to target the sense intronic transcripts, miC2_101 and miC4_101 showed a moderate knockdown (~50%) and miC31_101 showed a strong knockdown (~80%) (figure 3a). These were selected for further optimization. Amongst candidates predicted to target total *C9orf72*, miC32_101, miC33_101, miC38_451, miC39_451, miC40_451 and miC43_451 targeting exon 2 showed a strong knockdown of >80% (figure 3b). Similarly, miC46_101, miC49_451 and miC50_451 targeting exon 11 induced a strong knockdown (>80%) (figure 3c). Dilution of the selected miC candidates demonstrated that

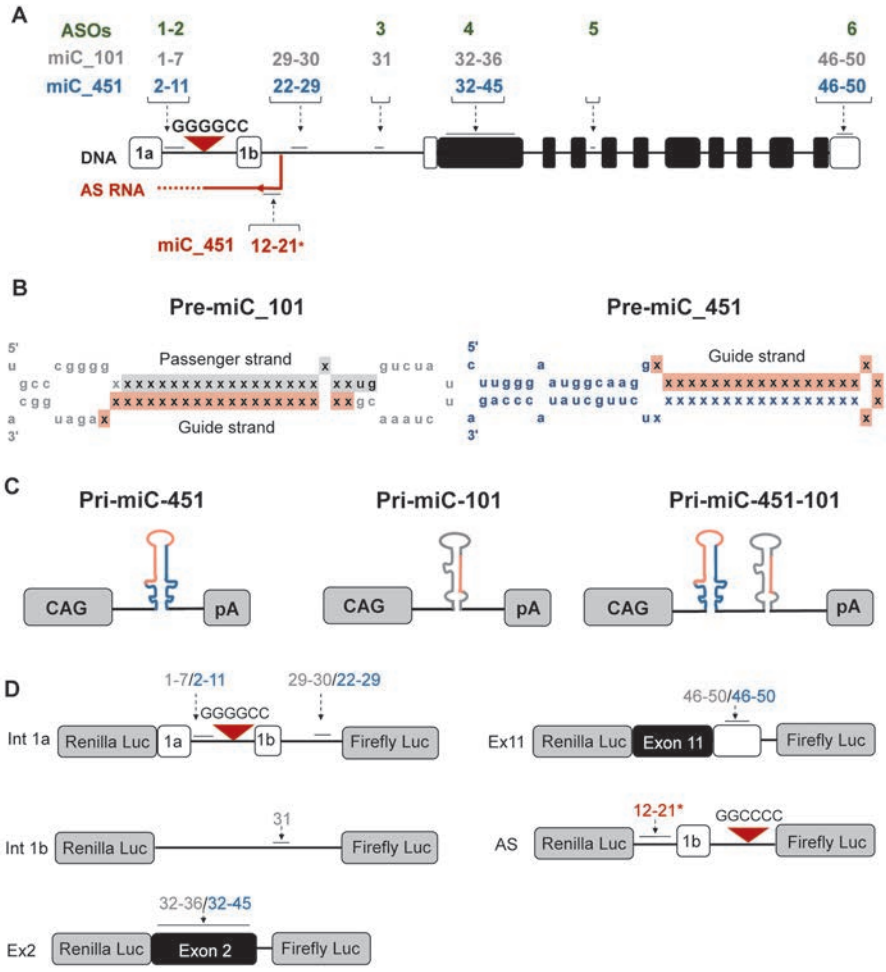

Figure 2. Design of artificial miC expression constructs targeting sense and antisense *C9orf72*. a) Schematic representation of the human *C9orf72* gene consisting show of 12 exons including the alternatively spliced exon 1a and 1b and the intronic G_4C_2 repeat. The positions of the miC target sites are indicated with numbers. Numbers in green shows position of ASO's described by Lagier-Tourenne et al.[18] In grey are the sense targeting miC candidates embedded in miR-101 scaffold, in blue are sense targeting miC candidates embedded in miR-451 scaffold, in red are antisense targeting miC candidates embedded in miR-451 scaffold. b) Schematic of the miC-101 and miC-451 secondary structures. The scaffolds were selected from miRBase database (www.mirbase.org). The guide strand was replaced by the mature miC sequence and the passenger strand was corrected in order to preserve pri-miC scaffolding. miR-101 can be processed into active guide strands (red) and in some cases passenger strands (grey). miR-451 produces only guide strands. c) Schematic of the pri-miC-451 and pri-miC-101 constructs consisting of the CAG promoter, pri-miC sequence and human growth hormone polyadenylation (hGH polyA) signal. d) Schematic of the reporter genes. To represent the *C9orf72* sense transcripts, sequences from *C9orf72* intron 1 (int 1a and int 1b), exon 2 (ex2) and exon 11 (ex11) were cloned downstream of the RL gene. In addition, FL was co-expressed from the vector as an internal control. For the antisense reporter (AS), the intronic antisense sequence was cloned.

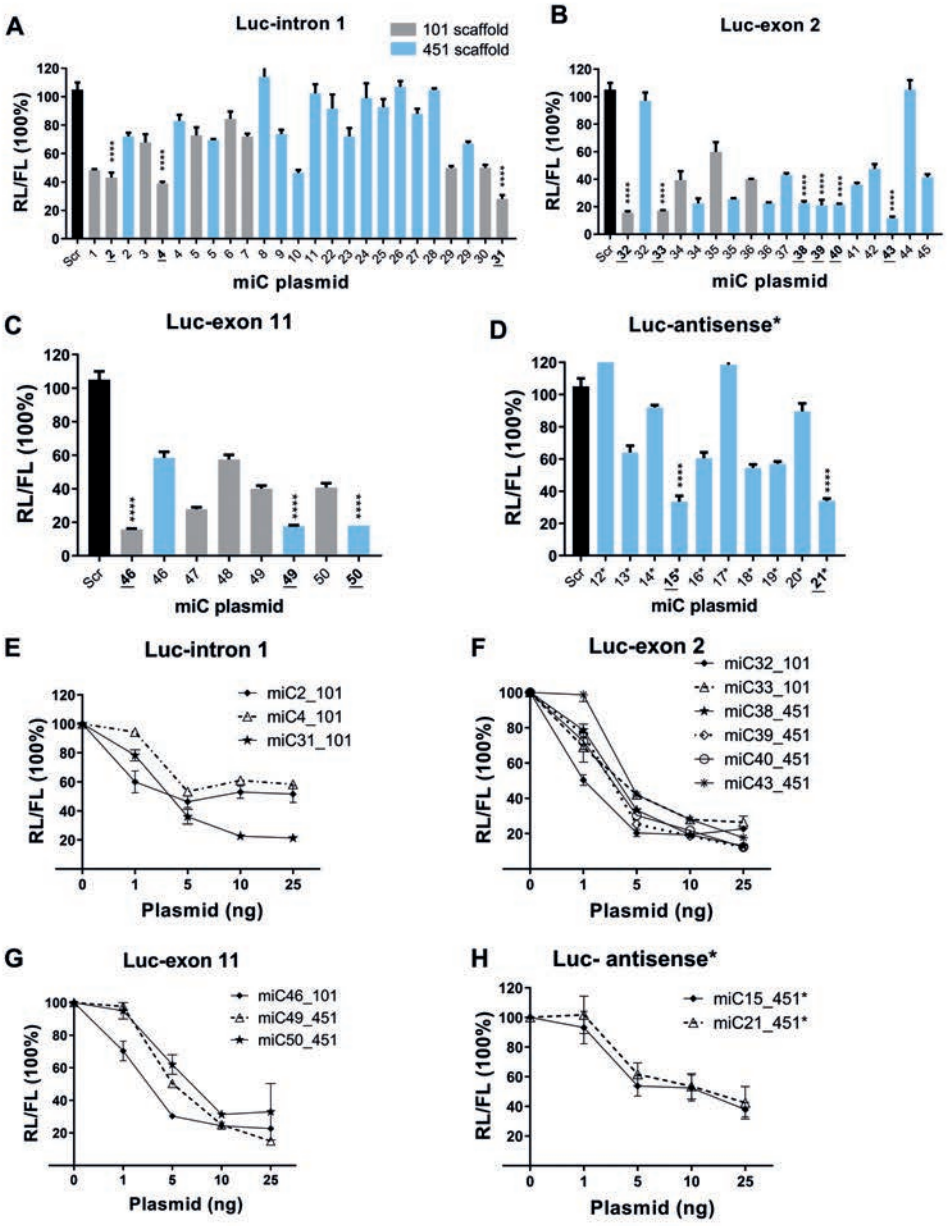

Figure 3. Silencing efficacy of miC candidates on luc reporters. a) knockdown by miC1 to miC11 and miC22 to miC31 targeting intron 1 either between exon 1a and the G_4C_2 repeat or between exon 1b and exon 2. HEK293T cells were co-transfected in a 1:1 ratio with luc reporters and the different miC variants embedded in miR-101 (grey bars) or miR-451 (blue bars) scaffold. RL and FL were measured 2 days post-transfection and RL was normalized to FL expression. Scrambled miRNA (miScr) served as a negative control and was set at 100%. Candidates selected for further testing are underlined. b-c) Knockdown of exon 2 reporter by miC32 to miC45 and exon 11 reporter by miC46 to miC50. d) knockdown of the antisense reporter by miC12_451* to miC21_451*. c). e-h)

Dose dependent effect of the selected miC candidates on luc reporters. HEK293T cells were co-transfected with 10ng of the Luc reporters and 1, 5, 10 and 25 ng of the selected miC constructs for intron 1 (e), exon 2 (f) and exon 11 (g) and the antisense transcript (f). RL and FL luciferases were measured as described above. Data were analyzed using a multiple comparison one-way ANOVA to determine statistically significances cells treated with scrambled and miC. The p values of miC candidates selected for further testing are listed in the graph by asterisks: ****p < 0.0001. Each bar represents the average and standard deviation of 3 independent experiments.

the most effective candidates were miC31_101 against intron 1 (figure 3e), miC32_101 against exon 2 (figure 3f) and miC46_101 against exon 11 (figure 3g).

For the antisense *C9orf72* transcript, miC15_451* and miC21_451* were selected as the most effective candidates with a knockdown efficiency of ~70% (figure 3d). Both miC15_451* and miC21_451* showed an equal dose dependent knockdown (figure 3h).

Our data demonstrate that intron 1 remains a difficult target region as all miC candidates in the highly structured repeat region between exon 1a and 1b failed to induce a strong knockdown. The most effective miC candidates were downstream of exon 1b or in exonic regions 2 and 11. Yet, if a moderate knockdown of the G_4C_2 repeat would be sufficient for a therapeutic effect, miC2_101 and miC4_101 could still be promising candidates to target the repeat containing transcripts in C9-ALS patients.

Bidirectional targeting of *C9orf72* is possible by introduction of a second miC concatenate

The region around the G_4C_2 repeat of *C9orf72* is transcribed in both sense and antisense transcripts and both strands have been linked to toxicity. Therefore, a therapy simultaneously targeting both strands could potentially add to therapeutic benefit. To investigate the feasibility for this approach using miRNAs we made concatenated constructs expressing two hairpins predicted to target both transcripts under control of the CAG-promotor (fig, 4a). The first hairpin from the concatenated hairpin miRNA construct was in a miR-451 scaffold and targets the antisense transcript. The second hairpin was in a miR-101 scaffold against the sense transcripts. The most effective candidates on luc reporters for intron 1 sense and antisense were selected. The miC15*+31 construct was designed to express miC15_451* and miC31_101 and was tested on the intron 1 and antisense reporters (figure 4b-c). A silencing of up to 60% was observed on the intron 1 sense and on the antisense reporter. Similarly, miC21*+31 expressing miC21_451* and miC31_101 was made and tested and up to 60% knockdown was observed on both reporter constructs (figure 4d-e). Both constructs showed a dose dependent reduction of the intron 1 sense and antisense reporters containing Luc. Our data demonstrates that two different miC can be properly processed and are active when expressed from a single promotor. Hence, a bidirectional miRNA-based approach to simultaneously target the sense and antisense transcripts of *C9orf72* is feasible, using two miC variants expressed in a concatenated fashion.

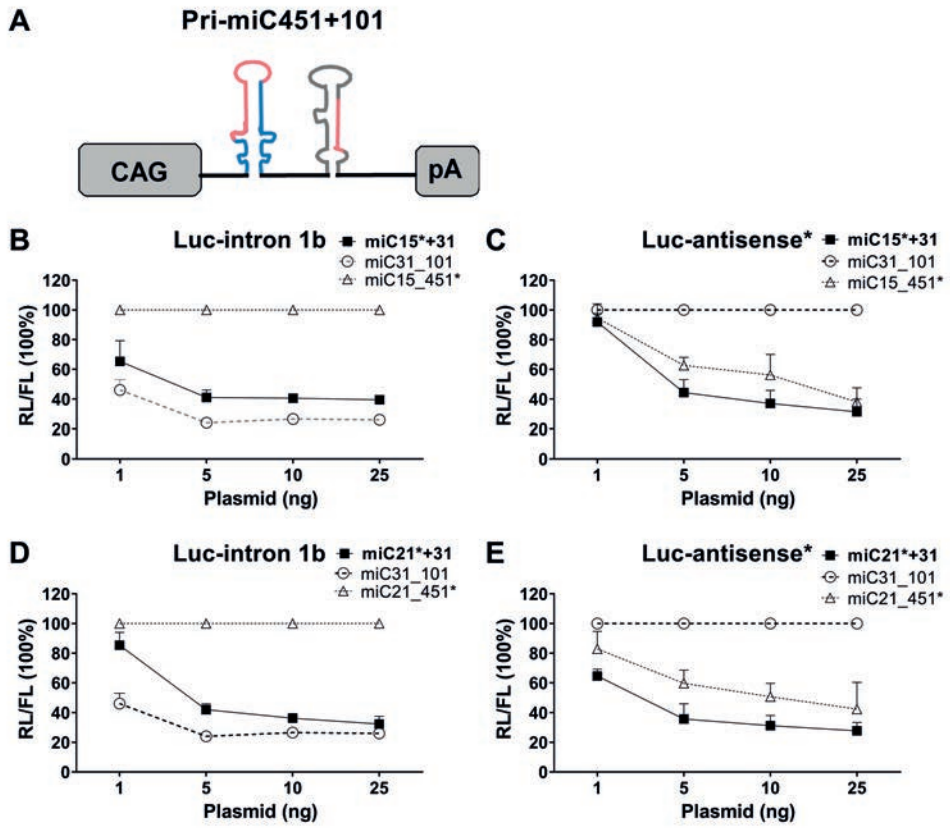

Figure 4. Efficacy of double hairpin constructs for bidirectional knockdown. a) Schematic of the concatenated pri-miC-451 and pri-miC-101 construct consisting of the CAG promoter, two pri-miC sequences in miR-451 and miR-101 scaffold, and human growth hormone polyadenylation (hGH polyA) signal. b) optimization of miC15*+31 on luc-intron 1b reporter. HEK293T cells were co-transfected with 10ng Luc-intron 1b reporter and 1, 5, 10 or 25 ng of miC15*+31 construct designed to simultaneously target both sense and antisense *C9orf72* transcripts. miC31_101 (targeting only sense) was used as positive control and miC15_451* served as negative control. RL and FL were measured as described in figure 3. c) Optimization of miC15*+31 on the antisense reporter. miC15*_451 was tested as positive control for the antisense reporter and miC31_101 as negative control. d) Knockdown of luc-intron 1b reporter by miC21*+31 with miC31_101 as positive and miC21_451* and negative controls. e) Dose dependent knockdown of the antisense reporter by miC21*+31. miC21_451* served as positive control and miC31_101 as negative control.

Endogenous knockdown of *C9orf72* expression in HEK293T cells by miC variants

We next investigated whether the selected miC candidates reduce the endogenous levels of *C9orf72* in HEK293T cells. Cells were transfected with the selected miC candidates and endogenous levels of *C9orf72* mRNA were determined 2 days post-transfection by RT-qPCR. As HEK293T cells lack the G_4C_2 expansion linked to the *C9orf72* pathology

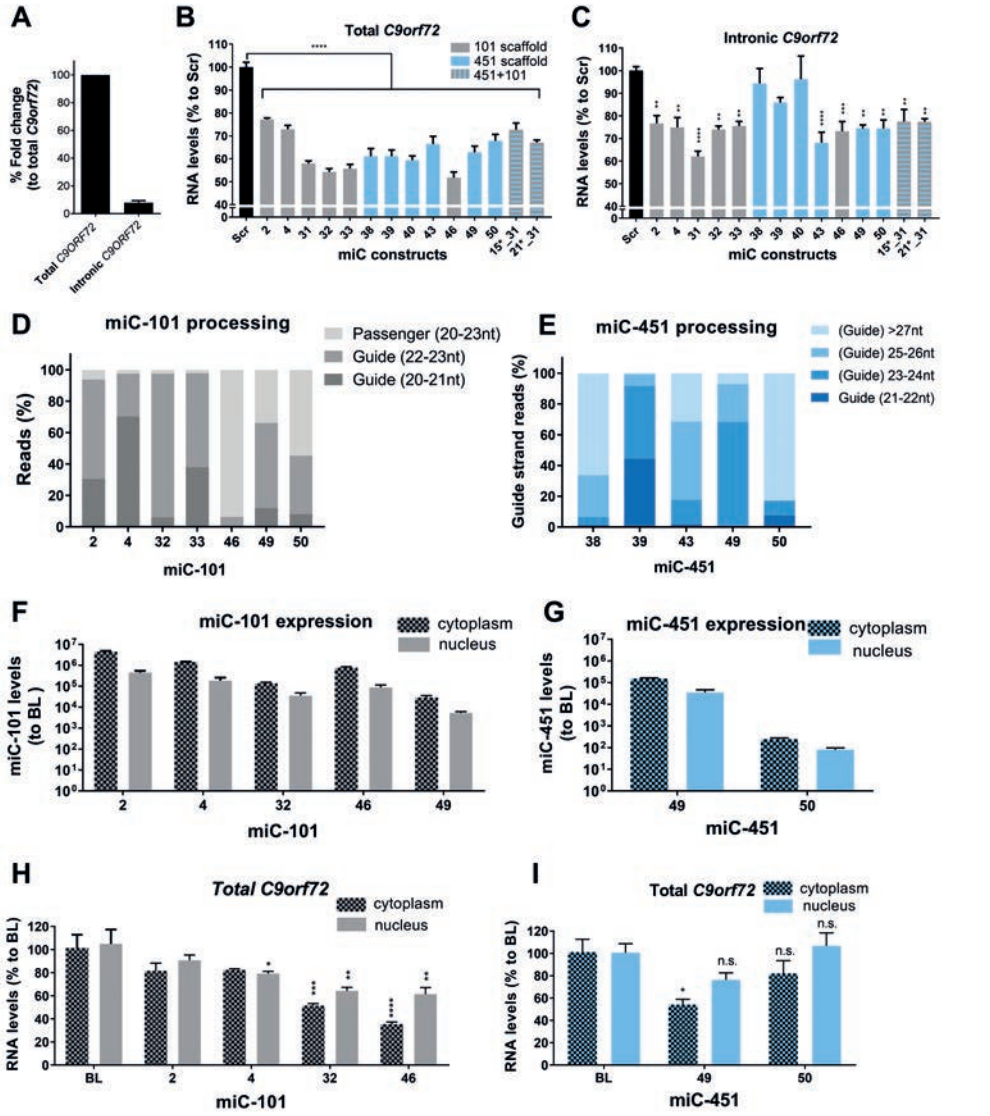

Figure 5. Lowering of endogenous *C9orf72* mRNA. a) Total and sense intronic *C9orf72* expression in HEK293T cells. RNA was isolated, and RT-qPCR was performed for total and sense intronic *C9orf72* transcripts. mRNA input levels were normalized to GAPDH and set relative to total *C9orf72* b-c) Endogenous knockdown of total *C9orf72* and sense intronic *C9orf72* by the selected miC candidates. RT-qPCR for total and sense *C9orf72* was performed on RNA from HEK293T cells that were transfected with 250 ng of different miC plasmids. mRNA input levels were normalized to GAPDH mRNA. miScr served as a negative control and was set at 100%. d) Processing of miC-101 candidates. HEK293T cells were transfected with 250 ng of the constructs, 48 hours post-transfection RNA was isolated and small RNA NGS was performed to determine the length and ratio of guide and passenger strands. e) Processing of miC-451 candidates. Performed as described in (d). f) Cytoplasmic and nuclear expression of miC candidates in miR_101 scaffold. RNA was isolated from cytoplasm and nucleus of HEK293T cells transfected with 250 ng of miC plasmid. miC levels

were measured by small RNA TaqMan and mRNA input levels was normalized to u6 small nuclear RNA and set relative to untreated (BL) cells. g) Expression of miC candidates in miR-451 in cytoplasm and nucleus. Performed as described in (f). h) Reduction of total *C9orf72* by miC-101 in cytoplasm and nucleus. RT-qPCR for total *C9orf72* was performed on cytoplasmic and nuclear fractions of transfected cells. mRNA input levels were corrected for GAPDH and BL was set at 100%. i) Total *C9orf72* reduction in nucleus and cytoplasm by miC-451. Performed as described in (h). Data were analyzed using a multiple comparison one-way ANOVA to determine statistically significances cells treated with scrambled or BL and miC. The p values are listed in the graph by asterisks: *p < 0.05; **p < 0.01; ***p < 0.001; ****p < 0.0001. Each graph represents the mean values with standard deviation of 2 independent experiment.

we first determined the expression of total *C9orf72* and intronic *C9orf72* mRNA. We found good expression of total *C9orf72,* while the intronic *C9orf72* was detectable but at very low levels (figure 5a). For miC candidates in miR-101 scaffold, total *C9orf72* mRNA was reduced up to 50% by miC32_101, miC33_101 and miC46_101 (figure 5b). The intronic *C9orf72* transcripts were also decreased by ~25% (figure 5c). miC2_101 and miC4_101 targeting intron 1 were less effective in lowering total *C9orf72* but the efficacy on intronic *C9orf72* was comparable to miC candidates targeting total *C9orf72.* Thus, both candidates may be targeting the repeat containing transcripts without significantly changing the total *C9orf72* expression. miC31_101 targeting intron 1 showed the best efficacy for the intronic *C9orf72* (40%) but despite its intronic localization, the total *C9orf72* RNA levels were also reduced by ~40% (figure 5b-c). Reduction of *C9orf72* was also observed by the selected miC candidates in miR-451 scaffold but their efficacy were slightly lower. Altogether, we demonstrated reduction of endogenous levels of *C9orf72* in HEK293T cells, confirming that the miC candidates are functional in cells.

Different processing pattern from miR-101 and miR-451 scaffolds

To assess the processing of the miC candidates, we analyzed the mature miC lengths and sequence composition of the guide and passenger strands by next-generation sequencing (NGS) for small transcriptome analysis (figure 5d-e). NGS was performed on small RNAs isolated from HEK293T cells that were transfected with the selected miC constructs. For each sample, we obtained between 15–30 million small RNA reads that were subsequently adaptor-trimmed and aligned against the corresponding reference sequence. All reads shorter than 10 nucleotide (nt), longer than 45 nt, or represented less than 10 times were excluded from the analysis.

miR-101 is processed into a miRNA duplex, first by Drosha cleavage and then by Dicer cleavage at the hairpin structure (supplementary figure S2). The miRNA duplex is then separated, and the guide strand is usually incorporated into the RNA-induced silencing complex (RISC) while in most cases the passenger strand is degraded.[42–44] The miC-101 candidates were processed into a 20-23 nt long mature miRNA, (figure 5d). The most frequently found length of guide strands was 22nt which is 1 nt longer than

the cleavage pattern predicted by miRBase (http://www.mirbase.org/) (supplementary table S1). The length of the passenger strands ranged between 19-23 nt. In most cases, Drosha cleavage sites of the mature miC-101 at 3' end of the pre-miC-101 candidates were precise and consistent with the prediction from miRBase except for miC33_101 and miC49_101. Following cleavage by Drosha, the hairpin of the pre-miC_101 is being cleaved by Dicer. Dicer cleavage in the hairpin generated more variability for almost all the miC variants. Processing of miC2_101, miC4_101, miC32_101 and miC33_101 yielded a high frequency of guide strands with very low percentage of the passenger strand. miC46_101 processing yielded more passenger strand, while miC49_101 and miC50_101 produced a relatively equal amount of guide and passenger strand.

The processing of the miC-451 candidates did not produce passenger strands but often generated longer guide strands than the predicted 22nt obtained from miRbase (figure 5e, supplementary table S2). Drosha cleavage sites at 5' end of the mature miC-451 were precise but the trimming of the 3' ends of the mature miC-451 by PARN were different for most candidates leading to a variety of mature lengths. miC39_451, miC43_451 and miC49_451 processing generated most often mature lengths between 21-26 nt long and processing of miC38_451 and miC50_451 often resulted in mature length longer than 27 nt.

Overall, we demonstrated that expressing different *C9orf72* target sequences from miR-101 scaffold yields a differential processing of mature guide and passenger strands. Using the miC-451, no passenger strands were detected, but this scaffold often generated longer mature guide strands.

miC-101 and miC-451 are active in the nucleus

pre-miRNAs are transported from the nucleus to cytoplasm for further processing and incorporation into the RISC.[42–44] However, because *C9orf72* related ALS and FTD are characterized by accumulation of the G_4C_2 containing transcripts in the nucleus, mature miC should be active in the cell nucleus to achieve therapeutic effect. Based on the efficacy *in vitro*, we selected miC2_101 and miC4_101 as the most promising candidates to target only the intronic transcripts. Similarly, miC32_101, miC46_101, miC49_451 and miC50_451 were selected for a total silencing approach based on their strong silencing efficacy *in vitro*. HEK293T cells were transfected with the different miC candidates, nuclear and cytoplasmic fractions were separated and expression of the mature miC2, miC4, miC32, miC46, miC49 and miC50 in nucleus and cytoplasm was evaluated. We detected mature miC in both nucleus and cytoplasmic fractions for all miC candidates but the expression levels in nucleus were consistently ~5 fold lower compared to cytoplasm (figure 5f-g). Next, we evaluated the silencing efficacy of the miC candidates in nucleus and cytoplasm by measuring the endogenous levels of total *C9orf72* mRNA. miC32_101, miC46_101 and miC49_451 caused a reduction of total *C9orf72* mRNA in both nucleus and cytoplasm (fig 5h, i). However, the silencing efficacy in the nucleus

was lower compared to cytoplasm, consistent with the lower miC levels detected in the nucleus. As expected, miC2_101 and miC4_101 which target the intronic *C9orf72* transcripts had limited to no effect on the total *C9orf72* expression. Thus, our data suggest that the mature miC-101 and miC-451 can both shuttle from the cytoplasm to the cell nucleus and can actively induce knockdown. Reduction of *C9orf72* was observed in both the nucleus and cytoplasm suggesting that both scaffolds can be used for further development into gene therapy for ALS and/or FTD.

Reduction of nuclear RNA foci by miC variants in $(G_4C_2)_{44}$ expressing cells

A hallmark of the RNA mediated toxicity in ALS and/or FTD is the formation of toxic RNA foci by the repeat-containing transcripts. We generated a cell model that develops nuclear RNA foci using methods similar to those described previously.[45,46] We expressed constructs consisting of $(G_4C_2)_{44}$ or $(G_4C_2)_3$ including 150 nt 5' and 50 nt 3' flanking regions linked to *C9orf72* exon 2 in HEK293T cells. Nuclear RNA foci were visualized by fluorescence *in situ* hybridization (FISH) using a TYE563-$(C_4G_2)_3$ locked nucleic acid (LNA) probe. However, we were not able to detect DPR proteins in these cells as the assay is technically challenging. Using a green fluorescence protein (GFP) construct the transfection efficiency was determined to be ~95-100% (data not shown). We observed sense RNA foci at 2 days post-transfection in ~40% of $(G_4C_2)_{44}$ cells (figure 6a) but antisense RNA foci were not detected (data not shown). RNA foci were primarily present in the nucleus. Control cells expressing a shorter $(G_4C_2)_3$ repeat did not accumulate RNA foci. To evaluate whether the foci were RNA specific, transfected cells were treated with RNAse or DNase (figure 6a). Almost all observed foci were degraded by RNAse but not DNAse, confirming that the observed foci are primarily composed of RNA.

miC4_101 and miC32_101 were evaluated for efficacy on RNA foci formation by co-transfection. Both miC candidates significantly decreased the percentage of $(G_4C_2)_{44}$ foci-positive cells by ~ 50% after 24 hours (figure 6b-c). miScr served as control and did not reduce the amount of foci in the cells. This confirms that our miC candidates are functional in reducing RNA foci in the cell nucleus.

Reduction of endogenous *C9orf72* in cells by AAV5-miC

To further investigate the silencing of *C9orf72* in context of a gene therapy for ALS and FTD, we selected miC32_101 as the best candidate to target total *C9orf72* based on the strong efficacy and low frequency of passenger strand formation. miC46_101 was selected as the most effective candidate based on silencing efficacy, but its high amount of passenger strand could make it less suitable to treat patients. Both candidates were incorporated in AAV5. Increasing doses of AAV5-miC32_101 and AAV5-miC46_101 were used to transduce HEK293T cells and iPSC derived frontal brain-like neurons from an FTD patient. Expression of the mature miC32 and miC46 was verified using TaqMan. Cells transduced with AAV5-GFP served as control for the transduction efficiency. At 3 days

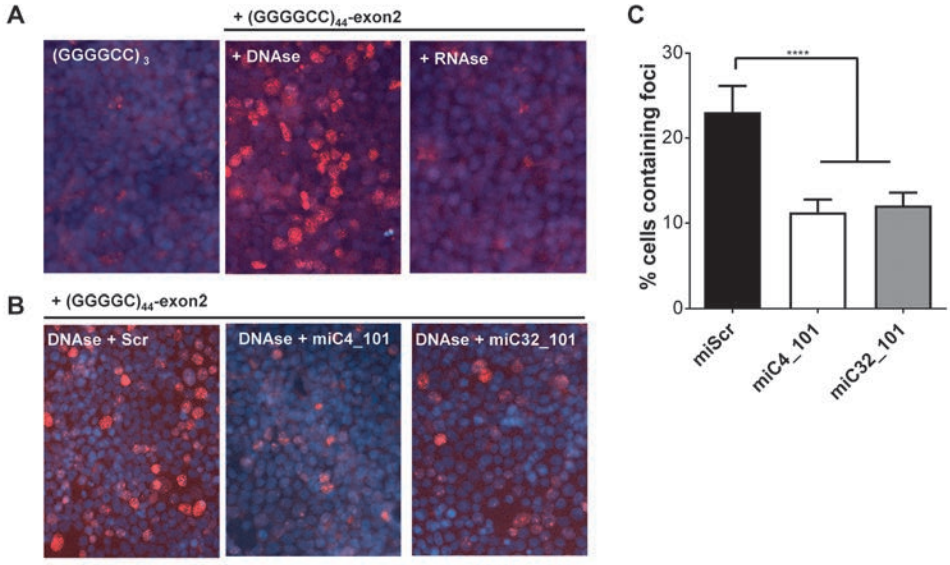

Figure 6. miC variants inhibit RNA foci formation in $(G_4C_2)_{44}$ expressing cells. a) RNA foci detected in HEK293T cells expressing $(G_4C_2)_{44}$. Cells were transfected with 250 ng of $(G_4C_2)_{44}$ and $(G_4C_2)_3$ plasmid and fixed 2 days post-transfection after treatment with DNAse or RNAse. RNA FISH was performed using a TYE563-$(CCCCGG)_3$ LNA probe (red) and nuclei were stained with DAPI (blue). Nuclear foci were resistant to DNAse but degraded by RNAse indicating RNA foci. b) Reduction of RNA foci by miC4_101 and miC32_101. Cells were co-transfected with 250 ng of $(G_4C_2)_{44}$ and 100 ng miC4_101, miC32_101 or miScr plasmid. Cells were fixed 2 days post- transfection and RNA FISH was performed as described in (a). c) Quantification of RNA foci in miC4_101 and miC32_101 transfected cells. A series of five images were made using a 10x magnification to quantify the number of cells containing nuclear foci using image J (mean ± standard deviation, one-way ANOVA, multiple comparison test, ***$p < 0.001$).

post-transduction, AAV5-GFP transduced ~80% of HEK293T cells (figure 7a). The mature guide strand expression of miC32 and miC46 was expressed at a dose-dependent manner and resulted in a dose dependent reduction of total *C9orf72* expression at a maximum of ~40-50% (figure 7b-c). The levels of mature miC32_101 and miC46_101 produced in transduced cells correlated well with *C9orf72* silencing (figure 7d-e). Similarly, miC expression and up to 50% lowering of *C9orf72* was observed in transduced frontal brain-like neurons (figure 7f-g). Hence, these data provide a strong rationale for further proof of concept studies in animal models of *C9orf72*-ALS leading towards a miRNA-based gene therapy to treat ALS and FTD.

Our results indicate that miRNAs could be used as therapeutics to reduce the gain of toxicity caused by the G_4C_2 expanded repeat of *C9orf72*. We demonstrated the feasibility of different targeting approaches by miC to silence the sense, antisense or both transcripts of *C9orf72*. In addition, the processing of miC in the miR-101 and miR-451 was demonstrated and both scaffolds produced mature miC that were functional in the cell

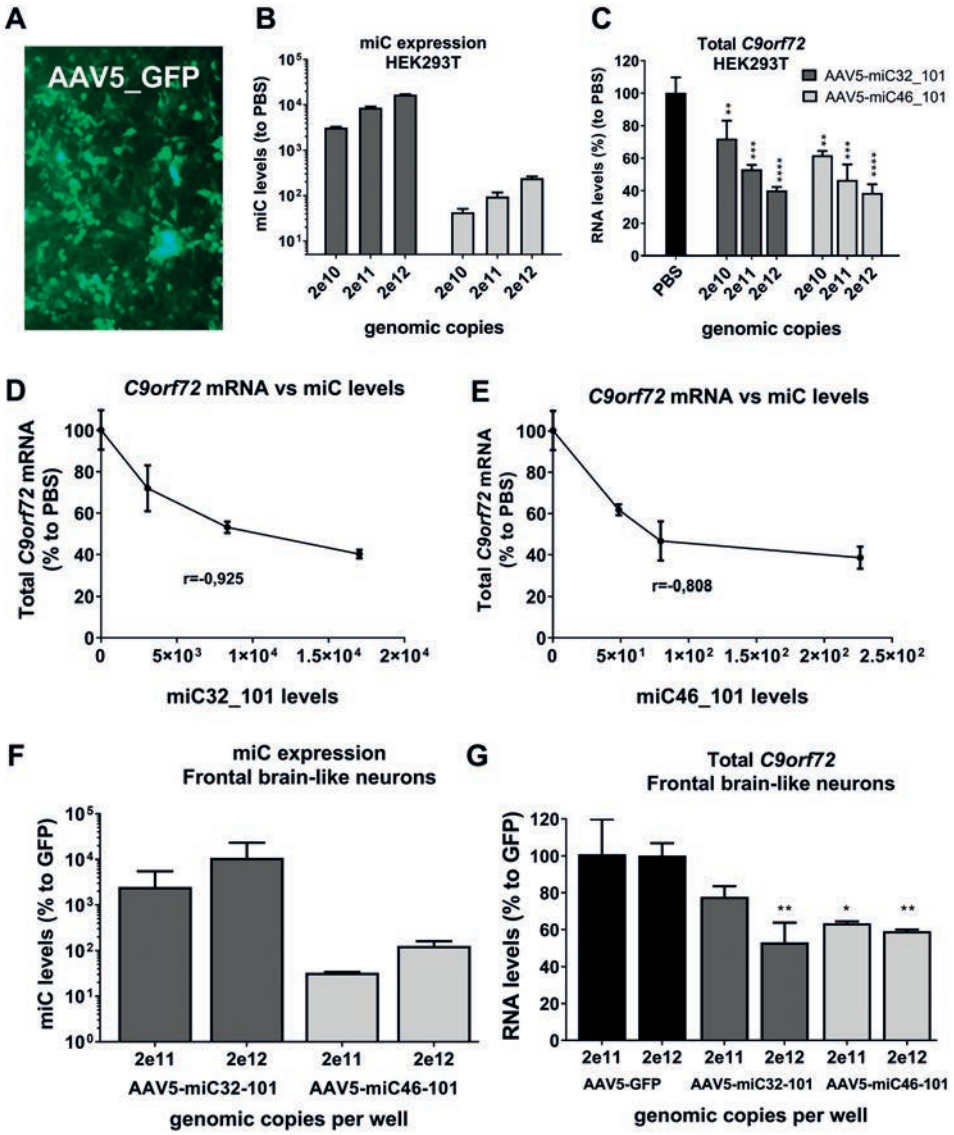

Figure 7. Silencing of endogenous *C9orf72* by AAV5-miC. a) Transduction efficiency by AAV5 in HEK293T cells. Cells were transduced with 1e12 genomic copies (gc) of AAV5-GFP and visualized 3 days post-transduction. b) Levels of mature miC32_101 and miC46_101 guide strands in transduced cells. Cells were transduced with 2e10, 2e11 and 2e12 gc of AAV5-miC32_101 and AAV5-miC46_101. RNA was isolated 3 days post-transduction to determine expression of the mature miC32_101 and miC46_101 by TaqMan. MicroRNA input levels were normalized to U6 small nuclear RNA and set relative to PBS treated cells. c) Silencing of *C9orf72* in transduced HEK293T cells. Performed as described in (b). Total *C9orf72* was determined by RT-qPCR. mRNA input was normalized to GAPDH and set relative to PBS treated cells. d) Correlation of miC32_101 expression levels and *C9orf72* knockdown in cells upon transduction with AAV5-miC32_101. Pearson correlation (r) = -0,925. e) Correlation of miC46_101 expression levels and *C9orf72* knockdown in cells transduced with AAV5-miC46_101 (r= -0,808). f) Levels of mature miC32_101

and miC46_101 guide strands in transduced iPSC-derived frontal brain-like neurons from an FTD patient. Cells were transduced with 2e11 and 2e12 gc of AAV5-miC32_101 and AAV5-miC46_101. RNA was isolated 7 days post-transduction to determine expression of the mature miC32_101 and miC46_101 by TaqMan. MicroRNA input levels were normalized to U6 small nuclear RNA and set relative to AAV5-GFP treated cells. g) Reduction of *C9orf72* in iPSC-derived frontal brain-like neurons from. Performed as described in (f) Total *C9orf72* levels were determined by RT-qPCR. mRNA input was normalized to GAPDH and set relative to cells treated with AAV5-GFP. Data were evaluated using two-way ANOVA multiple comparison test: *p < 0.05; **p < 0.01; ***p < 0.001; ****p < 0.0001. Each graph represents the mean values with standard deviation of 2 independent experiment.

nucleus and cytoplasm. Silencing of *C9orf72* by AAV5-miC was demonstrated in patient derived frontal brain-like neurons, proving promising results for further development of a miRNA-based gene therapy for ALS and FTD.

Discussion

A G_4C_2 repeat expansion in intron 1 of *C9orf72* is the most frequent cause of ALS and FTD, leading to accumulation of sense and antisense RNA foci in the cell nucleus and DPR proteins in the cytoplasm. Here we report on the design and characterization of an AAV-delivered miRNA-based approach to target *C9orf72* transcripts with potentially a long-lived therapeutic effect following a single administration. We analyzed RNA-seq data from C9-ALS patients to investigate *C9orf72* expression and sequence conservation to predict potential target regions for a miRNA-based targeting approach. We observed reduced levels of *C9orf72* in cortex and cerebellum from C9-ALS patients. This finding is consistent with other studies where significant reduction of *C9orf72* was also reported in brain and spinal cord tissues and in iPSC-derived neurons from patients.[2,39,47–49] Some studies reported that the V2 variant from *C9orf72* was the most affected transcript variant.[47,50] We did not find evidence that the reduction seen in patients was variant-specific. Reduced transcription of *C9orf72* in ALS patients could be a result of epigenetic silencing due to CpG hypermethylation of the G_4C_2 repeat and this raises the question whether haploinsufficiency also contributes to the pathology of the disease.[50] However, a significant body of evidences also support a G_4C_2-mediated toxicity.[49–52]

In order to identify potential miC target sites, we investigated the sequence conservation of *C9orf72*. Whereas exonic regions from exon 2 to exon 11 were completely covered, intronic regions were poorly represented and not much can be concluded about the conservation of intron 1 containing transcripts in patients. Despite the low coverage, read alignment for intronic regions was found in both patient and controls. Interestingly, the coverage of the introns 1-4 was relatively higher in C9-ALS patients than in controls, supporting findings that the impairment of full length *C9orf72* transcription in patients could be a result of accumulation of aberrant or unspliced *C9orf72* transcripts.[38,39] Directly targeting intron 1 is a challenging therapeutic strategy due to the low expression

and difficulty to detect intron 1 containing transcripts, as well as its high GC content. Moreover, GC rich regions are common in the genome and therapeutics targeting such region should be carefully investigated for off target effects. The coverage of the antisense transcript was very poor and limited coverage were found only in the 5'UTR of *C9orf72*. In contrast, exonic regions had complete coverage and therefore are much easier to target.

We designed miC candidates with intron 1 binding sites to target only the sense intronic transcripts and candidates binding within exon 2 and exon 11 to target all sense transcripts. miC candidates were also designed to specifically target the antisense transcripts of *C9orf72*.

In line with our difficulties to detect the repeat-containing transcripts with RNA-seq, the repeat region could also be less accessible for the mature miC due to its highly structured nature. Only two miC candidates targeting the G_4C_2 region showed a moderate knockdown of the intron 1 reporter. It is also possible that the high GC content of the mature miC itself interferes with strand loading and target recognition. miC candidates further downstream of the G_4C_2 repeat in intron 1, or in exon 2 and exon 11 showed a much stronger knockdown of the luc reporters and two miC candidates were also effective on the antisense reporter.

One challenge for our miC approach is simultaneous targeting of sense and antisense transcripts. To test the feasibility of such an approach, we designed a construct that expresses two miC molecules in a concatenated fashion against both sense and antisense transcripts. Silencing of both the intron 1 reporter and the antisense reporter constructs was achieved, demonstrating the feasibility for a bidirectional silencing of *C9orf72* by miC. Combining two or more miRNA hairpins in a single construct has been successfully performed previously and one study showed increased silencing efficacy by miRNAs in a polycistron setting.[53,54] Thus, expressing different miC in concatenated fashion could be promising to target both sense and antisense transcripts of *C9orf72*.

In the current study we used two differentially processed miRNA scaffolds, miR-101 and miR-451. The pre-miR-101 follows the canonical processing pathway as the further downstream processing in the cytoplasm involved Dicer cleavage of the hairpin to generate 5' arm strands and 3' arm strands. The 5' arm strand, which become the passenger strand, is usually degraded. Though, both strands could be incorporated into the RISC and loaded onto Argonaute (Ago), producing active guide- and passenger strands that cleaves the complimentary mRNA (supplementary figure S2). The pre-miR-451 follows the non-canonical pathway as it escapes Dicer cleavage producing only a 5' arm that is subsequently cleaved by Ago and trimmed by poly(a)-specific ribonuclease (PARN) into 22-24 nt guide strands that are incorporated into the RISC (supplementary figure S3). However, trimming of miR-451 can result into functional guide strands that are longer than the mature length.[31,55] Thus, both miR-101 and miR-451 are promising but simultaneous guide and passenger strand expression or mature miC much longer than the predicted length may increase the chance of hitting non-target genes due to miRNA-

like effects. Hence, it is important to determine the processing of miC candidates in both scaffolds and assess target similarity with other genes to minimize off-target effects.

The processing of the miC candidates was determined by NGS analysis. We confirmed a differential processing of the various miC-101 candidates, resulting in different ratios of guide and passenger strands. miC2_101, miC4_101, miC32_101 and miC33_101 produced low amounts of passenger strand and are predicted to have little off target effects. miC46_101, miC49_101 and miC50_101 may have an increased risk for off targets due to the high amount of passenger strands. The finding that the miC-101 candidates were differently processed, even in the same miRNA scaffold, support previous observations that not only the pri-miRNA scaffold, but also the miRNA sequence is critical for choosing which sequences of the duplex enters the RISC.[31,56–59] This strand selection has been extensively studied and seems to be also dependent on the difference in stability of the miRNA duplex at the 5′ ends of each strand.[31,57–62] miC-451 candidates did not show any passenger strand activity. However, miC38_451 and miC50_451 produced mature guide strands longer than 27nt and could also have increased risk for off targets. The different miC processing pattern suggest that selection of *C9orf72* silencing candidates should be based on a balanced assessment of silencing efficacy and NGS processing data.

The efficacy of the best miC candidates was further confirmed by their ability to reduce endogenously expressed *C9orf72* mRNA. We found up to ~50% reduction of total *C9orf72* mRNA and ~25% reduction of intronic transcripts by miC candidates targeting exon 2 or exon 11. The silencing efficacy of miC-451 was slightly lower compared to miC-101, consistent with the lower levels of mature miC-451 detected by NGS. Two miC candidates targeting the repeat region had limited effect on the total *C9orf72* mRNA expression but the reduction of the intronic transcripts was comparable with candidates targeting the total *C9orf72* mRNA. Thus, a total silencing approach and a mutant-specific approach can both result in lowering G_4C_2 repeat containing *C9orf72* transcripts.

Another challenge for therapeutic miC is the nuclear localization of the toxic transcripts. Thus, recognition of the transcripts by the miC candidates within the nucleus is required whereas the mature miC is produced in the cytoplasm. Nuclear RNA foci have been found in different neuronal cells of patients including spinal motor neurons, cerebellar Purkinje cells, cerebellar granule cells, hippocampal neurons and pyramidal cells in the motor cortex.[18] We report that the mature miC-101 and miC-451 candidates are detected in both nucleus and cytoplasm, and they lower *C9orf72* mRNA in both cellular structures. There is increasing evidence that miRNA-RISC components such as Ago and Dicer are present in the cell nucleus and retain their catalytic activity in the nucleus.[63,64] The current assumption is that miRNA-AGO complexes that are formed in the cytoplasm can travel back into the nucleus.[64] Indeed, we detected a reduction of nuclear RNA foci after treatment with miC candidates targeting intronic *C9orf72* or total *C9orf72* transcripts.

A critical factor determining the success of a gene therapy is the selected delivery system to the target cells or tissues. It is likely that a widespread transduction of neurons

in the whole brain and spinal cord including glia cells will be required to achieve disease modifying therapeutic effect in ALS and/or FTD patients. AAV vectors exhibit important advantages including a high transgene expression, long term stability and positive safety profile due to the non-pathogenic nature of the wild type form.[65] We demonstrated high expression of miC levels and up to 50% reduction of total *C9orf72* by AAV5-miC candidates in iPSC-derived frontal brain-like neurons from an FTD patient. It remains questionable how much reduction is required to achieve a rescue effect on the disease phenotype. However, previous findings using ASOs in an ALS mouse model without a clear clinical phenotype showed between 40-60% reduction of *C9orf72*, which appears to be sufficient to reduce RNA foci formation by ~50% and DPR proteins by ~80%.[26]

The delivery of RNAi-based AAV treatment strategies in ALS have predominantly been explored in preclinical studies to treat SOD1-ALS and have demonstrated to be promising.[66–69] AAV9 resulted in effective transduction of spinal cord and motor neurons, but sufficient widespread distribution in the adult CNS upon systemic injection remain challenging.[69–71] in children with spinal muscular atrophy type 1, a single intravenous infusion of AAV9 for gene replacement therapy resulted in widespread transduction of neurons within the spinal cord and significant clinical improvement.[72] However, for an RNAi based approach in adult with ALS and FTD patients, the blood–brain barrier (BBB) could still be a major obstacle for sufficient transduction of the CNS after systemic delivery. We have previously demonstrated strong transduction of the striatum and cortex, and lowering of mutant huntingtin protein in a Huntington's disease minipig model after direct injection of AAV5 into the striatum.[73] Furthermore, intrastriatal injection of AAV5 have shown to distribute via axons trough anterograde and/or retrograde transport and resulted into transduction of different type of neurons, astrocytes, microglia and oligodendrocytes.[73,74] Thus, a local delivery to the brain parenchyma is promising in patients with FTD for treatment of the symptoms associated with cortical degeneration. Parenchymal delivery of AAV also resulted in transduction of motor neurons along the corticospinal tract in non-human primates.[75] However, it needs to be assessed whether the transduction of motor neuron is sufficient to achieve therapeutic concentrations of AAV. An alternative approach could be intrathecal administration but further studies in large animals are required to predict the efficacy in the brain and spinal cord. Ultimately, intrathecal administration combined with parenchymal administration to the brain may be required to obtain sufficient transduction of the affected areas in ALS and/or FTD patients.

In summary, following an RNA sequence analysis of *C9orf72* in ALS patients and controls, we rationally designed miC candidates using the miR-101 and miR-451 scaffolds to target total, intronic and antisense *C9orf72* transcripts. We demonstrated that specifically targeting the G_4C_2 repeat by miC is possible but challenging. The feasibility of a bidirectional approach was also demonstrated by expressing two miC hairpins targeting the sense and antisense *C9orf72* in a concatenated fashion. The efficacy of the miC candidates was evaluated based on their ability to lower *C9orf72* mRNA and

the processing was determined by NGS. In addition, we also provided evidence that miC can be active in the nucleus by reduction of nuclear *C9orf72* mRNA and RNA foci.

2

Material and methods

RNA-seq and *C9orf72* target sequences

An RNA-seq library published by Prudencio et al was downloaded.[33] The data was analyzed by BaseClear B.V. In brief, we downloaded RNA-seq samples from the sequence reads archive(SRA) from NCBI Gene Expression Omnibus (http://www.ncbi.nlm.nih.gov/geo/) database under accession number GSE67196.[33] These samples were individually mapped to the human reference genome (GRCh38.p10) with Tophat version 2.1.1.[76] The mapped reads from Tophat are fragment per kilobase of transcript per million fragments mapped (FPKM) values. Differential gene and isoform expression was estimated on their relative abundance by Cufflinks 2.2.1.[77] With the CummeRbund 2.16 R package we visualized gene and isoform expression of *C9orf72*.[78] The alignment (.bam) and junctions file(.bed) generated by Tophat were used by the Integrative Genomics Viewer (IGV) 2.3.94.[79]

DNA constructs

To generate the miC vectors, we searched for sequences in intron 1, exon 2 and exon 11 of *C9orf72* that were mostly conserved between human, non-human primates and mouse. The miC sequences were incorporated into the cellular pri-miRNA miR-101-1 or miR-451 scaffold of the human. 200 nt 5' and 3' flanking regions were included with EcoRV and BamHI restriction sites and the mfold program (http://unafold.rna.albany.edu/?q=mfold) was used to determine if the miC candidates are folded correctly into their secondary structures. The complete sequences were ordered from GeneArt gene synthesis (Invitrogen). These constructs were subsequently cloned into an expression vector containing the CMV immediate-early enhancer fused to chicken β-actin (CAG) promoter (Inovio, Plymouth Meeting, PA) using the EcoRV and BamHI sites. For generation of the Luc reporters, sequences from *C9orf72* intron 1 (sense and antisense), exon 2 or exon 11 were synthesized at GeneArt gene synthesis and cloned in the 3'UTR of the renilla luciferase (RL) gene of the psiCHECK-2 vector (Promega, Madison, WI). The firefly luciferase (FL) gene was also expressed in this vector and served as internal control (figure 2d).

Culture and transfections of HEK293T cells

HEK293T were maintained in Dulbecco's modified Eagle's medium (DMEM) (Invitrogen) containing 10% fetal calf serum (Greiner, Kremsmünster, Austria), 100U/ml penicillin and 100U/ml streptomycin (Thermo Fisher, Waltham, MA), at 37 °C and 5% CO2. Transfections. For all assays, cells were seeded in 24-wells plates at a density of $0.1*10^6$ cells per well in DMEM. Transfections in HEK293T cells were performed

1-day post plating with Lipofectamine 2000 reagent (Invitrogen) according to the manufacturer's instructions.

Culture of iPSC-neurons

Frontotemporal Dementia (ND42765) iPSCs derived from fibroblast were ordered from Coriell Biorepository (https://www.coriell.org/) and was cultured on Matrigel (corning) -coated 6 wells plates in mTeSR1 (STEMCELL). For embryoid body-based neural induction, iPSCs were seeded on AggreWell800 plates and cultured in STEMdiff Neural Induction Medium (STEMCELL) for 5 days with daily medium changes. Embryoid bodies were harvested and plated on 6 wells plates coated with poly-D-lysine (Sigma-Aldrich) and laminin (Sigma-Aldrich) in STEMdiff Neural Induction Medium for 7 days with daily medium changes. Rosettes were selected with rosette selection medium and plated on poly-D-lysine and laminin coated 6-wells plates in STEMdiff Neural Induction Medium for 24 hours. For differentiation into frontal brain-like neurons, STEMdiff Neural Induction Medium was replaced for STEMdiff Neuron Differentiation Medium (STEMCELL) and neuroprogenitor cells were differentiated for 5 days. The neuroprogenitor cells were then plated on poly-D-lysine and laminin coated plates in STEMdiff Neuron Maturation Medium (STEMCELL) for one week. The mature frontal brain-like neurons were stored in liquid nitrogen in Neuroprogenitor Freezing Medium (STEMCELL).

Luciferase assays

HEK293T cells co-transfected with the miC expression constructs and Luc reporters were assayed at 48 hours post-transfection in 100 µl 1x passive lysis buffer (Promega) by gentle rocking for 15 minutes at room temperature. The cell lysates were centrifuged for 5 minutes at 4,000 rpm to get rid of cell debris and 10 µl of the supernatant was used to measure FL and RL activities with the Dual-Luciferase Reporter Assay System (Promega). Relative luciferase activity was calculated as the ratio between RL and FL activities.

RNA isolation

For all RNA isolation, cells were lysed in 200 ul Tryzol and RNA isolation was performed using the Direct-zol kit (R2061, ZYMO Research) according to the manufacturer protocol.

RT-qPCR, and miRNA TaqMan assay

To determine *C9orf72* mRNA knockdown, HEK293T cells were transfected with different concentrations of the miC variants. total RNA was isolated from the cells at 2 days post-transfection. Genomic DNA contamination was removed by DNAse treatment using recombinant shrimp DNase (ThemoFisher Scientific). First-strand complementary DNA was reverse transcribed using random hexamer primers with the Dynamo kit (Finnzymes, Espoo, Finland). Real-time PCR amplification was performed with primers targeting total *C9orf72*

(forward CGGAAAGGAAGAATATGGATGC, reverse CCATTACAGGAATCACTTCTCCA, probe AGCATTGGAATAATACTCTGACCCTGATCTTC) or sense intronic *C9orf72* (forward ACGCCTGCACAATTTCAGCCCAA, reverse CAAGTCTGTGTCATCTCGGAGCTG, probe TGAGGGCAGCAATGCAAGTCGGTGTG).[80] The assays were performed on ABI 7000 or ABI 7500 (Applied Biosystems, Foster City, CA, USA). The mRNA expression levels were normalized to human GAPDH (forward GAAGGTGAAGGTCGGAGTC, reverse GAAGATGGTGATGGGATTTC, probe CAAGCTTCCCGTTCTCAGCC) as an internal control, and the level of gene expression was calculated relative to cells transfected with a scrambled plasmid. To determine the expression of miC, a Custom TaqMan Small RNA Assay Design Tool (ThemoFisher Scientific) was used to design miC2 (assay ID CTEPR3R), miC4 (Assay ID: CTFVKNN), miC32 (assay ID CSGJPRB) and miC46, (assay ID CSHSNXJ) miC49 (Assay ID: CTGZE9K), miC50 (Assay ID: CTH49UH). All RT reaction and TaqMan for small RNAs were performed according to the manufacturer protocol.

RNA isolation from nucleus and cytoplasm separation

Nucleus and cytoplasm were isolated 2 days post transfections. Cells were washed with cold 1x PBS and 100 ul cold Nuclei EZ Lysis Buffer was added. Cells were incubated on a shaker on ice for 5 minutes and nucleus was collected by centrifugation at 500g for 5 minutes. The supernatant contains cytoplasmic components and was stored. The pellets were washed twice in 300 ul cold Nuclei EZ Lysis Buffer and the pellets containing nuclei components were stored. 200 ul Tryzol was added to both cytoplasmic and nuclei lysates and RNA was isolated as described in the previous section.

Next-generation sequencing (NGS) and data analysis

Small RNA sequencing libraries for the Illumina sequencing platform were generated using high-quality total RNA as input and the NEXTflex Small RNA Sequencing kit (Bioo Scientific, Austin, TX) as described before.[31] Briefly, the small RNA species were subjected to ligation with 3' and 5' RNA adapters, first strand reverse transcription, and polymerase chain reaction (PCR) amplification. Sample-specific barcodes were introduced in the PCR step. The PCR products were separated on TBE-PAGE electrophoresis and the expected band around 30bp was recovered for each sample. The resulting sequencing libraries were quantified on a BioAnalyzer (Agilent, Santa Clara, CA). The libraries were multiplexed, clustered, and sequenced on an Illumina HiSeq 2000 (TruSeq v3 chemistry) with a single-read 36 cycles sequencing protocol and indexing. The sequencing run was analyzed with the Illumina CASAVA pipeline (v1.8.2), with demultiplexing based on sample-specific barcodes. The raw sequencing data produced was processed removing the sequence reads which were of too low quality (only "passing filter" reads were selected). In total, between 15–35 million reads per sample were generated. NGS small RNA raw data sets were analyzed using the CLC Genomics Workbench 8 (Qiagen). The obtained reads were adaptor-trimmed, which decreased the average read size from ~50bp to ~25bp. All reads

containing ambiguity N symbols, reads shorter than 10 nt, longer than 45 nt, and reads represented less than 10 times were discarded. Next, the obtained unique small RNA reads were aligned to the reference sequences of the pre-miC constructs with a max. of 3 nt mismatches allowed. The percentages of reads based on the total number of reads matching the reference sequence were calculated (Table S1).

Cloning of $(G_4C_2)_{44}$-exon2 and $(G_4C_2)_3$-exon2 expression vectors

To generate $(G_4C_2)_{44}$ and $(G_4C_2)_3$ expression vectors we designed a sequence consisting of the intronic *C9orf72* repeat region. The sequence contained either 44 or 3 repeats of the G_4C_2 hexanucleotide and 150 nt of 5' and 50 nt' of 3' flanking regions was added. A restriction site ApaI was included at the 3' end to serve as cloning site. These sequences were synthesized and ordered from GeneArt gene synthesis (Invitrogen). In order to link the $(G_4C_2)_{44}$ and $(G_4C_2)_3$ vectors to exon 2, the *C9orf72* exon 2 sequence was ordered at GeneArt gene synthesis and cloned in in the $(G_4C_2)_{44}$ and $(G_4C_2)_3$ vectors using the ApaI site.

RNA foci fluorescence *in situ* hybridization (FISH)

RNA FISH was performed as described previously with some adjustments.[45] In brief, HEK293T cells were grown on poly-D-lysine coated 8 wells Nunc™ Lab-Tek™ Chamber Slide System at a density of 80k cells per well. The cells were transfected on day 2 with 200 ng $(G_4C_2)_{44}$ or $(G_4C_2)_3$ plasmid. On day 4, cells were fixed in 4% paraformaldehyde for 20 min, permeabilized in ice-cold methanol for 10 min, and washed 3 times with DEPC-treated PBS (DEPC-PBS). Optionally, cells were treated for 30min with 5mg/ml RNAse A (Qiagen) or 100 U RNAse free DNAse (Invitrogen). The cells were incubated for 1 hour in hybridization buffer (50% formamide, 10% dextran sulfate, 0.1 mg/mL yeast tRNA,2xSSC, 50 mM sodium phosphate) at 37°C and hybridize overnight with 40nm TYE563-$(C_4G_2)_3$ LNA probe in hybridization buffer at 37°C. Cells were then washed once with 40% formamide/1xSSC for 30 min at 37°C and 3x with DEPC-PBS at room temperature for 5 min. The slides were mounted with ProLong® Gold Antifade Mountant with DAPI (Invitrogen) and visualized using a LEICA DM2500 fluorescence microscope.

To determine the effect of miC4 and miC32 on foci formation, HEK293T cells co-transfected with 200 ng of $(G_4C_2)_{44}$ and 400ng of miC4, miC32 or miScr plasmid. Two days post-transfection, cells were fixed and subjected to FISH as described above. To quantify foci-bearing cells, ten fields were randomly selected under 10× magnification. For each field, the number of foci-positive nuclei and the total number of nuclei were counted using image J software. These counts were used to determine the average percentage of foci-positive cells for each condition.

AAV5 vector production and transductions

AAV5 encoding miC32_101 and miC46_101 were produced by a baculovirus-based AAV production system as described previously.[31] Briefly, the miC cassettes were obtained by digestion with restriction enzymes HindIII and PvuI and cloned in a uniQure transfer plasmid named pVD789 in order to generate an entry plasmid. The presence of the two inverted terminal repeats (ITRs) was confirmed by restriction digestion with SmaI. The ITR-CAG-miC cassettes were inserted in a recombinant baculovirus vector by homologous recombination in Spodoptera frugiperda Sf9 cells and clones were selected and screened by plague purification and PCR. The recombinant baculovirus containing the ITR-CAG-miC cassettes were further amplified till P6 in Sf+ cells and screened for the best production and stability by PCR and RT-qPCR. To generate AAV5, Sf+ cells were triple infected with three different recombinant baculoviruses expressing the ITRs-CAG-miC, the replicon enzyme and the capsid protein. The cells were lysed 72 hours after the triple infection and the crude lysate was treated with 50U/ml Benzonase (Merck, Darmstadt, Germany) for 1 hour at 37 °C. AAV5 was purified on an AVB Sepharose column (GE Healthcare, Little Chalfont, UK) using an AKTA purification system (GE Healthcare). The final titer concentration was determined by RT-qPCR with primers amplifying a 95bp fragment from the CAG promoter region.

For transductions with AAV, HEK293T cells were plated in 24-wells plates at $0.1x10^6$ cells per well in DMEM and transduced with AAV after 24 hours. Mature frontal brain-like neurons were plated at $0.3x10^6$ cells per well and transduced with AAV after one week. RNA isolation, and TaqMan for miC32_101, miC46_101 and total *C9orf72* Rt-qPCR was performed as described previously.

Statistical Analysis

Data were analyzed using the one-way ANOVA or Student's t-test to determine statistically significances between control and treated cells. A two-way ANOVA was used to determine statistically significances between multiple treated groups. The p values were either listed or represented by the following number of asterisks: *p < 0.05; **p < 0.01; ***p < 0.001; ****p < 0.0001.

Acknowledgments

The authors would like to thank Olivier ter Brake and Eileen Sawyer for reviewing the manuscript.

Author contributions

Conceptualization: P.K and R.M., Investigation: R.M., J.M.L., T.Z., J.M., J.S., Supervision: P.K, Formal analysis: R.M., J.M.L., I.K visualization and writing - initial draft: R.M., Project Administration and Writing – review and editing: P.K., S.D., M.M.E., H.P. Funding acquisition: P.K.

References

1. Renton, AE, Majounie, E, Waite, A, Simón-Sánchez, J, Rollinson, S, Gibbs, JR, *et al.* (2011). A hexanucleotide repeat expansion in *C9orf72* is the cause of chromosome 9p21-linked ALS-FTD. *Neuron* 72: 257–268.
2. DeJesus-Hernandez, M, Mackenzie, IR, Boeve, BF, Boxer, AL, Baker, M, Rutherford, NJ, *et al.* (2011). Expanded GGGGCC Hexanucleotide Repeat in Noncoding Region of *C9orf72* Causes Chromosome 9p-Linked FTD and ALS. *Neuron* 72: 245–256.
3. Mancuso, R and Navarro, X (2015). Amyotrophic lateral sclerosis: Current perspectives from basic research to the clinic. *Prog. Neurobiol.* 133: 1–26.
4. Nolan, M, Talbot, K and Ansorge, O (2016). Pathogenesis of FUS-associated ALS and FTD: insights from rodent models. *Acta Neuropathol. Commun.* 4: 99.
5. Heutink, P, Jansen, IE and Lynes, EM (2014). C9orf72; abnormal RNA expression is the key. *Exp. Neurol.* 262: 102–110.
6. Renton, AE, Majounie, E, Waite, A, Sim??n-S??nchez, J, Rollinson, S, Gibbs, JR, *et al.* (2011). A hexanucleotide repeat expansion in *C9orf72* is the cause of chromosome 9p21-linked ALS-FTD. *Neuron* 72: 257–268.
7. Gijselinck, I, Van Mossevelde, S, van der Zee, J, Sieben, A, Engelborghs, S, De Bleecker, J, *et al.* (2015). The C9orf72 repeat size correlates with onset age of disease, DNA methylation and transcriptional downregulation of the promoter. *Mol. Psychiatry* 21: 1–13.
8. van Blitterswijk, M, DeJesus-Hernandez, M and Rademakers, R (2012). How do *C9orf72* repeat expansions cause amyotrophic lateral sclerosis and frontotemporal dementia: can we learn from other noncoding repeat expansion disorders? *Curr. Opin. Neurol.* 25: 689–700.
9. Mis, MSC, Brajkovic, S, Tafuri, F, Bresolin, N, Comi, GP and Corti, S (2016). Development of Therapeutics for *C9orf72* ALS/FTD-Related Disorders. *Mol. Neurobiol.*: 1–11doi:10.1007/s12035-016-9993-0.
10. Gendron, TF, Belzil, V V., Zhang, YJ and Petrucelli, L (2014). Mechanisms of toxicity in C9FTLD/ALS. *Acta Neuropathol.* 127: 359–376.
11. Ling, SC, Polymenidou, M and Cleveland, DW (2013). Converging mechanisms in als and FTD: Disrupted RNA and protein homeostasis. *Neuron* 79: 416–438.
12. Ciura, S, Lattante, S, Le Ber, I, Latouche, M, Tostivint, H, Brice, A, *et al.* (2013). Loss of function of C9orf72 causes motor deficits in a zebrafish model of amyotrophic lateral sclerosis. *Ann. Neurol.* 74: 180–187.
13. Koppers, M, Blokhuis, AM, Westeneng, HJ, Terpstra, ML, Zundel, CAC, Vieira De Sá, R, *et al.* (2015). C9orf72 ablation in mice does not cause motor neuron degeneration or motor deficits. *Ann. Neurol.* 78: 426–438.
14. Jiang, J, Zhu, Q, Gendron, TF, Saberi, S, McAlonis-Downes, M, Seelman, A, *et al.* (2016). Gain of Toxicity from ALS/FTD-Linked Repeat Expansions in *C9orf72* Is Alleviated by Antisense Oligonucleotides Targeting GGGGCC-Containing RNAs. *Neuron* 90: 535–550.
15. Harms, MB, Cady, J, Zaidman, C, Cooper, P, Bali, T, Allred, P, *et al.* (2013). Lack of *C9orf72* coding mutations supports a gain of function for repeat expansions in amyotrophic lateral sclerosis. *Neurobiol. Aging* 34.
16. O'Rourke, JG, Bogdanik, L, Muhammad, AKMG, Gendron, TF, Kim, KJ, Austin, A, *et al.* (2015). C9orf72 BAC Transgenic Mice Display Typical Pathologic Features of ALS/FTD. *Neuron* 88: 892–901.
17. Almeida, S, Gascon, E, Tran, H, Chou, HJ, Gendron, TF, Degroot, S, *et al.* (2013). Modeling key pathological features of frontotemporal dementia with *C9orf72* repeat expansion in iPSC-derived human neurons. *Acta Neuropathol.* 126: 385–399.
18. Lagier-Tourenne, C, Baughn, M, Rigo, F, Sun, S, Liu, P, Li, H-R, *et al.* (2013). Targeted degradation of sense and antisense C9orf72 RNA foci as therapy for ALS and

frontotemporal degeneration. *Proc. Natl. Acad. Sci. U. S. A.* 110: E4530-9.

19. Gendron, TF, Bieniek, KF, Zhang, YJ, Jansen-West, K, Ash, PEA, Caulfield, T, *et al.* (2013). Antisense transcripts of the expanded *C9orf72* hexanucleotide repeat form nuclear RNA foci and undergo repeat-associated non-ATG translation in c9FTD/ALS. *Acta Neuropathol.* 126: 829–844.
20. Peters, OM, Cabrera, GT, Tran, H, Gendron, TF, McKeon, JE, Metterville, J, *et al.* (2015). Human *C9orf72* Hexanucleotide Expansion Reproduces RNA Foci and Dipeptide Repeat Proteins but Not Neurodegeneration in BAC Transgenic Mice. *Neuron* 88: 902–909.
21. Ash, PEA, Bieniek, KF, Gendron, TF, Caulfield, T, Lin, WL, DeJesus-Hernandez, M, *et al.* (2013). Unconventional Translation of *C9orf72* GGGGCC Expansion Generates Insoluble Polypeptides Specific to c9FTD/ALS. *Neuron* 77: 639–646.
22. Zu, T, Liu, Y, Banez-Coronel, M, Reid, T, Pletnikova, O, Lewis, J, *et al.* (2013). RAN proteins and RNA foci from antisense transcripts in *C9orf72* ALS and frontotemporal dementia. *Proc. Natl. Acad. Sci.* 110: E4968–E4977.
23. Hu, J, Liu, J, Li, L, Gagnon, KT and Corey, DR (2015). Engineering Duplex RNAs for Challenging Targets: Recognition of GGGGCC/CCCCGG Repeats at the ALS/FTD C9orf72 Locus. *Chem. Biol.* 22: 1505–1511.
24. Nordin, A, Akimoto, C, Wuolikainen, A, Alstermark, H, Forsberg, K, Baumann, P, *et al.* (2017). Sequence variations in C9orf72 downstream of the hexanucleotide repeat region and its effect on repeat-primed PCR interpretation: a large multinational screening study. *Amyotroph. Lateral Scler. Front. Degener.* 18: 256–264.
25. Hu, J, Rigo, F, Prakash, TP and Corey, DR (2017). Recognition of *c9orf72* Mutant RNA by Single-Stranded Silencing RNAs. *Nucleic Acid Ther.* 27: 87–94.
26. Jiang, J, Zhu, Q, Gendron, TF, Saberi, S, McAlonis-Downes, M, Seelman, A, *et al.* (2016). Gain of Toxicity from ALS/FTD-Linked Repeat Expansions in *C9orf72* Is Alleviated by Antisense Oligonucleotides Targeting GGGGCC-Containing RNAs. *Neuron* 90: 535–550.
27. Gendron, TF, Chew, J, Stankowski, JN, Hayes, LR, Zhang, YJ, Prudencio, M, *et al.* (2017). Poly(GP) proteins are a useful pharmacodynamic marker for *C9orf72*-associated amyotrophic lateral sclerosis. *Sci. Transl. Med.* 9.
28. Drouet, V, Perrin, V, Hassig, R, Dufour, N, Auregan, G, Alves, S, *et al.* (2009). Sustained effects of nonallele-specific huntingtin silencing. *Ann. Neurol.* 65: 276–285.
29. Stanek, LM, Sardi, SP, Mastis, B, Richards, AR, Treleaven, CM, Taksir, T, *et al.* (2014). Silencing mutant huntingtin by adeno-associated virus-mediated RNA interference ameliorates disease manifestations in the YAC128 mouse model of Huntington's disease. *Hum. Gene Ther.* 25: 461–74.
30. Boudreau, RL, Rodríguez-Lebrón, E and Davidson, BL (2011). RNAi medicine for the brain: Progresses and challenges. *Hum. Mol. Genet.* 20.
31. Miniarikova, J, Zanella, I, Huseinovic, A, van der Zon, T, Hanemaaijer, E, Martier, R, *et al.* (2016). Design, Characterization, and Lead Selection of Therapeutic miRNAs Targeting Huntingtin for Development of Gene Therapy for Huntington's Disease. *Mol. Ther. Nucleic Acids* 5: e297.
32. Snøve, O and Rossi, JJ (2006). Toxicity in mice expressing short hairpin RNAs gives new insight into RNAi. *Genome Biol.* 7.
33. Prudencio, M, Belzil, V V., Batra, R, Ross, CA, Gendron, TF, Pregent, LJ, *et al.* (2015). Distinct brain transcriptome profiles in C9orf72-associated and sporadic ALS. *Nat. Neurosci.* 18: 1175–1182.
34. Lee, Y, Kim, M, Han, J, Yeom, K-H, Lee, S, Baek, SH, *et al.* (2004). MicroRNA genes are transcribed by RNA polymerase II. *EMBO J.* 23: 4051–4060.
35. Gregory, RI, Yan, KP, Amuthan, G, Chendrimada, T, Doratotaj, B, Cooch, N, *et al.* (2004). The Microprocessor complex mediates the genesis of microRNAs. *Nature* 432: 235–240.

36. Han, J, Lee, Y, Yeom, KH, Kim, YK, Jin, H and Kim, VN (2004). The Drosha-DGCR8 complex in primary microRNA processing. *Genes Dev.* 18: 3016–3027.
37. Auyeung, VC, Ulitsky, I, McGeary, SE and Bartel, DP (2013). Beyond secondary structure: Primary-sequence determinants license Pri-miRNA hairpins for processing. *Cell* 152: 844–858.
38. Niblock, M, Smith, BN, Lee, Y-B, Sardone, V, Topp, S, Troakes, C, *et al.* (2016). Retention of hexanucleotide repeat-containing intron in C9orf72 mRNA: implications for the pathogenesis of ALS/FTD. *Acta Neuropathol. Commun.* 4: 18.
39. Haeusler, AR, Donnelly, CJ, Periz, G, Simko, EAJ, Shaw, PG, Kim, MS, *et al.* (2014). C9orf72 nucleotide repeat structures initiate molecular cascades of disease. *Nature* 507: 195–200.
40. Zu, T, Liu, Y, Banez-Coronel, M, Reid, T, Pletnikova, O, Lewis, J, *et al.* (2013). RAN proteins and RNA foci from antisense transcripts in *C9orf72* ALS and frontotemporal dementia. *Proc. Natl. Acad. Sci.* 110: E4968–E4977.
41. Klein, RL, Hamby, ME, Gong, Y, Hirko, AC, Wang, S, Hughes, JA, *et al.* (2002). Dose and promoter effects of adeno-associated viral vector for green fluorescent protein expression in the rat brain. *Exp. Neurol.* 176: 66–74.
42. Grimm, D, Streetz, KL, Jopling, CL, Storm, TA, Pandey, K, Davis, CR, *et al.* (2006). Fatality in mice due to oversaturation of cellular microRNA/short hairpin RNA pathways. *Nature* 441: 537–541.
43. McBride, JL, Boudreau, RL, Harper, SQ, Staber, PD, Monteys, AM, Martins, I, *et al.* (2008). Artificial miRNAs mitigate shRNA-mediated toxicity in the brain: Implications for the therapeutic development of RNAi. *Proc. Natl. Acad. Sci.* 105: 5868–5873.
44. Cifuentes, D, Xue, H, Taylor, DW, Patnode, H, Mishima, Y, Cheloufi, S, *et al.* (2010). A novel miRNA processing pathway independent of dicer requires argonaute2 catalytic activity. *Science (80-.).* 328: 1694–1698.
45. Su, Z, Zhang, Y, Gendron, TF, Bauer, PO, Chew, J, Yang, WY, *et al.* (2014). Discovery of a Biomarker and Lead Small Molecules to Target r(GGGGCC)-Associated Defects in c9FTD/ALS. *Neuron* 83: 1043–1050.
46. Stepto, A, Gallo, JM, Shaw, CE and Hirth, F (2014). Modelling *C9orf72* hexanucleotide repeat expansion in amyotrophic lateral sclerosis and frontotemporal dementia. *Acta Neuropathol.* 127: 377–389.
47. van Blitterswijk, M, Gendron, TF, Baker, MC, DeJesus-Hernandez, M, Finch, NCA, Brown, PH, *et al.* (2015). Novel clinical associations with specific *C9orf72* transcripts in patients with repeat expansions in *C9orf72*. *Acta Neuropathol.* 130: 863–876.
48. Donnelly, CJ, Zhang, PW, Pham, JT, Heusler, AR, Mistry, NA, Vidensky, S, *et al.* (2013). RNA Toxicity from the ALS/FTD *C9orf72* Expansion Is Mitigated by Antisense Intervention. *Neuron* 80: 415–428.
49. Shi, Y, Lin, S, Staats, KA, Li, Y, Chang, W-H, Hung, S-T, *et al.* (2018). Haploinsufficiency leads to neurodegeneration in *C9orf72* ALS/FTD human induced motor neurons. *Nat. Med.*doi:10.1038/nm.4490.
50. Liu, EY, Russ, J, Wu, K, Neal, D, Suh, E, McNally, AG, *et al.* (2014). C9orf72 hypermethylation protects against repeat expansion-associated pathology in ALS/FTD. *Acta Neuropathol.* 128: 525–541.
51. Fratta, P, Poulter, M, Lashley, T, Rohrer, JD, Polke, JM, Beck, J, *et al.* (2013). Homozygosity for the C9orf72 GGGGCC repeat expansion in frontotemporal dementia. *Acta Neuropathol.* 126: 401–409.
52. Liu, Y, Pattamatta, A, Zu, T, Reid, T, Bardhi, O, Borchelt, DR, *et al.* (2016). C9orf72 BAC Mouse Model with Motor Deficits and Neurodegenerative Features of ALS/FTD. *Neuron* 90: 521–534.
53. Liu, YP, Haasnoot, J, ter Brake, O, Berkhout, B and Konstantinova, P (2008). Inhibition of HIV-1 by multiple siRNAs expressed from a single microRNA polycistron. *Nucleic Acids Res.* 36: 2811–2824.
54. Sun, D, Melegari, M, Sridhar, S, Rogler, CE and Zhu, L (2006). Multi-miRNA hairpin method that improves gene knockdown efficiency and provides linked multi-gene knockdown. *Biotechniques* 41: 59–63.
55. Mayuko Yoda, Daniel Cifuentes, Natsuko Izumi, Yuriko Sakaguchi, Tsutomu Suzuki,

AJG and YT (2013). PARN mediates 3'-end trimming of Argonaute2-cleaved precursor microRNAs 5.

56. Schwarz, DS, Hutvágner, G, Du, T, Xu, Z, Aronin, N and Zamore, PD (2003). Asymmetry in the assembly of the RNAi enzyme complex. *Cell* 115: 199–208.
57. Vitsios, DM, Davis, MP, Dongen, S Van and Enright, AJ (2016). Large-scale analysis of microRNA expression, epi-transcriptomic features and biogenesis. *Genome Biol. Evol.*: 1–12doi:10.1093/gbe/evw245.
58. Maczuga, P, Verheij, J, Loos, C Van Der, Logtenstein, R Van, Hooijer, G, Martier, R, *et al.* (2013). Therapeutic expression of hairpins targeting apolipoprotein B100 induces phenotypic and transcriptome changes in murine liver. *Gene Ther.* 21: 60–70.
59. Maczuga, P, Koornneef, A, Borel, F, Petry, H, van Deventer, S, Ritsema, T, *et al.* (2012). Optimization and comparison of knockdown efficacy between polymerase II expressed shRNA and artificial miRNA targeting luciferase and Apolipoprotein B100. *BMC Biotechnol.* 12: 42.
60. Slezak-Prochazka, I, Durmus, S, Kroesen, B-J and Berg, A van den (2010). MicroRNAs, macrocontrol: Regulation of miRNA processing. *RNA* 16: 1087–1095.
61. Guo, L and Lu, Z (2010). The fate of miRNA* strand through evolutionary analysis: Implication for degradation as merely carrier strand or potential regulatory molecule? *PLoS One* 5.
62. Diederichs, S and Haber, DA (2007). Dual Role for Argonautes in MicroRNA Processing and Posttranscriptional Regulation of MicroRNA Expression. *Cell* 131: 1097–1108.
63. Gagnon, KT, Li, L, Chu, Y, Janowski, BA and Corey, DR (2014). RNAi factors are present and active in human cell nuclei. *Cell Rep.* 6: 211–221.
64. Catalanotto, C, Cogoni, C and Zardo, G (2016). MicroRNA in control of gene expression: An overview of nuclear functions. *Int. J. Mol. Sci.* 17.
65. Saraiva, J, Nobre, RJ and Pereira de Almeida, L (2016). Gene therapy for the CNS using AAVs: The impact of systemic delivery by AAV9. *J. Control. Release* 241: 94–109.
66. Borel, F, Gernoux, G, Cardozo, B, Metterville, JP, T. Cabrera, G, Song, L, *et al.* (2016). Therapeutic rAAVrh10 Mediated *SOD1* Silencing in Adult *SOD1* ^{G93A} Mice and Nonhuman Primates. *Hum. Gene Ther.* 27: 19–31.
67. M.G., B, M., C-T, B., G, M., R, S., A, T., M, *et al.* (2015). A newaav-based gene therapy approach for SOD1-linked als. *Amyotroph. Lateral Scler. Front. Degener.* 16: 20–21.
68. Dirren, E, Aebischer, J, Rochat, C, Towne, C, Schneider, BL and Aebischer, P (2015). SOD1 silencing in motoneurons or glia rescues neuromuscular function in ALS mice. *Ann. Clin. Transl. Neurol.* 2: 167–184.
69. Foust, KD, Salazar, DL, Likhite, S, Ferraiuolo, L, Ditsworth, D, Ilieva, H, *et al.* (2013). Therapeutic AAV9-mediated suppression of mutant SOD1 slows disease progression and extends survival in models of inherited ALS. *Mol. Ther.* 21: 2148–59.
70. Stoica, L, Todeasa, SH, Cabrera, GT, Salameh, JS, Elmallah, MK, Mueller, C, *et al.* (2016). Adeno-associated virus-delivered artificial microRNA extends survival and delays paralysis in an amyotrophic lateral sclerosis mouse model. *Ann. Neurol.* 79: 687–700.
71. Wang, W, Wen, D, Duan, W, Yin, J, Cui, C, Wang, Y, *et al.* (2018). Systemic administration of scAAV9-IGF1 extends survival in SOD1G93AALS mice via inhibiting p38 MAPK and the JNK-mediated apoptosis pathway. *Brain Res. Bull.* 139: 203–210.
72. Mendell, JR, Zaidy, S Al, Shell, R, Arnold, WD, Klapac, LRR, Prior, TW, *et al.* (2017). Single-Dose Gene-Replacement Therapy for Spinal Muscular Atrophy. *N. Engl. J. Med.* 377: 1713–1722.
73. Evers, MM, Miniarikova, J, Juhas, S, Vallès, A, Bohuslavova, B, Juhasova, J, *et al.* (2018). AAV5-miHTT Gene Therapy Demonstrates Broad Distribution and Strong Human Mutant Huntingtin Lowering in a Huntington's Disease Minipig Model. *Mol. Ther.* 26: 2163–2177.
74. Aschauer, DF, Kreuz, S and Rumpel, S (2013). Analysis of Transduction Efficiency, Tropism and Axonal Transport of AAV

Serotypes 1, 2, 5, 6, 8 and 9 in the Mouse Brain. *PLoS One* 8.

75. Samaranch, L, Blits, B, San Sebastian, W, Hadaczek, P, Bringas, J, Sudhakar, V, *et al.* (2017). MR-guided parenchymal delivery of adeno-associated viral vector serotype 5 in non-human primate brain. *Gene Ther.* 24: 253–261.
76. Trapnell, C, Pachter, L and Salzberg, SL (2009). TopHat: Discovering splice junctions with RNA-Seq. *Bioinformatics* 25: 1105–1111.
77. Trapnell, C, Williams, BA, Pertea, G, Mortazavi, A, Kwan, G, Van Baren, MJ, *et al.* (2010). Transcript assembly and quantification by RNA-Seq reveals unannotated transcripts and isoform switching during cell differentiation. *Nat. Biotechnol.* 28: 511–515.
78. Goff, LA, Trapnell, C and Kelley, D (2012). CummeRbund: visualization and exploration of Cufflinks high-throughput sequencing data. *(http://compbio.mit.edu/cummeRbund/)*.
79. Robinson, JT, Thorvaldsdóttir, H, Winckler, W, Guttman, M, Lander, ES, Getz, G, *et al.* (2011). Integrative genomics viewer. *Nat. Biotechnol.* 29: 24–26.
80. Liu, J, Hu, J, Ludlow, AT, Pham, JT, Shay, JW, Rothstein, JD, *et al.* (2017). c9orf72 Disease-Related Foci Are Each Composed of One Mutant Expanded Repeat RNA. *Cell Chem. Biol.* 24: 141–148.

Supplementary material

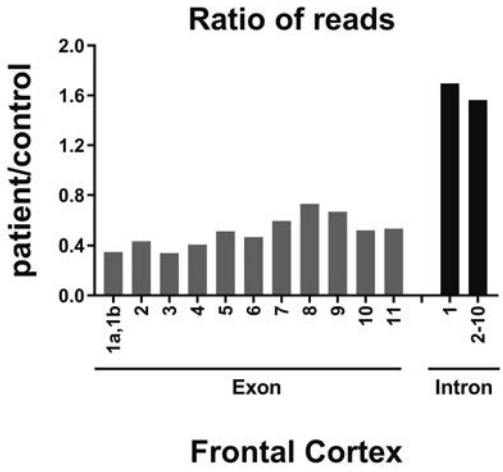

Figure S1. Ratio of reads between C9-ALS patients and controls in cortex. The total amount of reads counted in different intronic and exonic regions from C9-ALS patients were divided by the total amount of reads from the same region of control donors.

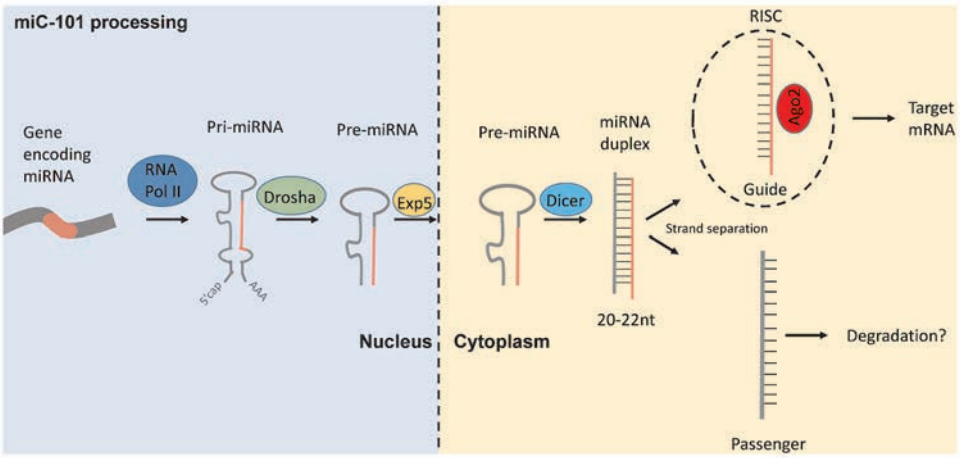

Figure S2. Processing of miC-101 in the cell. In the canonical pathway**,** miC-101 is transcribed by RNA pol II and produces a primary miRNA (pri-miC) hairpin, which is processed by Drosha to generate a precursor miRNA (pre-miC). The pre-miC is transported by exportin 5 (exp 5) into the cytoplasm for further processing by Dicer to produce a miC duplex of ~20-22 basepairs. An Argonaute (Ago2) protein binds the duplex and incorporates the mature miC-101 guide strand in the RNA-induced silencing complex (RISC) to suppress downstream target gene expression. The passenger strand of the miC-101 duplex is usually discarded but can also be functional.[1]

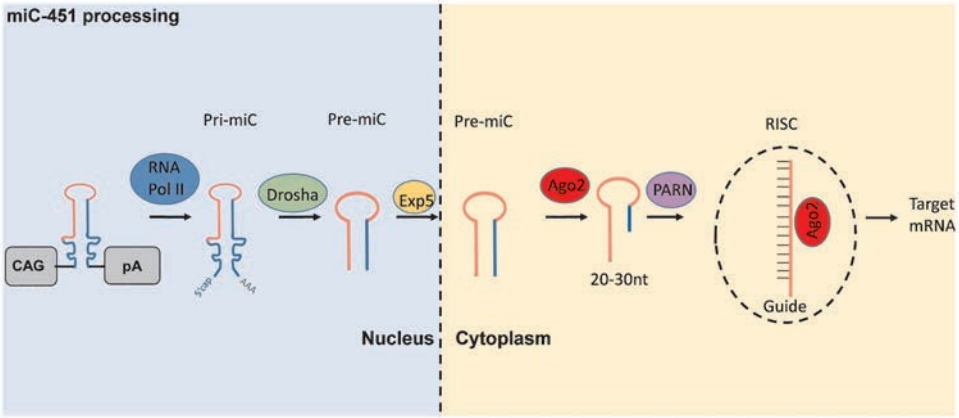

Figure S3. Processing of miC-451 in the cell. In the non-canonical pathway, miC-451 follows the same Drosha dependent processing in the nucleus into a pre-miC. The pre-miC-451 is too short to be cleaved by dicer and is directly loaded into Ago proteins. Ago2 cleaves the 3' arm of pre-miR-451 by its slicer activity and yields a ~30-nt intermediate that is further trimmed by PARN to generate a mature miC of ~23nt. The trimming of the miC-451 is not essential for efficiency and miC-451 can be functional with mature guide strands longer than the mature length.[2]

miC	mature miRNA (Guide strand)	lenght	reads	% reads	mature miRNA (passenger strand)	nt lengt	reads	% reads
miC2_101								
Total expression valı 1E+06								
5' passenger	1 TCACCCTCAGCGAGTACTGTGA	22	636099	57,6%	1 ACAGTACTCGCTGAGGGTTGACG	23	11703	1,1%
u cuggc u gucua	2 CACCCTCAGCGAGTACTGTGA	21	265198	24,0%	2 ACAGTACTCGCTGAGGGTTGAC	22	4773	0,4%
gcc cacaguacucgcugaggg ugac u	3 TCACCCTCAGCGAGTACTGTG	21	73556	6,7%	3 ACAGTACTCGCTGAGGGTTG	20	4136	0,4%
cgg gugucaugagcgacuccc acug u	4 CACCCTCAGCGAGTACTGTGAG	22	23444	2,1%	4 ACAGTACTCGCTGAGGGTTGACT	23	4102	0,4%
a uagga aaauc	5 TCACCCTCAGCGAGTACTGTGT	22	21217	1,9%	5 ACAGTACTCGCTGAGGGTTGA	21	3800	0,3%
3' guide	6 CACCCTCAGCGAGTACTGTGAGA	23	20599	1,9%	6 ACAGTACTCGCTGAGGGTT	19	1618	0,1%
	7 CACCCTCAGCGAGTACTGTGAA	22	18592	1,7%	7 ACAGTACTCGCTGAGGGTTGACA	23	1042	0,1%
	8 CACCCTCAGCGAGTACTGTG	20	14071	1,3%	8 CACAGTACTCGCTGAGGGTTG	21	774	0,1%
			total	97,1%			total	2,9%
miC4_101								
Total expression valı 3400199								
5' passenger	1 CTAGCGCGCGACTCCTGAGTT	21	1955837	63,2%	1 CTCAGGAGTCGCGCGCTGA	19	47230	1,5%
u cuggc g cucua	2 CTAGCGCGCGACTCCTGAGTTA	22	378744	12,2%	2 ACTCAGGAGTCGCGCGCTGA	20	5763	0,2%
gcc acucaggagucgcgcgcu aggg u	3 CTAGCGCGCGACTCCTGAGTTT	22	334594	10,8%	3 CTCAGGAGTCGCGCGCTG	18	5187	0,2%
cgg ugaguccucagcgcgcga uccu u	4 CTAGCGCGCGACTCCTGAGT	20	192640	6,2%	4 CTCAGGAGTCGCGCGCTGAGGG	22	4382	0,1%
a uaggu aaauc	5 CTAGCGCGCGACTCCTGAGTTAA	23	61917	2,0%	5 CTCAGGAGTCGCGCGCTGAGGGT	23	3151	0,1%
3' guide	6 CTAGCGCGCGACTCCTGAGTTG	22	37869	1,2%	6 CACTCAGGAGTCGCGCGCTGA	21	3128	0,1%
	7 CCTAGCGCGCGACTCCTGAGTT	22	34766	1,1%	7 CTCAGGAGTCGCGCGCTGT	19	2365	0,1%
	8 TAGCGCGCGACTCCTGAGTT	20	24587	0,8%	8 CTCAGGAGTCGCGCGCTGAGGGA	23	2311	0,1%
			Total	97,6%			Total	2,4%
miC32_101								
Total expression valı 3464421								
5' passenger	1 TCCTTACTCTAGGACCAAGAAT	22	2606713	79,5%	1 TCTTGGTCCTAGAGTAACGGACG	22	24762	0,8%
u cuggc c gucua	2 TCCTTACTCTAGGACCAAGAATT	23	269810	8,2%	2 TCTTGGTCCTAGAGTAACGGA	21	16762	0,5%
gcc uucuugguccuagaguaa ggac u	3 CCTTACTCTAGGACCAAGAAT	21	142674	4,4%	3 TCTTGGTCCTAGAGTAACGG	20	7759	0,2%
cgg aagaaccaggaucucauu ccug u	4 CCTTACTCTAGGACCAAGAATT	22	75024	2,3%	4 TTCTTGGTCCTAGAGTAACGGA	22	6829	0,2%
a uaggu aaauc	5 TCCTTACTCTAGGACCAAGAA	21	37463	1,1%	5 TCTTGGTCCTAGAGTAACGGAC	22	6535	0,2%
3' guide	6 TCCTTACTCTAGGACCAAGAATTT	24	36928	1,1%	6 TCTTGGTCCTAGAGTAACG	19	6513	0,2%
	7 TCCTTACTCTAGGACCAAGAAC	22	16022	0,5%	7 TTCTTGGTCCTAGAGTAACGG	21	6217	0,2%
	8 TCCTTACTCTAGGACCAAGA	20	13809	0,4%	8 TCTTGGTCCTAGAGTAACGGACGT	24	4317	0,1%
			total	97,6%			total	2,4%

Table S1. miC-101 processing by NGS. Sequence distribution (%) of guide- and passenger strands of reads mapping to miC2_101, miC4_101, miC32_101, miC33_101, miC46_101, miC49_101 and miC50_101. Human embryonic kidney (HEK)293T cells were transfected with 250ng of the constructs. RNA was isolated 48 hours post-transfection and small RNA NGS was performed. The scaffold for each candidate is shown in the first column. Based on miRBase, the predicted guide and passenger strand sequences of the cellular pri-miRNA scaffolds are indicated in red and blue, respectively. The 5′ and 3′ flanking nucleotides are indicated in black.

miC33_101									
Total expression valı 1E+06									
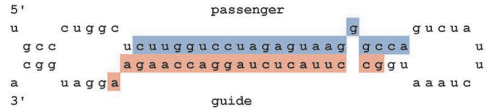	1 GCCTTACTCTAGGACCAAGAAT	22	304832	25,5%	1 CTTGGTCCTAGAGTAAGGGCC	21	10472	0,9%
	2 GCCTTACTCTAGGACCAAGA	20	260199	21,7%	2 TCTTGGTCCTAGAGTAAGGG	20	3471	0,3%
	3 GCCTTACTCTAGGACCAAGAA	21	193939	16,2%	3 TCTTGGTCCTAGAGTAAGG	19	2371	0,2%
	4 GCCTTACTCTAGGACCAAGAATT	23	143923	12,0%	4 CTTGGTCCTAGAGTAAGGGC	20	2109	0,2%
	5 GCCTTACTCTAGGACCAAGACC	22	82239	6,9%	5 TCTTGGTCCTAGAGTAAGGGC	21	1873	0,2%
	6 GCCTTACTCTAGGACCAAGAAA	22	73716	6,2%	6 TCTTGGTCCTAGAGTAAGGGCC	22	1442	0,1%
	7 GCCTTACTCTAGGACCAAGAAG	22	69331	5,8%	7 CTTGGTCCTAGAGTAAGGGCCA	22	1299	0,1%
	8 GCCTTACTCTAGGACCAAGACT	22	44100	3,7%	8 CTTGGTCCTAGAGTAAGGG	19	1184	0,1%
			total	98,0%			total	2,0%
miC46_101									
Total expression valı 2E+05									
	1 TTATCTTCAGGTTCCGAAGAGA	22	10318	5,6%	1 TCTTCGGAACCTGAAGATTGACG	23	126624	68,3%
	2 TTATCTTCAGGTTCCGAAGAG	21	340	0,2%	2 TCTTCGGAACCTGAAGATTGAC	22	16393	8,8%
	3 TTATCTTCAGGTTCCGAAGAGT	22	240	0,1%	3 TCTTCGGAACCTGAAGATTGACGT	24	15479	8,3%
	4 TTATCTTCAGGTTCCGAAGAGAA	23	199	0,1%	4 TCTTCGGAACCTGAAGATTGACT	23	5010	2,7%
	5 TATCTTCAGGTTCCGAAGAGA	21	198	0,1%	5 TCTTCGGAACCTGAAGATTGA	21	4479	2,4%
	6 TTATCTTCAGGTTCCGAAG	19	151	0,1%	6 TCTTCGGAACCTGAAGATTGACGTCTATTCTAAAG	35	2069	1,1%
	7 TTATCTTCAGGTTCCGA	17	144	0,1%	7 TCTTCGGAACCTGAAGATTGACGTT	25	1939	1,0%
	8 TTATCTTCAGGTTCCGAA	18	105	0,1%	8 CTTCGGAACCTGAAGATTGACG	22	1779	1,0%
			total	6,3%			total	93,7%
miC49_101									
Total expression 4E+05									
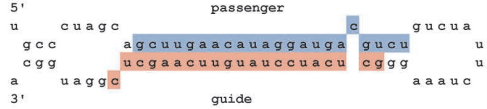	1 GCTCATCCTATGTTCAAGCTCG	22	142575	42,9%	1 AGCTTGAACATAGGATGACGTC	22	73189	22,0%
	2 CTCATCCTATGTTCAAGCTCG	21	34782	10,5%	2 AGCTTGAACATAGGATGACGT	21	14962	4,5%
	3 GCTCATCCTATGTTCAAGCTCT	22	21281	6,4%	3 AGCTTGAACATAGGATGACGTCT	23	8609	2,6%
	4 CTCATCCTATGTTCAAGCTCGG	22	5304	1,6%	4 GCTTGAACATAGGATGACGTC	21	6126	1,8%
	5 GCTCATCCTATGTTCAAGCTC	21	4672	1,4%	5 AGCTTGAACATAGGATGACG	20	4119	1,2%
	6 GCTCATCCTATGTTCAAGCTCGT	23	4018	1,2%	6 AGCTTGAACATAGGATGACGTCA	23	2509	0,8%
	7 CTCATCCTATGTTCAAGCTCGA	22	3894	1,2%	7 CAGCTTGAACATAGGATGACGT	22	2150	0,6%
	8 GCTCATCCTATGTTCAAGCTCGA	23	3608	1,1%	8 AGCTTGAACATAGGATGACGTT	22	905	0,3%
			total	66,2%			total	33,8%
miC50_101									
Total expression valı 1E+06									
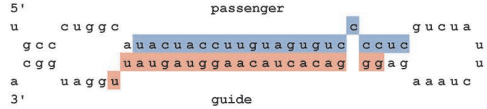	1 AGGGACACTACAAGGTAGTATT	22	455665	35,7%	1 TACTACCTTGTAGTGTCCCCTCG	23	349594	27,4%
	2 AGGGACACTACAAGGTAGTAT	21	73542	5,8%	2 TACTACCTTGTAGTGTCCCCTCGT	24	85200	6,7%
	3 AGGGACACTACAAGGTAGTA	20	15195	1,2%	3 TACTACCTTGTAGTGTCCCCTC	22	65164	5,1%
	4 GGGACACTACAAGGTAGTATT	21	12306	1,0%	4 TACTACCTTGTAGTGTCCCCTCT	23	62606	4,9%
	5 AGGGACACTACAAGGTAGTATTT	23	9717	0,8%	5 TACTACCTTGTAGTGTCCCCTCGA	24	61009	4,8%
	6 AGGGACACTACAAGGTAGTATTA	23	5461	0,4%	6 TACTACCTTGTAGTGTCCCCT	21	38667	3,0%
	7 GGGACACTACAAGGTAGTATTG	22	3372	0,3%	7 ATACTACCTTGTAGTGTCCCCTCT	24	20936	1,6%
	8 GGGACACTACAAGGTAGTAT	20	2861	0,2%	8 TACTACCTTGTAGTGTCCCCTCGTT	25	15182	1,2%
			total	45,3%				54,7%

Table S1. (continued)

miC	mature miRNA (Guide strand)	lenght	reads	% reads
miC38_451				
Total expression valu 62120				
1	AGCAATCTCTGTCTTGGCAACAGCC	25	12263	22,2%
2	AGCAATCTCTGTCTTGGCAACAGCCAT	27	11500	20,8%
3	AGCAATCTCTGTCTTGGCAACAGCCAAT	28	7931	14,3%
4	AGCAATCTCTGTCTTGGCAACAGCCAAGA	29	4655	8,4%
5	AGCAATCTCTGTCTTGGCAACAGCCAAG	28	3896	7,0%
6	AGCAATCTCTGTCTTGGCAACAGCCAA	27	2978	5,4%
7	AGCAATCTCTGTCTTGGCAACAGCCT	26	2973	5,4%
8	AGCAATCTCTGTCTTGGCAACAGC	23	2773	5,0%
9	AGCAATCTCTGTCTTGGCAACAGCCATT	28	2732	4,9%
10	AGCAATCTCTGTCTTGGCAACAGCCAAGT	29	1779	3,2%
11	AGCAATCTCTGTCTTGGCAACAGCCAAA	28	1048	1,9%
12	AGCAATCTCTGTCTTGGCAACA	22	805	1,5%
			total	100,0%
miC39_451				
Total expression valu 205272				
1	TAAAGCAATCTCTGTCTTGGCA	22	76916	39,1%
2	TAAAGCAATCTCTGTCTTGGCAA	23	75442	38,4%
3	TAAAGCAATCTCTGTCTTGGCAAA	24	13838	7,0%
4	TAAAGCAATCTCTGTCTTGGCAAAG	25	11180	5,7%
5	TAAAGCAATCTCTGTCTTGGC	21	6379	3,2%
6	TAAAGCAATCTCTGTCTTGGCAAT	24	2638	1,3%
7	AAAGCAATCTCTGTCTTGGCAA	22	2314	1,2%
8	TAAAGCAATCTCTGTCTTGGCAAAGA	26	2238	1,1%
9	TAAAGCAATCTCTGTCTTGGCAT	23	1613	0,8%
10	AAAGCAATCTCTGTCTTGGCA	21	1502	0,8%
11	AAAGCAATCTCTGTCTTGGCAAAG	24	1248	0,6%
12	TAAAGCAATCTCTGTCTTGGCAAAGT	26	1243	0,6%
			total	99,9%
miC43_451				
Total expression valu 13621				
1	TTGGCAAGAAAAGTTATTTCTCAAT	25	5312	42,7%
2	TTGGCAAGAAAAGTTATTTCTCAATAACT	29	1853	14,9%
3	TTGGCAAGAAAAGTTATTTCTCA	23	1387	11,1%
4	TTGGCAAGAAAAGTTATTTCTCAATAAC	28	1253	10,1%
5	TTGGCAAGAAAAGTTATTTCTCAATA	26	1015	8,2%
6	TTGGCAAGAAAAGTTATTTCTCAATAACTT	30	556	4,5%
7	TTGGCAAGAAAAGTTATTTCTCAA	24	525	4,2%
8	TTGGCAAGAAAAGTTATTTCTCAATAA	27	272	2,2%
9	TTGGCAAGAAAAGTTATTTCTC	22	228	1,8%
10	TTGGCAAGAAAAGTTATTTCT	23	54	0,4%
11				0,0%
12				0,0%
			total	100,0%
miC49_451				
Total expression valu 136609				
1	AGCTCATCCTATGTTCAAGCTCTT	24	76725	58,6%
2	AGCTCATCCTATGTTCAAGCTCTTG	25	14652	11,2%
3	AGCTCATCCTATGTTCAAGCTCTTGA	26	13511	10,3%
4	AGCTCATCCTATGTTCAAGCTCT	23	11970	9,1%
5	AGCTCATCCTATGTTCAAGCTCTTGAAC	28	6402	4,9%
6	AGCTCATCCTATGTTCAAGCTCTTGT	26	2060	1,6%
7	AGCTCATCCTATGTTCAAGCTCTTGAA	27	1982	1,5%
8	AGCTCATCCTATGTTCAAGCTCTTT	25	1321	1,0%
9	AGCTCATCCTATGTTCAAGCTCTTGAACA	29	693	0,5%
10	GCTCATCCTATGTTCAAGCTCTT	23	634	0,5%
11	AGCTCATCCTATGTTCAAGCTCTTA	25	534	0,4%
12	AGCTCATCCTATGTTCAAGCTCTTGAT	27	406	0,3%
			total	100,0%
miC50_451				
Total expression valu 10569				
1	TGGGACACTACAAGGTAGTATTCTACCTT	29	5354	55,9%
2	TGGGACACTACAAGGTAGTATTCTACCT	28	961	10,0%
3	TGGGACACTACAAGGTAGTATT	22	611	6,4%
4	TGGGACACTACAAGGTAGTATTC	23	560	5,8%
5	TGGGACACTACAAGGTAGTATTCTACCTTT	30	485	5,1%
6	TGGGACACTACAAGGTAGTATTCTACCTTG	30	461	4,8%
7	TGGGACACTACAAGGTAGTATTCT	24	284	3,0%
8	TGGGACACTACAAGGTAGTATTCTACC	27	274	2,9%
9	TGGGACACTACAAGGTAGTATTCTACCTTGT	31	252	2,6%
10	TGGGACACTACAAGGTAGTATTCTACCTTA	30	149	1,6%
11	TGGGACACTACAAGGTAGTATTCTACCTA	29	126	1,3%
12	GGGACACTACAAGGTAGTATTCTACCTT	28	73	0,8%
			total	100,0%

Table S2. miC-451 processing by NGS. Sequence distribution (%) of guide strands of reads mapping to miC38_451, miC39_451, miC43_451, miC49_451 and miC 50_451. Performed as described in table S1.

References

1. Miniarikova, J, Zanella, I, Huseinovic, A, van der Zon, T, Hanemaaijer, E, Martier, R, *et al.* (2016). Design, Characterization, and Lead Selection of Therapeutic miRNAs Targeting Huntingtin for Development of Gene Therapy for Huntington's Disease. *Mol. Ther. Nucleic Acids* **5**: e297.
2. Mayuko Yoda, Daniel Cifuentes, Natsuko Izumi, Yuriko Sakaguchi, Tsutomu Suzuki, AJG and YT (2013). PARN mediates 3′-end trimming of Argonaute2-cleaved precursor microRNAs **5**.

Chapter 3

Targeting RNA-mediated toxicity in *C9orf72* ALS/FTD by RNAi-based gene therapy

Raygene Martier[1,2], Jolanda M. Liefhebber[1], Ana García-Osta[3], Jana Miniarikova[1,2], Mar Cuadrado-Tejedor[3], Maria Espelosin[3], Susana Ursua[3], Harald Petry[1], Sander J. van Deventer[1,2], Melvin M. Evers[1], Pavlina Konstantinova[1]

[1]Department of Research & Development, uniQure Biopharma B.V., Amsterdam, the Netherlands;
[2]Department of Gastroenterology and Hepatology, Leiden University Medical Center, Leiden, the Netherlands;
[3]Neurosciences Division, Center for Applied Medical Research, CIMA, University of Navarra, Pamplona, Spain.

Mol. Ther. Nucleic. Acids. (2019); 16: 26-37

Summary

A hexanucleotide GGGGCC expansion in intron 1 of chromosome 9 open reading frame 72 (*C9orf72*) gene is the most frequent cause of amyotrophic lateral sclerosis (ALS) and frontotemporal dementia (FTD). The corresponding repeat-containing sense and antisense transcripts cause a gain of toxicity through accumulation of RNA foci in the nucleus and deposition of dipeptide-repeat (DPR) proteins in the cytoplasm of the affected cells. We have previously reported on the potential of engineered artificial miRNAs (miC) targeting *C9orf72* to reduce gain of toxicity caused by the repeat-containing transcripts. In the current study, we tested the silencing efficacy of AAV5-miC in human-derived iPSC-neurons and in an ALS mouse model. We demonstrated that AAV5-miC transduces different types of neuronal cells and can reduce the accumulation of repeat-containing *C9orf72* transcripts. Additionally, we demonstrated silencing of *C9orf72* in both nucleus and cytoplasm which has an added value for treatment of ALS/FTD patients. A proof of concept in an ALS mouse model demonstrated significant reduction of the repeat-containing *C9orf72* transcripts and RNA foci after treatment. Taken together, these findings support the feasibility of a gene therapy for ALS and FTD based on reduction of toxicity caused by the repeat-containing *C9orf72* transcripts.

Introduction

Amyotrophic lateral sclerosis (ALS) and frontotemporal dementia (FTD) are two severe neurodegenerative diseases with overlapping pathologic and genetic features, but distinct clinical features. ALS is the most common adult onset motor neuron degenerative disorder that affects mainly the upper and lower motor neurons in the brain and corticospinal tract.[1,2] FTD is a presenile dementia characterized by degeneration of neurons in the frontal and temporal lobes of the brain.[2,3] A significant number of patients develop both diseases (ALS-FTD).[4]

The most common genetic mutation in both ALS and FTD is a hexanucleotide GGGGCC (G_4C_2) repeat expansion in the first intron of the chromosome 9 open reading frame 72 (*C9orf72*) gene.[4–6] ALS and FTD patients display hundreds to a few thousand copies of the G_4C_2 repeat in the *C9orf72* gene.[5] The contribution of this mutation to the pathogenesis of both diseases has been debated for several years, with loss of *C9orf72* function (haploinsufficiency), gain of toxicity or a combination of both being implicated.[7,8] Reduced *C9orf72* mRNA levels in patients due to hypermethylation of the G_4C_2 repeat supports haploinsufficiency.[6,9] On the other hand, a causal role for RNA-mediated toxicity is supported by accumulation of the repeat-containing transcripts that fold into stable structures forming RNA foci enriched with RNA binding proteins in the nucleus.[5,10–13] RNA foci are detected in several repeat expansion diseases and can sequester RNA binding proteins. RNA foci produced from both the sense (G_4C_2) and antisense (G_2C_4) repeat transcripts are detected in tissues and in induced pluripotent stem cell (iPSC)-derived neurons from ALS and FTD patients, proving that the repeat region is bidirectionally transcribed.[14,15]

Gain of toxicity is also supported by repeat-associated non-AUG-dependent (RAN) translation of the sense and antisense repeat transcripts resulting in accumulation of five aberrant dipeptide-repeat (DPR) proteins (poly(GA), poly(GR), poly(GP), poly(PA), poly(PR)) in the cytoplasm, all with different toxicity profiles shown *in vitro* and *in vivo*.[12,16,17] In addition, DPRs disrupt the nucleocytoplasmic transport system of cells.[18,19] Furthermore, autopsy studies revealed that ~90% of *C9orf72* ALS and ~50% of FTD patients have cytoplasmic aggregation of the transactive response DNA-binding protein of 43 kDa (TDP-43; encoded by *TARDBP*).[8,20] Abnormal aggregation of P62 and ubiquitin have also been described in *C9orf72* related ALS and FTD patients.[21–23] A recently developed BAC transgenic mouse model expressing the human *C9orf72* including the expanded G_4C_2 repeat showed gain of toxicity features such as RNA foci, DPRs, TDP43 and p62 inclusions.[24] These mice also develop neurodegeneration and ALS/FTD-like phenotypes, suggesting that these inclusions result into gain of toxicity and contribute to the pathology observed in ALS and FTD.[24]

Regardless of the contribution of either RNA mediated toxicity or haploinsufficiency, a therapy reducing the repeat-containing transcripts could potentially translate into reduction of RNA foci and DPR proteins, slowing down the disease progression. Silencing

of *C9orf72* transcripts by RNA interference (RNAi) strategies such as duplex and single-stranded siRNAs or by the RNAse H mediated antisense oligonucleotides (ASOs) indeed resulted in reduction of RNA foci and DPR proteins in patient-derived iPSC-neurons and in mouse models.[15,25–28] Interestingly, targeting only the sense strand of *C9orf72* with ASOs not only reduced RNA foci but also rescued the disrupted nucleocytoplasmic transport in patient-derived iPSC-neurons.[19] Another promising strategy to achieve similar outcomes is by adeno-associated virus (AAV) delivered artificial microRNAs (miRNAs) engineered to target *C9orf72*. miRNAs are short non-coding RNAs that bind to a complementary mRNA through specific base pairing, inducing its degradation and/or translational repression. As AAVs express stable extrachromosomal nuclear episomes, the primary miRNA transcripts can be continually produced resulting in a longer-lasting therapeutic effect. The primary miRNA transcripts are processed into precursor miRNAs that are transported to the cytoplasm for further processing and incorporation into the RNA-induced silencing complex (RISC).[29] Thus, one mayor challenge to overcome for a miRNA-based gene therapy approach is targeting of the repeat-containing *C9orf72* transcripts within the cell nucleus. In one study, siRNAs which are also processed by RISC demonstrated silencing of *C9orf72* mRNA in patient derived iPSC neurons but the nuclear repeat-containing transcripts and RNA foci were unaffected, indicating a predominant efficacy in the cytoplasm.[15] We previously reported on miRNAs sequences (miC) that target the sense, antisense or both transcripts of *C9orf72* and demonstrated *in vitro* using luciferase reporter systems that all three approaches are feasible.[30] In addition, we used cell models and showed crucial evidence that miC can be functional in the cell nucleus, where the repeat-containing transcripts accumulates and form RNA foci.

In the current study, we investigated the efficacy of AAV-delivered miC on lowering of *C9orf72* in human derived iPSCs-neurons and in the Tg(*C9orf72*_3) line 112 mice as a proof of concept for an AAV-based gene therapy.[31] Different human neuronal cell types were transduced and the *C9orf72* lowering efficacy in the nucleus and cytoplasm was investigated. In addition, we showed evidence that miC targeting *C9orf72* in the mouse brain causes reduction of nuclear RNA foci. Our study provides strong evidence that AAV delivered miC can target *C9orf72* in the cell nucleus and may be promising to alleviate the RNA mediated toxicity in ALS and FTD patients.

Results

AAV5 can efficiently transduce neuronal and non-neuronal cells

The neuronal cells affected in ALS and FTD deviate. The main affected cells in ALS patients are motor neurons in the brain and spinal cord, whereas neurons in the frontal and temporal lobes of the brain are mainly affected in patients with FTD. About 15% of patients develop both ALS and FTD, where different types of neurons in the brain and spinal cord are affected.[32] Besides motor neurons, other CNS cell types such as astrocytes, microglia, and oligodendrocytes may contribute to the progression of the diseases.[33–36]

For example, it has been shown that astrocytes carrying the *C9orf72* hexanucleotide expansion are toxic to motor neurons.[33,35] Although the underlying mechanisms remain unclear, intercellular seeding and transmission of DPRs between the two cell types could be a contributing factor.[33,37] Thus, ideally a therapeutic drug for ALS and/or FTD should target a large variety of neuronal and non-neuronal cell types. We generated and characterized different human derived iPSC-neurons and astrocytes to validate the transduction of AAV5 in different CNS cell types (Figure 1). iPSCs were induced into a neural progenitor state and differentiated into frontal brain like neurons (FBN) or astrocytes (Supplementary Figure S1). In addition, commercially available mature dopaminergic neurons and motor neurons from a healthy person were obtained. Immunohistochemistry was performed and about 60% of FBN were ß-tubulin III positive and glial fibrillary acidic protein (GFAP) negative, implicating a successful differentiation rate of iPSCs into mature neurons. Similarly, mature astrocytes were ~90% GFAP positive, confirming a successful differentiation of iPSCs into astrocytes. Mature dopaminergic neurons were ~90% tyroxine hydroxylase (TH) positive, confirming successful differentiation. Mature motor neurons were also successfully differentiated as ~85% were choline acetyltransferase (CHAT) positive. Following transduction with AAV5-GFP, ~90% of all the different cell types expressed GFP (Figure 1a). Immunohistochemistry for GFP combined with either ß-tubulin III, TH, GFAP or CHAT antibodies confirmed that all four cell types were transduced by AAV5 (Figure 1b). To compare the AAV transduction tropism of the different cell types, we isolated DNA and RNA of transduced cells and quantitated vector copies and GFP mRNA expression in the cells (Figure 1c-d). A similar dose-dependent transduction efficiency was observed in all cell types and transduction correlated with GFP expression. Thus, AAV5 efficiently transduces different human CNS specific cell types including FBN, dopaminergic neurons, motor neurons and astrocytes and hence is a promising vector to deliver therapeutic genes to the CNS to treat neurogenerative diseases such as ALS and FTD.

C9orf72 expression is reduced in neuronal cells derived from an FTD patient

iPSCs from an FTD patient (ND42765) and a healthy non-diseased person (ND42245) were differentiated into FBN (FTD-FBN) and astrocytes to compare the levels of *C9orf72* mRNA and repeat-containing transcripts (Supplementary Figure S1). RT-qPCR was performed 2 weeks after maturation for total *C9orf72* mRNA (detecting all transcript variants), and the sense intronic transcripts (detecting sense transcripts containing G_4C_2 repeat) to compare the expression levels in these cells. Primers amplifying a region spanning exon 2 to exon 4 were used to detect total *C9orf72* mRNA (Figure 2a).[10] The sense intronic transcripts were detected with primers amplifying a region in intron 1.[10] The levels of total *C9orf72* mRNA were significantly reduced in the FTD-patient derived cells: A reduction of ~60% was observed in FBN and ~25% in astrocytes from the FTD patient as compared to healthy cells (Figure 2b). Interestingly, although at a low level, sense intronic transcript

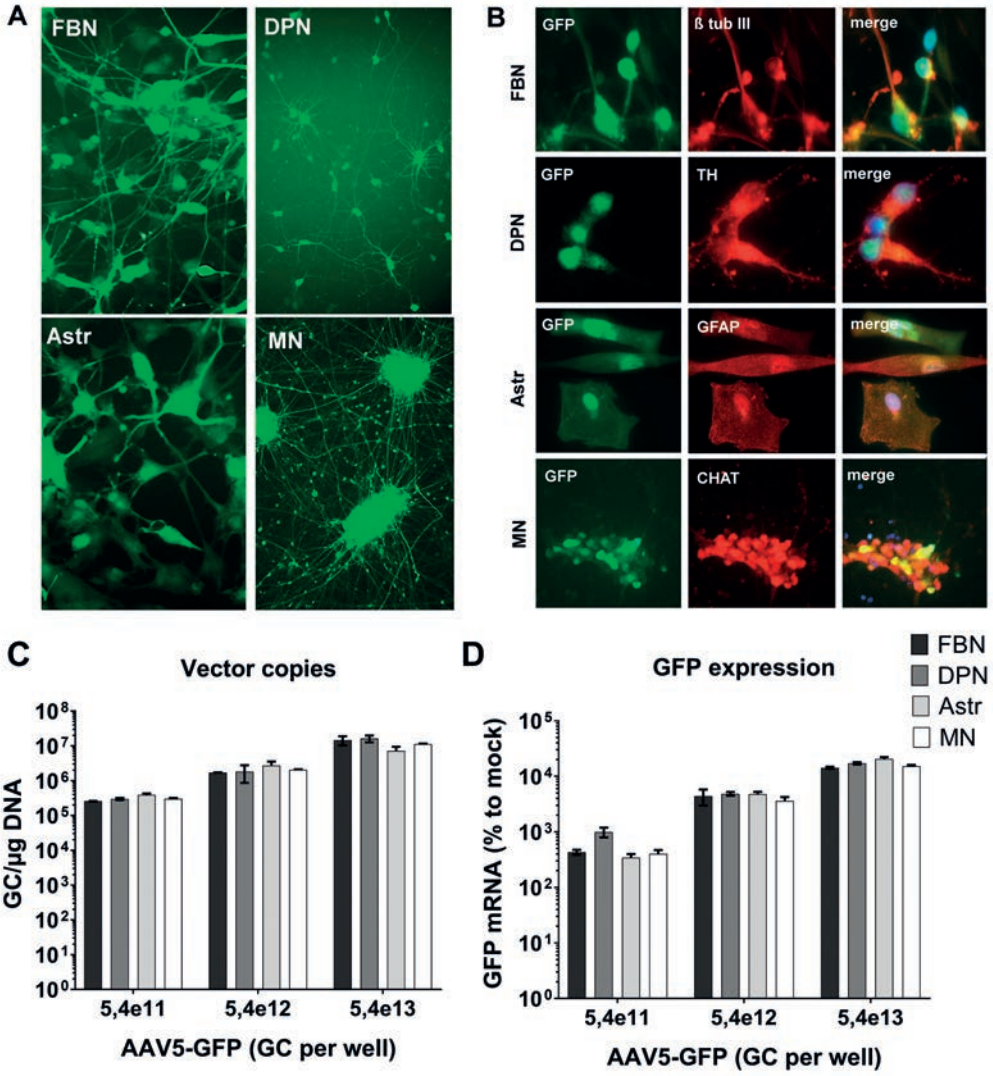

Figure 1. Transduction of different iPSC-derived cells by AAV5. a) Human iPSCs were differentiated into mature frontal brain like neurons (FBN), dopaminergic neurons (DPN), astrocytes (Astr) and motor neurons (MN). The cells were transduced with 5e12 genomic copies (GC) of AAV5-CAG-GFP and live cell imaging was performed at 2 weeks post transduction. b) Characterization of iPSC-derived cells. FBN, DPN, Astr and MN were transduced with AAV5-CAG-GFP and fixed at 2 weeks post transduction. Immunohistochemistry was performed with antibodies detecting β-tubulin III (β tub III) for mature FBN, tyrosine hydroxylase (TH) for mature DPN, glial fibrillary acidic protein (GFAP) for mature astrocytes and choline acetyltransferase (ChAT) for mature MN. c-d) Transduction efficiency of AAV5 in iPSC-derived neurons. FBN, DPN, Astr and MN were transduced with increasing doses of AAV5-CAG-GFP. The vector copy distribution and GFP mRNA expression were evaluated at 2 weeks post transduction. Vector copies were calculated using a standard curve. For GFP mRNA expression, the input of RNA was corrected for GAPDH and expression was calculated relative to cells treated with the formulation buffer (mock).

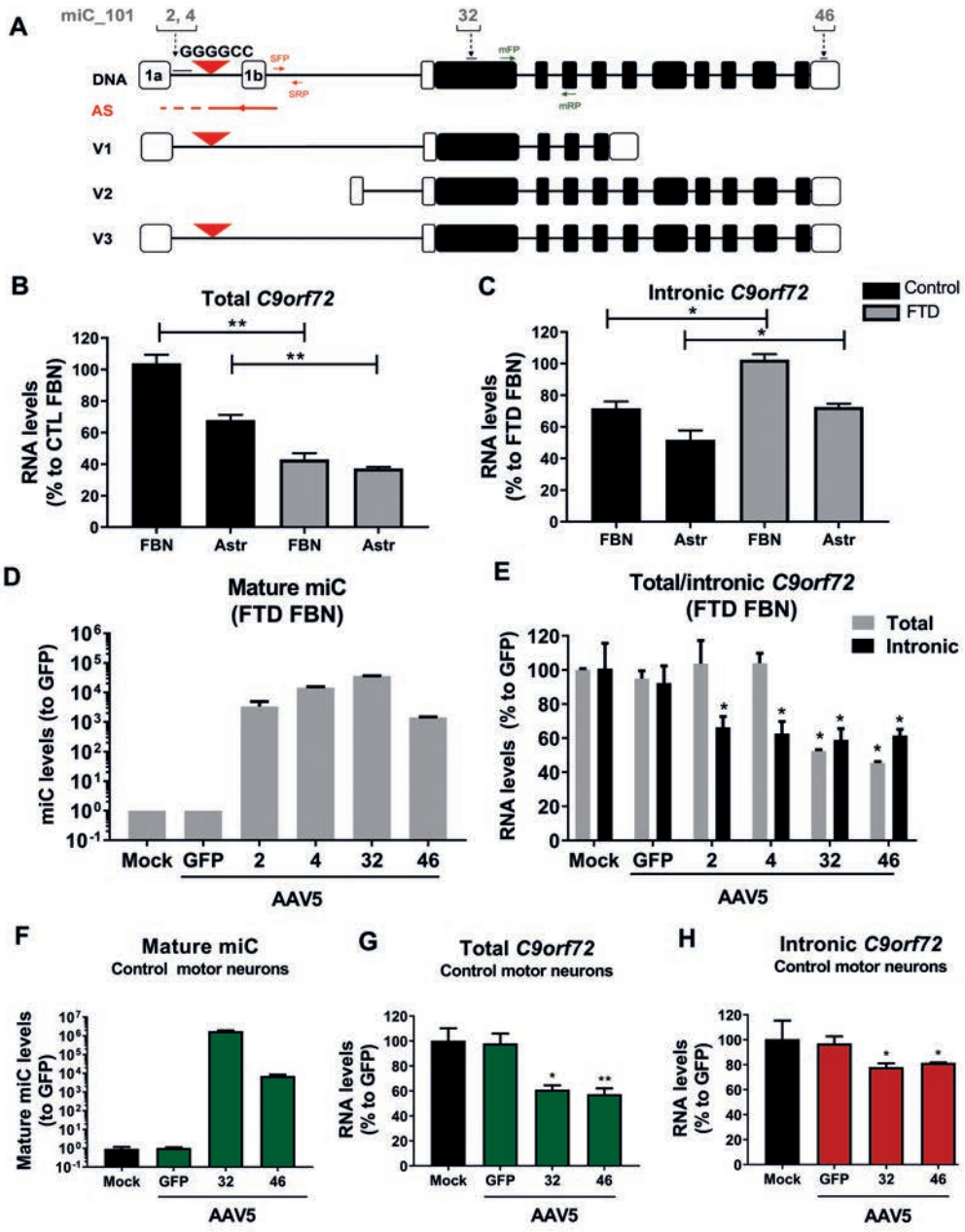

Figure 2. Silencing of *C9orf72* in iPSC-neurons by AAV5-miC. a) Schematic of *C9orf72* gene and location of the miC binding sites. The *C9orf72* gene consists of 12 exons, including two alternatively spliced exon 1a and exon 1b. The G_4C_2 expansion is in the first intron between exon 1a and 1b. the gene produces three sense transcripts (V1, V2 and V3) and an antisense transcript. miC candidates were designed with binding sites in intron 1 (miC2 and miC4), exon 2 (miC32) and exon 11 (miC46). Primersets in intron 1 were used to detect the sense intronic transcripts of *C9orf72* (SFP-SRP). Total *C9orf72 mRNA* was detected with primers spanning exon 2 and exon 4 (mFP-mRP) as described

by others.[10] b-c) Expression of *C9orf72* mRNA and sense intronic transcripts in FBN and Astrocytes. iPSCs were differentiated into FBN and astrocytes. RNA was isolated from cells after 2 weeks of maturation and RT-qPCR was performed to detect the endogenous expressed total *C9orf72 mRNA* and sense intronic transcripts (intronic *C9orf72*). The RNA input levels were corrected to GAPDH and calculated relative to the cell line with the highest expression of *C9orf72* (FBN). Error bars indicate the mean of two independent experiments. Data were evaluated using Student's t test: (*p < 0.05; **p < 0.01). d) Expression of the mature miC guide strands in FBN after transduction with AAV5. Mature FTD FBNs were transduced with 2e12 gc of AAV5-miC2, AAV5-miC4, AAV5-miC32 and AAV5-miC46. Cells treated with the formulation buffer (mock) or AAV5-GFP served as controls. RNA was isolated 7 days post-transduction and expression of the mature miC2, miC4, miC32 and miC46 were determined by TaqMan. MicroRNA input levels were normalized to U6 small nuclear RNA and set relative to cells treated with AAV5-GFP. e) Silencing of *C9orf72* mRNA and sense intronic transcripts in iPSC derived FBNs. Mature FTD FBNs were transduced with 2e12 gc of AAV5-miC2, AAV5-miC4, AAV5-miC32 and AAV5-miC46. RNA was isolated 7 days post-transduction. The levels of total *C9orf72* mRNA and the sense intronic transcripts were determined by RT-qPCR. mRNA input was normalized to GAPDH and set relative to cells treated with AAV5-GFP. Data were evaluated using a one-way ANOVA with Dunnett's multiple comparison test (*p < 0.05) to compare cells treated with AAV5-miC to AAV5-GFP. f) miC32 and miC46 expression in transduced motor neurons. Healthy motor neurons differentiated from human iPSCs were transduced with AAV5-GFP, AAV5-miC32 and AAV5-miC46 for two weeks. Total RNA was isolated and small RNA TaqMan was performed to detect the mature miC32 and miC46 as described in (d). g-h) *C9orf72* reduction in motor neurons by AAV5-miC. RNA was isolated from transduced motor neurons two weeks post transduction and RT-qPCR was performed to detect the total *C9orf72* mRNA (g) and sense intronic transcripts (h) as described in (e). Error bars represent the mean of two independent experiments. Data were evaluated using a one-way ANOVA with Dunnett's multiple comparison test (*p < 0.05; **p < 0.01) to compare cells treated with AAV5-miC to AAV5-GFP.

levels were increased by ~ 30% in FBN and ~20% in astrocytes of the FTD patient cells as compared to healthy cells (Figure 2c). Thus, while total *C9orf72* mRNA levels were reduced, sense intronic transcripts seems to accumulate in iPSC-derived FBNs and astrocytes from the FTD patient.

AAV5-miC can lower the repeat-containing transcripts of *C9orf72* in iPSC-neurons

Sequences on the human *C9orf72* were previously selected to design artificial anti-*C9orf72*-targeting miRNAs (miC).[30] The miC sequences were embedded in the primary miR-101 and/or miR-451 scaffold by replacing the naturally expressed guide strand sequences. Four lead miC candidates were selected in the miR-101 scaffold based on their efficacy on reporter genes and their ability to reduce the endogenously expressed *C9orf72* mRNA and sense intronic transcripts in cells.[30] miC32 and miC46 were designed to target *C9orf72* exon 2 and exon 11 respectively, targeting all sense *C9orf72* transcripts (Figure 2a). miC2 and miC4 were designed in intron 1 to selectively silence the sense G_4C_2 sense intronic transcripts.

To determine whether miC delivered by AAV5 is functional in patient-derived cells, FTD-FBNs were transduced with AAV5-miC2, AAV5-miC4, AAV5-miC32 and AAV5-

miC46. Two weeks following transduction, all four mature miC were expressed, suggesting a successful transduction by AAV5-miC and efficient processing into a mature miC (Figure 2d). Sense intronic transcript levels were reduced by ~40% in FBNs transduced with miC2 and miC4, while the *C9orf72* mRNA levels were not affected (Figure 2e). Thus, both candidates exclusively target the sense intronic transcripts while preserving normal levels of *C9orf72* mRNA. Of the candidates targeting the total *C9orf72* mRNA, both miC32 and miC46 reduced the levels of *C9orf72* mRNA (~50%) and the sense intronic transcript (~40%). Thus, the sense intronic transcripts could be also targeted by silencing total *C9orf72* mRNA.

Additionally, we investigated silencing of *C9orf72* in a healthy motor neuron cell line, as motor neurons are highly affected in ALS. The expression of *C9orf72* was first evaluated in control (non-transduced) motor neurons and both total and intronic *C9orf72* was detected. However, the intronic *C9orf72* expression in this cell line, that lacks the G_4C_2 expansion, was very low and slightly above the detection limit (data not shown). Having established that *C9orf72* can be detected in healthy motor neurons, the cells were transduced with AAV5-miC32 and AAV5-miC46 for 2 weeks. We found expression of miC32 and miC46, confirming that AAV5 efficiently transduces human motor neurons (Figure 2f). Consistently, we observed a ~40% reduction of total *C9orf72* mRNA by both miC candidates and a mild reduction of the intronic *C9orf72* (~20%) (Figure 2g-h). Altogether, we demonstrated reduction of total and intronic *C9orf72* levels in FBNs and motor neurons, confirming that both neuronal cell types are transduced, and that the miC candidates are effective in lowering *C9orf72* these cells.

Efficient silencing of *C9orf72* in the nucleus of iPSC derived neurons by AAV-miC

Accumulation of the G_4C_2 repeat-containing transcripts in the cell nucleus seems to highly contribute to the progression of both ALS and FTD. These transcripts form RNA foci in the cell nucleus that sequester RNA binding proteins and inhibit their function, or are transported to the cytoplasm for repeat-associated non-ATG (RAN) translation into toxic DPRs.[14,17,38,39] Thus, for a therapeutic approach, efficacy within the cell nucleus is required to effectively target the RNA-mediated toxicity in ALS and FTD. The processing of miRNAs occurs through a multi-step process involving a nuclear and cytoplasmic phase, but the mature miRNA product is produced in the cytoplasm.[29,40–42] Therefore, miRNAs were initially thought to be predominantly expressed and active in the cytoplasm. We previously demonstrated that active mature miC is also detected in the nucleus of cells transfected with miC constructs, but at lower levels than in the cytoplasm.[30] Here we evaluated whether transduction of iPSC neurons by AAV5-miC is sufficient to express the mature miC and reduce *C9orf72* levels in nucleus (Figure 3).

FTD-FBNs were transduced with AAV5-miC32 and AAV5-miC46 and after a week RNA was isolated from nuclear and cytoplasmic fractions to calculate the percentage of RNA transcripts in both cellular compartments. In control FBN, ~80% of total *C9orf72* mRNA

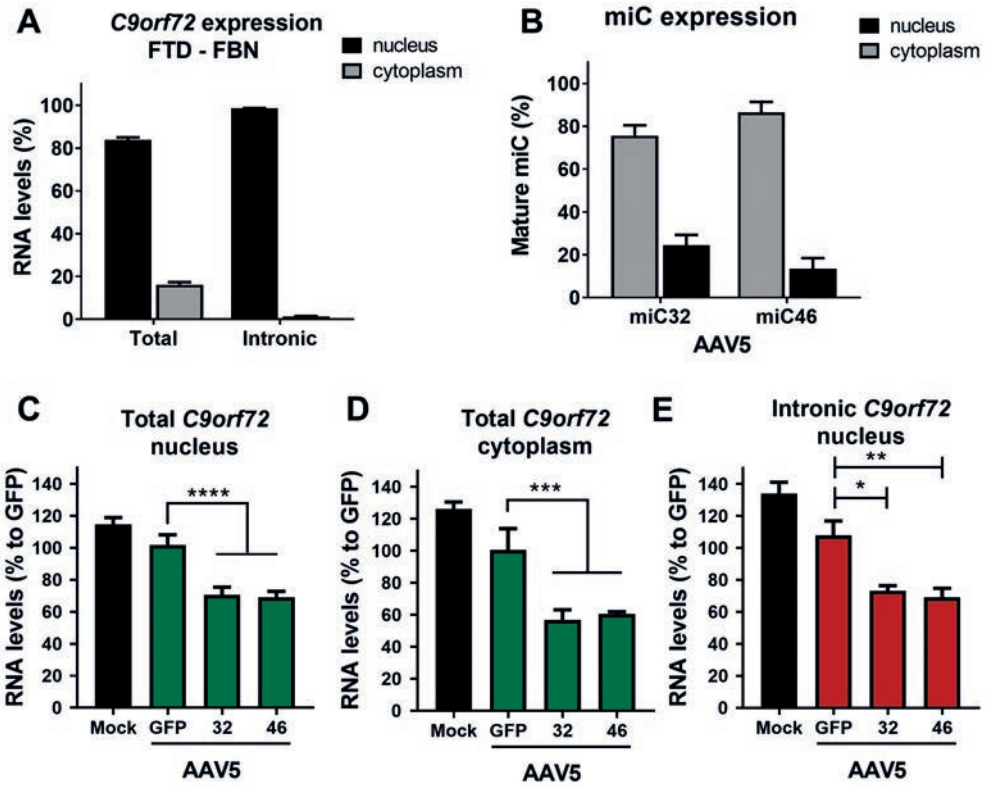

Figure 3. Reduction of *C9orf72* in the nucleus by miC. a) Nuclear and cytoplasmic expression of *C9orf72* in FTD FBN. RNA was isolated from nuclear and cytoplasmic fractions of mature FTD FBN and RT-qPCR was performed to detect the total *C9orf72* mRNA (total *C9orf72*) and sense intronic transcripts (intronic *C9orf72*). Total and intronic *C9orf72* mRNA levels were normalized to GAPDH (n=4). The sum of nuclear and cytoplasmic *C9orf72* expression values were set at 100%. (2^-Δct nuclear *C9orf72* RNA + 2^-Δct cytoplasmic *C9orf72* RNA = 100%). b) Mature miC expression in nucleus and cytoplasm. FTD FBNs were transduced with mock, AAV5-GFP, AAV5-miC31 and AAV5-miC46 for 7 days (n=4). RNA was isolated from nucleus and cytoplasm and expression of mature miC31 and miC46 were determined by small RNA TaqMan. mRNA input levels were normalized to GAPDH. The sum of nuclear and cytoplasmic miC expression values was set at 100%. c-d) Silencing of total *C9orf72* in nucleus and cytoplasm. RNA was isolated from nucleus (c) and cytoplasm (d) of FTD FBN transduced for 7 days with mock, AAV5-GFP, AAV5-miC31 and AAV5-miC46. mRNA levels were normalized to GAPDH and total *C9orf72* expression was determined relative to AAV5-GFP treated cells. e) Reduction of intronic *C9orf72* in nucleus of FTD FBN. Performed as described in (c-d) intronic *C9orf72* expression was determined relative to AAV5-GFP treated cells. Data were evaluated using a one-way ANOVA with Dunnett's multiple comparison test (*$p < 0.05$; **$p < 0.01$; ***$p < 0.001$; ****$p < 0.0001$) to compare cells treated with AAV5-miC to AAV5-GFP (n=4).

was detected in the nucleus and ~20% was measured in the cytoplasm, whereas, sense intronic transcripts were predominately (~95%) found in nucleus of FTD-FBNs (Figure 3a). Thus, both *C9orf72* mRNA and sense intronic transcript levels were significantly higher in the nucleus of FTD-FBNs. Next, the percentage of the mature miC and the silencing of *C9orf72* was determined in nucleus and cytoplasm after transducing FTD-FBNs with AAV5-miC32 and AAV5-miC46. About 20% of the mature miC32 was detected in the nucleus while ~80% was measured in the cytoplasm (Figure 3b). In cells treated with AAV5-miC46, ~10% of the mature miC was expressed in the nucleus and ~90% in the cytoplasm. Interestingly, both AAV5-miC32 and AAV5-miC46 resulted in ~30% reduction of *C9orf72* mRNA in the nucleus and ~40% reduction in the cytoplasm (Figure 3c-d). Consistently, ~25% reduction of the sense intronic transcripts was observed in the nucleus (Figure 3e). Our data show that the mature miC32 and miC46 can both shuttle from the cytoplasm to the cell nucleus and can reduce levels of both *C9orf72* mRNA and the sense intronic transcripts in the nucleus as well as in the cytoplasm.

AAV5-miC32 and AAV5-miC46 can both reduce *C9orf72* in Tg(*C9orf72_3*) line 112 mice

Having established the efficacy of AAV5-miC in different human neuronal cell types we next evaluated their efficacy *in vivo* in Tg(*C9orf72*_3) line 112 mice.[31] This mouse model is based on several tandem copies of the human *C9orf72* with repeat sizes ranging from 100-1000 repeats. Although the progressive neurodegeneration seen in ALS and FTD patients is not observed in these mice, they do exhibit some of the pathological features seen in patients such as RNA foci (starting at ~3 months of age) and poly GP protein (starting at ~6-20 months of age). Three months old mice were injected bilaterally in the striatum with AAV5-GFP, AAV5-miC32 and AAV5-miC46. Mice were sacrificed 6 weeks post injection to determine distribution of AAV5, mature miC expression, *C9orf72* lowering, and the effect of miC on RNA foci formation. A widespread distribution of AAV5 to the cortex, striatum and midbrain was observed after administration in the striatum (Figure 4a). A weak transduction of the cerebellum was observed while the spinal cord was not transduced. Consistent with the AAV5 distribution, small RNA TaqMan showed high expression of miC32 and miC46 in the cortex and striatum which resulted in a 20-40% lowering of *C9orf72* mRNA and the sense intronic transcripts (Figure 4b-d). Both AAV5-miC32 and AAV5-miC46 also target the mouse *C9orf72* ortholog (3110043O21 Rik) and indeed lowered the target 3110043O21 Rik. No behavioral and/or phenotypic changes were observed in mice treated with AAV5-miC32 or AAV5-miC46 (Supplementary Figure S3).

AAV5-miC32 and AAV5-miC46 are processed differently in mice brain

We further investigated the fidelity of miC processing in the mouse brain. Following transcription of the miC construct, the primary miR-101 is processed by Drosha cleavage

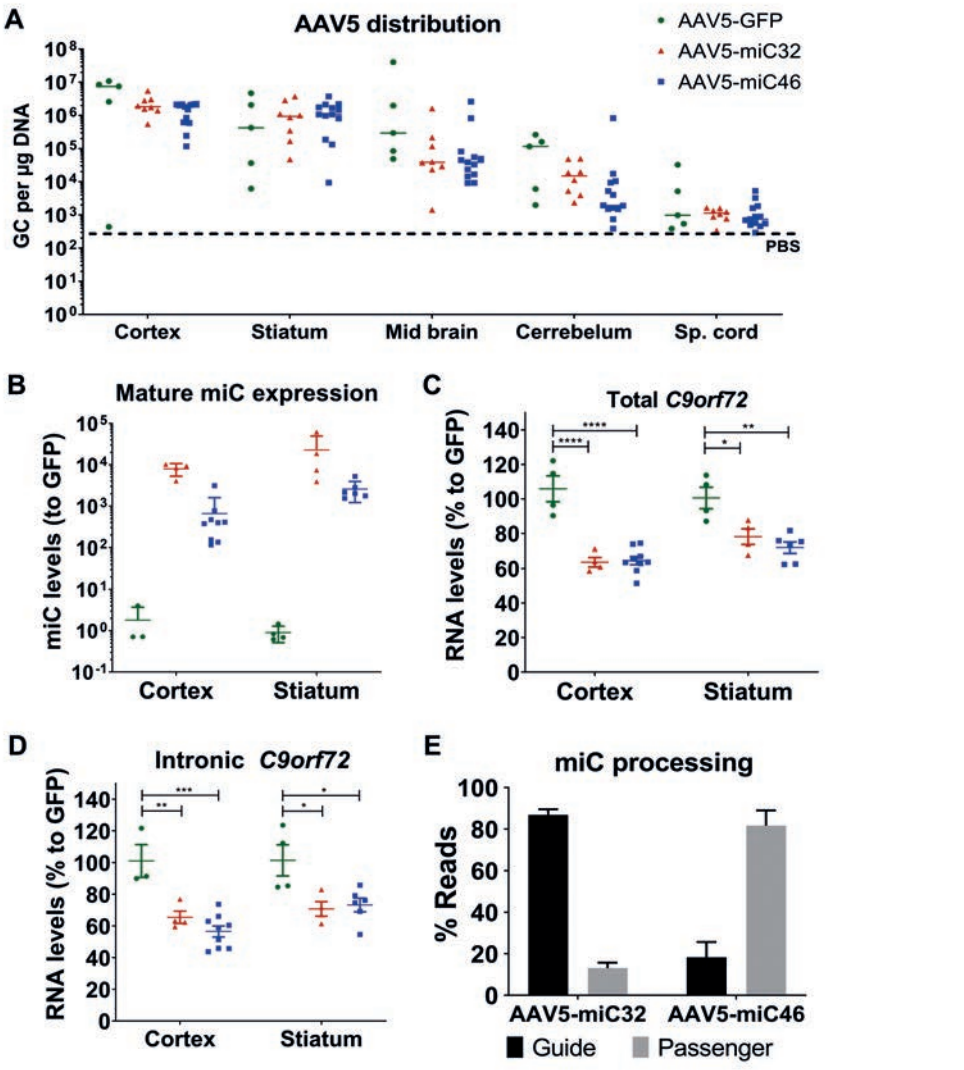

Figure 4. Reduction of *C9orf72* in C9BAC mice. a) Vector copy distribution of AAV5 upon intrastriatal injection. Three months old Tg(*C9orf72*_3) line 112 mice were injected with AAV5-GFP (5e10gc), AAV5-miC32 (5e10gc) and AAV5-miC46 (1e10gc) bilaterally in the striatum. All mice were sacrificed 6 weeks after surgeries and frontal cortex, striatum, mid brain, cerebellum and spinal cord were collected. DNA was isolated from the tissues and qPCR was performed with primers amplifying a 95bp fragment from the CAG promoter region. The GC per tissue was calculated using a standard curve. b) Expression of mature miC32 an miC46 guide strands cortex and striatum of Tg(*C9orf72*_3) line 112 mice. Performed as described in (a). Total RNA was isolated from the cortex and striatum for small RNA TaqMan. MicroRNA input levels was normalized to U6 small nuclear RNA and set relative to AAV-GFP treated mice. c-d) Lowering of total and intronic *C9orf72* by miC in Tg(*C9orf72*_3) line 112 mice. Performed as described in (a). Total RNA was isolated from the cortex and striatum and RT-qPCR was performed using primers for total *C9orf72* mRNA and sense intronic transcripts. RNA input levels were normalized to GAPDH and set relative to AAV-GFP mice. e) Processing of miC32 and miC46 in mice. Small RNA NGS was performed on RNA isolated from the striatum

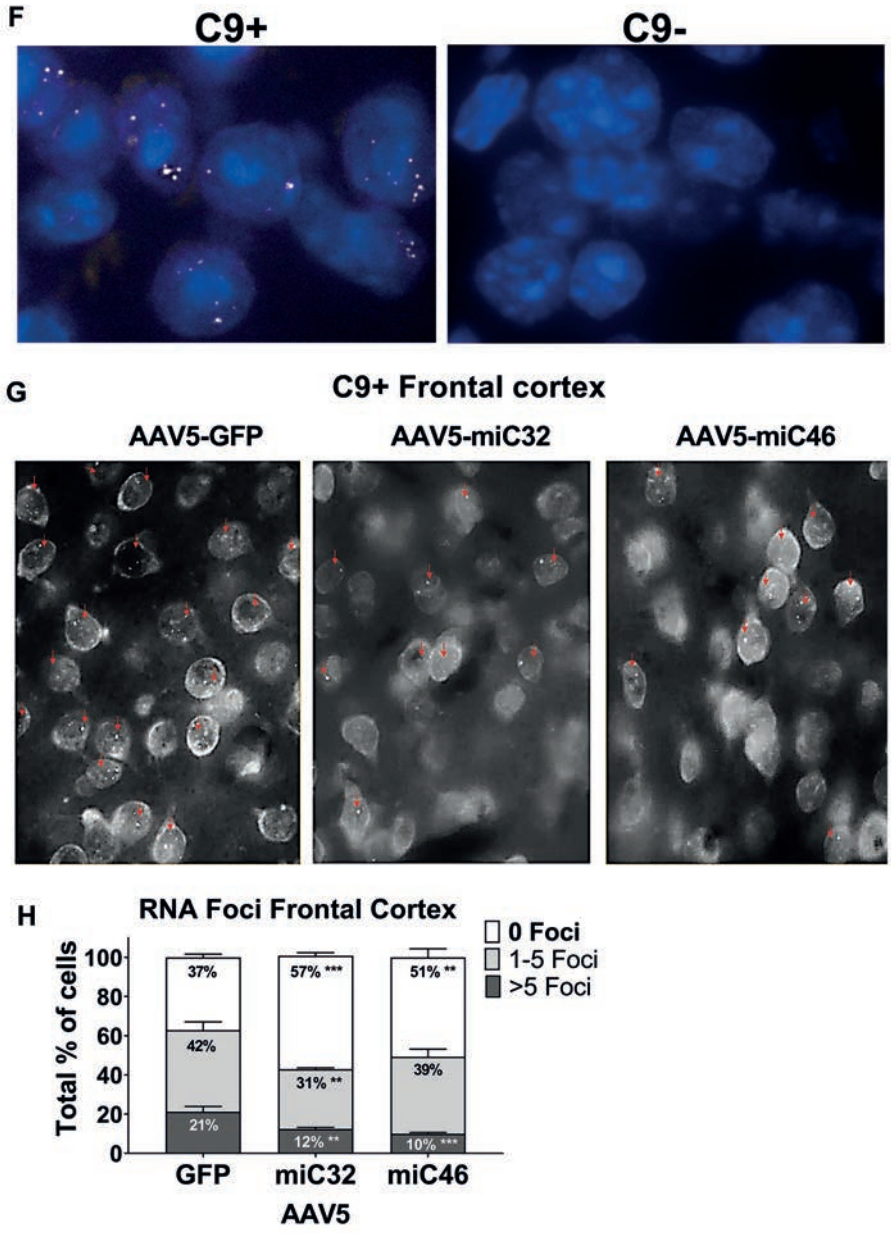

to determine the length and ratio of guide and passenger strands. f) detection of RNA foci in cortex of Tg(*C9orf72*_3) line 112 mice. Mice brain was frozen and sectioned in OCT. RNA FISH was performed using a TYE563-$(CCCCGG)_3$ LNA probe to detect the sense foci. Sense foci (shown as white spots) was detected in Tg(*C9orf72*_3) line 112 mice (C9+) but not in control littermates (C9-) g-h) Reduction of RNA foci in frontal cortex. Cells with 0, 1-5 or >5 foci were counted in control (AAV5-GFP) and treated groups (AAV5-miC32 and AAV5-miC46). The percentage of cells containing 0, 1-5 or >5 foci were calculated from 6 different images per treatment group (N=3). Red arrows show the cells that contain RNA foci. Data were evaluated using a one-way ANOVA with Dunnett's multiple comparison test (*$p < 0.05$; **$p < 0.01$; ***$p < 0.001$; ****$p < 0.0001$).

and then by Dicer cleavage into a miRNA duplex. The miRNA duplex is then separated, and the guide strand is usually incorporated into the RNA-induced silencing complex (RISC) while in most cases the passenger strand is degraded. The processing of the miC32 and miC46 was analyzed by small RNA sequencing to determine the ratio of guide and passenger strands that are produced. Small transcriptome analysis was performed on RNA isolated from the striatum of four mice that were injected with AAV5-miC32 or AAV5-miC46. For each sample, we obtained between 15–30 million small RNA reads that were subsequently adaptor-trimmed and aligned against the corresponding reference sequence. All reads shorter than 10 nucleotides, longer than 45 nucleotides, or represented less than 10 times were excluded from the analysis. miC32 was processed into predominantly guide strands (~87%) of 19-20 nucleotides long with low percentage of the passenger strand (~13%). However, miC46 processing yielded more passenger strands (~82%) of between 19-22 nucleotides long and low amounts (~18%) of guide strands (Figure 4e, Supplementary Table S1).

AAV5-miC reduces RNA foci in Tg(*C9orf72_3*) line 112 mice

RNA foci formation by the repeat-containing transcripts is considered a hallmark of the RNA mediated toxicity in ALS/FTD.[4,11,13,14] Fluorescence in situ hybridization (FISH) using a TYE563-$(C_4G_2)_3$ locked nucleic acid (LNA) probe showed that ~60-80% of cells in cortex, hippocampus and cerebellum of the Tg(*C9orf72*_3) line 112 mice contained RNA foci (fig. 4f).[31] After confirming the presence of sense and antisense RNA foci in the cortex, hippocampus and cerebellum, the efficacy of AAV5-miC32 and AAV5-miC46 to reduce RNA foci was determined. Both miC candidates caused a significant drop of sense RNA foci in cortex and hippocampus and the number of cells containing RNA foci, as well in as the total amount of RNA foci per cell (Figure 4g-h, Supplementary Figure S2). AAV5-miC32 resulted in a 20% drop of cells containing RNA foci and the number of cells containing 1-5 RNA foci and >5 RNA foci were reduced by 11% and 9% respectively. Similarly, AAV5-miC46 treatment resulted in 14% reduction of foci-containing cells, 3% reduction in cells containing 1-5 foci and 11% reduction in cell containing >5 RNA foci. Hence, these data confirm that AAV5 delivered miC candidates against total *C9orf72* mRNA are functional in reducing nuclear sense RNA foci in brain tissues of the Tg(*C9orf72*_3) line 112 mice.

Overall, we demonstrated that AAV5 can transduce different CNS cell types relevant for ALS/FTD treatment and that miC candidates targeting *C9orf72* are successfully delivered and are functional in mice brain. Furthermore, we showed that total *C9orf72* mRNA and sense intronic *C9orf72* transcripts can be lowered in both nucleus and cytoplasm of cells, increasing the potential for achieving therapeutic benefit in patients.

Discussion

The intronic G_4C_2 repeat of *C9orf72* produces repeat-containing transcripts that cause RNA foci and DPR proteins which contribute to ALS/FTD pathology. Thus, a therapy reducing these gain of toxicity features could slow down disease progression in ALS/FTD patients. In the current study we provide evidence that AAV5-delivered miRNAs targeting *C9orf72* reduce gain of toxicity features caused by the G_4C_2 repeat in a murine model.

Initially described as a pure motor neuron disease, it is now thought that other cell types, including resident glial cells, are involved in ALS.[43,44] Abnormal neuropsychological testing is observed in ~50% of ALS patients, indicating that besides motor neurons, other neuronal cell types in the brain are affected.[32] In addition, some patients develop both ALS and FTD, affecting different types of neurons in the brain and spinal cord. Delivery of therapeutics to the affected cell types is a mayor challenge for ALS/FTD therapy. We demonstrated that AAV5 can transduce various cell types of the CNS that are relevant to both diseases.

We observed a reduction of *C9orf72* mRNA in astrocytes and FBN derived from an FTD patient compared to healthy cells. This finding was consistent with several other studies that reported a reduction of *C9orf72* mRNA and protein in iPSC neurons, and in brain and spinal cord tissues from *C9orf72* related ALS/FTD patients.[6,9,45–48] This reduction is caused by methylation of the repeat region of *C9orf72* which is located in or near the promotor region, leading to transcription inhibition.[49–51] However, *C9orf72* haploinsufficiency alone is most likely not sufficient to cause neurodegeneration. Reduction of *C9orf72* in mice was tolerable while complete elimination of *C9orf72* caused splenomegaly and enlarged lymph nodes but not neurodegeneration or mis-localization of TDP-43.[52–54]

Compared to *C9orf72* mRNA levels, the expression of sense intronic transcripts were low in FTD and control cells. Yet, sense intronic transcripts were increased in FTD cells as compared to healthy cells, consistent with what have been reported by others.[10] The elevated sense intronic transcript levels detected in the FTD cells seems to be caused by defective splicing of intron 1 due to presence of the G_4C_2 repeat.[5,55] The corresponding transcripts containing the G_4C_2 repeat may be protected from degradation which allow them to accumulate in the cell.[46,55–57] Despite a relatively low abundance as compared to *C9orf72* mRNA, the intronic transcripts could still be sufficient to accumulate into RNA foci over time.[30,49,55] Furthermore, it has been estimated that hundreds of protein products could be produced by a single mRNA, suggesting that even low levels of intronic transcripts are sufficient to cause accumulation of toxic DPR proteins in the cell.[9,58]

Several approaches such as antisense oligonucleotides, duplex and single-stranded siRNAs and small compounds have been tested and proved promising to reduce gain of toxicity features caused by the G_4C_2 repeat.[27,39,59] In the current study we investigated the feasibility for a miRNA-based gene therapy to obtain long-term silencing of the repeat-containing transcripts of *C9orf72*. Four AAV5-miC candidates were tested on human derived iPSC neurons and all four resulted in sufficient transduction to express

therapeutically relevant levels of the corresponding mature miC. Selective reduction of the sense intronic transcripts was achieved with miC targeting intron 1, without affecting normal *C9orf72* mRNA levels. This approach could prevent RNA-mediated toxicity without further reducing *C9orf72* protein. However, as sequence variations within intron 1 have been observed, genomic screening of patients for selection could be necessary when targeting this region.[60] Thus, sequence conservation of miC2 and miC4 targets should be determined in larger cohort studies. We previously used a publicly available RNAseq data of patients to investigate the conservation of miC2 and miC4 target sites in intron 1, but the intronic transcript levels detected were too low to determine their conservation.[30,61] The target sequences of miC32 and miC46, targeting either exon 2 or exon 11, were well conserved between the patients and both candidates also reduced levels of the sense intronic transcripts in iPSC-neurons. The reduction of sense intronic transcripts by miC32 and miC46 supports previous findings that intron 1 is still present in the mature *C9orf72* mRNA, suggesting defective splicing.[55] Although miC32 and miC46 also reduced the levels of normal *C9orf72* mRNA, its expression was not completely eliminated. Additionally, we observed transduction, mature miC expression and reduction of *C9orf72* mRNA in a healthy motor neuron cell line. As expected, the expression of the sense intronic transcripts in this cell line was very low as the repeat expansion is absent in healthy individuals.

Having established that miC delivered by AAV5 are effective in human derived iPSC neurons, we specifically studied their efficacy in the cell nucleus where *C9orf72* mRNA and intronic transcripts are predominantly expressed. Although the primary and precursor miRNAs originate from the cell nucleus, their transport to the cytoplasm to exert post transcriptional gene silencing via the RISC have been well described.[29,40,41,62] Indeed, most studies have initially focused on post transcriptional gene silencing of miRNAs in the cytoplasm. However, the discovery of several mature miRNA and RISC components enriched in the nucleus indicate that nuclear miRNAs do exists.[63] Additionally, several proteins mediating nucleus – cytoplasm shuttling of small RNAs have been identified.[63,64] We found ~5 times lower levels of mature miC in the nucleus compared to cytoplasm of transduced iPSC-neurons, but the nuclear miC levels were still sufficient to reduce the levels of *C9orf72* mRNA and the sense intronic transcripts in the nucleus. Thus, AAV-delivered miC can lower the repeat-containing transcripts that accumulate in the nucleus of ALS/FTD patients.

Moving forward to an *in vivo* proof of concept study, we tested the delivery and efficacy of AAV5-miC in the BAC transgenic Tg(*C9orf72*_3) line 112 mouse model.[31] These mice exhibit pathologic features such as sense and antisense RNA foci and poly GP protein but no TDP-43 or P62 inclusions. These mice also do not develop ALS and/or FTD-like phenotype in their lifespan, possibly due to lack of 5' and 3' regulatory elements needed to control sufficient expression of sense and antisense transcripts.[24,31] Intrastriatal injection of AAV5 resulted in a strong localized transduction on the injection site and surrounding areas including frontal cortex and midbrain area but was not sufficient to

transduce the spinal cord. Thus, further studies in larger animals are required to predict the best routes of injection into the CSF to transduce the brain and spinal cord of patients. Intrastriatal delivery of AAV5-miC caused high expression of mature miC and significant lowering of *C9orf72* mRNA and the sense intronic transcripts in the transduced areas. The efficacy of AAV5-miC in the nucleus was further confirmed by the finding of a significant reduction of nuclear sense RNA foci in the cortex and hippocampus, suggesting that the mature miC is functional in the nucleus of transduced neurons *in vivo*. Moreover, reduction of the mice *C9orf72* ortholog was also observed and was well tolerated in mice (3110043O21Rik). The processing of the miC in the mice brain revealed that miC32 has a low amount of passenger strand decreasing the risk for off target effects in comparison to miC46. In the present study all mice were sacrificed at 5 months of age and future studies in older mice that have more accumulation of poly GP proteins would be needed to investigate the effect of miC on the DPR protein accumulation. However, based on the observed reduction of the sense intronic transcripts, a reduction of poly GP protein would be expected as fewer repeat-containing transcripts are available to undergo RAN translation.

Taken together, these studies provide proof of concept for silencing of *C9orf72* by AAV5-miC in relevant cell types as a potential treatment approach for ALS/FTD. miC32 offers the superior profile as a candidate to reduce gain of toxicity in ALS/FTD due to the sense intronic transcripts. We showed nuclear and cytoplasmic silencing, increasing the potential for a therapeutic effect of a miC32-based gene therapy that silences *C9orf72*.

Material and methods

Cell culture

Human control (ND42245) and Frontotemporal Dementia (ND42765) iPSC cells derived from fibroblast were ordered from Coriell Biorepository and was cultured on Matrigel (corning) -coated 6 wells plates in mTeSR1 (STEMCELL). For embryoid body-based neural induction, iPS cells were seeded on AggreWell800 plates and cultured in STEMdiff Neural Induction Medium (STEMCELL) for 5 days with daily medium changes. Embryoid bodies were harvested and plated on 6 wells plates coated with poly-D-lysine (Sigma-Aldrich) and laminin (Sigm-Aldrich) in STEMdiff Neural Induction Medium for 7 days with daily medium changes. Rosettes were harvested with STEMdiff Neural Rosette Selection Reagent (STEMCELL) and plated on poly-D-lysine and laminin coated 6-wells plates in STEMdiff Neural Induction Medium for 24 hours. For differentiation into FBN, STEMdiff Neural Induction Medium was replaced for STEMdiff Neuron Differentiation Medium (STEMCELL) and neuroprogenitor cells were differentiated for 5 days. For differentiation into astrocytes, neuroprogenitor cells were differentiated in STEMdiff Astrocyte Differentiation Medium (STEMCELL). The neuroprogenitor cells were then plated on poly-D-lysine and laminin coated plates in STEMdiff Neuron Maturation Medium (STEMCELL) for one week

or STEMdiff Astrocytes Maturation Medium for 3 weeks. The mature FBN and astrocytes were stored in liquid nitrogen in Neuroprogenitor Freezing Medium (STEMCELL).

Cryopreserved non- diseased mature dopaminergic neurons (iCELL Dopaneurons, 01279, Cat# C1028, Lot# 102477) were ordered at FUJIFILM Cellular Dynamics, Inc. Cryopreserved non-diseased mature motor neurons (cat# 40HU-005, lot#400089) were ordered at iXCells Biotechnologies.

Generation of AAV5-miC vectors and transductions

The design and cloning of the miC constructs was performed as described previously.[30,65] The miC constructs were all expressed by the synthetic CMV early enhancer/chicken β actin (CAG) promotor. To produce AAV5, the CAG-miC2, CAG-miC4, CAG-miC32 and CAG-miC46 cassettes were obtained by digestion with restriction enzymes HindIII and PvuI and cloned in a uniQure transfer plasmid in order to generate an entry plasmid. The presence of the two inverted terminal repeats (ITRs) was confirmed by restriction digestion with SmaI. The ITR-CAG-miC cassettes were inserted in a recombinant baculovirus vector by homologous recombination in Spodoptera frugiperda Sf9 cells and clones were selected by plague purification and insert PCR. The recombinant baculovirus containing the ITR-CAG-miC were further amplified till P6 in Sf+ cells and screened for the best production and stability by PCR and RT-qPCR. To generate AAV5, Sf+ cells were triple infected with three different recombinant baculoviruses expressing the ITRs-CAG-miC, the replicon enzyme and the capsid protein. The cells were lysed 72 hours after the triple infection and the crude lysate was treated with 50U/ml Benzonase (Merck, Darmstadt, Germany) for 1 hour at 37 °C. AAV5 was purified on an AVB Sepharose column (GE Healthcare, Little Chalfont, UK) and eluted in a formulation buffer consisting of 1x PBS and 4% sucrose. the final titer was determined by RT-qPCR with primers amplifying a 95bp fragment from the CAG promoter region.

For transductions with AAV, FBN, DPN and MN were plated in 24-wells plates at $0.3*10^6$ cells per well. Astrocytes were plated at $0.1*10^6$ cells per well in STEMdiff Astrocyte Maturation Medium (STEMCELL) on matrigel coated plates. FBN were plated in STEMdiff Neuron Maturation Medium (STEMCELL) on poly-D-lysine and laminin coated plates. Dopaminergic neurons were plated in iCell Neural Base Medium (FUJIFILM Cellular Dynamics, Inc) according to the manufacturer's description on poly-D-lysine and laminin coated plates. Motor neurons were plated in Motor Neuron Maintenance Medium according to the manufacturer's description on matrigel coated plates. After 1 week of acclimation, cells were transduced with AAV5 for 1-2 weeks.

RNA and DNA isolation

For RNA, plated cells and tissues were lysed in 300ul TRizol. RNA was isolated from TRizol using the DIRECT-ZOL miniprep kit (cat# R2050, ZYMO Research). DNA was isolated using the DNeasy Blood & Tissue Kit (cat# 69506, Qiagen) according to the manufacturer's protocol.

Next-generation sequencing (NGS)

Small RNA sequencing libraries for the Illumina sequencing platform were generated using high-quality total RNA as input and the NEXTflex Small RNA Sequencing kit (Bioo Scientific, Austin, TX). Briefly, the small RNA species were subjected to ligation with 3′ and 5′ RNA adapters, first strand reverse transcription, and polymerase chain reaction (PCR) amplification. Sample-specific barcodes were introduced in the PCR step. The PCR products were separated on TBE-PAGE electrophoresis and the expected band around 30bp was recovered for each sample. The resulting sequencing libraries were quantified on a BioAnalyzer (Agilent, Santa Clara, CA). The libraries were multiplexed, clustered, and sequenced on an Illumina HiSeq 2000 (TruSeq v3 chemistry) with a single-read 36 cycles sequencing protocol and indexing. The sequencing run was analyzed with the Illumina CASAVA pipeline (v1.8.2), with demultiplexing based on sample-specific barcodes. The raw sequencing data produced was processed removing the sequence reads which were of too low quality (only "passing filter" reads were selected). In total, we generated between 15–35 mln reads per sample.

NGS data analysis

NGS small RNA raw data sets were analyzed using the CLC Genomics Workbench 8 (Qiagen). The obtained reads were adaptor-trimmed, which decreased the average read size from ~50bp to ~25bp. All reads containing ambiguity N symbols, reads shorter than 10 nt, longer than 45 nt, and reads represented less than 10 times were discarded. Next, the obtained unique small RNA reads were aligned to the reference sequences of the pre-miC9 constructs with a max. of 3 nt mismatches allowed. The percentages of reads based on the total number of reads matching the reference sequence were calculated (Supplementary Table S1).

RT-qPCR, and miRNA TaqMan assay

To determine *C9orf72* mRNA knockdown in cells, RNA was isolated, and first-strand complementary DNA was reverse transcribed using random hexamer primers with the Dynamo kit (Finnzymes, Espoo, Finland). Real-time PCR amplification was performed with primers to detect total *C9orf72* mRNA and the sense intronic transcripts of human. Total *C9orf72* mRNA was detected with primers: mFP 5′-CGGAAAGGAAGAATATGGATGC-3′, mRP 5′-CCATTACAGGAATCACTTCTCCA-3′ and probe mPRB 5′-AGCATTGGAATAATACTCTGACCCTGATCTTC-3′. The sense intronic transcripts was detected with primers SFP 5′-ACGCCTGCACAATTTCAGCCCAA-3′, SRP 5′-CAAGTCTGTGTCATCTCGGAGCTG-3′ and probe SPRB 5′-TGAGGGCAGCAATGCAAGTCGGTGTG-3′. The mRNA expression levels were normalized to human GAPDH (forward GAAGGTGAAGGTCGGAGTC, reverse GAAGATGGTGATGGGATTTC, probe CAAGCTTCCCGTTCTCAGCC) as an internal control. PCR reaction conditions were: 95 °C for 10 min, followed by 40 cycles of 15

s at 95 °C and 1 min at 60 °C. The assays were performed on ABI 7000 or ABI 7500 (Applied Biosystems, Foster City, CA, USA). Gene expression levels were normalized to GAPDH as an internal control, and the level of gene expression was calculated relative to control cells. To determine the expression of miC2, miC5, miC32 and miC46, Custom TaqMan® Small RNA Assay (ThemoFisher Scientific) was used; miC2 (assay ID CTEPR3R), miC4 (Assay ID: CTFVKNN), miC32 (assay ID CSGJPRB) and miC46 (assay ID CSHSNXJ). The RT reaction and TaqMan was performed according to the manufacturer's protocol.

Animals

Two breeding couples were ordered at the Jacksons Laboratory (stock number: 023099) and were kept and bred at the Neurosciences Division, Center for Applied Medical Research, CIMA, University of Navarra, Pamplona, Spain. The animals were housed 4–5 per cage with ad libitum access to food and water and maintained in a temperature controlled. environment on a 12-h dark/light cycle. All procedures were carried out in accordance with the current European and Spanish regulations (86/609/EEC; RD1201/2005). This study was approved by the Ethical Committee of the University of Navarra (no. 137/010).

Intrastriatal injection in Tg[C9orf72_3] line 112 mice

Surgeries were performed as described previously.[66] In brief, 3 months old mice were anesthetized with ketamine/xylazine (80/10 mg/kg, i.p.) and placed in a stereotactic frame. The scalp was shaved, and a longitudinal incision was made along the midline of the skull. The dorsal surface of the skull was then exposed, and two burr holes were drilled above the infusion sites. 2 or 5 µL of virus suspension or PBS solution (sham mice) was infused bilaterally to striatum (+0.8 mm AP, +/- 2 mm ML, -4.0 mm DV to bregma) according to the Paxinos and Watson mouse brain atlas (1998). A 5 µL Hamilton syringe (or 10 for ventricle surgeries) was used for the infusion (Hamilton Co., Reno, NV). The infusion rate was 0.2 µL/min and the needle remained in place for 5 min after the infusion for vector absorption. Finally, the site was stitched closed.

RNA foci fluorescence in situ hybridization (FISH)

RNA FISH was performed as described previously with some adjustments.[24,31,59] In brief, whole mice brain were fixed in 4% PFA for 1 week at 4°C. Brains were transferred into 15 ml tubes containing 10 ml of 30% PBS/sucrose andleft at 4°C until brains sinks to the bottom. The brains were then frozen in OCT and 25 µM thick cryostat sections were prepared. Brain sections were permeabilize in 0.2% Triton/1x PBS for 10 min and incubated for 1 hour in hybridization buffer (50% formamide, 10% dextran sulfate, 0.1 mg/mL yeast tRNA,2xSSC, 50 mM sodium phosphate) at 55°C. Hybridization was performed overnight with 40nm TYE563-$(C_4G_2)_3$ LNA probe in hybridization buffer at 55°C. Brain sections were then washed once with 40% formamide/1xSSC for 30 min at 55°C, 2x in 2x SSC/0.1% Tween-20 at room temperature for 5 min and 3x in

0.1x SSC for 10 min at room temperature. The slides were mounted with ProLong® Gold Antifade Mountant with DAPI (Invitrogen) and visualized using a LEICA DM2500 fluorescence microscope.

Statistical Analysis

Data were analyzed using Student's t test or ordinary one-way ANOVA to determine statistically significances. The p values are represented by the following number of asterisks: *p < 0.05; **p < 0.01; ***p < 0.001; ****p < 0.0001.

Acknowledgments

The authors would like to thank Ellen Broug and Eileen Sawyer for reviewing the manuscript.

Author contributions

Conceptualization: P.K and R.M. Investigation: R.M., J.M.L., A.O., J.M., Recourses: A.O, M.C, M.E, S.U.. Supervision, formal analysis, visualization and writing - initial draft: P.K, R.M., M.E., S.D Project Administration and Writing – review and editing: P.K., S.D., H.P. Funding acquisition: P.K.

References

1. Geser, F, Lee, VMY and Trojanowski, JQ (2010). Amyotrophic lateral sclerosis and frontotemporal lobar degeneration: A spectrum of TDP-43 proteinopathies. *Neuropathology* 30: 103–112.
2. Ferrari, R, Kapogiannis, D, Huey, ED and Momeni, P (2011). FTD and ALS: a tale of two diseases. *Curr. Alzheimer Res.* 8: 273–94.
3. Liscic, RM, Grinberg, LT, Zidar, J, Gitcho, MA and Cairns, NJ (2008). ALS and FTLD: Two faces of TDP-43 proteinopathy. *Eur. J. Neurol.* 15: 772–780.
4. Renton, AE, Majounie, E, Waite, A, Sim??n-S??nchez, J, Rollinson, S, Gibbs, JR, *et al.* (2011). A hexanucleotide repeat expansion in *C9orf72* is the cause of chromosome 9p21-linked ALS-FTD. *Neuron* 72: 257–268.
5. DeJesus-Hernandez, M, Mackenzie, IR, Boeve, BF, Boxer, AL, Baker, M, Rutherford, NJ, *et al.* (2011). Expanded GGGGCC Hexanucleotide Repeat in Noncoding Region of *C9orf72* Causes Chromosome 9p-Linked FTD and ALS. *Neuron* 72: 245–256.
6. Heutink, P, Jansen, IE and Lynes, EM (2014). C9orf72; abnormal RNA expression is the key. *Exp. Neurol.* 262: 102–110.
7. Gendron, TF, Belzil, V V., Zhang, YJ and Petrucelli, L (2014). Mechanisms of toxicity in C9FTLD/ALS. *Acta Neuropathol.* 127: 359–376.
8. Ling, SC, Polymenidou, M and Cleveland, DW (2013). Converging mechanisms in als and FTD: Disrupted RNA and protein homeostasis. *Neuron* 79: 416–438.
9. Shi, Y, Lin, S, Staats, KA, Li, Y, Chang, W-H, Hung, S-T, *et al.* (2018). Haploinsufficiency leads to neurodegeneration in *C9orf72* ALS/FTD human induced motor neurons. *Nat. Med.*doi:10.1038/nm.4490.
10. Liu, J, Hu, J, Ludlow, AT, Pham, JT, Shay, JW, Rothstein, JD, *et al.* (2017). c9orf72 Disease-Related Foci Are Each Composed of One Mutant Expanded Repeat RNA. *Cell Chem. Biol.* 24: 141–148.
11. Cooper-Knock, J, Walsh, MJ, Higginbottom, A, Highley, JR, Dickman, MJ, Edbauer, D, *et al.* (2014). Sequestration of multiple RNA recognition motif-containing proteins by C9orf72 repeat expansions. *Brain* 137: 2040–2051.
12. Zu, T, Liu, Y, Banez-Coronel, M, Reid, T, Pletnikova, O, Lewis, J, *et al.* (2013). RAN proteins and RNA foci from antisense transcripts in *C9orf72* ALS and frontotemporal dementia. *Proc. Natl. Acad. Sci.* 110: E4968–E4977.
13. Wojciechowska, M and Krzyzosiak, WJ (2011). Cellular toxicity of expanded RNA repeats: Focus on RNA foci. *Hum. Mol. Genet.* 20: 3811–3821.
14. Zu, T, Liu, Y, Banez-Coronel, M, Reid, T, Pletnikova, O, Lewis, J, *et al.* (2013). RAN proteins and RNA foci from antisense transcripts in *C9orf72* ALS and frontotemporal dementia. *Proc. Natl. Acad. Sci.* 110: E4968–E4977.
15. Lagier-Tourenne, C, Baughn, M, Rigo, F, Sun, S, Liu, P, Li, H-R, *et al.* (2013). Targeted degradation of sense and antisense C9orf72 RNA foci as therapy for ALS and frontotemporal degeneration. *Proc. Natl. Acad. Sci. U. S. A.* 110: E4530-9.
16. Freibaum, BD and Taylor, JP (2017). The Role of Dipeptide Repeats in *C9orf72*-Related ALS-FTD. *Front. Mol. Neurosci.* 10.
17. Ash, PEA, Bieniek, KF, Gendron, TF, Caulfield, T, Lin, WL, DeJesus-Hernandez, M, *et al.* (2013). Unconventional Translation of *C9orf72* GGGGCC Expansion Generates Insoluble Polypeptides Specific to c9FTD/ALS. *Neuron* 77: 639–646.
18. Jovičič, A, Mertens, J, Boeynaems, S, Bogaert, E, Chai, N, Yamada, SB, *et al.* (2015). Modifiers of C9orf72 dipeptide repeat toxicity connect nucleocytoplasmic transport defects to FTD/ALS. *Nat. Neurosci.* 19: 1226–1229.
19. Zhang, K, Donnelly, CJ, Haeusler, AR, Grima, JC, Machamer, JB, Steinwald, P, *et al.* (2015). The C9orf72 repeat expansion disrupts nucleocytoplasmic transport. *Nature* 525: 56–61.
20. Scaber, J and Talbot, K (2016). What is the role of TDP-43 in C9orf72-related amyotrophic

lateral sclerosis and frontemporal dementia? *Brain* 139: 3057–3059.

21. Gijselinck, I, Van Langenhove, T, van der Zee, J, Sleegers, K, Philtjens, S, Kleinberger, G, *et al.* (2012). A C9orf72 promoter repeat expansion in a Flanders-Belgian cohort with disorders of the frontotemporal lobar degeneration-amyotrophic lateral sclerosis spectrum: A gene identification study. *Lancet Neurol.* 11: 54–65.
22. Al-Sarraj, S, King, A, Troakes, C, Smith, B, Maekawa, S, Bodi, I, *et al.* (2011). P62 positive, TDP-43 negative, neuronal cytoplasmic and intranuclear inclusions in the cerebellum and hippocampus define the pathology of C9orf72-linked FTLD and MND/ALS. *Acta Neuropathol.* 122: 691–702.
23. Brettschneider, J, Van Deerlin, VM, Robinson, JL, Kwong, L, Lee, EB, Ali, YO, *et al.* (2012). Pattern of ubiquilin pathology in ALS and FTLD indicates presence of *C9orf72* hexanucleotide expansion. *Acta Neuropathol.* 123: 825–839.
24. Liu, Y, Pattamatta, A, Zu, T, Reid, T, Bardhi, O, Borchelt, DR, *et al.* (2016). C9orf72 BAC Mouse Model with Motor Deficits and Neurodegenerative Features of ALS/FTD. *Neuron* 90: 521–534.
25. Jiang, J, Zhu, Q, Gendron, TF, Saberi, S, McAlonis-Downes, M, Seelman, A, *et al.* (2016). Gain of Toxicity from ALS/FTD-Linked Repeat Expansions in *C9orf72* Is Alleviated by Antisense Oligonucleotides Targeting GGGGCC-Containing RNAs. *Neuron* 90: 535–550.
26. Gendron, TF, Chew, J, Stankowski, JN, Hayes, LR, Zhang, YJ, Prudencio, M, *et al.* (2017). Poly(GP) proteins are a useful pharmacodynamic marker for *C9orf72*-associated amyotrophic lateral sclerosis. *Sci. Transl. Med.* 9.
27. Hu, J, Rigo, F, Prakash, TP and Corey, DR (2017). Recognition of c*9orf72* Mutant RNA by Single-Stranded Silencing RNAs. *Nucleic Acid Ther.* 27: 87–94.
28. Hu, J, Liu, J, Li, L, Gagnon, KT and Corey, DR (2015). Engineering Duplex RNAs for Challenging Targets: Recognition of GGGGCC/CCCCGG Repeats at the ALS/FTD C9orf72 Locus. *Chem. Biol.* 22: 1505–1511.
29. Graves, P and Zeng, Y (2012). Biogenesis of Mammalian MicroRNAs: A Global View. *Genomics, Proteomics Bioinforma.* 10: 239–245.
30. Martier R, Liefhebber J, Miniarikova J, van der Zon T, Snapper J, Kolder I, Petry H, van Deventer S, Evers M, KP. Artificial microRNAs targeting *C9orf72* have the potential to reduce accumulation of the intra-nuclear transcripts in ALS and FTD patients. *Mol. Ther. - Nucleic Acids*.
31. O'Rourke, JG, Bogdanik, L, Muhammad, AKMG, Gendron, TF, Kim, KJ, Austin, A, *et al.* (2015). C9orf72 BAC Transgenic Mice Display Typical Pathologic Features of ALS/FTD. *Neuron* 88: 892–901.
32. Lee, S and Huang, EJ (2017). Modeling ALS and FTD with iPSC-derived neurons. *Brain Res.* 1656: 88–97.
33. Meyer, K, Ferraiuolo, L, Miranda, CJ, Likhite, S, McElroy, S, Renusch, S, *et al.* (2014). Direct conversion of patient fibroblasts demonstrates non-cell autonomous toxicity of astrocytes to motor neurons in familial and sporadic ALS. *Proc. Natl. Acad. Sci.* 111: 829–832.
34. Di Giorgio, FP, Boulting, GL, Bobrowicz, S and Eggan, KC (2008). Human Embryonic Stem Cell-Derived Motor Neurons Are Sensitive to the Toxic Effect of Glial Cells Carrying an ALS-Causing Mutation. *Cell Stem Cell* 3: 637–648.
35. Haidet-Phillips, AM, Hester, ME, Miranda, CJ, Meyer, K, Braun, L, Frakes, A, *et al.* (2011). Astrocytes from familial and sporadic ALS patients are toxic to motor neurons. *Nat. Biotechnol.* 29: 824–828.
36. Ilieva, H, Polymenidou, M and Cleveland, DW (2009). Non-cell autonomous toxicity in neurodegenerative disorders: ALS and beyond. *J. Cell Biol.* 187: 761–772.
37. Selvaraj, BT, Livesey, MR and Chandran, S (2017). Modeling the *C9orf72* repeat expansion mutation using human induced pluripotent stem cells. *Brain Pathol.* 27: 518–524.
38. Peters, OM, Cabrera, GT, Tran, H, Gendron, TF, McKeon, JE, Metterville, J, *et al.*

(2015). Human *C9orf72* Hexanucleotide Expansion Reproduces RNA Foci and Dipeptide Repeat Proteins but Not Neurodegeneration in BAC Transgenic Mice. *Neuron* 88: 902–909.

39. Jiang, J, Zhu, Q, Gendron, TF, Saberi, S, McAlonis-Downes, M, Seelman, A, *et al.* (2016). Gain of Toxicity from ALS/FTD-Linked Repeat Expansions in *C9orf72* Is Alleviated by Antisense Oligonucleotides Targeting GGGGCC-Containing RNAs. *Neuron* 90: 535–550.
40. Lee, Y, Kim, M, Han, J, Yeom, K-H, Lee, S, Baek, SH, *et al.* (2004). MicroRNA genes are transcribed by RNA polymerase II. *EMBO J.* 23: 4051–4060.
41. Kim, VN and Nam, JW (2006). Genomics of microRNA. *Trends Genet.* 22: 165–173.
42. Winter, J, Jung, S, Keller, S, Gregory, RI and Diederichs, S (2009). Many roads to maturity: microRNA biogenesis pathways and their regulation. *Nat. Cell Biol.* 11: 228–234.
43. Tyzack, G, Lakatos, A and Patani, R (2016). Human Stem Cell-Derived Astrocytes: Specification and Relevance for Neurological Disorders. *Curr. Stem Cell Reports* 2: 236–247.
44. Madill, M, McDonagh, K, Ma, J, Vajda, A, McLoughlin, P, O'Brien, T, *et al.* (2017). Amyotrophic lateral sclerosis patient iPSC-derived astrocytes impair autophagy via non-cell autonomous mechanisms. *Mol. Brain* 10.
45. Xu, Z, Poidevin, M, Li, X, Li, Y, Shu, L, Nelson, DL, *et al.* (2013). Expanded GGGGCC repeat RNA associated with amyotrophic lateral sclerosis and frontotemporal dementia causes neurodegeneration. *Proc. …* 110: pp 7778–7783.
46. Haeusler, AR, Donnelly, CJ, Periz, G, Simko, EAJ, Shaw, PG, Kim, MS, *et al.* (2014). C9orf72 nucleotide repeat structures initiate molecular cascades of disease. *Nature* 507: 195–200.
47. van Blitterswijk, M, Gendron, TF, Baker, MC, DeJesus-Hernandez, M, Finch, NCA, Brown, PH, *et al.* (2015). Novel clinical associations with specific *C9orf72* transcripts in patients with repeat expansions in *C9orf72*. *Acta Neuropathol.* 130: 863–876.
48. Donnelly, CJ, Zhang, PW, Pham, JT, Heusler, AR, Mistry, NA, Vidensky, S, *et al.* (2013). RNA Toxicity from the ALS/FTD *C9orf72* Expansion Is Mitigated by Antisense Intervention. *Neuron* 80: 415–428.
49. Rizzu, P, Blauwendraat, C, Heetveld, S, Lynes, EM, Castillo-Lizardo, M, Dhingra, A, *et al.* (2016). C9orf72 is differentially expressed in the central nervous system and myeloid cells and consistently reduced in C9orf72, MAPT and GRN mutation carriers. *Acta Neuropathol. Commun.* 4: 37.
50. Dodge, JC, Treleaven, CM, Fidler, JA, Hester, M, Haidet, A, Handy, C, *et al.* (2010). AAV4-mediated expression of IGF-1 and VEGF within cellular components of the ventricular system improves survival outcome in familial ALS mice. *Mol. Ther.* 18: 2075–84.
51. Rizzu, P, Blauwendraat, C, Heetveld, S, Lynes, EM, Castillo-Lizardo, M, Dhingra, A, *et al.* (2016). C9orf72 is differentially expressed in the central nervous system and myeloid cells and consistently reduced in C9orf72, MAPT and GRN mutation carriers. *Acta Neuropathol. Commun.* 4: 37.
52. Koppers, M, Blokhuis, AM, Westeneng, HJ, Terpstra, ML, Zundel, CAC, Vieira De Sá, R, *et al.* (2015). C9orf72 ablation in mice does not cause motor neuron degeneration or motor deficits. *Ann. Neurol.* 78: 426–438.
53. Sudria-Lopez, E, Koppers, M, de Wit, M, van der Meer, C, Westeneng, HJ, Zundel, CAC, *et al.* (2016). Full ablation of C9orf72 in mice causes immune system-related pathology and neoplastic events but no motor neuron defects. *Acta Neuropathol.* 132: 145–147.
54. O'Rourke, JG, Bogdanik, L, Yáñez, A, Lall, D, Wolf, AJ, Muhammad, AKMG, *et al.* (2016). C9orf72 is required for proper macrophage and microglial function in mice. *Science (80-.).* 351: 1324–1329.
55. Niblock, M, Smith, BN, Lee, Y-B, Sardone, V, Topp, S, Troakes, C, *et al.* (2016). Retention of hexanucleotide repeat-containing intron in C9orf72 mRNA: implications for the pathogenesis of ALS/FTD. *Acta Neuropathol. Commun.* 4: 18.

56. Fratta, P, Mizielinska, S, Nicoll, AJ, Zloh, M, Fisher, EMC, Parkinson, G, *et al.* (2012). C9orf72 hexanucleotide repeat associated with amyotrophic lateral sclerosis and frontotemporal dementia forms RNA G-quadruplexes. *Sci. Rep.* 2: 1016.
57. Reddy, K, Zamiri, B, Stanley, SYR, Macgregor, RB and Pearson, CE (2013). The disease-associated r(GGGGCC) nrepeat from the C9orf72 gene forms tract length-dependent uni- and multimolecular RNA G-quadruplex structures. *J. Biol. Chem.* 18: 9860–9866.
58. Schwanhüusser, B, Busse, D, Li, N, Dittmar, G, Schuchhardt, J, Wolf, J, *et al.* (2011). Global quantification of mammalian gene expression control. *Nature* 473: 337–342.
59. Su, Z, Zhang, Y, Gendron, TF, Bauer, PO, Chew, J, Yang, WY, *et al.* (2014). Discovery of a Biomarker and Lead Small Molecules to Target r(GGGGCC)-Associated Defects in c9FTD/ALS. *Neuron* 83: 1043–1050.
60. Nordin, A, Akimoto, C, Wuolikainen, A, Alstermark, H, Forsberg, K, Baumann, P, *et al.* (2017). Sequence variations in C9orf72 downstream of the hexanucleotide repeat region and its effect on repeat-primed PCR interpretation: a large multinational screening study. *Amyotroph. Lateral Scler. Front. Degener.* 18: 256–264.
61. Prudencio, M, Belzil, V V., Batra, R, Ross, CA, Gendron, TF, Pregent, LJ, *et al.* (2015). Distinct brain transcriptome profiles in C9orf72-associated and sporadic ALS. *Nat. Neurosci.* 18: 1175–1182.
62. Han, J, Lee, Y, Yeom, KH, Kim, YK, Jin, H and Kim, VN (2004). The Drosha-DGCR8 complex in primary microRNA processing. *Genes Dev.* 18: 3016–3027.
63. Liu, H, Lei, C, He, Q, Pan, Z, Xiao, D and Tao, Y (2018). Nuclear functions of mammalian MicroRNAs in gene regulation, immunity and cancer. *Mol. Cancer* 17.
64. Schraivogel, D and Meister, G (2014). Import routes and nuclear functions of Argonaute and other small RNA-silencing proteins. *Trends Biochem. Sci.* 39: 420–431.
65. Miniarikova, J, Zanella, I, Huseinovic, A, van der Zon, T, Hanemaaijer, E, Martier, R, *et al.* (2016). Design, Characterization, and Lead Selection of Therapeutic miRNAs Targeting Huntingtin for Development of Gene Therapy for Huntington's Disease. *Mol. Ther. Nucleic Acids* 5: e297.
66. Pascual-Lucas, M, Viana da Silva, S, Di Scala, M, Garcia-Barroso, C, Gonzalez-Aseguinolaza, G, Mulle, C, *et al.* (2014). Insulin-like growth factor 2 reverses memory and synaptic deficits in APP transgenic mice. *EMBO Mol. Med.* 6: 1246–1262.

Supplementary material

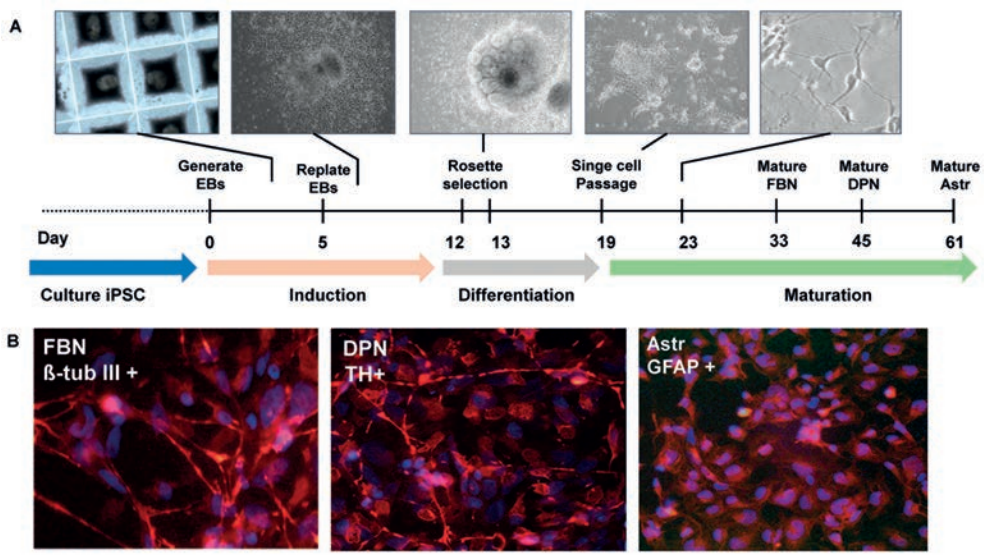

Figure S1. Differentiation and characterization of iPSC neurons. a) iPSC cells were seeded on AggreWell800 plates and cultured in STEMdiff Neural Induction Medium until day 5 to induce embryoid bodies formation. Embryoid bodies were harvested and replated in STEMdiff Neural Induction Medium for 7 days. At day 12, Rosettes were selected with rosette selection medium and differentiated in STEMdiff Neuron Differentiation medium or STEMdiff astrocyte Differentiation medium (STEMCELL) for 5 days. The cells were then maturated into mature FBN or astrocytes for one week.

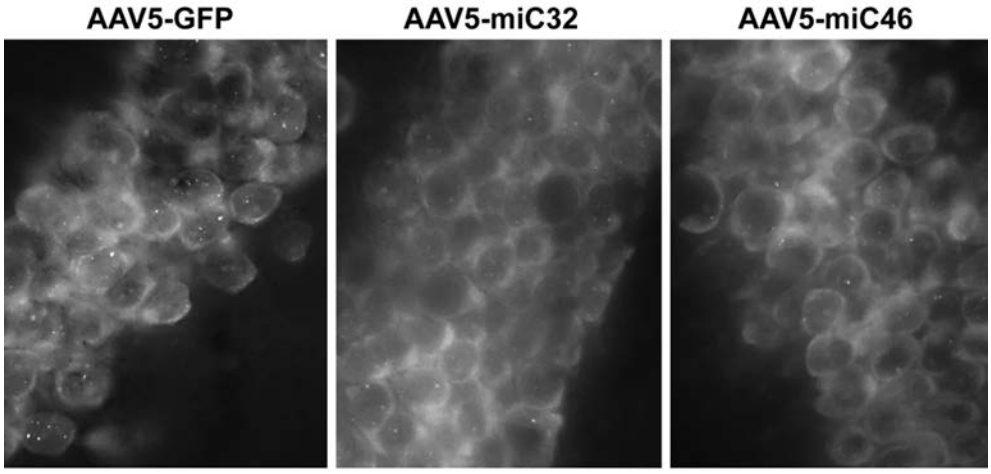

Figure S2. Reduction of RNA foci in hippocampus of Tg(*C9orf72_3*) line 112 mice.

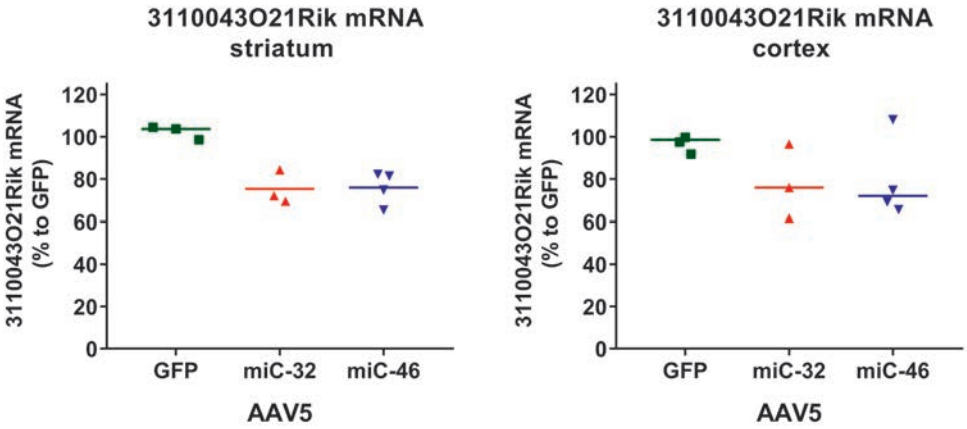

Figure S3. Reduction of the mouse *C9orf72* in striatum and cortex of C9BAC mice. Total RNA was isolated from the striatum and cortex of mice treated with AAV5-miC32 and AAV5-miC46. RT-qPCR was performed using primers to detect the mouse *C9orf72* ortholog (3110043O21Rik). RNA input levels were normalized to GAPDH and set relative to AAV-GFP treated mice.

miC precursor	mature miRNA (Guide strand)	lenght	reads	% reads	mature miRNA (passenger strand)	nt length	reads	% reads
C9BAC mouse striatum 333 (AAV5_miC32)								
Total expression values: 454435								
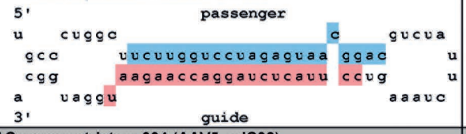	1 CCTTACTCTAGGACCAAGAA	20	317977	70,0%	1 CTTGGTCCTAGAGTAACGG	19	17591	3,9%
	2 CTTACTCTAGGACCAAGAA	19	22720	5,0%	2 CTTGGTCCTAGAGTAACGGA	20	11244	2,5%
	3 CTTACTCTAGGACCAAGAAT	20	9351	2,1%	3 CTTGGTCCTAGAGTAACGGAC	21	9383	2,1%
			total	77,0%			total	8,4%
C9BAC mouse striatum 334 (AAV5_miC32)								
Total expression values: 394961								
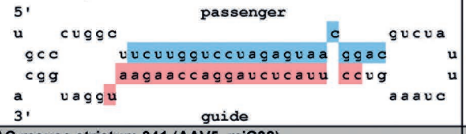	1 CCTTACTCTAGGACCAAGAA	20	255155	64,6%	1 CTTGGTCCTAGAGTAACGG	19	25219	6,4%
	2 CTTACTCTAGGACCAAGAA	19	18480	4,7%	2 CTTGGTCCTAGAGTAACG	18	14210	3,6%
	3 CTTACTCTAGGACCAAGAAT	20	7553	1,9%	3 CTTGGTCCTAGAGTAACGGA	21	13098	3,3%
			total	71,2%			total	13,3%
C9BAC mouse striatum 341 (AAV5_miC32)								
Total expression values: 257715								
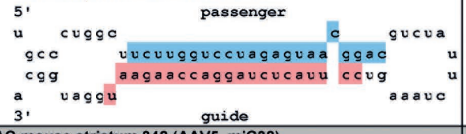	1 CCTTACTCTAGGACCAAGAA	20	169312	65,7%	1 CTTGGTCCTAGAGTAACGG	19	15032	5,8%
	2 CTTACTCTAGGACCAAGAA	19	12731	4,9%	2 CTTGGTCCTAGAGTAACGGA	20	9099	3,5%
	3 CTTACTCTAGGACCAAGAAT	20	4820	1,9%	3 CTTGGTCCTAGAGTAACG	18	8177	3,2%
			total	72,5%			total	12,5%
C9BAC mouse striatum 342 (AAV5_miC32)								
Total expression values: 423128								
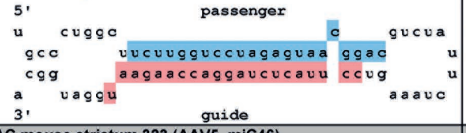	1 CCTTACTCTAGGACCAAGAA	20	283816	67,1%	1 CTTGGTCCTAGAGTAACGG	19	19759	4,7%
	2 CTTACTCTAGGACCAAGAA	19	22210	5,2%	2 CTTGGTCCTAGAGTAACGGA	20	12406	2,9%
	3 CTTACTCTAGGACCAAGAAT	20	8896	2,1%	3 CTTGGTCCTAGAGTAACGGAC	18	11793	2,8%
			total	74,4%			total	10,4%
C9BAC mouse striatum 323 (AAV5_miC46)								
Total expression values: 22153								
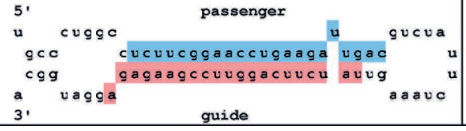	1 TATCTTCAGGTTCCGAAGAG	20	870	3,9%	1 CTTCGGAACCTGAAGATTGAC	21	16507	74,5%
	2 TATCTTCAGGTTCCGAA	17	343	1,5%	2 CTTCGGAACCTGAAGATTGA	20	1310	5,9%
	3 TATCTTCAGGTTCCGA	16	277	1,3%	3 CTTCGGAACCTGAAGATTGACG	22	460	2,1%
				6,7%			total	82,5%

Table S1. miC processing in mice brain. Sequence distribution (%) of guide- and passenger strands of reads mapping to miC32 and miC46. RNA was isolated from striatum of mice that were injected with AAV5-miC32 and AAV5-miC46 and small RNA NGS was performed. The scaffold is shown in Table

C9BAC mouse striatum 324 (AAV5_miC46)										
Total expression values: 14529										
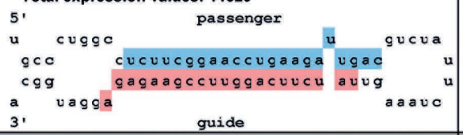	1 TATCTTCAGGTTCCGAAGAG	20	1873	12,9%	1 CTTCGGAACCTGAAGATTGAC	21	9167	63,1%
	2 TATCTTCAGGTTCCGAA	17	580	4,0%	2 CTTCGGAACCTGAAGATTGA	20	737	3,3%
	3 TATCTTCAGGTTCCGAAGA	19	196	1,3%	3 CTTCGGAACCTGAAGATTGACG	22	301	1,4%
				18,2%			total	67,8%
C9BAC mouse striatum 353 (AAV5_miC46)										
Total expression values: 20523										
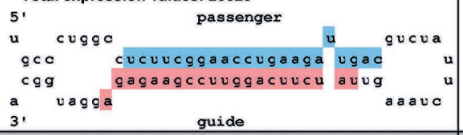	1 TATCTTCAGGTTCCGAAGAG	20	2751	13,4%	1 CTTCGGAACCTGAAGATTGAC	21	11058	53,9%
	2 TATCTTCAGGTTCCGAA	17	469	2,3%	2 CTTCGGAACCTGAAGATTGA	20	1297	6,3%
	3 TCAGGTTCCGAAGAG	15	239	1,2%	3 TCGGAACCTGAAGATTGAC	19	1012	4,9%
				16,9%			total	65,1%
C9BAC mouse striatum 358 (AAV5_miC46)										
Total expression values: 7758										
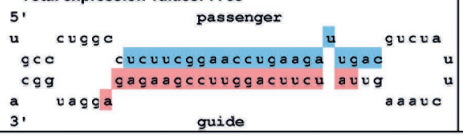	1 TATCTTCAGGTTCCGAAGAG	20	1386	17,9%	1 CTTCGGAACCTGAAGATTGAC	21	4871	62,8%
	2 TATCTTCAGGTTCCGAA	17	153	2,0%	2 CTTCGGAACCTGAAGATTGA	20	280	3,6%
	3 TATCTTCAGGTTCCGAAGA	19	132	1,7%	3 CTTCGGAACCTGAAGATTGACG	22	135	1,7%
				21,5%			total	68,1%

Table S1. (continued). the first column. Based on miRBase, the predicted guide and passenger strand sequences of the cellular pri-miRNA scaffolds are indicated in red and blue, respectively. The 5′ and 3′ flanking nucleotides are indicated in black. The three most abundant guide and passenger strand sequences are shown.

Chapter 4

Development of an AAV-based microRNA gene therapy to treat Machado-Joseph disease

Raygene Martier[1,2], Marina Sogorb-Gonzalez[1,2], Janice Stricker-Shaver[3], Jeannette Hübener-Schmid[3], Sonay Keskin[1], Jiri Klima[4], Lodewijk J. Toonen[1], Stefan Juhas[4], Jana Juhasova[4], Zdenka Ellederova[4], Jan Motlik[4], Eva Haas[3], Sander van Deventer[1,2], Pavlina Konstantinova[1], Huu Phuc Nguyen[5], Melvin M. Evers[1].

[1]Department of Research & Development, uniQure Biopharma B.V., Amsterdam, the Netherlands;
[2]Department of Gastroenterology and Hepatology, Leiden University Medical Center, Leiden, the Netherlands;
[3]Institute of Medical Genetics and Applied Genomics, University of Tuebingen, Tuebingen, Germany;
[4]Institute of Animal Physiology and Genetics, Libechov, Czech Republic
[5]Department of Human Genetics, Medical Faculty, Ruhr University Bochum, Bochum, Germany.

Mol Ther Methods Clin Dev. (2019); 15: 343-358

Abstract

Spinocerebellar ataxia type 3 (SCA3) or Machado-Joseph disease (MJD) is a progressive neurodegenerative disorder caused by a CAG expansion in the *ATXN3* gene. The expanded CAG repeat is translated into a prolonged polyglutamine repeat in the ataxin-3 protein and accumulates within inclusions, acquiring toxic properties, which results in degeneration of the cerebellum and brain stem.

In the current study, a non-allele specific *ATXN3* silencing approach was investigated using artificial microRNAs engineered to target various regions of the *ATXN3* gene (mi*ATXN3*). The mi*ATXN3* candidates were screened *in vitro* based on their silencing efficacy on a luciferase reporter co-expressing *ATXN3*. The three best mi*ATXN3* candidates were further tested for target engagement and potential off-target activity in induced-pluripotent stem cells (iPSC) differentiated into frontal brain-like neurons and in a SCA3 knock-in mouse model. Besides a strong reduction of *ATXN3* mRNA and protein, small RNA sequencing revealed efficient guide strand processing without passenger strands being produced. We used different methods to predict alteration of off-target genes upon AAV5-mi*ATXN3* treatment and found no evidence for unwanted effect.

Furthermore, we demonstrated in a large animal model, the minipig, that intrathecal delivery of AAV5 can transduce the main areas affected in SCA3 patients. These results proved a strong basis to move forward to investigate distribution, efficacy and safety of AAV5-miATXN3 in large animals.

Introduction

Spinocerebellar ataxia type 3 (SCA3), or Machado-Joseph disease (MJD), is the most common spinocerebellar ataxia worldwide and the second most common polyglutamine (polyQ) disease after Huntington disease (HD)[1–5]. Similar to the other polyQ disorders, SCA3 is inherited in an autosomal dominant manner, which is progressively neurodegenerative and ultimately fatal. SCA3 is caused by an expanded stretch of CAG triplets in the coding region of the *ATXN3* gene[6]. Healthy individuals have up to 44 CAG repeats, whilst affected individuals have between 52 and 86 glutamine repeats[6–8]. Repeat ranges from 45 to 51 are associated with incomplete penetrance of the disease. There is a clear correlation between CAG repeat size and age of onset, though CAG repeat length only accounts for approximately 50% of the total variability in age of onset[9]. Age at onset of SCA3 is highly variable but most commonly in the second to fifth decade, with an average age at onset of 40 years[10]. The CAG expansion has full penetration as patients harboring the mutation will inevitably develop the disease and have 50% chance to pass it on to their offspring.

The *ATXN3* transcript is alternatively spliced and produces different isoforms of the ataxin-3 protein[10,11]. The most abundant protein isoform contains an N-terminal Josephin domain which has a deubiquitinase activity and a C-terminal region that has three ubiquitin-interacting motifs (UIM), implicating a role of ataxin-3 in the ubiquitin-proteasome pathway[1,12]. The expanded CAG repeat in the *ATXN3* gene leads to formation of an expanded polyQ tract in the C-terminal region of the ataxin-3 protein. This mutated ataxin-3 protein causes toxic gain of function and leads to formation of neuronal aggregates which is a hallmark of polyQ diseases[13]. Despite extensive research the mechanisms leading to the observed neurodegeneration in SCA3 patients have not been completely elucidated. Ataxin-3 is normally ubiquitously found throughout the cell and can translocate from the cytoplasm to the nucleus and vice versa[14]. In neurons, ataxin-3 is predominantly expressed in the cytoplasm while the mutated protein mainly accumulates in the nucleus and acquires toxic properties [13–17]. Formation of neuronal aggregates comprising the mutated ataxin-3 protein is a typical neuropathological hallmark of the disease. Besides protein toxicity, RNA toxicity may also contribute to pathogenicity of the disease[18], as the expanded CAG repeat, and CUG-containing RNA molecules can form RNA foci, which colocalize with RNA binding proteins and sequester their functions. For example, colocalization of CAG and CUG-containing RNA foci with the muscleblind-like 1 (MBNL1) splicing factor in nuclei of both muscle cells and neurons resulted in inactivation of MBNL1, leading to dysregulation of alternative splicing[18–22].

Neuropathological studies have detected widespread neuronal loss in the cerebellum, thalamus, midbrain and spinal cord of SCA3 patients[17]. Although widespread pathology is reported in later disease stage of SCA3 patients, the general consensus is that the main neuropathology in SCA3 patients is located in the cerebellum and brain stem[23]. The main clinical symptom observed in SCA3 patients is progressive ataxia, affecting balance, gait and speech[18]. Other frequently described symptoms include pyramidal

signs, progressive external ophthalmoplegia, dysarthria, dysphagia, rigidity, distal muscle atrophies and double vision[2]. Most of the patients die due to pulmonary complications, usually within 6 to 29 years after onset, and up to now there is no disease modifying treatment available.[2425]

From a therapeutic standpoint, an advantage of monogenetic disorders such as SCA3 is that reducing expression of the responsible gene should result in alleviation of mutant RNA and protein toxicity[18]. Silencing approaches by RNA interference (RNAi) or antisense oligonucleotides (ASOs) are attractive to achieve silencing of the mutant ataxin-3. The silencing can be allele-specific; silencing only the mutant ataxin-3, or non-allele specific; silencing both wildtype and mutant allele. Both approaches demonstrated that neuropathology in SCA3 rodents can be improved[26–28].

In the current study, we investigated a non-allele specific RNAi based gene therapy for SCA3 patients with a potentially long-lived therapeutic effect. The therapeutic product is an adeno-associated virus (AAV) vector expressing a microRNA that binds *ATXN3* mRNA leading to its degradation via the RNA-induced silencing complex (RISC). Non-allele specific silencing of ataxin-3 by RNAi have been tested in wildtype and SCA3 rodent models and demonstrated improvement of the observed neuropathology[27]. This approach was well tolerated despite the concomitant reduction of the wildtype ataxin-3. We engineered artificial microRNAs (mi*ATXN3*) to target various exons within the *ATXN3* mRNA. The mi*ATXN3* candidates were incorporated in the primary-miR451 scaffold which has been extensively studied by us and proved to be safe in rodents, pigs and non-human primates[29–31]. By targeting both wildtype and mutant ataxin-3 and using a scaffold that is known to produce no passenger strands, we are aiming for a therapy to treat the whole SCA3 patient population while significantly reduce the risk for off-target effect. Since miR451 has not passenger activity, the effects of the passenger strand is completely eliminated. A preselection for the most efficient mi*ATXN3* candidates was performed *in vitro* on a luciferase (Luc) reporter. The best candidates were incorporated in AAV serotype 5 (AAV5) and their efficacies were tested in human-derived induced-pluripotent stem cells (iPSC)-neurons and in a knock-in SCA3 mouse model. We observed strong reduction of *ATXN3* mRNA and mutant ataxin-3 protein, suggesting that our AAV-microRNA-based approach could have therapeutic benefits in SCA3 human patients. In addition, we investigated the intrathecal delivery of AAV5 in a minipig and confirmed that the main areas affected in SCA3 patients are transduced at a therapeutically relevant dose. These data demonstrate that AAV-based RNAi gene therapy has potential for use in SCA3 treatment by lowering of the mutant ataxin-3 protein in the central nervous system.

Results

Design of artificial mi*ATXN3* constructs and prescreening on Luc reporter

Silencing of mutant *ATXN3* mRNA should result in alleviation of toxicity caused by the mutant ataxin-3 protein. Using this rationale, we engineered artificial microRNAs

complementary to various regions of the *ATXN3* gene aiming at a knockdown of *ATXN3* mRNA. Different regions of the human *ATXN3* gene were selected to design anti-*ATXN3* microRNAs (mi*ATXN3*) constructs (Figure 1a). All mi*ATXN3* constructs were designed to specifically target the human *ATXN3* transcripts with high to full conservation for non-human primates, mouse and rat *ATXN3*. The mi*ATXN3* sequences were embedded in the engineered pre-miR-451 scaffold and expressed by the ubiquitous CAG promoter that consists of the cytomegalovirus immediate-early enhancer fused to chicken β-actin promoter (Figure 1b). This promoter has been broadly used in central nervous system (CNS) indications, showing stable and high transgene expression[32]. To test the silencing efficacy of the mi*ATXN3* constructs, we designed a Luc reporter bearing complementary *ATXN3* target mRNA fused to the renilla luciferase (RL) gene (Figure 1c). The firefly luciferase (FL) gene was independently expressed from RL in the same reporter to correct for transfection efficiency. We co-transfected the mi*ATXN3* constructs with the Luc reporter and prescreened for the best candidates. mi*ATXN3*_7, mi*ATXN3*_9 and mi*ATXN3*_11 were selected for further testing as these candidates showed knockdown on the Luc reporter at lower concentrations and reached up to 80-90% knockdown efficiencies at higher concentrations (Figure 1D).

Strong silencing of endogenous *ATXN3* and ataxin-3 protein by miATXN3

We next investigated whether the selected mi*ATXN3* candidates were capable of reducing the endogenous levels of total *ATXN3* mRNA and protein in HEK293T cells. Cells were transfected with the mi*ATXN3*_7, mi*ATXN3*_9 or mi*ATXN3*_11 and the endogenous levels of *ATXN3* mRNA was determined 2 days post-transfection by quantitative reverse transcription PCR (RT-qPCR). A significant reduction was observed by all three mi*ATXN3* constructs (Figure 2a). The most effective candidate was mi*ATXN3*_9 with a silencing efficacy of 52%. Consistently, silencing of the *ATXN3* mRNA also resulted in significant reduction of ataxin-3 protein with up to 75% reduction achieved with mi*ATXN3*_9 (Figure 2b). Thus, all three selected candidates can reduce *ATXN3* mRNA and protein in transfected cells, mi*ATXN3*_9 being the most potent.

AAV5-mi*ATXN3* is highly effective in human iPSC-neurons

To further confirm the silencing of *ATXN3* in the context of a gene therapy for SCA3, we incorporated all three candidates in AAV5. Subsequently, increasing doses of AAV5-mi*ATXN3* were tested in iPSC-neurons. Human iPSCs were differentiated into frontal brain-like neurons which represent mainly neurons of the frontal cortex. About 90% of these neurons expressed beta tubulin III indicating a successful differentiation.[33] The cells were transduced with AAV5-mi*ATXN3*_7, AAV5-mi*ATXN3*_9 or AAV5-mi*ATXN3*_11 for two weeks. As shown previously, at this time point, about 80% of cells are GFP positive.[33] Following mi*ATXN3* transductions, the silencing efficacy of *ATXN3* mRNA was determined. *ATXN3* mRNA were reduced up to 65% in a dose dependent manner by all three mi*ATXN3*

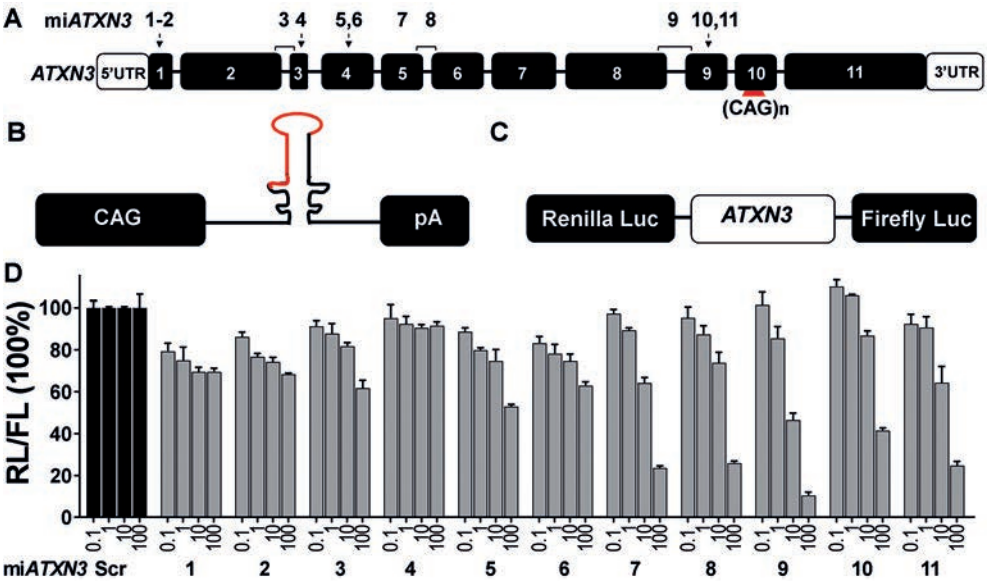

Figure 1. Design and screening of engineered mi*ATXN3* constructs. a) Schematic representation of the human *ATXN3* gene and mi*ATXN3* binding sites. The *ATXN3* gene (NG_008198.2) consists of 11 exons shown by the numbered black boxes. The white boxes represent the 5' and 3' UTR's. The CAG expansion in exon 10 is depicted by a red triangle. The position of the mi*ATXN3* candidates are shown on top of the exons and indicated with numbers 1 till 11. mi*ATXN3*_3, mi*ATXN3*_8 and mi*ATXN3*_9 are exon spanning. b) Schematic representation of the mi*ATXN3* constructs. Each construct was expressed by the CAG promotor, followed by the primary mi*ATXN3* sequence in the miR-451 scaffold, and a human growth hormone polyadenylation (hGH polyA) signal. c) Schematic representation of the Luc reporter. The whole sequence of the *ATXN3* mRNA (NM_004993.5) was cloned downstream of the RL gene. In addition, FL was co-expressed from the vector as an internal control. d) Dose dependent knockdown of *ATXN3* Luc reporter by mi*ATXN3* constructs. HEK293T cells were co-transfected with 50 ng of the Luc reporter and 0.1, 1, 10 and 100 ng of the mi*ATXN3* constructs. RL and FL were measured 2 days post-transfection and RL was normalized to FL expression. Scrambled microRNA (miScr) served as a negative control and was set at 100%.

candidates (Figure 3a). Consistent with the knockdown of the Luc reporter, AAV5-mi*ATXN3*_9 had the strongest silencing efficacy in iPSC-neurons. The mature mi*ATXN3* guide strands levels were also determined by a small RNA TaqMan assay. All three mature mi*ATXN3* were expressed in the cell in a dose dependent manner, suggesting a successful transduction by AAV5-mi*ATXN3* and processing into a mature microRNA (Figure 3b).

No Saturation of endogenous RNAi machinery by mi*ATXN3*

As microRNA overexpression can lead to toxicity, we determined the overall expression of the mi*ATXN3* candidates in human transduced iPSC-neurons relative to other endogenous microRNAs. Small transcriptome analysis was performed on total RNAs

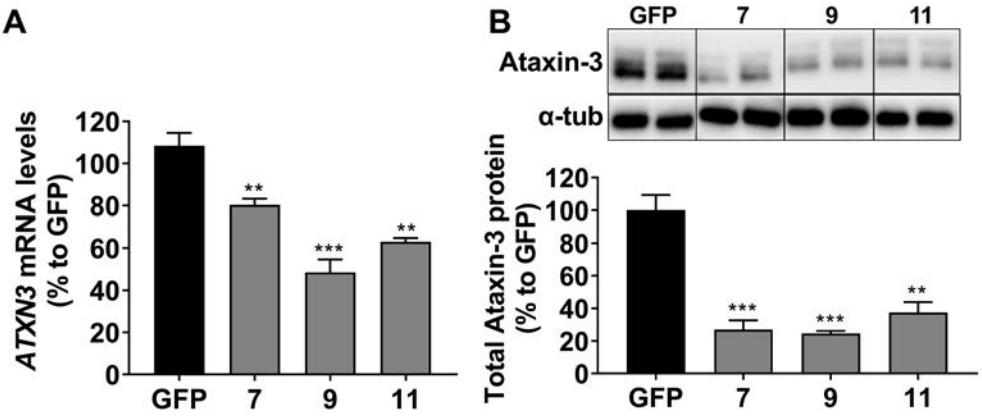

Figure 2. Silencing of *ATXN3* mRNA and protein in HEK293T cells. a) Endogenous knockdown *ATXN3* mRNA by the selected mi*ATXN3* candidates. RT-qPCR *ATXN3* mRNA was performed on RNA from HEK293T cells that were transfected with 250 ng of mi*ATXN3*_7, mi*ATXN3*_9 or mi*ATXN3*_11 for 3 days. mRNA input levels were normalized to GAPDH mRNA. Cells transfected with a GFP construct served as negative control and was set at 100%. b) Silencing of total ataxin-3 protein. HEK293T cells were transfected as describe in A and protein expression was determined by western blot. α tubulin was included as internal control. Western blot intensity bands of ataxin-3 was quantitated and the knockdown was calculated relative to GFP. Data were analyzed using a multiple comparison one-way ANOVA to determine statistically significances of cells treated the mi*ATXN3* constructs. The p-values are listed in the graph by asterisks: *p < 0.05; **p < 0.01; ***p < 0.001; ****p < 0.0001. Each graph represents the mean values with standard deviation (n=3).

isolated from frontal brain-like neurons that were transduced with AAV5-mi*ATXN3*_7, AAV5-mi*ATXN3*_9 or AAV5-mi*ATXN3*_11 for two weeks. We then compared the total amount of reads corresponding to the mature guide strand sequences of mi*ATXN3*_7, mi*ATXN3*_9 and mi*ATXN3*_11 to the total amount of reads of other natural expressed microRNAs found in the cell (Figure 3c). All three mi*ATXN3* candidates were expressed at normal levels and within the expression range of other natural microRNAs in the cell, thus the microRNA biogenesis system was not overloaded. mi*ATXN3*_9 had the highest expression, consistent with its strong silencing efficacy.

mi*ATXN3* is processed into exclusively guide strands in human iPSC-neurons

The mi*ATXN3* candidates were incorporated in the natural human precursor miR-451 scaffold. miR-451 is processed in the non-canonical pathway, first by Drosha to generate a precursor microRNA (pre-mi*ATXN3*). The pre-mi*ATXN3* is then transported by exportin 5 (EXP5) into the cytoplasm for further processing by Argonaute 2 (AGO2) and poly(A)-specific ribonuclease (PARN)[34–38]. Ago2 cleaves the 3' arm of pre-miR-451 by its slicer activity and generates a ~30-nt intermediate that is further trimmed by PARN to generate

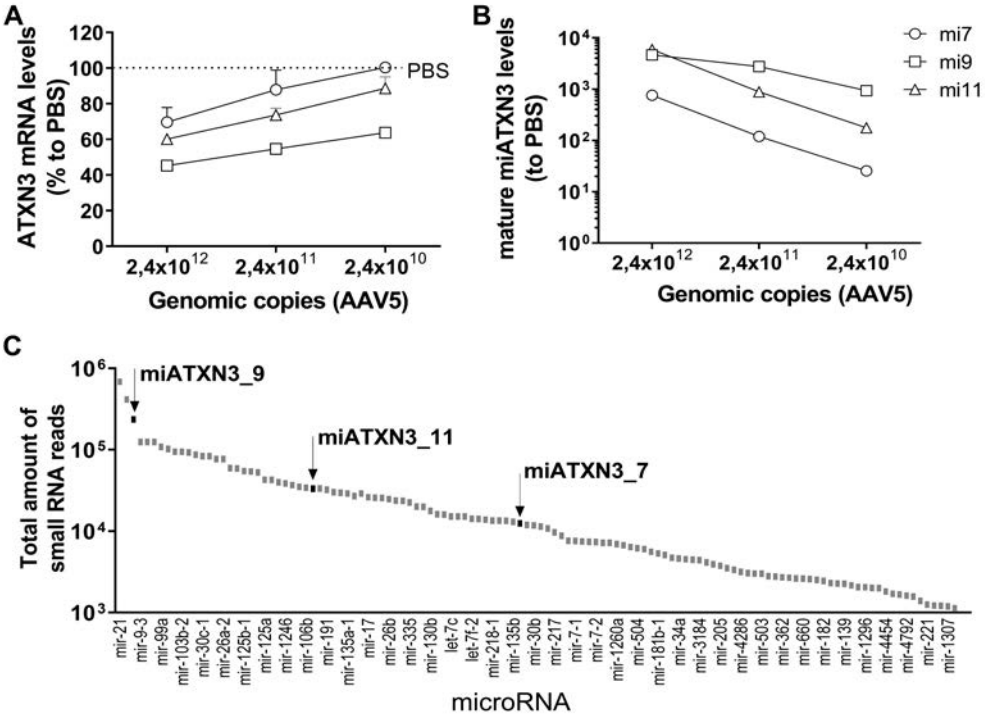

Figure 3. Silencing of *ATXN3* mRNA by AAV5-miC in human iPSC-neurons. a) Dose dependent silencing of *ATXN3* in transduced iPSC-neurons. Frontal brain-like neurons were transduced with 2.4e12, 2.4e11 and 2.4e10 gc of mi*ATXN3*_7, mi*ATXN3*_9 or mi*ATXN3*_11 incorporated into AAV5. RNA was isolated 2 weeks post-transduction and *ATXN3* mRNA levels was determined by RT-qPCR. mRNA input was normalized to GAPDH and set relative to PBS treated cells. b) Levels of mature mi*ATXN3* guide strands in transduced cells. Performed as described in (a). Expression of the mature mi*ATXN3*_7, mi*ATXN3*_9 and mi*ATXN3*_11 were determined by small RNA TaqMan. MicroRNA input levels were normalized to U6 small nuclear RNA and set relative to PBS treated cells. c) Relative mi*ATXN3* expression levels in transduced cells by small RNA sequencing. Frontal brain-like neurons were transduced with 2.4e12 gc mi*ATXN3*_7, mi*ATXN3*_9 or mi*ATXN3*_11 incorporated in AAV5. Small RNA sequencing was performed 2 weeks post-transduction. The total amount of small RNA reads corresponding the three lead mi*ATXN3* candidates shown by the black arrows. The total amount of reads from other natural expressed endogenous microRNAs are shown in grey. d) Processing of mi*ATXN3* in iPSC-neurons by small RNA sequencing. Frontal brain-like neurons were transduced as described in (c). The secondary mi*ATXN3* structure based on miRbase prediction are shown on the first row, including their predicted 22 nucleotide guide strands shown in red. The sequence distribution of the different guide strand length (nt) mapping to mi*ATXN3*_7, mi*ATXN3*_9 and mi*ATXN3*_11 pre-microRNA sequences in miR451 scaffold were calculated in percentage (% reads).

a mature mi*ATXN3* of ~22 nucleotides. The trimming is not essential for efficiency and mature guide strands longer than the mature length can still be functional[39]. However, mature microRNAs that are too long could increase the risk of binding to off-target genes.

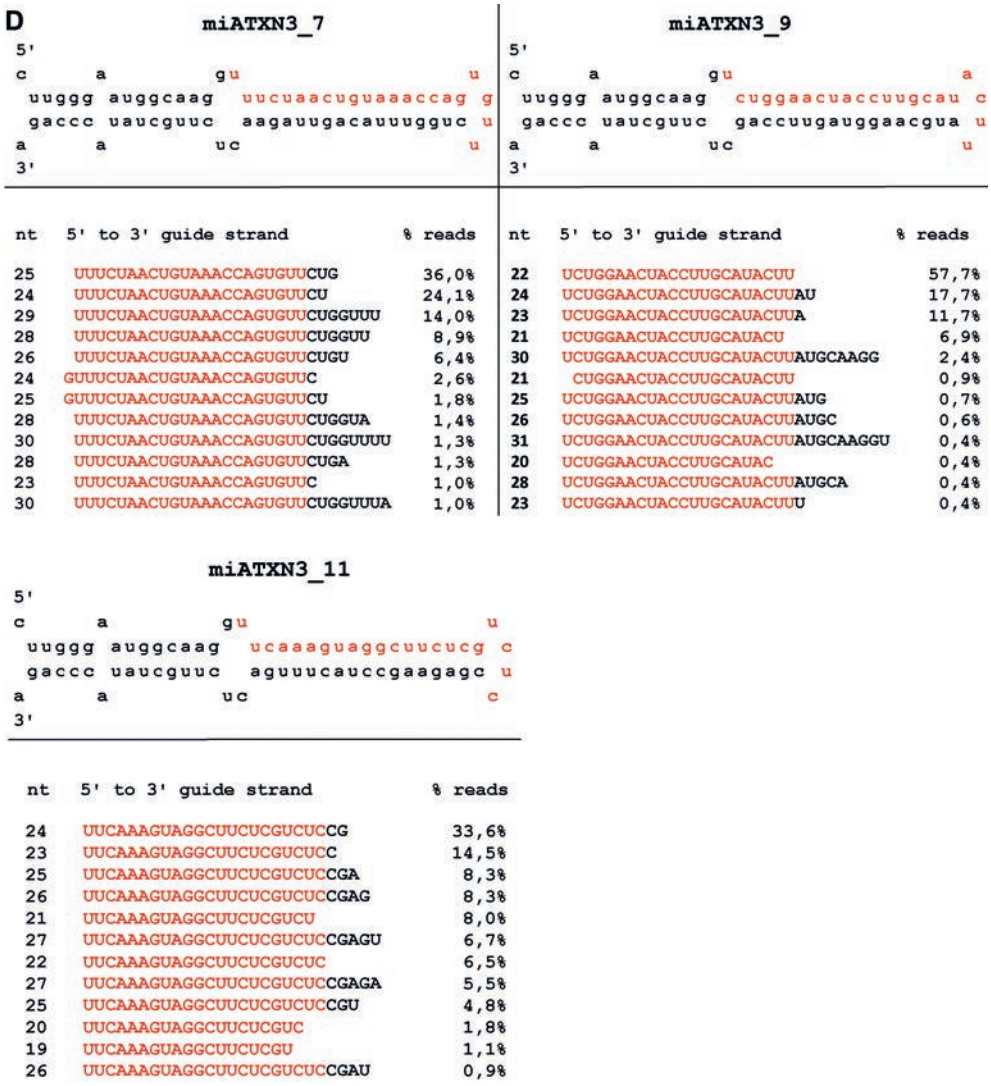

Figure 3. (continued)

The processing was investigated by small transcriptome analysis and all three mi*ATXN3* candidates resulted into exclusively guide strands between 19 to 30 nucleotides long, with no passenger strands detected (Figure 3d). However, the individual length of mature guide strands that were generated varied between the three mi*ATXN3* candidates. The majority of mi*ATXN3*_7 guide strands were between 2 to 7 nucleotides longer at the 3' end than the in silico 22-nucleotide prediction. mi*ATXN3*_9 was processed into primarily 22 nucleotides guide strands, as was predicted on mfold. The processing of mi*ATXN3*_11 mainly generated guide strands between 1 to 4 extra nucleotides at the 3'

end than predicted. Thus, Drosha cleavage sites at 5' end of the mature guide strand was precise for all the mi*ATXN3* candidates but the trimming at the 3' ends by PARN was different and resulted to a variety of mature lengths.

Overall, no passenger strands were detected by the mi*ATXN3* candidates, and the processing of mi*ATXN3*_9 was the closest to our prediction.

Diffused AAV5 transduction of cerebellum and brain stem upon administration in the cisterna magna or DCN of SCA3 knock-in mice

The primary pathology in SCA3 is degeneration of the cerebellum and brain stem. Thus, for an AAV-based gene therapy for SCA3, diffused transduction of both brain structures is required in order to prevent neuronal dysfunction caused by mutant ataxin-3 protein. To determine the most effective delivery route needed for transduction of the cerebellum and brain stem, a study was conducted in a SCA3 knock-in mouse model. The SCA3 knock-in mouse model was generated using Zinc Finger technology by cutting the murine (CAG)6 and subsequent homologous recombination with a (CAACAGCAG)48 donor vector with interrupted repeat. This mouse model was characterized to express a mutant ataxin-3 protein with a 304 glutamine repeat. Three routes of injection were explored; (1) intracerebroventricular (ICV), (2) intracisterna magna, or (3) bilateral into the deep cerebellar nuclei (DCN) (Figure 4a). Injections were performed with AAV5-mi*ATXN3*_7, AAV5-mi*ATXN3*_9 or AAV5-mi*ATXN3*_11, whereas AAV5-GFP was taken along as control: The animals were sacrificed 6 weeks post-surgery and qPCR of the transgene was performed on the *miATXN3* or GFP to determine the biodistribution in the cortex, cerebellum and brain stem. ICV administration resulted in a relative low vector copy distribution to all three analyzed tissues. Some transduction was observed only in the cortex (Figure 4b). Administration into the cisterna magna resulted in low transduction of the cortex but strong transduction of the brain stem and cerebellum (Figure 4c). The highest transduction was detected in the brain stem with up to 2.9 $x10^7$ genome copies (gc)/µg tissue DNA. One mouse that received AAV5-mi*ATXN3*_9 in the cisterna magna was excluded because no genomic copies were detected, suggesting that the injection failed. Direct injection into the DCN also resulted in relatively high transduction of the cerebellum and the brain stem. Compared to cisterna magna administration, DCN injection resulted in better transduction of the cerebellum and less transduction of the brain stem (Figure 4d). Up to 4.6 $x10^6$ gc/µg tissue DNA was detected in the cerebellum. Based on the current observation, we concluded that administration into the cisterna magna resulted in the highest combined transduction of both cerebellum and brain stem of mice.

Significant reduction of *ATXN3* mRNA in SCA3 knock-in mice brain

Having established distribution of AAV5 upon different routes of injection, we further investigated the efficacy of the AAV5-mi*ATXN3* candidates to reduce the total *ATXN3*

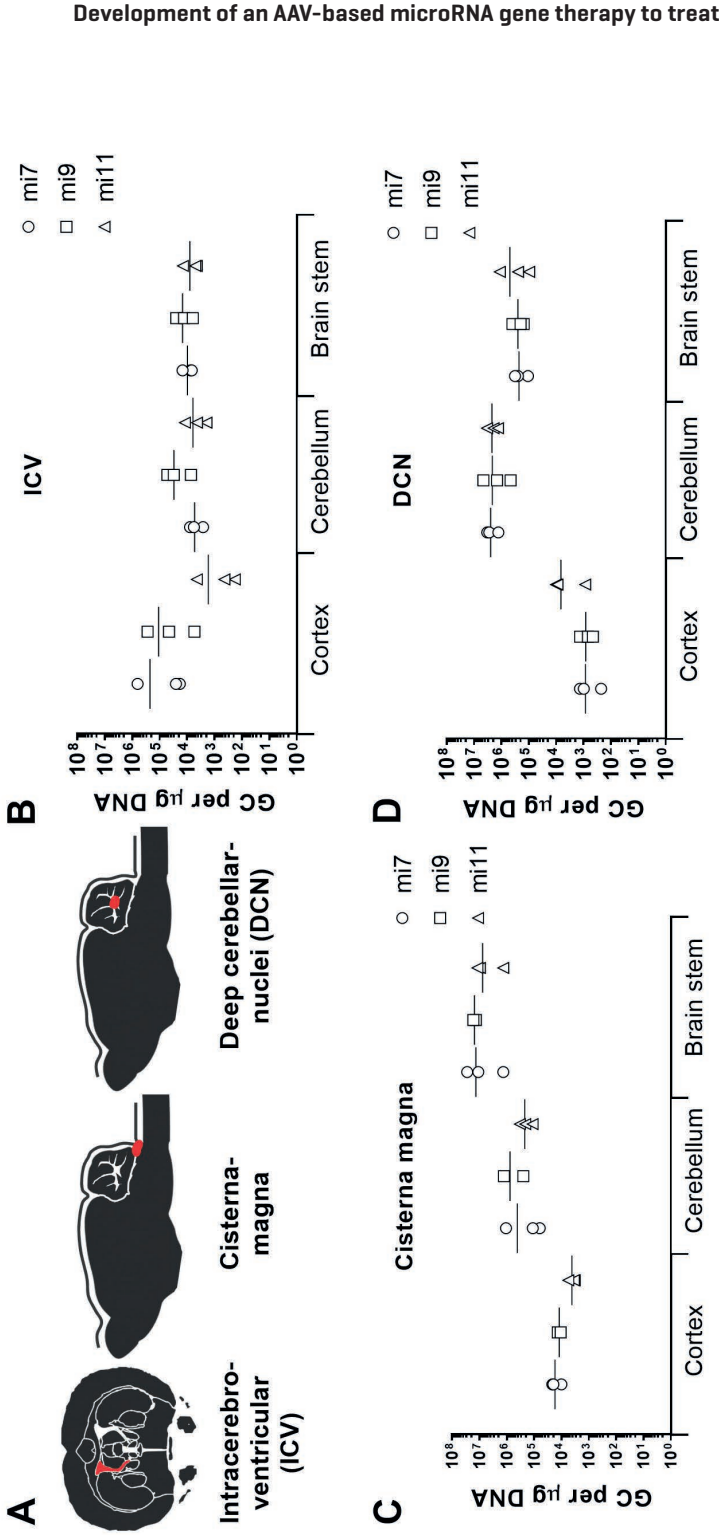

Figure 4. Vector copy distribution of AAV5 in SCA3 knock-in mice. a) Schematic representation of the routes of administration. Three months old mice (N=3) were injected ICV, or in the cisterna magna, or DCN with 2.43x10^{13} gc/mL of AAV5-mi*ATXN3*_7, AAV5-mi*ATXN3*_9 or AAV5-mi*ATXN3*_11. 10 µl of AAV5 were injected either ICV or in the cisterna magna and 2 µl were injected bilaterally in the DCN. The injection sites are depicted in red. All mice were sacrificed 6 weeks after surgeries. b-d) Vector copy distribution in cortex, cerebellum and brain stem. DNA was isolated from the cortex, cerebellum and brain stem tissues and RT-qPCR was performed to determine the vector copy distribution. The genomic copies per µg DNA was calculated for each brain region using a standard curve. No genomic copies were detected in untreated mice. Data were analyzed using student's t-test comparing untreated to treatment group. The p-values were ****p < 0.0001 for all treatments.

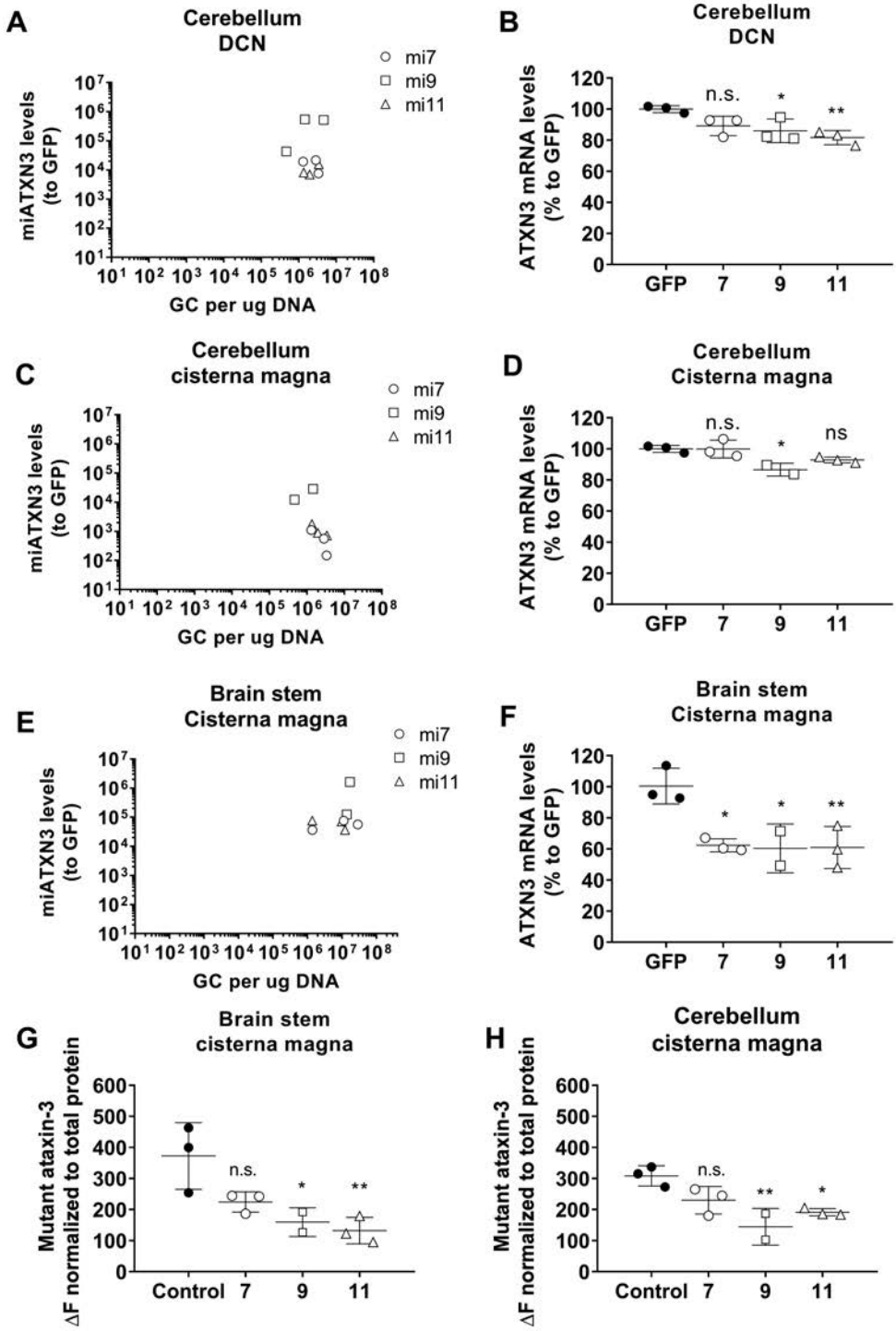
A
Cerebellum
DCN
mi7
mi9
mi11
miATXN3 levels
(to GFP)
GC per ug DNA
B
Cerebellum
DCN
ATXN3 mRNA levels
(% to GFP)
n.s.
*
**
GFP
7
9
11
C
Cerebellum
cisterna magna
D
Cerebellum
Cisterna magna
ns
E
Brain stem
Cisterna magna
F
Brain stem
Cisterna magna
G
Brain stem
cisterna magna
Mutant ataxin-3
ΔF normalized to total protein
Control
H
Cerebellum
cisterna magna

mRNA in the transduced tissues. Direct injection into the DCN showed highest expression of mature mi*ATXN3* in the cerebellum (Figure 5a). mi*ATXN3*_9 had the highest microRNA expression, consistent with the observation *in vitro*. The microRNA expression correlated well with a mild (~15-20%) but significant reduction of *ATXN3* mRNA by mi*ATXN3*_9 and mi*ATXN3*_11 in the cerebellum (Figure 5b). Administration to the cisterna magna resulted into lower mature microRNA expression in the cerebellum as compared to DCN injection (Figure 5c). Nevertheless, mi*ATXN3*_9 was best expressed and resulted in significant lowering (~15%) of *ATXN3* mRNA in the cerebellum (Figure 5d). The highest microRNA expression and silencing efficacy from all three delivery routes was observed in the brain stem after administration in the cisterna magna (Figure 5e-f). Expression of the mi*ATXN3* candidates were high in the brain stem and all led to a strong reduction of *ATXN3* mRNA of about 40%. Both AAV5-mi*ATXN3*_9 and AAV5-mi*ATXN3*_11 had comparable efficacies in the brain stem although the significance of AAV5-mi*ATXN3*_9 was smaller because one mouse was excluded. Overall, we concluded that administration of AAV5-mi*ATXN3*_9 to the cisterna magna resulted in *ATXN3* mRNA reduction in both cerebellum and brain stem, which are the main areas affected in SCA3 patients.

Reduction of mutant ataxin-3 protein in brain stem and cerebellum of mice

Heterozygous SCA3 knock-in mice showed reduced body weight in male mice with 48 weeks in life. Additionally, male and female SCA3 knock-in mice developed an ataxic gait with 18 months of age. Neuropathologically, accumulation of mutant ataxin-3 and protein aggregates were found in cerebellum, DCNs and pons of heterozygous SCA3 knock-in mice starting at the age of three months with higher amounts at later age.

Figure 5. Silencing of mutant ataxin-3 in SCA3 knock-in mice. a) Expression of mature mi*ATXN3* guide strands in the cerebellum after DCN administration. Total RNA was isolated from the cerebellum for small RNA TaqMan. MicroRNA input levels was normalized to U6 small nuclear RNA and set relative to AAV-GFP treated mice. b) Lowering of total *ATXN3* mRNA in cerebellum of DCN injected mice. Total RNA was isolated from cerebellum and RT-qPCR was performed to detect the mouse wildtype *ATXN3* mRNA. RNA input levels were normalized to GAPDH and set relative to AAV-GFP treated mice. c) Expression of mature mi*ATXN3* guide strands in the brain stem after cisterna magna administration. Performed as described in (a). d) Lowering of total *ATXN3* mRNA in cerebellum of cisterna magna injected mice. Performed as described in (b). e) Expression of mature mi*ATXN3* guide strands in the brain stem after cisterna magna administration. Performed as described in (a). f) Lowering of total *ATXN3* mRNA in brain stem of cisterna magna injected mice. Performed as described in (b). g) Reduction of mutant ataxin-3 protein in the brain stem after cisterna magna delivery. TR-FRET immuno-assay was performed on tissue homogenates to specifically detect the mutant ataxin-3 protein containing more than 37 glutamine repeats (no detection of wildtype mouse ataxin-3). H) Reduction of mutant ataxin-3 protein in the cerebellum after cisterna magna delivery.

The polyQ expansion within the mutant ataxin-3 protein causes toxic gain-of-function, leading to the formation of neuronal intranuclear inclusions, neuronal dysfunction and degeneration[15,26]. Decreasing the levels of the mutant proteins leads to therapeutic benefit in several preclinical models[18,26–28,40]. We used a time-resolved fluorescence energy transfer (TR-FRET) immuno-assay to measure the levels of mutant ataxin-3 in cerebellum and brain stem homogenates of treated mice[41]. We found a strong lowering of up to 64% of the mutant ataxin-3 protein in the cerebellum and brain stem homogenates of mice receiving AAV5-mi*ATXN3*_9 and AAV5-mi*ATXN3*_11 in the cisterna magna (Figure 5g-h). The reduction of the mutant ataxin-3 protein in the cerebellum and brain stem of mice confirmed the feasibility of an RNAi based gene therapy approach for lowering of mutated ataxin-3 protein in the affected brain regions of patients.

Prediction of off-target genes due to mi*ATXN3* treatment

We next investigated whether mi*ATXN3* treatment results in major alterations in RNA expression profile in SCA3 knock-in mouse brain and human-derived iPSC-neurons. Although the mi*ATXN3* candidates were designed to specifically target *ATXN3* mRNA transcript, complementarity with other transcripts might result in off-target lowering of other genes. The off-target activity of AAV5-mi*ATXN3*_7, AAV5-mi*ATXN3*_9 and AAV5-mi*ATXN3*_11 was predicted using BLAST to search for transcripts with (partial) complementarity with the guide strand using the homo sapiens reference RNA sequence database (refseq_rna [taxid 9606]). The BLAST results were subsequently compared to RNA sequencing expression values that were performed on total RNA from human-derived frontal brain-like neurons transduced with the three AAV5-mi*ATXN3* candidates and the formulation buffer (control). As expected, all three candidates showed a 100% coverage to *ATXN3* mRNA and RNA sequencing data revealed a significant downregulation of *ATXN3* mRNA (Table S2). Some other genes showed partial coverage to *ATXN3* mRNA and minor alterations (<1.5-fold) were found in those genes by RNA sequencing.

microRNAs can act by binding along the entire mRNA, but studies have shown that the 3′ untranslated region (3′ UTR) of transcripts is the most frequently target site for microRNAs.[42] Further analysis was performed on all three mi*ATXN3* candidates using siSPOTR to predict the binding of their predicted seed sequences to the 3′ UTR of human target transcripts.[43] The transcript Probability of off-Target Score (tPOTS) were calculated by siSPOTR based on the number and type of seed matches (8mer, 7mer-M8, 7mer-1A and 6mer) found in each transcript.[43] The top 20 genes with the highest tPOTS were compared to the gene expression values obtained by RNA sequencing in human-derived frontal brain-like neurons treated with AAV5-mi*ATXN3*_7, AAV5-mi*ATXN3*_9, AAV5-mi*ATXN3*_11 or control (Table S3-S5). We did not find a correlation between tPOTS and gene expression. In the most cases, only minor changes in gene expression (<1.5-fold) were accompanied with the mi*ATXN3*-mediated reduction of *ATXN3*. In frontal brain-like neurons treated with AAV5-mi*ATXN3*_7, expression of all 20 genes were smaller than

1.5-fold. For AAV5-mi*ATXN3*_9 treated cells, only two genes showed a higher alteration in expression. Prostaglandin-endoperoxide synthase 1(PTGS1) was found downregulated (-3.4 fold change) and Formin 1 (FMN1) was upregulated (2.1 fold change). In AAV5-mi*ATXN3*_11 treated cells, Tudor Domain Containing 6 (TDRD6) was found downregulated (-1.6 fold change) and Lysyl oxidase (LOX) was upregulated (1.8 fold change).

The 3' UTR off-target analysis was also performed on RNA derived from brain stem of SCA3 knock-in mice. We selected mice injected with AAV5-mi*ATXN3*_9 in the cisterna magna, as we observed the strongest knockdown using this route of administration. Consistent with the human cells, no correlation was found between tPOTS values and the expression of two genes was slightly over the 1.5 -fold threshold (table S6). Overall, we found no major alterations in gene expression after treatment with the three mi*ATXN3* candidates, suggesting that the risks for off-target effects are limited.

Widespread AAV5-GFP transduction in minipig brain after intrathecal administration

The translation of preclinical studies performed in rodent models to the clinic is a challenging process, particularly due to the relatively small brain and spinal cord sizes of rodents. Successful delivery of AAV to reach the target tissues in humans is likely dependent on brain size and structure. Therefore, we further investigated the delivery of AAV5 in a minipig CNS in order to predict the biodistribution of AAV5 more precisely. The brain stem and cerebellum are the primary affected regions in SCA3 patients and transduction of these brain region is required for an *ATXN3*-based lowering gene therapy. Because cisterna magna injection in minipig was not feasible due the relatively thick neck, we investigated the biodistribution of AAV5 upon intrathecal injection in the lumbar region of the spinal cord. The biodistribution of AAV5 was determined by vector DNA genome copies and immunohistochemistry for the transgene (GFP). We found a relatively equal distribution of the vector DNA across the whole brain, including the cerebellum and brain stem (Figure 6a). The cerebellar cortex, DCN and brain stem were transduced at therapeutically relevant doses of ~10^5 genomic copies per µg DNA. To visualize AAV5 distribution in the brain, GFP immunohistochemical analysis was performed and the widespread GFP expression in the minipig brain confirmed an equally distribution of AAV5 (Figure 6b). Overall, the current data suggest that intrathecal administration of AAV5 could be sufficient for an AAV-based *ATXN3*-lowering gene therapy.

Discussion

In the current study we focused on the development of a microRNA-based gene therapy that could benefit the entire human SCA3 patient population. We aimed for a non-allele selective reduction of human *ATXN3* mRNA as this approach has been tested in several rodent preclinical models and showed no overt symptoms or toxicity[27,44]. Furthermore,

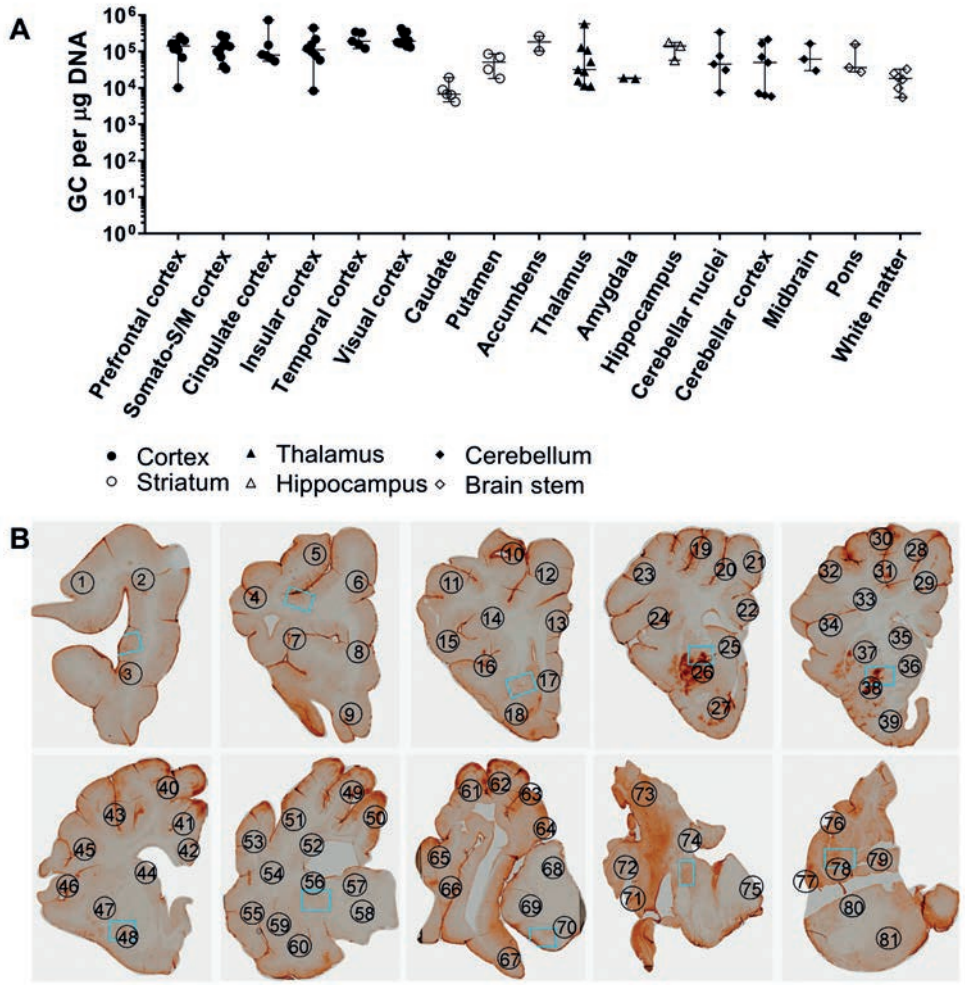

ataxin-3 knock-out mice have no major abnormalities suggesting that lowering of ataxin-3 in the context of SCA3 is safe and effective[44]. An additional advantage of this approach is that the entire human patient population can be treated. Allele-specific approaches for downregulation of only the mutant ataxin-3 have also been tested. For example, allele specific silencing was achieved using short hairpin (sh)RNAs directed against a single nucleotide polymorphisms (SNP) unique to the mutant ataxin-3 transcript which seems to be present in over 70% of SCA3 patients. The SNP-specific shRNA was able to specifically silence mutant ataxin-3 and was found to be neuroprotective in SCA3 mouse and rat models[45]. Single-stranded silencing RNAs (ssRNAs), ASO and peptide nucleic acids (PNAs) directly targeting the expanded CAG repeat also resulted in translational blockage of only the mutant ataxin-3[46–49]. The latter approach is very interesting because it may be used to treat multiple polyQ diseases but knockdown of several other endogenous CAG

repeat-containing transcripts, like huntingtin (HTT), TATA-binding protein (TBP) and other ATXNs might be detrimental.

Several mi*ATXN3* were designed in the natural human miR-451 scaffold to target different regions within exons of *ATXN3* mRNA by using the knowledge and technologies developed for a Huntington's disease RNAi gene therapy[29–31]. A pre-screening of the mi*ATXN3* candidates were performed on a Luc reporter construct and mi*ATXN3*_7, mi*ATXN3*_9 and mi*ATXN3*_11 showed the highest silencing efficacy. All three candidates also successfully reduced the endogenous *ATXN3* mRNA and protein levels in cells and the strongest efficacy was consistently obtained with mi*ATXN3*_9.

For clinical development, it is important to establish the fidelity of cellular processing of the microRNA in the target human tissue and select the candidates with the least probability for off-target effects. For this reason, we analyzed the microRNA processing patterns in iPSC-neurons transduced with the three selected AAV5-mi*ATXN3* candidates by small RNA sequencing. We found high expression of all three mi*ATXN3* in transduced iPSC-neurons, but they were not overexpressed, even after transducing the cells with very high concentration of AAV-mi*ATXN3*. Furthermore, no dysregulation in microRNA molecules was observed, strongly limiting the possibility of off-target effects due to the saturation

Figure 6. AAV5 biodistribution in brain of minipig upon intrathecal administration. A) Vector copy distribution in brain of a 7 months old Gottingen minipig. The minipig was injected with 5 mL of AAV5-GFP (4 x 10^{13} gc/ml) into the lumbar region. The minipig was sacrificed 4 weeks post injection and DNA was isolated from several punches of the brain. RT-qPCR was performed to determine the vector copy distribution. The genomic copies per µg DNA were calculated for each brain region using a standard curve. B) Widespread GFP expression in minipig brain transduced with AAV5-GFP. Brains were fixed in paraformaldehyde, embedded in paraffin and serially cut in 5 µm sections. GFP staining was performed to visualize GFP expression throughout the brain. Different area of the brain was numbered according to Atlas of the Gottingen minipig brain (Cense): 1) PFC lateral, 2) PFC lateral, 3) PFC ventral, 4) Motor cortex M1, 5) Motor cortex M1, 6) Cingulate cortex, 7) PFC lateral, 8) PFC medial, 9) PFC ventral, 10) Motor cortex, 11) Somatosensory S1 dorsal,12) Frontal lobe WM, 13) Cingulate cortex, 14) Centrum semioval WM , 15) Somatosensory S1 ventral, 16) Insular cortex, 17) PFC medial, 18) Olfactory cortex 19) M1/S1 cortex, 20) M1 cortex, 21) M1 cortex, 22) Cingulate cortex, 23) Somatosensory S1dorsal, 24) Insular cortex, 25) Nuc Caudate (frontal), 26) Putamen (F), 27) Nucleus Accumbens, 28) Motor cortex M1, 29) Cingulate cortex, 30) Occipital lobe (Visual cortex), 31) Occipital lobe (Visual cortex), 32) Somatosensory S1 ventral , 33) Centrum semioval WM 34) Insular lobe , 35) Caudate, 36) Caudate, 37) Putamen, 38) Putamen 39) Nucleus Accumbens, 40) Occipital lobe (Visual cortex), 41) Cingulate cortex, 42) Cingulate cortex, 43) Somatosensory S1 ventral, 44) Caudate, 45) Insular cortex, 46) Insular cortex, 47) Putamen, 48) Globus pallidus, 49) Visual cortex, 50) Cingulate cortex, 51) Visual cortex, 52) Centrum semiovale WM, 53) Temporal cortex, 54) Temporal lobe WM, 55) Insular cortex, 56) Caudate, 57) Thalamus anterior, 58) Thalamus ventral, 59) Putamen, 60) Globus pallidus, 61) Visual cortex, 62) Visual cortex, 63) Visual cortex, 64) Occipital lobe, 65)Temporal cortex, 66) Insular cortex, 67) Hippocampus, 68) Thalamus (Medial), 69) Thalamus (lateral), 70) Thalamus (ventral), 71) Temporal cortex, 72) Occipital cortex (Visual cortex), 73) Cerebellum lobe, 74) Cerebellum lobe, 75) Reticular formation (pons), 76) Cerebellum lobe, 77) Cerebellum lobe, 78) Cerebellar nuclei, 79) Medulla oblongata, 80) Cerebellar peduncle, 81) Reticular formation (pons).

of the endogenous RNAi pathway. We detected a typical variability in the read length (19-30 nucleotides) occurring when the miR-451 precursor is intracellularly processed. This observation is consistent with expected processing mechanism of miR-451 which escapes Dicer cleavage in the cytoplasm and is instead processed by Ago2. Ago2 cleavage generates a 30-nucleotide guide strand which is further trimmed by PARN leading to the observed variability in length. The processing and expression varied per mi*ATXN3*, and mi*ATXN3*_9 was the most efficiently processed and the highest expressed of the three tested mi*ATXN3s*. The higher expression could be a result of a more efficient processing because the thermodynamic stability at the loop of mi*ATXN3*_9 is lower, compared to mi*ATXN3*_7 and mi*ATXN3*_11. mi*ATXN3*_9 has a A-U nucleotide at the loop, thus less energy may be needed to break this A-U bond by PARN. mi*ATXN3*_7 and mi*ATXN3*_11 both have a G-C nucleotide. The efficient processing and high expression of mi*ATXN3*_9 is likely to be responsible for its strong silencing efficacy. For mi*ATXN3*_9 the most abundant reads were, as predicted *in silico*, 22 nucleotides long and showed the exact miATNX3 guide strand sequence. The second most abundant reads had either 1 or 2 extra nucleotides at the 3' end and no passenger strands were detected, indicating that off-target effects due to microRNA-like effect of the passenger strand can be excluded. The absence of a passenger strand associated with the miR-451 precursor also confirms our previous findings in the human neuronal cells and animal models, that this scaffold does not produce a passenger strand.[30,50]

The success of a RNAi-based gene therapy for SCA3 is also dependent on the delivery method to reach the affected brain regions. AAV vectors are of particular interest due to their high safety profile and different AAV serotypes have proven to be stable and safe, each with different tropism for a wide range of tissues[51–54]. AAVs can be delivered to the CNS either by systemic administration, direct intraparenchymal administration or in the cerebrospinal fluid (CSF). Systemic AAV infusion has been used in preclinical models and in clinical studies and some serotypes were identified that can cross the blood brain barrier[55,56]. Based on our own experience we anticipate that intravenous (IV) infusion of AAV would not be sufficient to achieve silencing of *ATXN3* in the cerebellum and brain stem with the current technology. Direct injection of AAV in the parenchyma of brain is more invasive but studies in rodents, minipig and non-human primates consistently showed very strong transduction of the deeper brain structures and vector spread to the adjacent brain areas[29,57]. The target regions in SCA3 patients are the cerebellum and brain stem and they are the primary affected areas in the early stages of the disease. Therefore, direct intraparenchymal administration would not result in spread of the vector to those areas and a CSF-mediated delivery would be necessary. In SCA3 mouse models, ICV injection of ASOs resulted into sufficient reduction of the mutant ataxin-3 in the cerebellum and brain stem[58]. microRNAs delivered by AAV directly in the cerebellum (DCN) also reduced mutant ataxin-3 in the cerebellum, while the effect was not evaluated in the brain stem[28,59]. We investigated the transduction of cerebellum and brain stem of mice injected with AAV5-mi*ATXN3* in the CSF via ICV injection or cisterna magna, or directly to the cerebellum via

DCN injection. Upon ICV injection, the transduction of the cerebellum and brain stem of mice was low and not sufficient to expect a therapeutic benefit. In contrast, intracisterna magna administration resulted in transduction of the brain stem and cerebellum, with the highest transduction in the brain stem. DCN injection also transduced both brain regions but transduction was the highest in the cerebellum. However, a single delivery to the cisterna magna resulted in the most optimal transduction of cerebellum and brain stem combined. Consistently, lowering of *ATXN3* mRNA and the mutant ataxin-3 protein were observed in both cerebellum and brain stem of SCA3 knock-in mice injected with AAV5-mi*ATXN3*_9 and AAV5-mi*ATXN3*_11 in the cisterna magna. The efficacy of both mi*ATXN3* candidates were comparable, despite the fact that AAV5-mi*ATXN3*_9 was the most effective candidate in our *in vitro* screening. A logical explanation is that while the mi*ATXN3*_11 target sequence had 100% homology with the human and mouse *ATXN3* gene, mi*ATXN3*_9 had one nucleotide mismatch with the mouse *ATXN3*. This means that the efficacy of mi*ATXN3*_9 seen could be underestimated in the mouse model used in this study as mismatches interferes with the binding efficacy of a microRNA. Nevertheless, we showed that mi*ATXN3*_9 and mi*ATXN3*_11 are highly effective by mediating a strong knock-down of the mutant ataxin-3 protein in the cerebellum and brain stem after a single administration in the cisterna magna. Previous studies using RNAi and ASO's showed that reduction of about 37 up to 80% of the mutant ataxin 3 protein is sufficient to reverse molecular phenotypes associated with mutant ataxin-3 gain of toxicity in SCA3. We are aiming for a 40-50% reduction of the mRNA and showed that we can reach more that 50% knockdown of *ATXN3* mRNA and mutant ataxin-3 protein lowering of 53.1% in the cerebellum and 64% in the brain stem which is within the therapeutic range. To further predict potential off-target genes, we examined the impact of AAV5-mi*ATXN3* treatment on the overall gene expression profile. *In-silico* analysis was performed using BLAST to search for off-target genes with partial guide-strand complementarity to human and mice microRNA and siSPOTR tool was used to predict potential off-target effects related to the mi*ATXN3* seed sequence. The data obtain by BLAST and siSPOTR was compared to an unbiased RNA sequencing to look at differential changes in gene expression upon treatment. We selected an exclusion criterion of -1.5 – 1.5-fold change, based on observations from previous studies in large animals that most of the genes within this range do not show significant changes when this data is revalidated with other applications such as qPCR. Two genes (PTGS1 and FMN) were differentially expressed upon AAV5-mi*ATXN3*_9 treatment. PTGS1 encodes the enzyme Cyclooxygenase (COX) which is involved in conversion of arachinodate to prostaglandin. PTGS1 is also downregulated by nonsteroidal anti-inflammatory drugs such as aspirin and ibuprofen suggesting its downregulation is tolerable in humans.[60] Interestingly, ibropufen was found to have neuroprotective properties in SCA3 mouse model by increasing levels of neural progenitors proliferation and synaptic markers.[61] Whether PTGS1 downregulation by ibropufen may have play a role is unclear and may be worth investigating. If this is the case, a combination therapy based on PTGS1 lowering

and *ATXN3* downregulation could add to therapeutic benefit. FMN belongs to the formin family of proteins and is involved in actin nucleation.[62] Upregulation of FMN has not been linked to diseases. Similarly, two genes (TDRD6 and LOX1) were slightly modulated upon AAV5-mi*ATXN3*-11 treatment. TDRD6 encodes a protein that is specific to the male germ line and essential for chromatoid body structure.[63] TDRD6 is usually only expressed in mid prophase I spermatocytes. Thus, its downregulation in the brain is not expected to be relevant. LOX1 is a member of the lysyl oxidase family and has a role in crosslinking of collagens and elastin.[64] Its role in disease is unclear as it has been reported to enhance metastasis of certain cancers, but it was also shown to have tumor suppressor function.[65–68] Overall, dysregulation in one of these genes were not directly linked to any known diseases, increasing our confidence that AAV5-mi*ATXN3* mediated silencing of *ATXN3* mRNA may have limited risk for off-target effects. However, further investigation will be needed across multiple human cellular systems and larger animal models transduced with therapeutically relevant doses of AAV5-mi*ATXN3* to better predict gene dysregulation and their effects after treatment with AAV5-mi*ATXN3* in humans.

We demonstrated thus far that AAV5-mi*ATXN3* can successfully lower the mutant *ATXN3* mRNA and protein in iPSC-neurons and SCA3 knock-in mice. One major challenge remains the translation of AAV5 delivery results acquired from the mouse model to humans. Multiple neuronal systems are affected in SCA3 patients and degeneration of neurons is especially observed in the cerebellum, brainstem, basal ganglia, some cranial nerves and the spinal cord.[1,17,69] In the cerebellum, neurodegeneration is observed in dentate nucleus. The cerebellar cortex seems less affected but loss of granule and Purkinje cells has been reported in the cerebellar vermis.[1,70–73] Main areas affected in the brainstem include the vestibular, pontine and motor nuclei.[1,71,74] Other regions such as the cerebral cortex, autonomic ganglia, striatum, substantia nigra, nerve motor nuclei, Clarke's column nuclei, the anterior horn of the spinal cord are also affected[1,45,72,75] . We investigated AAV5 delivery and distribution in a larger minipig model with a brain and spinal cord size that closely resemble the situation in humans. Because administration into the cisterna magna was not feasible, AAV5-GFP was administered intrathecally. Next to widespread vector distribution and transgene expression, successful transduction of the structures mostly affected in SCA3 patients was observed. The current data increase of our confidence that mutant ataxin-3 protein can be modulated in these brain regions. Moving forward, further studies in large animal models is needed to determine the silencing efficacy and tolerability AAV5-mi*ATXN3*.

In summary, we presented the development of a gene therapy for SCA3 patients based on non-allele specific lowering of *ATXN3* mRNA and protein by AAV5-mi*ATXN3*. We demonstrated the efficacy in cellular models and in a SCA3 knock-in mouse model. In addition, we demonstrated that administration of AAV5 to the cisterna magna of mice can be successfully translated to intrathecal administration of a minipig to simultaneously transduce the cerebellum and brain stem, and potentially lower *ATXN3* mRNA and mutant

ataxin-3 protein in these brain regions. The current preclinical data support the feasibility for an AAV-based microRNA gene therapy and further studies in animals with a larger brain would be required to investigate the translation of the current observations in the small mouse brain to a larger brain size closer to humans.

Material and methods

DNA constructs

To generate the mi*ATXN3* vectors, we searched for sequences on *ATXN3* gene that were mostly conserved between human, non-human primates and rodents. The sequences were incorporated into the cellular miR-451 scaffold of humans. 200 nt 5' and 3' flanking regions were included with EcoRV and BamHI restriction sites and the mfold program (http://unafold.rna.albany.edu/?q=mfold) was used to determine if the mi*ATXN3* candidates are folded correctly into their secondary structures. The complete sequences were ordered from GeneArt gene synthesis (Invitrogen). These constructs were subsequently cloned into an expression vector containing the CMV immediate-early enhancer fused to chicken β-actin (CAG) promoter (Inovio, Plymouth Meeting, PA) using the EcoRV and BamHI sites. For generation of the Luc reporter, the complete *ATXN3* mRNA (NM_004993.5) sequence was synthesized at GeneArt gene synthesis and cloned in the 3'UTR of the renilla luciferase (RL) gene of the psiCHECK-2 vector (Promega, Madison, WI). The firefly luciferase (FL) gene was also expressed in this vector and served as internal control.

Culture and transfections of HEK293T cells

Human embryonic kidney (HEK)293T were maintained in Dulbecco's modified Eagle's medium (DMEM) (Invitrogen) containing 10% fetal calf serum (Greiner, Kremsmünster, Austria), 100U/ml penicillin and 100U/ml streptomycin (Thermo Fisher, Waltham, MA), at 37 °C and 5% CO2. Transfections: For all assays, cells were seeded in 24-wells plates at a density of $0.1*10^6$ cells per well in DMEM. Transfections in HEK293T cells were performed 1 day post-plating with Lipofectamine 2000 reagent (Invitrogen) according to the manufacturer's instructions.

Luciferase assays

HEK293T cells were co-transfected with the mi*ATXN3* expression constructs and the Luc reporter. The cells were lysed at 48 hours post-transfection in 100 µl 1x passive lysis buffer (Promega) by gentle rocking for 15 minutes at room temperature. The cell lysates were centrifuged for 5 minutes at 4,000 rpm to get rid of cell debris and 10 µl of the supernatant was used to measure FL and RL activities with the Dual-Luciferase Reporter Assay System (Promega). Relative luciferase activity was calculated as the ratio between RL and FL activities.

Culture of iPSC-neurons

Frontal brain-like neurons were generated as described previously.[33] Control iPSC cells (ND42245) derived from fibroblast were ordered from Coriell biorepository and were cultured on Matrigel (corning) -coated 6 wells plates in mTeSR1 (STEMCELL). For embryoid body-based neural induction, iPSC cells were seeded on AggreWell800 plates and cultured in STEMdiff Neural Induction Medium (STEMCELL) for 5 days with daily medium changes. Embryoid bodies were harvested and plated on 6 wells plates coated with poly-D-lysine (Sigma-Aldrich) and laminin (Sigm-Aldrich) in STEMdiff Neural Induction Medium for 7 days with daily medium changes. Rosettes were selected with rosette selection medium and plated on poly-D-lysine and laminin coated 6-wells plates in STEMdiff Neural Induction Medium for 24 hours. For differentiation into frontal brain-like neurons, STEMdiff Neural Induction Medium was replaced for STEMdiff Neuron Differentiation medium (STEMCELL) and neuroprogenitor cells were differentiated for 5 days. The neuroprogenitor cells were then plated on poly-D-lysine and laminin coated plates in STEMdiff Neuron Maturation medium (STEMCELL) for one week. The mature frontal brain-like neurons were stored in liquid nitrogen in neuroprogenitor freezing medium (STEMCELL).

Western blot

Western blot was performed to detect wildtype ataxin-3 protein expression in transfected HEK293T cells. In brief, cells were lysed using RIPA lysis buffer solution, containing Tris-HCL (pH 8,0), NaCl, 1% IGEPAL CA-630, 0,5% DOC and cOmplete protease inhibitor and extracted by centrifugation. Equal amounts of tissue (30°g) were loaded through a 10% SDS-PAGE gel. The gel was transferred to a bio-rad nitrocellulose membrane using bio-rad turbo transfer system, running for 30 minutes at 90V. Membranes were blocked for one hour in 3% milk in TBS, containing 0,1% Tween-20 (TBST), and incubated overnight with primary antibody mouse anti-*ATXN3* (Abcam ab61392 1:1000) and mouse anti-α tubulin (Abcam ab13533 1:1000) at 4°C. Secondary antibody incubation was with horseradish peroxidase (HRP) conjugated rabbit anti-mouse (DAKO 1:5000) for one hour at room temperature.

AAV5 vector production

AAV5 encoding mi*ATXN3*_7, mi*ATXN3*_9 and mi*ATXN3*_11 were produced by a baculovirus-based AAV production system as described previously[30]. Briefly, the mi*ATXN3* cassettes were obtained by digestion with restriction enzymes HindIII and PvuI and cloned in an uniQure transfer plasmid in order to generate an entry plasmid. The presence of the two inverted terminal repeats (ITRs) was confirmed by restriction digestion with SmaI. The ITR-CAG-miC cassettes were inserted in a recombinant baculovirus vector by homologous recombination in Spodoptera frugiperda Sf9 cells and clones were selected and screened by plague purification and PCR. The recombinant baculovirus containing the ITR-CAG-miC casettes were further amplified till P6 in Sf+ cells and screened for

the best production and stability by PCR and RT-qPCR. To generate AAV5, Sf+ cells were triple infected with three different recombinant baculoviruses expressing the ITRs-CAG-mi*ATXN3*, the replicon enzyme and the capsid protein. The cells were lysed 72 hours after the triple infection and the crude lysate was treated with 50U/ml Benzonase (Merck, Darmstadt, Germany) for 1 hour at 37 °C. AAV5 was purified on an AVB Sepharose column (GE Healthcare, Little Chalfont, UK) using an AKTA purification system (GE Healthcare). The final titer concentration was determined by RT-qPCR with primers amplifying a 95bp fragment from the CAG promoter region.

Transduction of iPSC-neurons

Mature frontal brain-like neurons were plated in 500µL STEMdiff Neuron Maturation medium (STEMCELL) at $0.3*10^6$ cells per well in 24-wells plates. 1 week after plating, the cells were transduced with the 100µL, 10µL or 1µL of $2.42x10^{13}$ gc/mL of AAV5-mi*ATXN3*_7, AAV5-mi*ATXN3*_9, AAV5-mi*ATXN3*_11 or AAV5-GFP. The cells were incubated with AAV for 2 weeks and medium were changed twice a week.

SCA3 mice and treatment groups

All procedures were approved by the local ethics committee at the Regierungspraesidium Tuebingen and performed in accordance with the German Animal Welfare Act and the guidelines of the Federation of European Laboratory Animal Science Associations based on the European Union legislation (Directive 2010/63/EU). All efforts were made to minimize the suffering and the number of animals used.

Heterozygous SCA3 knock-in animals expressing 304 glutamines within the murine ataxin-3 polyQ locus were used in this study and maintained in a controlled facility in a 12-hour light/dark cycle with free access to food and water. 3 animals (2 males and 1 female) were recruited to each treatment group (Table S1).

Viral delivery by stereotaxic injections and tissue collection in mice

Animals were injected at 3 months of age. For each injection, the animal was initially anaesthetized with 5 % isoflurane in an oxygen-air mixture in the induction box. After induction, the animal was injected intraperitoneally with a combination of fentanyl 0.05 mg/kg, midazolam 5 mg/kg and medetomidine 0.5 mg/kg and transferred to the stereotaxic frame. Isoflurane was then delivered via the facemask and reduced to 1.5-2.0 % depending on the weight and responses of the animal. Eye ointment was given to the animal to prevent the eyes from drying during surgery. The body temperature of the animal was monitored and maintained at 37 ± 0.5 °C through a rectal probe and a negative feedback controlled heat pad (Harvard Apparatus, US). The depth of anesthesia was checked by the lack of pedal withdrawal to a firmly pinched hind toe or foot. The head was shaved and disinfected, and local anesthetic agent (2% lidocaine, 5 mg/kg) was injected subcutaneously. For ICV and DCN injections, bregma and lambda

were used for alignments and locating the injection sites after midline skin incision. Small skull hole was drilled to expose the dura over the injection site. Craniotomy (0.5-0.8 mm in diameter) was performed using a microscope or magnifying glass and a pneumatic drill. In the case of cisterna magna injections, skin incision was performed at the neck region. Dura mater was exposed by blunt dissection of the subcutaneous neck muscles. The animal received bilateral DCN (AP-6.5, ML±1, DV-2.8), ICV (AP+0.3, ML+1, DV-3) or cisterna magna injection according to the assigned treatment group. 2.0 µl per hemisphere (bilateral DCN) or 10 µl (ICV and cisterna magna) of AAV5-mi*ATXN3*_7, AAV5-mi*ATXN3*_9, AAV5-mi*ATXN3*_11 or AAV5-GFP was delivered at a rate of 0.25 µl/min using a microinjection pump (UMP3-1, WPI) with a 10 µl Hamilton syringe and a 32-gauge needle. The AAVs were titer matched at $2{,}42x10^{13}$ gc/mL. After the injection, the needle remained at the injection site for 5 mins before withdrawal. The animal was then sutured and given carprofen (5 mg/kg) subcutaneously as analgesics post-surgery. For recovery from anesthesia, the animal was given a mixture of naloxone (1.2 mg/kg), flumazenil (0.5 mg/kg) und atipamezole (2.5mg/kg) subcutaneously and transferred to a warm (37°C) environment with access to food and water. The operated animal was returned to its home cage after recovery from anesthesia. All animals were given carprofen (5 mg/kg) subcutaneously every 24 hours and provided with antibiotics (enrofloxacin, 10mg/kg)-containing water until the 3rd and 7th day post-surgery respectively. Health and other conditions of all animals were closely monitored throughout the project duration using score sheets.

All treated animals were euthanized 6 weeks after viral delivery. For the untreated group, animals were sacrificed at 4.5 months of age. The animals were given saturated carbon dioxide in the home cage until death. Tissues were dissected and snap frozen in liquid nitrogen and stored at -80°C for subsequent analyses.

RNA isolation

For all RNA isolation, cells and tissues were lysed in 300 µl Tryzol and RNA isolation was performed using the Direct-zol kit (R2061, ZYMO Research) according to the manufacturer protocol.

RT-qPCR, and microRNA TaqMan assay

To determine *ATXN3* mRNA knockdown, total RNA was isolated as described above. Genomic DNA contamination was removed by DNAse treatment using recombinant shrimp ds DNase (ThemoFisher Scientific). First-strand complementary DNA was reverse transcribed using random hexamer primers with the Dynamo kit (Finnzymes, Espoo, Finland). Real-time PCR amplification was performed with a customizes TaqMan for human *ATXN3* (assay ID Hs01026440_g1) or mouse *ATXN3* (assay ID Mm00804702_m1) on ABI 7000 or ABI 7500 (Applied Biosystems, Foster City, CA, USA). The mRNA expression levels were normalized to human GAPDH (assay ID Hs02758991_g1) or mouse GAPDH

(assay ID Mm99999915_g10 as an internal control. A custom TaqMan Small RNA Assay Design Tool (ThemoFisher Scientific) was used to design microRNA TaqMan for the mature mi*ATXN3*_7 (assay ID CTCE3VJ), mi*ATXN3*_9 (Assay ID CTEPRZE) and mi*ATXN3*_11 (assay ID CTFVKKC). The microRNA expression levels were normalized to U6 snRNA (assay ID 001973) as an internal control. All reverse transcription reaction and TaqMan for small RNAs were performed according to the manufacturer protocol.

Next-generation sequencing (NGS) and data analysis (small RNAs)

Mature frontal brain-like neurons were plated in 500µL STEMdiff Neuron Maturation medium (STEMCELL) at $0.3*10^6$ cells per well in 24-wells plates. 1 week after plating, the cells were transduced with the 100µL of $2.\ 42x10^{13}$ gc/mL of AAV5-mi*ATXN3*_7, AAV5-mi*ATXN3*_9 or AAV5-mi*ATXN3*_11. Small RNA sequencing libraries for the Illumina sequencing platform were generated using high-quality total RNA as input and the NEXTflex Small RNA Sequencing kit (Bioo Scientific, Austin, TX). Briefly, the small RNA species were subjected to ligation with 3′ and 5′ RNA adapters, first strand reverse transcription, and polymerase chain reaction (PCR) amplification. Sample-specific barcodes were introduced in the PCR step. The PCR products were separated on TBE-PAGE electrophoresis and the expected band around 30bp was recovered for each sample. The resulting sequencing libraries were quantified on a BioAnalyzer (Agilent, Santa Clara, CA). The libraries were multiplexed, clustered, and sequenced on an Illumina HiSeq 2000 (TruSeq v3 chemistry) with a single-read 36 cycles sequencing protocol and indexing. The sequencing run was analyzed with the Illumina CASAVA pipeline (v1.8.2), with demultiplexing based on sample-specific barcodes. The raw sequencing data produced was processed removing the sequence reads which were of too low quality (only "passing filter" reads were selected). In total, between 15–35 million reads per sample were generated. NGS small RNA raw data sets were analyzed using the CLC Genomics Workbench 8 (Qiagen). The reads were adaptor-trimmed and aligned against the corresponding reference sequence. Reads that were shorter than 10 nucleotide (nt), longer than 45 nt, or represented less than 10 times were excluded from the analysis. The custom adapter sequenced used for trimming all the bases extending 5′ was: GTGACTGGAGTTCCTTGGCACCCGAGAATTCCA. Next, the obtained unique small RNA reads were aligned to the reference sequences of the pre-mi*ATXN3* constructs with a max. of 3 nt mismatches allowed. The percentages of reads based on the total number of reads matching the reference sequence were calculated.

RNA sequencing and transcriptome analysis

For human transcriptome-related off-target analysis, total RNA from healthy human-derived frontal brain-like neurons treated with the AAV5-mi*ATXN3* candidates or formulation buffer as control. For analysis in mice, total RNA was isolated from brain stem of SCA3 knock-in mice transduced with mi*ATXN3*_9 or the formulation buffer. Total RNA was reverse transcribed and single-end sequence reads were generated using the Illumina

HiSeq2500 system (BaseClear B.V., Leiden, The Netherlands). FASTQ sequence files were generated using the Illumina Casava pipeline version 1.8.3. Initial quality assessment was based on data passing the Illumina Chastity filtering. Subsequently, reads containing PhiX control signal were removed using an in-house filtering protocol. In addition, reads containing (partial) adapters were clipped (up to minimum read length of 50bp). The second quality assessment was based on the remaining reads using the FASTQC quality control tool version 0.10.0. The analysis of the weighted proportions fold change and p-value scores between the conditions were calculated using the Baggerley's Beta-binomial test. The fold change in gene expression was calculated for each comparison (AAV5-mi*ATXN3*_7 versus control, AAV5-mi*ATXN3*_9 versus control and AAV5-mi*ATXN3*_11 versus control).

TR-FRET assay

TR-FRET assay was performed as described before.[41] Brain tissues were lysed by sonication in 10x v/w of ice-cold lysis buffer (PBS +1% TritonX100+1X protease inhibitor cocktail (Roche)). Anti-ataxin-3 clone 1H9 (MAB5360, Millipore) was labeled with donor Lumi4-Tb-fluorophore (Cisbio). Anti-ploy glutamine expansion marker clone 5TF1-1C2 (MAB1574, Millipore) was labeled with D2 acceptor fluorophore (Cisbio). The combination of 1H9 and 5TF1-1C allow detection of more than 37 glutamine repeats. After optimization of antibody titers and incubation conditions, quantification of mutant ataxin-3 levels was performed in low volume polystyrene 384 microtiter plates (Greiner Bio-One) with 5 µl sample volume and addition of 1 µl antibody solution (50 mM NaHPO4+400 mM NaF +0.1% BSA +0.05% Tween-20 +1 ng/ml 1H9-Tb +10 ng/ml 1C2-D2). Plates were then incubated at 4°C for 20 h and analyzed by time-resolved fluorescence at 620 nm and 665 nm on an Envision Multilabel reader (Perkin Elmer).

AAV5 injection in minipigs

A male 7 month old Gottingen minipig was selected at the Institute of Animal Physiology and Genetics in Libechov (Czech Republic). General anaesthesia was induced by intramuscular application of tiletamine (4 mg/kg), zolazepam (4 mg/kg Zoletil 100; Virbac), ketamine (5 mg/kg Narketan 10: Chassot), and xylazine (1 mg/kg (Rometar 2%; Spofa) mixture followed by intravenous ear cannulation and intubation. Artificial ventilation and isoflurane/nitrous oxide anaesthesia was used during the rest of the procedure. For intrathecal administration, a spinal needle (Yale; 121884; 1.2x90 mm) attached to a 5-mL syringe was used. 5 mL of AAV5-GFP (4 x 10^{13} gc/ml) was delivered slowly (over approximately 5 min) by hand injection into the lumbar region of the minipig. 4 weeks after treatment the minipig was sacrificed using pentobarbital sodium intravenous injection (100 mg/kg) followed by a bilateral thoracotomy. The animal was transcardially perfused with 500-1,000 mL of heparinized PBS. Once removed from the skull, the brain

was coronally sliced into 3-4 mm blocks from frontal to occipital. The left hemisphere was used for biomolecular analyses, where 102 brain punches were taken and stored at -80 °C. The right hemisphere was fixed by paraformaldehyde (PFA) for immunostaining of GFP protein (at Libechov, Czech Republic).

DNA isolation from minipig brain tissue

DNA isolation from brain tissue punches was performed using the DNeasy Blood and Tissue kit (QIAGEN, Germany). Primers specific for the CAG promoter sequence were used to measure the vector genome copies (gc) by SYBR Green Fast qPCR (Thermo Fisher Scientific). The amount of vector DNA was calculated based on a plasmid standard curve. Results were reported as gc per microgram of genomic DNA.

Immunohistochemistry on minipig prain tissues

PFA-fixed blocks were sliced in 20-25 coupes of approximately 5um (100-125 coupes/ brain). For immunostaining analysis, the endogenous peroxidase activity was blocked with a solution of 0.3% of hydrogen peroxide in methanol for 20 min, and the brain sections were immunostained using the rabbit primary antibodies anti-GFP (1:1,000, ab6556; Abcam). Sections were then treated with a biotinylated donkey anti-rabbit secondary antibody (1:400, RPN 1004V; GE Healthcare Life Sciences) followed by an avidin-peroxidase complex (1:400, A3151; Sigma-Aldrich). The avidin-peroxidase complex was visualized by incubation with solution containing a dissolved 3, 3 -diaminobenzidine tablet (4170; Kementec Diagnostics). The sections were dehydrated and mounted with DePeX (Sigma). Images were acquired using a histological scanner (Virtual Slide Microscope VS120-5 fluorescence; Olympus), and quantitative analysis of IHC-stained brain sections was performed using Fiji ImageJ distribution (https://fiji.sc/).

Statistical Analysis

Data were analyzed using the one-way ANOVA or Student's t-test to determine statistically significances between control and treated cells. A two-way ANOVA was used to determine statistically significances between multiple treated groups. The p-values were either listed or represented by the following number of asterisks: *$p < 0.05$; **$p < 0.01$; ***$p < 0.001$; ****$p < 0.0001$.

Acknowledgements

The authors would like to thank Ellen Broug and Eileen Sawyer for reviewing this manuscript. The research leading to these results has received funding from the European Community's Seventh Framework Programme (FP7/2007-2013) under grant agreement

n° 2012-305121 "Integrated European –omics research project for diagnosis and therapy in rare neuromuscular and neurodegenerative diseases (NEUROMICS)".

Author contribution

Conceptualization, M.E., R.M., P.K., and S.D. ; Methodology, R.M., J.H., H.N., J.S. ; Investigation, R.M., J.S., S.K., J.H., and E.H. ; Writing – Original Draft, R.M. and M.E.; Writing –Review & Editing, R.M., J.S., J.H., E.H., P.K., H.N., S.D., M.E ; Funding Acquisition, M.E., H.N., P.K.

References

1. Matos, C, Pereira de Almeida, L and Nóbrega, C (2018). Machado-Joseph disease / Spinocerebellar ataxia type 3:lessons from disease pathogenesis and clues into therapy. *J. Neurochem.* doi:10.1111/jnc.14541.
2. Couthino, P and Andrade, C (1978). Autosomal dominant system degeneration in Portuguese families of the Azores Islands: A new genetic disorder involving cerebellar, pyramidal, extrapyramidal and spinal cord motor functions. *Neurology* 28: 703–703.
3. Rosenberg, RN (1992). Machado-Joseph disease: An autosomal dominant motor system degeneration. *Mov. Disord.* 7: 193–203.
4. Ranum, LP, Lundgren, JK, Schut, LJ, Ahrens, MJ, Perlman, S, Aita, J, *et al.* (1995). Spinocerebellar ataxia type 1 and Machado-Joseph disease: incidence of CAG expansions among adult-onset ataxia patients from 311 families with dominant, recessive, or sporadic ataxia. *Am.J.Hum. Genet.* 57: 603–608.
5. Schöls, L, Bauer, P, Schmidt, T, Schulte, T and Riess, O (2004). Autosomal dominant cerebellar ataxias: Clinical features, genetics, and pathogenesis. *Lancet Neurol.* 3: 291–304.
6. Kawaguchi, Y, Okamoto, T, Taniwaki, M, Aizawa, M, Inoue, M, Katayama, S, *et al.* (1994). CAG expansions in a novel gene for Machado-Joseph disease at chromosome 14q32.1. *Nat. Genet.* 8: 221–228.
7. Maciel, P, Do Carmo Costa, M, Ferro, A, Rousseau, M, Santos, CS, Gaspar, C, *et al.* (2001). Improvement in the molecular diagnosis of Machado-Joseph disease. *Arch. Neurol.* 58: 1821–1827.
8. Cummings, CJ and Zoghbi, HY (2000). Trinucleotide repeats: Mechanisms and pathophysiology. *Annu Rev Genomic Hum Genet* 1: 281–328.
9. Maciel, P, Gaspar, C, DeStefano, A, Silveira, I, Coutinho, P, Radvany, J, *et al.* (1995). Correlation between CAG Repeat Length and Clinical Features in Machado-Joseph Disease. *Am. J. Hum. Genet* 57: 54–61.
10. Bettencourt, C and Lima, M (2011). Machado-Joseph disease: From first descriptions to new perspectives. *Orphanet J. Rare Dis.* 6.
11. Goto, J, Watanabe, M, Ichikawa, Y, Yee, SB, Ihara, N, Endo, K, *et al.* (1997). Machado-Joseph disease gene products carrying different carboxyl termini. *Neurosci. Res.* 28: 373–377.
12. Ichikawa, Y, Goto, J, Hattori, M, Toyoda, A, Ishii, K, Jeong, SY, *et al.* (2001). The genomic structure and expression of MJD, the Machado-Joseph disease gene. *J. Hum. Genet.* 46: 413–422.
13. Paulson, HL, Perez, MK, Trottier, Y, Trojanowski, JQ, Subramony, SH, Das, SS, *et al.* (1997). Intranuclear inclusions of expanded polyglutamine protein in spinocerebellar ataxia type 3. *Neuron* 19: 333–344.
14. Macedo-Ribeiro, S, Cortes, L, Maciel, P and Carvalho, AL (2009). Nucleocytoplasmic shuttling activity of ataxin-3. *PLoS One* 4.
15. Schmidt, T, Bernhard Landwehrmeyer, G, Schmitt, I, Trottier, Y, Auburger, G, Laccone, F, *et al.* (1998). An isoform of ataxin-3 accumulates in the nucleus of neuronal cells in affected brain regions of SCA3 patients. *Brain Pathol.* 8: 669–679.
16. Trottier, Y, Cancel, G, An-Gourfinkel, I, Lutz, Y, Weber, C, Brice, A, *et al.* (1998). Heterogeneous intracellular localization and expression of ataxin-3. *Neurobiol. Dis.* 5: 335–347.
17. Riess, O, Rüb, U, Pastore, A, Bauer, P and Schöls, L (2008). SCA3: neurological features, pathogenesis and animal models. *Cerebellum* 7: 125–137.
18. Evers, MM, Toonen, LJA and Van Roon-Mom, WMC (2014). Ataxin-3 protein and RNA toxicity in spinocerebellar ataxia type 3: Current insights and emerging therapeutic strategies. *Mol. Neurobiol.* 49: 1513–1531.
19. Wang, LC, Chen, KY, Pan, H, Wu, CC, Chen, PH, Liao, YT, *et al.* (2011). Muscleblind participates in RNA toxicity of expanded CAG and CUG repeats in Caenorhabditis elegans. *Cell. Mol. Life Sci.* 68: 1255–1267.

20. Miller, JW (2000). Recruitment of human muscleblind proteins to (CUG)n expansions associated with myotonic dystrophy. *EMBO J.* 19: 4439–4448.
21. Fardaei, M, Larkin, K, Brook, JD and Hamshere, MG (2001). In vivo co-localisation of MBNL protein with DMPK expanded-repeat transcripts. *Nucleic Acids Res.* 29: 2766–2771.
22. Jiang, H, Mankodi, A, Swanson, MS, Moxley, RT and Thornton, CA (2004). Myotonic dystrophy type 1 is associated with nuclear foci of mutant RNA, sequestration of muscleblind proteins and deregulated alternative splicing in neurons. *Hum. Mol. Genet.* 13: 3079–3088.
23. Eichler, L, Bellenberg, B, Hahn, HK, Köster, O, Schöls, L and Lukas, C (2011). Quantitative assessment of brain stem and cerebellar atrophy in spinocerebellar ataxia types 3 and 6: Impact on clinical status. *Am. J. Neuroradiol.* 32: 890–897.
24. Sudarsky, L, Corwin, L and Dawson, DM (1992). Machado-Joseph disease in New England: Clinical description and distinction from the olivopontocerebellar atrophies. *Mov. Disord.*doi:10.1002/mds.870070303.
25. Sequeiros J, CP, Sequeiros, J and Coutinho, P (1993). Epidemiology and clinical aspects of Machado-Joseph disease. *Adv Neurol* 61: 139–153.
26. Nóbrega, C, Nascimento-Ferreira, I, Onofre, I, Albuquerque, D, Hirai, H, Déglon, N, *et al.* (2013). Silencing Mutant Ataxin-3 Rescues Motor Deficits and Neuropathology in Machado-Joseph Disease Transgenic Mice. *PLoS One* 8.
27. Alves, S, Nascimento-Ferreira, I, Dufour, N, Hassig, R, Auregan, G, Nóbrega, C, *et al.* (2010). Silencing ataxin-3 mitigates degeneration in a rat model of Machado-Joseph disease: No role for wild-type ataxin-3? *Hum. Mol. Genet.* 19: 2380–2394.
28. Rodríguez-Lebrón, E, Costa, MD, Luna-Cancalon, K, Peron, TM, Fischer, S, Boudreau, RL, *et al.* (2013). Silencing mutant *ATXN3* expression resolves molecular phenotypes in SCA3 transgenic mice. *Mol. Ther.* 21: 1909–1918.
29. Evers, MM, Miniarikova, J, Juhas, S, Vallès, A, Bohuslavova, B, Juhasova, J, *et al.* (2018). AAV5-miHTT Gene Therapy Demonstrates Broad Distribution and Strong Human Mutant Huntingtin Lowering in a Huntington's Disease Minipig Model. *Mol. Ther.* 26: 2163–2177.
30. Miniarikova, J, Zanella, I, Huseinovic, A, van der Zon, T, Hanemaaijer, E, Martier, R, *et al.* (2016). Design, Characterization, and Lead Selection of Therapeutic miRNAs Targeting Huntingtin for Development of Gene Therapy for Huntington's Disease. *Mol. Ther. Nucleic Acids* 5: e297.
31. Miniarikova, J, Evers, MM and Konstantinova, P (2018). Translation of MicroRNA-Based Huntingtin-Lowering Therapies from Preclinical Studies to the Clinic. *Mol. Ther.* 26: 947–962.
32. Klein, RL, Hamby, ME, Gong, Y, Hirko, AC, Wang, S, Hughes, JA, *et al.* (2002). Dose and promoter effects of adeno-associated viral vector for green fluorescent protein expression in the rat brain. *Exp. Neurol.* 176: 66–74.
33. Martier, R, Liefhebber, JM, Garcia-Osta, A, Miniarikova, J, Cuadrado-Tejedor, M, Espelosin, M, *et al.* (2019). Targeting RNA-Mediated Toxicity in *C9orf72* ALS and/or FTD by RNAi-Based Gene Therapy. *Mol. Ther. Nucleic Acids* 16: 26–37.
34. Yang, J-S, Maurin, T, Robine, N, Rasmussen, KD, Jeffrey, KL, Chandwani, R, *et al.* (2010). Conserved vertebrate mir-451 provides a platform for Dicer-independent, Ago2-mediated microRNA biogenesis. *Proc. Natl. Acad. Sci.* 107: 15163–15168.
35. Cifuentes, D, Xue, H, Taylor, DW, Patnode, H, Mishima, Y, Cheloufi, S, *et al.* (2010). A novel miRNA processing pathway independent of dicer requires argonaute2 catalytic activity. *Science (80-.).* 328: 1694–1698.
36. Cheloufi, S, Dos Santos, CO, Chong, MMW and Hannon, GJ (2010). A dicer-independent miRNA biogenesis pathway that requires Ago catalysis. *Nature* 465: 584–589.
37. Yoda, M, Cifuentes, D, Izumi, N, Sakaguchi, Y, Suzuki, T, Giraldez, AJ, *et al.* (2013). Poly(A)-specific ribonuclease mediates 3'-end trimming of argonaute2-cleaved precursor microrna. *Cell Rep.* 5: 715–726.

38. Herrera-Carrillo, E and Berkhout, B (2017). Dicer-independent processing of small RNA duplexes: mechanistic insights and applications. *Nucleic Acids Res.* 45: 10369–10379.
39. Mayuko Yoda, Daniel Cifuentes, Natsuko Izumi, Yuriko Sakaguchi, Tsutomu Suzuki, AJG and YT (2013). PARN mediates 3'-end trimming of Argonaute2-cleaved precursor microRNAs 5.
40. Bezprozvanny, I and Klockgether, T (2009). Therapeutic prospects for spinocerebellar ataxia type 2 and 3. *Drugs Future* 34: 991–999.
41. Nguyen, HP, Hübener, J, Weber, JJ, Grueninger, S, Riess, O and Weiss, A (2013). Cerebellar Soluble Mutant Ataxin-3 Level Decreases during Disease Progression in Spinocerebellar Ataxia Type 3 Mice. *PLoS One* 8.
42. Plass, M, Rasmussen, SH and Krogh, A (2017). Highly accessible AU-rich regions in 3' untranslated regions are hotspots for binding of regulatory factors. *PLoS Comput. Biol.*doi:10.1371/journal.pcbi.1005460.
43. Boudreau, RL, Spengler, RM, Hylock, RH, Kusenda, BJ, Davis, HA, Eichmann, DA, *et al.* (2013). SiSPOTR: A tool for designing highly specific and potent siRNAs for human and mouse. *Nucleic Acids Res.* doi:10.1093/nar/gks797.
44. Schmitt, I, Linden, M, Khazneh, H, Evert, BO, Breuer, P, Klockgether, T, *et al.* (2007). Inactivation of the mouse Atxn3 (ataxin-3) gene increases protein ubiquitination. *Biochem. Biophys. Res. Commun.* 362: 734–739.
45. Alves, S, Nascimento-Ferreira, I, Auregan, G, Hassig, R, Dufour, N, Brouillet, E, *et al.* (2008). Allele-specific RNA silencing of mutant ataxin-3 mediates neuroprotection in a rat model of Machado-Joseph disease. *PLoS One* 3.
46. Evers, MM, Pepers, BA, van Deutekom, JCT, Mulders, SAM, den Dunnen, JT, Aartsma-Rus, A, *et al.* (2011). Targeting several CAG expansion diseases by a single antisense oligonucleotide. *PLoS One* 6.
47. Hu, J, Matsui, M, Gagnon, KT, Schwartz, JC, Gabillet, S, Arar, K, *et al.* (2009). Allele-specific silencing of mutant huntingtin and ataxin-3 genes by targeting expanded CAG repeats in mRNAs. *Nat. Biotechnol.* 27: 478–484.
48. Liu, J, Yu, D, Aiba, Y, Pendergraff, H, Swayze, EE, Lima, WF, *et al.* (2013). Ss-siRNAs allele selectively inhibit ataxin-3 expression: Multiple mechanisms for an alternative gene silencing strategy. *Nucleic Acids Res.* 41: 9570–9583.
49. Datson, NA, González-Barriga, A, Kourkouta, E, Weij, R, Van De Giessen, J, Mulders, S, *et al.* (2017). The expanded CAG repeat in the huntingtin gene as target for therapeutic RNA modulation throughout the HD mouse brain. *PLoS One* 12.
50. Martier R, Liefhebber J, Miniarikova J, van der Zon T, Snapper J, Kolder I, Petry H, van Deventer S, Evers M, KP. Artificial microRNAs targeting *C9orf72* have the potential to reduce accumulation of the intra-nuclear transcripts in ALS and FTD patients. *Mol. Ther. - Nucleic Acids*.
51. Colella, P, Ronzitti, G and Mingozzi, F (2018). Emerging Issues in AAV-Mediated In Vivo Gene Therapy. *Mol. Ther. - Methods Clin. Dev.* 8: 87–104.
52. Saraiva, J, Nobre, RJ and Pereira de Almeida, L (2016). Gene therapy for the CNS using AAVs: The impact of systemic delivery by AAV9. *J. Control. Release* 241: 94–109.
53. Hocquemiller, MM, Giersch, L, Audrain, M, Parker, S and Cartier, N (2016). Adeno-Associated Virus-Based Gene Therapy for CNS Diseases. *Hum. Gene Ther.* 27: 478–496.
54. Zincarelli, C, Soltys, S, Rengo, G and Rabinowitz, JE (2008). Analysis of AAV serotypes 1-9 mediated gene expression and tropism in mice after systemic injection. *Mol. Ther.* 16: 1073–1080.
55. Foust, KD, Nurre, E, Montgomery, CL, Hernandez, A, Chan, CM and Kaspar, BK (2009). Intravascular AAV9 preferentially targets neonatal neurons and adult astrocytes. *Nat. Biotechnol.* 27: 59–65.
56. Mendell, JR, Zaidy, S Al, Shell, R, Arnold, WD, Klapac, LRR, Prior, TW, *et al.* (2017). Single-Dose Gene-Replacement Therapy for Spinal Muscular Atrophy. *N. Engl. J. Med.* 377: 1713–1722.
57. Samaranch, L, Blits, B, San Sebastian, W, Hadaczek, P, Bringas, J, Sudhakar, V, *et al.*

(2017). MR-guided parenchymal delivery of adeno-associated viral vector serotype 5 in non-human primate brain. *Gene Ther.* 24: 253–261.

58. Toonen, LJA, Rigo, F, van Attikum, H and van Roon-Mom, WMC (2017). Antisense Oligonucleotide-Mediated Removal of the Polyglutamine Repeat in Spinocerebellar Ataxia Type 3 Mice. *Mol. Ther. - Nucleic Acids* 8: 232–242.
59. Do Carmo Costa, M, Luna-Cancalon, K, Fischer, S, Ashraf, NS, Ouyang, M, Dharia, RM, *et al.* (2013). Toward RNAi therapy for the polyglutamine disease Machado-Joseph disease. *Mol. Ther.* 21: 1898–1908.
60. Dean, B, Gibbons, A, Gogos, A, Udawela, M, Thomas, E and Scarr, E (2018). Studies on prostaglandin-endoperoxide synthase 1: Lower levels in schizophrenia and after treatment with antipsychotic drugs in conjunction with aspirin. *Int. J. Neuropsychopharmacol.* doi:10.1093/ijnp/pyx092.
61. Mendonça, LS, Nóbrega, C, Tavino, S, Brinkhaus, M, Matos, C, Tomé, S, *et al.* (2019). Ibuprofen enhances synaptic function and neural progenitors proliferation markers and improves neuropathology and motor coordination in Machado-Joseph disease models. *Hum. Mol. Genet.*doi:10.1093/hmg/ddz097.
62. Zhou, F, Leder, P and Martin, SS (2006). Formin-1 protein associates with microtubules through a peptide domain encoded by exon-2. *Exp. Cell Res.* doi:10.1016/j.yexcr.2005.12.035.
63. Akpınar, M, Lesche, M, Fanourgakis, G, Fu, J, Anasstasiadis, K, Dahl, A, *et al.* (2017). TDRD6 mediates early steps of spliceosome maturation in primary spermatocytes. *PLoS Genet.*doi:10.1371/journal.pgen.1006660.
64. Wang, TH, Hsia, SM and Shieh, TM (2017). Lysyl oxidase and the tumor microenvironment. *Int. J. Mol. Sci.*doi:10.3390/ijms18010062.
65. Erler, JT, Bennewith, KL, Nicolau, M, Dornhöfer, N, Kong, C, Le, QT, *et al.* (2006). Lysyl oxidase is essential for hypoxia-induced metastasis. *Nature*doi:10.1038/nature04695.
66. Cox, TR, Gartland, A and Erler, JT (2016). Lysyl oxidase, a targetable secreted molecule involved in cancer metastasis. *Cancer Res.* doi:10.1158/0008-5472.CAN-15-2306.
67. Kaneda, A, Wakazono, K, Tsukamoto, T, Watanabe, N, Yagi, Y, Tatematsu, M, *et al.* (2004). Lysyl oxidase is a tumor suppressor gene inactivated by methylation and loss of heterozygosity in human gastric cancers. *Cancer Res.*doi:10.1158/0008-5472.CAN-04-1543.
68. Ozdener, GB, Bais, M V. and Trackman, PC (2016). Determination of cell uptake pathways for tumor inhibitor lysyl oxidase propeptide. *Mol. Oncol.*doi:10.1016/j.molonc.2015.07.005.
69. Scherzed, W, Brunt, ER, Heinsen, H, De Vos, RA, Seidel, K, Bürk, K, *et al.* (2012). Pathoanatomy of cerebellar degeneration in spinocerebellar ataxia type 2 (SCA2) and type 3 (SCA3). *Cerebellum*doi:10.1007/s12311-011-0340-8.
70. Sudarsky, L and Coutinho, P (1995). Machado-Joseph disease. *Clin. Neurosci.*
71. Dürr, A, Stevanin, G, Cancel, G, Duyckaerts, C, Abbas, N, Didierjean, O, *et al.* (1996). Spinocerebellar ataxia 3 and Machado-Joseph disease: Clinical, molecular, and neuropathological features. *Ann. Neurol.* doi:10.1002/ana.410390411.
72. Yamada, M, Sato, T, Tsuji, S and Takahashi, H (2008). CAG repeat disorder models and human neuropathology: Similarities and differences. *Acta Neuropathol.* doi:10.1007/s00401-007-0287-5.
73. Muñoz, E, Rey, MJ, Milà, M, Cardozo, A, Ribalta, T, Tolosa, E, *et al.* (2002). Intranuclear inclusions, neuronal loss and CAG mosaicism in two patients with Machado-Joseph disease. *J. Neurol. Sci.* doi:10.1016/S0022-510X(02)00110-7.
74. Rüb, U, Brunt, ER and Deller, T (2008). New insights into the pathoanatomy of spinocerebellar ataxia type 3 (Machado-Joseph disease). *Curr. Opin. Neurol.* 21: 111–116.
75. Paulson, HL, Das, SS, Crino, PB, Perez, MK, Patel, SC, Gotsdiner, D, *et al.* (1997). Machado-Joseph disease gene product is a cytoplasmic protein widely expressed in brain. *Ann. Neurol.* doi:10.1002/ana.410410408.

Supplementary material

Table S1. Treatment group design of the in vivo investigations. AAV5-mi*ATXN3*_7, -9 and -11 were tested *in vivo* and delivered to the SCA3 knock-in mice by 3 different routes of administration.

Groups	Treatment	Route of injection	Number of animals (n)	Amount of injection (µl)
1	AAV5-mi*ATXN3*_7	ICV	3	10
2		Cisterna magna	3	10
3		Bilateral DCN	3	4 = 2+2
4	AAV5-mi*ATXN3*_9	ICV	3	10
5		Cisterna magna	3	10
6		Bilateral DCN	3	4 = 2+2
7	AAV5-mi*ATXN3*_11	ICV	3	10
8		Cisterna magna	3	10
9		Bilateral DCN	3	4 = 2+2
10	AAV5-GFP	Bilateral DCN	3	4 = 2+2
11	No treatment	Not applicable	3	0

Table S2. Prediction of off-target genes based on BLAST search and RNA sequencing. BLAST search was performed with the guide sequences of mi*ATXN3*_7, mi*ATXN3*_9 and mi*ATXN3*_11. The blast results were then compared to RNA sequencing expression values obtained from human-derived frontal brain-like neurons treated with the AAV5-mi*ATXN3* candidates or the formulation buffer. P-values >0.05 were excluded

Treatment	Transcript (Blast)	% coverage (Blast)	Fold Change (treatment vs PBS)	p-value (treatment vs PBS)
mi*ATXN3*_7	*ATXN3*	100%	-1.2	9.4E-03
mi*ATXN3*_7	GNPTAB	63%	1.1	4.2E-03
mi*ATXN3*_7	SOX5	63%	-1.1	2.6E-02
mi*ATXN3*_7	GNPTAB	63%	1.1	4.2E-03
mi*ATXN3*_7	CTSC	63%	1.3	2.2E-16
mi*ATXN3*_9	*ATXN3*	100%	-1.5	3.4E-16
mi*ATXN3*_9	TNFRSF6B	59%	1.3	4.4E-02
mi*ATXN3*_9	FGD6	59%	-1.2	9.1E-03
mi*ATXN3*_11	*ATXN3*	100%	-1.3	1.0E-06
mi*ATXN3*_11	ICA1	68%	1.3	4.8E-03
mi*ATXN3*_11	CACNA1D	63%	1.5	2.9E-02

Table S3. Prediction of off-target genes in human by siSPOTR and RNA sequencing after AAV5-mi*ATXN3*_7 treatment. A search was performed on siSPOTR with the seed sequence of mi*ATXN3*_7 to check for binding within 3'UTR of human transcripts. The top 20 genes with highest tPOTS were compared to RNA sequencing expression values in human-derived frontal brain-like neurons. RNA sequencing was performed on RNA isolated from human-derived frontal brain-like neurons treated with AAV5-mi*ATXN3*_7 or the formulation buffer for 7 days. The genes with p-value < 0.05 were excluded.

Gene name	TPOTS value	8mer	7mer-M8	7mer-1A	6mer	Fold Change (mi7 vs PBS)	p-value (mi7 vs PBS)
WDR72	0.816	1	1	9	1	-1.4	9.5E-03
SCAI	0.615	1	0	7	0	-1.3	3.4E-05
GDA	0.547	3	0	1	2	-2.3	6.9E-03
FOXP2	0.526	2	2	1	1	-1.3	2.9E-02
DNAL1	0.525	0	1	7	0	-1.3	1.5E-02
AAK1	0.522	2	0	3	7	1.1	3.3E-02
KCNMA1	0.488	1	0	5	3	1.3	1.8E-03
ONECUT2	0.487	1	0	5	2	-1.2	6.9E-04
FBXL20	0.428	1	1	3	3	-1.2	3.6E-03
IKZF2	0.426	1	1	3	1	-1.4	3.2E-02
BMPR1B	0.426	1	1	3	1	-1.3	1.6E-04
CSRNP3	0.403	0	2	4	3	-1.3	1.4E-02
LIFR	0.367	1	2	1	2	-1.4	1.5E-03
ZNF652	0.36	1	1	2	0	-1.1	3.1E-03
LONRF2	0.36	1	0	3	5	1.2	8.9E-05
CPNE3	0.36	1	1	2	0	-1.2	7.7E-03
PHF6	0.357	1	0	3	2	-1.2	1.3E-02
C21orf91	0.357	1	0	3	2	-1.2	1.2E-02
TMEM47	0.356	1	0	3	1	-1.3	1.3E-02
ARL3	0.355	1	0	3	0	-1.1	2.0E-03
ATXN3	0.295	1	1	1	0	-1.2	9.4E-03

Table S4. Prediction of off-target genes in human by siSPOTR and RNA sequencing for AAV5-mi*ATXN3*_9 treatment. Performed as described in table S3 for AAV5-mi*ATXN3*_9.

Gene name	TPOTS value	8mer	7mer-M8	7mer-1A	6mer	Fold Change (mi9 vs PBS)	p-value (mi9 vs PBS)
PHC3	0.651	2	1	4	1	-1.3	1.2E-03
HIF3A	0.617	3	1	1	2	-1.4	3.1E-02
ONECUT2	0.606	0	3	6	6	-1.2	3.4E-13
UBE2R2	0.515	2	0	3	0	-1.1	1.5E-04
H6PD	0.493	1	1	4	3	-1.2	6.0E-16
RAB3B	0.43	1	1	3	5	-1.3	6.3E-10
PTGS1	0.427	1	1	3	2	-3.4	1.3E-121
KSR2	0.412	0	4	2	2	1.4	2.1E-04
TTC14	0.391	2	1	0	1	-1.1	1.9E-05
BBX	0.391	2	1	0	1	-1.2	3.2E-04
ZNF286B	0.385	2	0	1	0	-1.2	3.4E-03
SYT2	0.385	2	0	1	0	-1.2	2.2E-05
SYP	0.385	2	0	1	0	1.3	0.0E+00
THY1	0.365	1	2	1	0	1.3	7.2E-03
TFDP2	0.365	1	2	1	0	-1.4	1.3E-17
PRLR	0.357	1	0	3	2	-1.2	8.0E-03
FMN1	0.328	0	0	5	3	2.1	2.6E-05
PRX	0.326	0	0	5	1	-1.2	1.1E-02
NCALD	0.326	0	0	5	1	-1.1	1.9E-05
ATXN3	0.001	0	0	0	1	-1.5	3.4E-16

Table S5. Prediction of off-target genes in human by siSPOTR and RNA sequencing for AAV5-mi*ATXN3*_11 treatment. Performed as described in table S3 for AAV5-mi*ATXN3*_11.

Gene name	TPOTS value	8mer	7mer-M8	7mer-1A	6mer	Fold Change (mi11 vs PBS)	p-value (mi11 vs PBS)
SPTY2D1	0.615	3	1	1	0	-1.1	9.3E-05
ENAH	0.586	2	1	3	1	1.2	3.0E-08
TDRD6	0.55	3	1	0	0	-1.6	2.8E-02
PRKAB2	0.546	3	0	1	1	1.1	9.2E-05
TAB3	0.525	2	2	1	0	-1.2	5.4E-04
C1orf21	0.518	2	0	3	3	-1.3	4.7E-57
SMAD2	0.517	2	0	3	2	-1.1	2.4E-03
BRWD1	0.515	2	0	3	0	-1.1	4.0E-17
EXD2	0.498	1	2	3	3	-1.2	4.1E-05
NFYA	0.497	1	2	3	2	-1.3	1.0E-35
AAK1	0.484	0	5	2	4	1.2	8.7E-06
RRAGD	0.456	2	1	1	1	-1.2	6.7E-03
RBM43	0.455	2	1	1	0	-1.4	2.3E-07
ATRNL1	0.455	2	1	1	0	-1.1	8.8E-04
ZFHX3	0.451	2	0	2	1	1.1	1.5E-02
LYSMD3	0.451	2	0	2	1	-1.2	3.6E-02
LOX	0.451	2	0	2	1	1.8	1.6E-12
LPP	0.446	1	4	0	6	1.2	1.1E-02
PAPOLG	0.432	1	2	2	2	-1.1	2.9E-02
C21orf91	0.426	1	1	3	1	-1.2	4.9E-02
ATXN3	0	0	0	0	0	-1.3	9.96E-07

Table S6. Prediction of off-target genes in mice by siSPOTR and RNA sequencing for AAV5-mi*ATXN3*_9 treatment. Performed as described in table S3. siSPOTR search was performed against mouse transcripts. RNA sequencing was performed on RNA isolated from brain stem of SCA3 knock-in mice treated with AAV5-mi*ATXN3*_9 or control (untreated) by injection in the cisterna magna.

Gene name	TPOTS value	8mer	7mer-M8	7mer-1A	6mer	Fold Change (mi9 vs untreated)	p-value (mi9 vs untreated)
Ncl	0.657	2	2	3	2	1.3	8.3E-03
Aak1	0.51	1	4	1	5	-1.6	5.0E-05
Onecut2	0.497	1	2	3	2	-1.2	1.3E-03
Nhsl2	0.461	0	1	6	1	-1.5	1.5E-04
Cacna1e	0.458	2	1	1	3	-1.0	5.0E-05
Nav1	0.435	1	2	2	5	-1.4	5.0E-05
Ttc14	0.422	1	0	4	2	-1.6	5.0E-05
Fzd3	0.408	0	3	3	3	-1.3	5.0E-05
Srgap3	0.396	0	1	5	1	-0.8	3.0E-04
Pde5a	0.391	2	1	0	1	-1.0	2.0E-03
Lonrf2	0.385	2	0	1	0	-1.3	5.0E-05
Zfp704	0.37	1	2	1	5	-1.1	5.0E-05
Mecp2	0.368	1	2	1	3	-1.5	5.0E-05
Cldn12	0.362	1	1	2	2	-1.3	5.0E-05
Dnajc18	0.361	1	1	2	1	-0.6	1.2E-02
0610030E20Rik	0.361	1	1	2	1	-1.2	2.0E-04
Dhx33	0.36	1	1	2	0	-0.7	5.8E-03
Pdzd2	0.356	1	0	3	1	-1.2	5.0E-05
D430041D05Rik	0.355	1	0	3	0	-1.4	5.0E-05
Atxn3	0.16	1	0	0	0	-1.7	5.0E-05

Chapter 5

Transduction patterns in the CNS following various routes of AAV5-mediated gene delivery

Kimberly L. Pietersz[1,2,3], Raygene Martier[1,2,4], Sumiati Baatje[2], Jolanda M. Liefhebber[2], Cynthia Brouwers[2], Stephan Pouw[2], Lianne Fokkert[2], Jacek Lubelski[2], Harald Petry[2], Gerard J.M. Martens[3], Sander van Deventer[2,4], Pavlina Konstantinova[2] and Bas Blits[2,5]

[1]these authors contributed equally
[2]Department of Research & Development, uniQure biopharma B.V., Amsterdam, the Netherlands
[3]Department of Molecular Animal Physiology, Donders Institute for Brain, Cognition and Behaviour, Centre for Neuroscience, Faculty of Science, Radboud University, Nijmegen, The Netherlands
[4]Department of Gastroenterology and Hepatology, Leiden University Medical Center, Leiden, the Netherlands
[5]Current address: Blits Biopharma Consultancy, The Netherlands

Gene Ther. Accepted, March 2020

Abstract

Various administration routes of adeno-associated virus (AAV)-based gene therapy have been examined to target the central nervous system. In this study, we evaluated a recently improved AAV5 vector system for its capability to target the central nervous system via intrastriatal, intrathalamic or intracerebroventricular delivery routes. AAV5 is an ideal candidate for gene therapy because of its relatively low level of existing neutralizing antibodies compared to other serotypes, and its broad tissue and cell tropism. Intrastriatal administration of AAV5-GFP resulted in centralized localized vector distribution and expression in the frontal part of the brain. Intrathalamic injection showed transduction and gradient expression from the rostral brain into lumbar spinal cord, while intracerebroventricular administration led to a more evenly, albeit relatively superficially distributed, transduction and expression throughout the central nervous system. To visualize the differences between localized and intra-cerebral spinal fluid administration routes, we compared intrastriatal to intracerebroventricular and intrathecal administration of AAV5-GFP. Together, our results demonstrate that for efficient transgene expression in neuronal cell bodies of deeper brain structures local administration is necessary and that, depending on the desired AAV transduction pattern and transgene expression level, various administration routes can be applied.

Introduction

Since the first clinical protocol was published for the treatment of Canavan's disease (CD) in 2002 [1], great progress has been made in the field of adeno-associated virus (AAV)-based gene therapy for neurological diseases. Long-term follow-up studies have shown that although intra-cortical administration of AAV2-based therapy was safe, no clear benefit of the therapy has been observed, most likely due to insufficient delivery and hence inadequate expression of the therapeutic gene at the correct location [1]. The 2002 clinical study has illustrated the importance of effective delivery to all affected sites. Cortical delivery of AAV2 resulted in relatively low transduction of tissue beyond the injection site. Therefore, other areas affected in CD, such as the brainstem and cerebellum, were not transduced. Additionally, in the brain the substrate of the mutated enzyme is found mostly in oligodendrocytes and their progenitor cells with smaller amounts in microglia and brainstem neurons. As AAV2 predominantly transduces neurons, the affected cells are not targeted by this serotype.

AAV5 is an ideal candidate for gene therapy as it has relatively low seroprevalence, i.e. antibodies against the capsid, compared to other serotypes [2] and a broad tropism for muscle, liver and CNS [3, 4]. Intrastriatal (IStr) delivery of AAV5 to the murine brain has resulted in the highest degree of transduction of the striatum when compared to AAV serotypes 1,2,4,6,8 and 9 [3]. IStr administration of AAV5 to rats [5] and primates [6, 7] showed improvement in transgene expression with regards to expression levels and scope of target cell population for AAV5 compared to other serotypes tested. Furthermore, following IStr administration AAV5 is transduced into neurons, astrocytes, microglia and oligodendrocytes [3] and into distant nuclei such as substantia nigra (SN) reticulata, globus pallidus, cortex and thalamus [8]. Thus, AAV5 is a promising vector for disease indications that require a global transduction of the brain.

AAV can be administered through various routes, e.g. directly into the parenchyma (brain or spinal cord), into the cerebral spinal fluid (CSF) or intravenously (IV), in an effort to specifically target affected sites, whereby each route has its characteristics with specific advantages and disadvantages. In human subjects, intrathecal (IT) delivery is a relatively non-invasive procedure consisting of a lumbar puncture. Schuster and colleagues [9] have shown that at the lumbar site IT administration of AAV5-GFP in rats led to GFP expression throughout the spinal cord and in discrete regions of the CNS throughout the rostro-caudal extent of the neuroaxis [9, 8]. Broader transduction of the rostral part of the brain may be achieved with an intracerebroventricular (ICV) injection into the lateral ventricle. These studies have also shown that AAV5 does not cross the blood-brain barrier after IV transduction and hence this delivery route was not taken into consideration in the current study.

Different transduction patterns are desirable in order to target various diseases. For instance, in Parkinson's Disease (PD) neurodegeneration mainly occurs in dopaminergic cells of the SN [10], while prominent neuropathology in Huntington Disease (HD) occurs within

the striatal part of the basal ganglia, and secondary marked neuronal loss and shrinkage is observed in the deep layers of the cerebral cortex [11]. Parenchymal administration of AAV could result in significant transduction for production of therapeutic protein in these areas. In the monogenetic disease Niemann Pick Type C, a progressive loss of Purkinje cells is observed [12], the cerebellum and brainstem is the genesis of neuropathology in spinocerebellar ataxias (SCAs), and the hippocampus is the earliest brain region affected in Alzheimer's Disease (AD). Direct administration of therapeutic-encoding AAV2/5 to the hippocampus in an AD model has been shown to ameliorate disease progression [13]. These studies make hippocampal and cerebellar transduction of interest for transgene delivery. In order to develop a therapy for these disorders, it is essential to characterize to what extent a transgene is delivered by AAV to the brain or spinal cord. In some cases, a broader delivery spectrum may be needed, such as in patients with Amyotrophic Lateral Sclerosis (ALS) where both the upper and lower motor neurons of the brain and spinal cord are affected. Another example is the neurological phenotype of infantile Pompe´s disease where the brain stem motor and sensory neurons, spinal cord motor-, sensory- and interneurons are affected [14]. For these indications, a broader transduction pattern seems necessary, e.g. via an intrathecal approach. Recently, a phase-1 trial for San Filippo B disease has shown that 16 intraparenchymal injections of AAV2/5 encoding the deficient enzyme alpha-N-acetylglucosaminidase (NaGlu) into white matter of the cortex were well tolerated [14]. Theoretically, by infusing into a more central area in the brain, it might be possible to reach the affected areas with one bilateral IStr or intrathalamic (ITH) administration. Both sites have multiple anterograde and retrograde projections throughout the brain. These projections can be used to predict the distribution of the transgene product. Moreover, the choice of serotype can also influence the expression pattern, expanding the possibilities and necessities of a so-called AAV toolbox even further.

In this study, we explored the transduction pattern of AAV5 following IStr, ITH, ICV or IT administration. Predictable transduction patterns will aid the design of new therapeutic strategies.

Results

IStr, ICV and ITH administration of AAV5 leads to distinct vector DNA distributions and transgene RNA expression patterns in rats

To evaluate the capability of AAV5 to transduce the brain after parenchymal or CSF-mediated administration, AAV5 was administered to rats IStr, ICV or ITH (fig 1). IStr injection of AAV5-GFP resulted in vector DNA and GFP RNA expression in the cortex, striatum, thalamus, and hippocampus (fig. 2a brain). Vector DNA was not detected above background levels ($1x10^3$ genome copies(gc)/µg genomic DNA) in the cerebellum, brain stem, spinal cord or peripheral organs (fig. 2a).

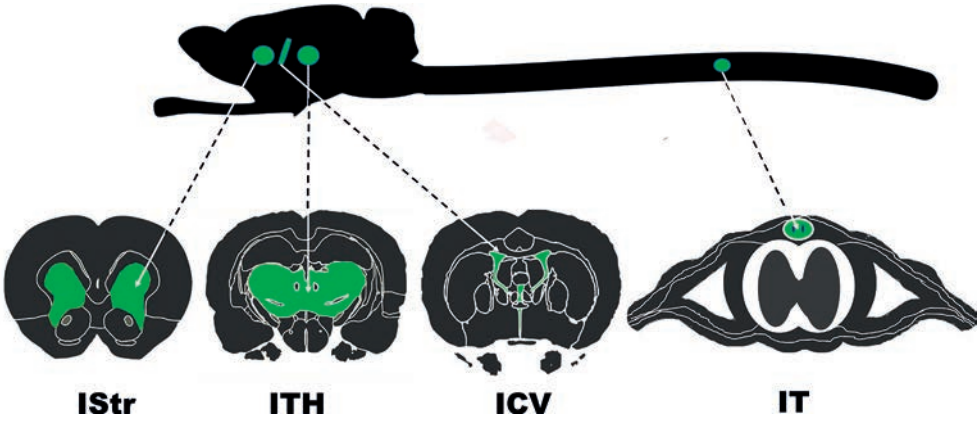

Figure 1. Overview of injection routes Intrastriatal (IStr), intrathalamic(ITH), intracerebroventricular (ICV) and intrathecal (IT) injections in the rat have been performed in this study. Green areas indicate the site of injection and the predicted spread of the fluid containing the vector.

Thalamic administration of AAV5-GFP led to the transduction (both presence of vector and GFP RNA expression) in the cortical-, striatal-, thalamic-, hippocampal-, cerebellar area, and brainstem (fig. 2b, brain). Furthermore, we also observed vector DNA and GFP RNA presence in the spinal cord, albeit at a lower level than in the brain (fig. 2b, spinal cord). Surprisingly, vector DNA was detected in the spleen. However, this did not result in GFP relative expression above background levels. (fig. 2b peripheral organs).

ICV-administered rats showed a more even distribution pattern with similar amounts of vector DNA, and GFP RNA expression throughout the brain and spinal cord (fig. 2c brain and spinal cord). Vector DNA was also retrieved in liver, kidney, and spleen (fig. 2c peripheral organs). However, in the peripheral organs there was no GFP RNA detected above background levels, even though the CAG promoter is classified as a ubiquitous expression promoter [14].

Distinct protein expression pattern observed at macro level when comparing IStr administration of AAV5-GFP to ICV and IT in rats

We delved further into the potential use of AAV5 for diseases affecting the brain and spinal cord by aiming for a larger area of transduction. As shown in the previous experiment, ICV administration in rats leads to broad transduction of the cerebral areas and spinal cord on DNA and RNA level. To assess the maximum capability of AAV5, the vector was administered ICV and IT (fig. 1) at the highest titer available, $1x10^{14}$ GC/ml, and compared to IStr administration (as local administration method) at the same high titer, but the volume was adjusted depending on the administration method.

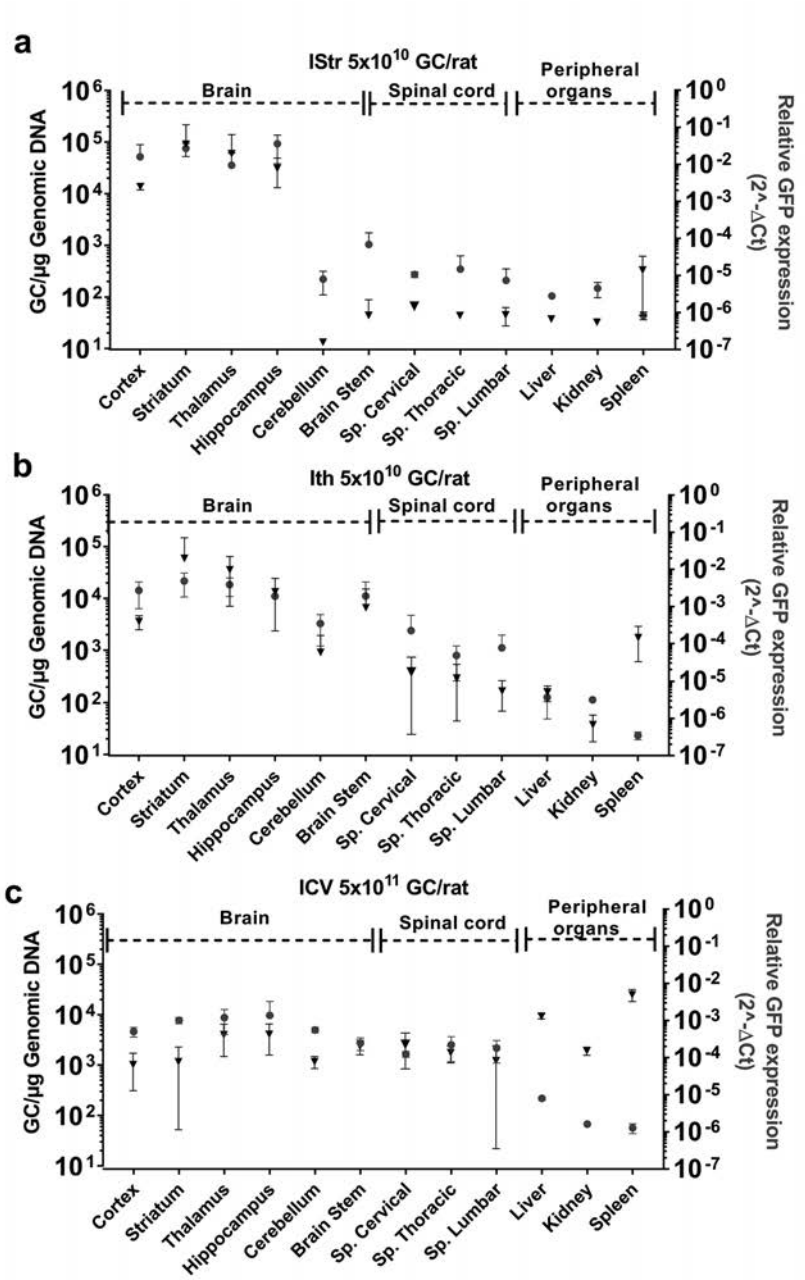

Figure 2. Vector distribution and GFP expression following various cerebral administration routes of AAV5-GFP in rats. Rats(n=3) received a total of 5E10 genomic copies (GC) of AAV5-CAG-GFP bilaterally by intrastriatal (IS) (a), intrathalamic (ITH) (b), or 5E11GC total via Intracerebroventricular (ICV) (c) administration. Tissues were collected eight weeks post surgery, and DNA and RNA were isolated to determine the vector distribution and GFP expression. IS-administration resulted into distribution and expression in the frontal areas, basal ganglia, and midbrain. ITH-administration les to a more spread gene expression compared to IS-administration. Black triangles represent GC/µg genomic DNA, whereas grey circles represent relative GFP expression (RNA). Sp: spinal cord.

Figure 3 gives an overview of the results following the three administration routes in rat brain. In the frontal area, both IStr (fig. 3a) and ICV (fig. 3b) administration of AAV5-GFP resulted in GFP expression in the striatum and the cortex. At this magnification level, staining was only observed in the cortex of IT-administered rats (fig. 3c). In the striatal area of IStr-injected rats, the complete caudate putamen was transduced. In comparison, GFP staining was concentrated around the ventricles surrounding the striatum and the cortex in the brains of ICV-administered rats.

In the hippocampal structure of IStr-administered rats, only the Cornu Ammonis (CA)1 area showed moderate GFP expression. In ICV-administered rats, the complete hippocampal structure appeared to be transduced. IT-administration showed propensity towards a low degree of GFP expression in the molecular layer of the hippocampus. In the midbrain area, both ICV- and IStr-administered rats displayed GFP staining in the SN, while this area was negative in IT rats. The hypothalamus shows some GFP-positive staining in both the ICV and IT administered rats. At the occipital end of the cerebral area, the cerebellum of ICV- and IT-injected rats appeared to have some GFP-positive areas (Fig3C)

IT, IS and ICV administration of AAV5 leads to different GFP expression profiles in the frontal area

Upon taking a closer look at the frontal brain area, we observed a striking difference between the three injection routes. In the striatum of IStr-injected rats, neurons and surrounding matter were GFP positive (fig.4a, ST). In the cortical area of these rats, GFP-positive neurons were observed, yet the intensity of staining in the surrounding area was less intense compared to that in rats injected in the ICV or IT (fig 4a, CR). In ICV-administered rats, the frontal area showed GFP expression in neurons and surrounding matter in the striatum and cortex (fig. 4b). In contrast to the pattern seen in ICV- and IStr-administered rats, in the striatum of IT- administered rats GFP-positive neurons and axons were observed, however surrounding striatal white matter showed no GFP expression (fig. 4c).

ICV administration of AAV5-GFP leads to GFP expression in the hippocampal structure of rat

IStr administration of AAV5-GFP in rats led to GFP staining of the hippocampal layers within the CA1 area, such as the pyramidal cell, lacunosum molecular and oriens layers. Some sparse neurons of the CA2 showed positive staining, but most of this area was negative. Neurons of the CA3 pyramidal cell layer were GFP positive as well as neurons and dendrites in the Dentate Gyrus (DG), but the surrounding matter and layers of the DG were negative for GFP expression (fig. 5a).

In the ICV-administered rats, the core area of the hippocampus was thoroughly transduced, aiding in clear visualization of its structural architecture. For instance, at

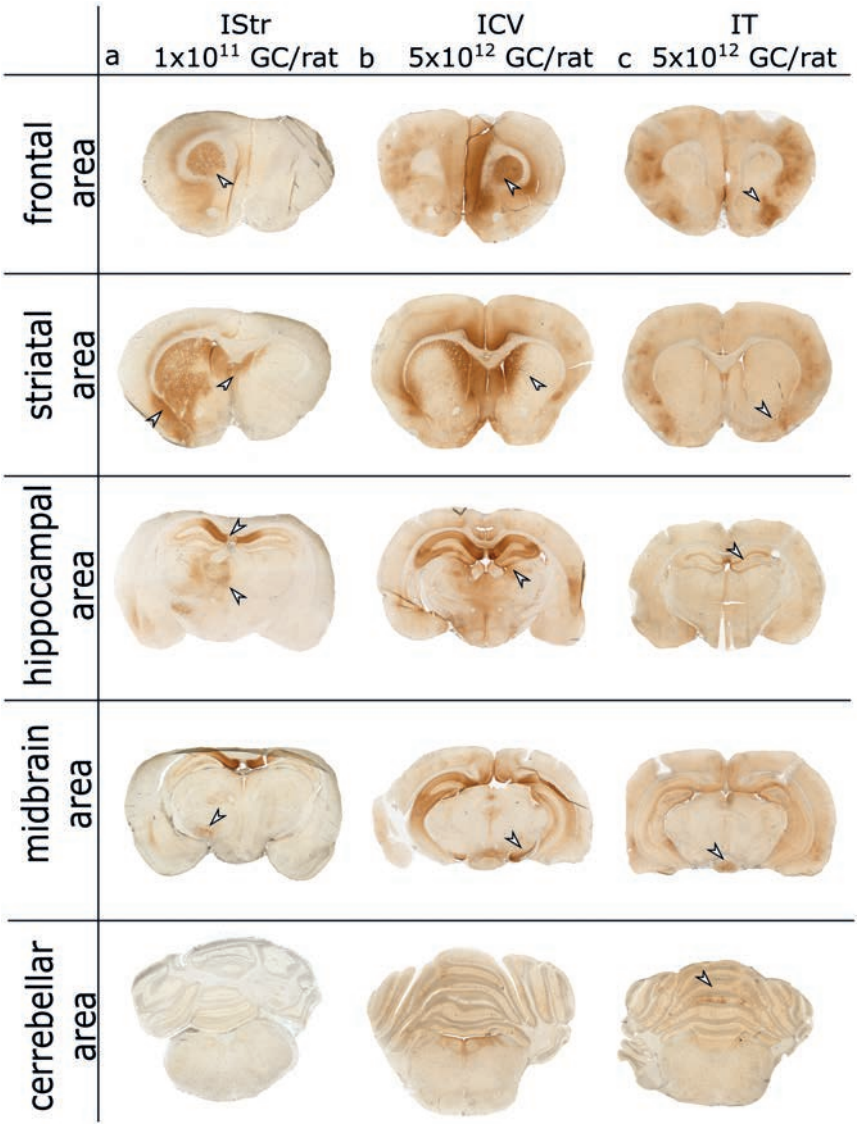

Figure 3. GFP expression throughout the rat brain following intrastriatal (IStr), intracerebroventricular (ICV) or intrathecal (IT) administration of AAV5-GFP. Rats(n=3) were administered with AAV5-GFP at $1x10^{14}$ GC/ml, respectively 1, 50 and 50 µl and sacrificed after one month. Brains were extracted, fixed in 4% paraformaldehyde, embedded in gelatin and serially cut with a vibratome to 50 µm sections. a) IS-administered rats show GFP staining (shown in brown) in the striatum, neocortex, and upper septum region. Beyond the injection site, also the Cornu Ammonis 1 field of the hippocampus, rostral part of the thalamus and the substantia nigra were positive for GFP signal. b) ICV-administered rats showed partial GFP IR in the striatal area and neocortex, rostral part of the thalamus, the complete hippocampus and the substantia nigra. c) IT-administered rats showed primarily transduction of the neocortex and hypothalamus, and some layers of the cerebellum. At this magnification level, staining was not observed in the basal ganglia or thalamus. Areas of interest indicated by white arrows. Figure is representative from 3 animals.

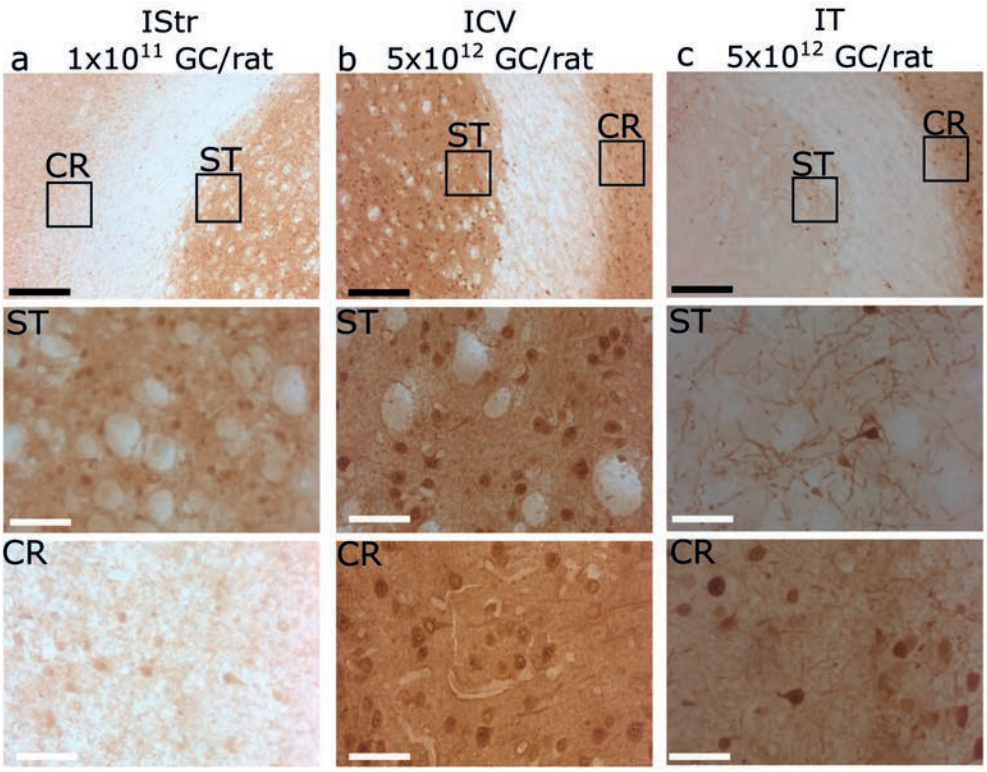

Figure 4. GFP expression in cortex and striatum in rat brain following intrastriatal (IStr), intracerebroventricular (ICV) or intrathecal (IT) administration of AAV5-GFP Overview of striatal (ST) and cortical (CR) area from a) IS administered rat, b) ICV administered rats, c) IT administered rats. Both IS- and ICV-administration in rats result in GFP stained neurons and the surrounding fibers in the ST area. Striatal area of IT administered rats displayed GFP staining neurons and neurites. However, no GFP staining was observed in the surrounding area. In the cortical area a similar transduction pattern is seen in IT- and ICV-administered rats. In the cortical area of IS-administered rats, the matter staining is less intense compared to the other routes of injection. Black bar represents 1 mm and white bar represents 100µm for scale.

the transition from CA1 to CA2 there was a difference in the intensity of GFP staining. Also, a clear distinction could be made in the morphology of the pyramidal layer of CA2 versus CA1. In the DG neurons of the granular layer were GFP positive as well as surrounding matter and molecular layers (fig. 5b).

In IT-administered rats, strong GFP staining of middle and outer molecular layer of the DG was observed. Positive neurons, dendrites, and axons could be observed in the granular layer of the DG. The morphology of stained cells in the granular layer differs from that of ICV injected rats. In the ICV DG, a tightly packed layer of neurons was seen, whilst the IT neurons were spaced with longer neurites Therefore, it seems that these neurons are in the subgranular zone rather than the granular layer itself. In the CA2

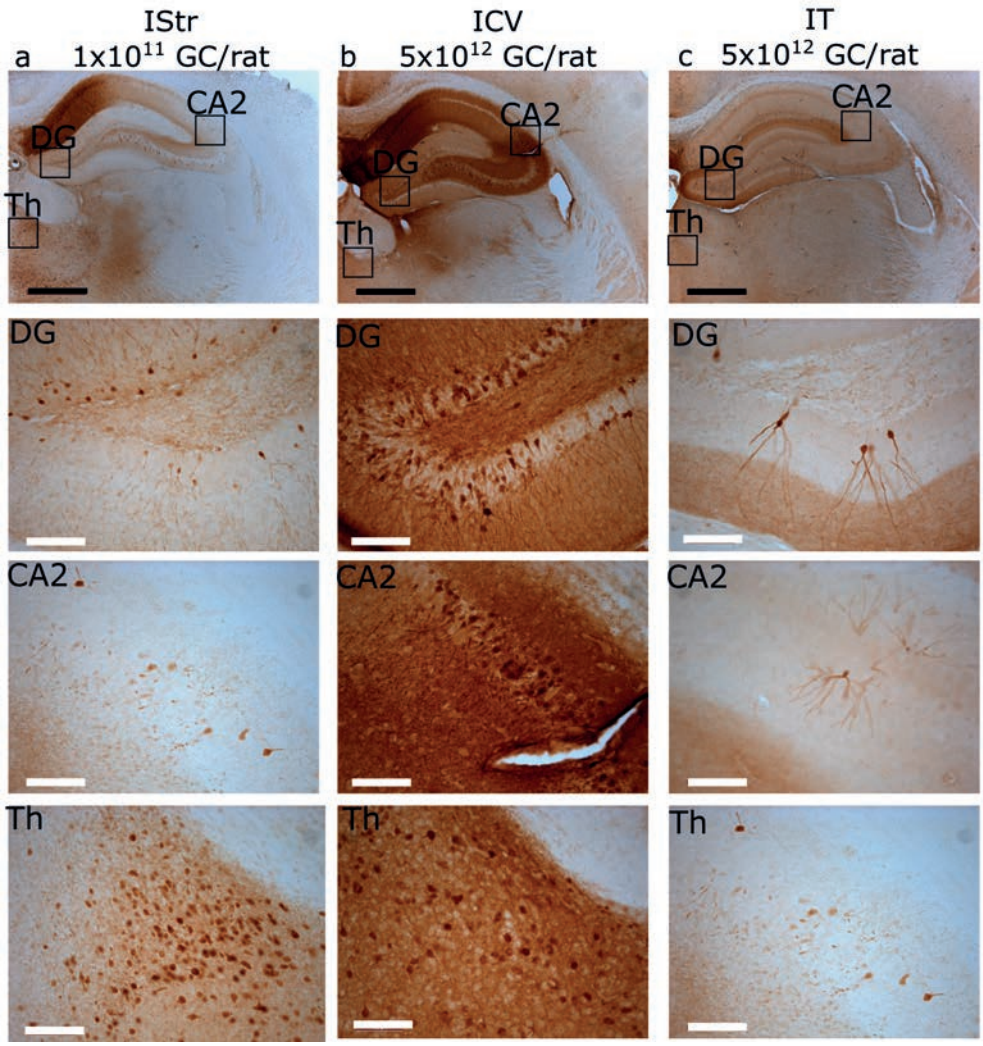

Figure 5. GFP expression in the hippocampal area in rat brain intrastriatal (IStr), intracerebroventricular (ICV) or intrathecal (IT) administration of AAV5-GFP. a) IS-administered rat, b) ICV-administered rats, c) IT-administered rats. Dentate gyrus (DG) of ICV-administered rats showed GFP staining in the Hilus area which was not seen in the other administration routes. The IStr-administrated animals show GFP stained neurons in the inner molecular area compared to the ICV where the complete CA2 showed GFP staining. Intrathecal (IT)-administered rats had sparse transduction of neurons. In the Thalamic (Th) area, both IStr- and ICV-administered rats showed GFP staining in the thalamic area of neurons and surrounding area. IT administration resulted in GFP stained neurons, however not in the surrounding area. Black bar represents 1mm scale and white bar represents 100 µm scale

layer multipolar neurons were seen with branching dendrites. However, the layers were negative for GFP staining (fig. 5c).

Altogether, the results suggest that depending on the injection route AAV-mediated transduction patterns involve different neuronal pathways.

IT, IStr and ICV administration of AAV5 results in different GFP- expression profiles in SNpc hypothalamus and cerebellum of rats

In the midbrain area, the SN pars compacta (SNpc) and pars recticulata (SNrc) as well as in the Ventral Tegmental Area (VTA) neurons were positive for GFP in brains of IStr-administered rats. All other areas of the midbrain were negative (fig 6a). After ICV injection, the SNrc and VTA are positive for GFP but not the SNpc. In the medial mammillary body of the hypothalamus GFP positive neurons are perceived (fig 6b).

In brains from IT-administered rats, predominantly neurons of the mammillary body were positive for GFP (fig. 6c). In the cerebellum of IStr-administered rats, no positive neurons could be discerned (fig. 6d). ICV injection led to sparse transduction of the cerebellum, but positive Purkinje and Golgi cells were identified (fig. 6e). In the cerebellum of IT-administered rats, more layers with positive cells were identified, for example in Purkinje cells, Bergman Glia and Golgi cells based on morphology and location (fig. 6f).

ICV- and IT-administration of AAV5-GFP results in GFP expression in spinal cord and dorsal root ganglia of rats

Along the entire length of the spinal cord (SC) and aligned Dorsal Root Ganglia (DRG) of IStr-administered rats, no GFP-positive cells were observed (fig. 7a). The cervical SC of ICV-injected rats did also not show staining for GFP. However, positive cells were observed in the cervical DRG. In the thoracic area, sporadic positive neurites in the dorsal root entry zone could be observed in the dorsal horn. Also, GFP-positive neurons in the DRG were observed. At the lowest part of the spinal cord at the lumbar section, GFP-stained neurons were visualized in the SC and DRG (fig. 7b). IT administration led to positive neurons at the injection site in the lumbar spinal cord and attached DRG, moving upwards to the thoracic section positive cells can also be observed in both SC and DRG. In the cervical SC and DRG, no GFP-positive cells were observed (fig. 7c).

Discussion

In this study we demonstrated that the distribution profile of AAV in the CNS is highly dependent on its delivery method. Thus, depending on the disease for which therapy is being developed each method has its own merits. IStr and ITH are more suited for diseases in which a high concentration of therapeutic compound is needed in the frontal to mid brain areas, such as PD and HD. ICV is suited for low to mid-range transgene

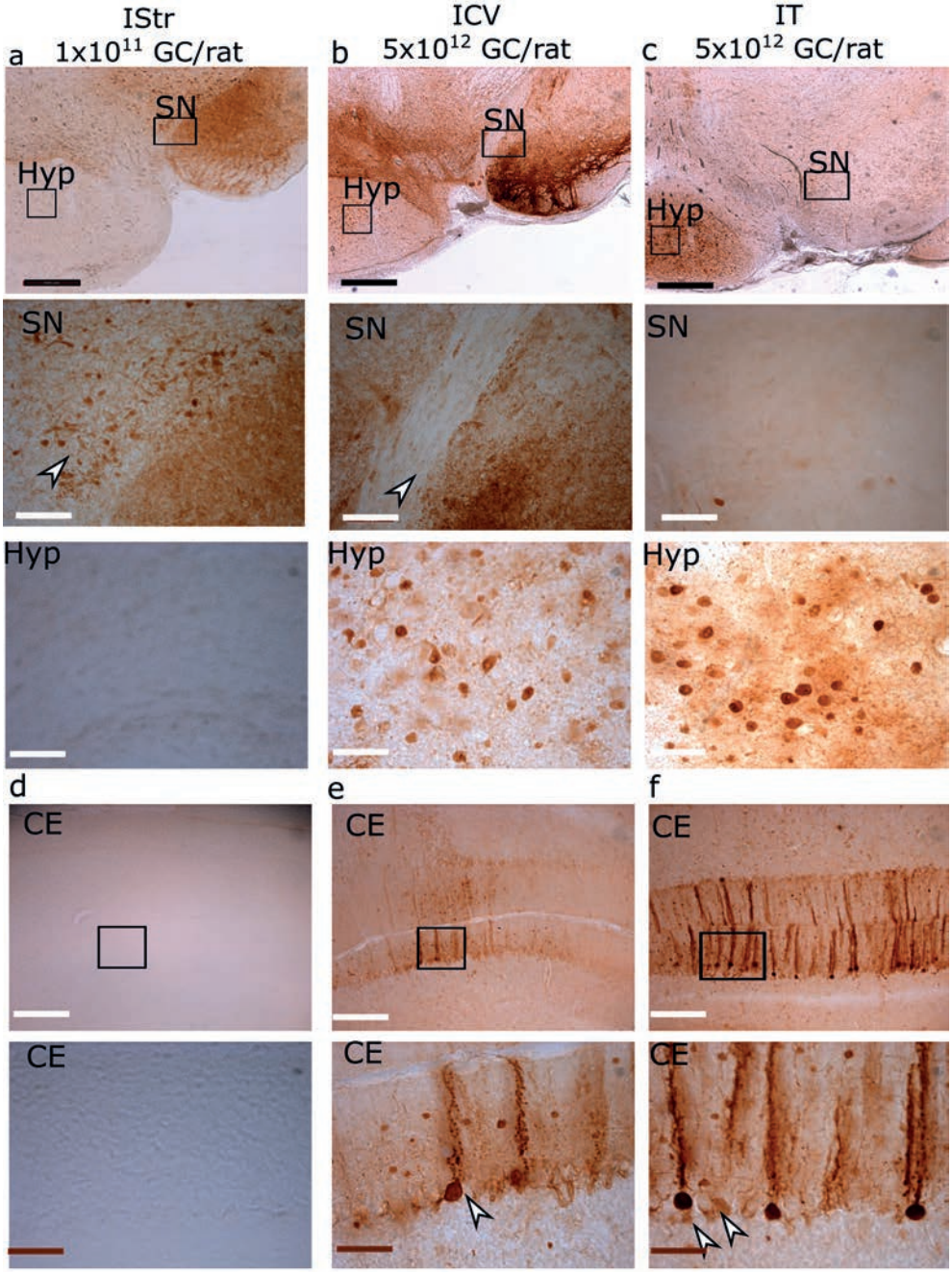
IStr
1x10^11 GC/rat
ICV
5x10^12 GC/rat
IT
5x10^12 GC/rat
a
b
c
SN
Hyp
SN
Hyp
SN
Hyp
SN
SN
SN
Hyp
Hyp
Hyp
d
e
f
CE
CE
CE
CE
CE
CE

delivery in a broad distribution throughout the CNS with somewhat less penetration into deeper brain structures but could be useful for e.g. lysosomal storage diseases.

In brains of IStr-administered rats, vector and transgene expression were detected in the thalamus, cortex, and hippocampus, and thus outside the injected nucleus. There are strong indications that AAV travels beyond the injection site by axonal transport [12]. Following IStr administration of AAV5 in NHP, AAV5 transduced the SNpc, cortex and thalamus by retrograde transduction and SNpr by anterograde transduction [8]. Anterograde transport is characterized by transduction of vector distal to the injection site after cell body-mediated uptake. Retrograde transport involves the uptake of viral particles by nerve terminals at the site of injection, which are then transported to the cell body of the neuron. Samaranch et al [8] showed the same pattern of GFP-positive nuclei in NHP as we observed in rats. Therefore, in rats as well as NHP AAV5 may well use the same anterograde and retrograde mode of transport. This has great implications for the capability to predict the transduction patterns across species.

ICV administration only targets the SNpr and not the SNpc. In an earlier study comparing IStr- to ITH-delivery in NHP, it was also observed that ITH delivery does not result in the transduction of the SNpc whilst IStr administration does. [8]. These results suggest that of the delivery methods studied for PD, IStr administration of AAV5-based therapy is currently the best option to deliver meaningful amounts of therapeutic to the SNpc.

Our distribution analysis showed that vector copies were detected evenly across all tissues analyzed following ICV infusion of AAV5. In contrast to direct infusion into the striatum, where almost the complete nucleus was GFP positive, only the nuclei in the vicinity of the lateral ventricle were positive for GFP after ICV administration. However, ICV injection led to complete transduction of the hippocampus making this a feasible alternative to direct administration into the hippocampal formation. This knowledge is crucial for the development of AAV-based therapies for AD.

The SNpr, cerebellum and spinal cord could be transduced via the subarachnoid space. During the systolic phase, CSF flows from the ventricles into the subarachnoid space and spinal cord via the foramen located below the cerebellum. The SNpr projects to the thalamus, resulting in retrograde transduction of the thalamus. The thalamus has

Figure 6. GFP staining in the midbrain area and cerebellum in rat brain following intrastriatal (IS), intracerebroventricular (ICV) or intrathecal (IT) administration of AAV5-GFP. a-c) overview of midbrain area. 20X magnification of the substantia nigra of IS administrated rats showed GFP stained neurons in the substantia nigra pars compacta and pars reticulata, ICV administered rats showed GFP staining in the pars reticulata but not in the pars compacta. In the hypothalamus (hyp) GFP IR neurons were observed in ICV- and IT administered rats for which IStr administered rats are negative. d-f) In the cerebellum of IT-administered rats, show GFP staining in Purkinje cells and Bergman cells. Neuronal staining also found in ICV-administered rats. However, transduced cells are more sporadic as compared to IT administration. No staining observed in IStr- administered rats. Black bar represents 500 µm, white bar 100µm and brown bar 50 µm for scale.

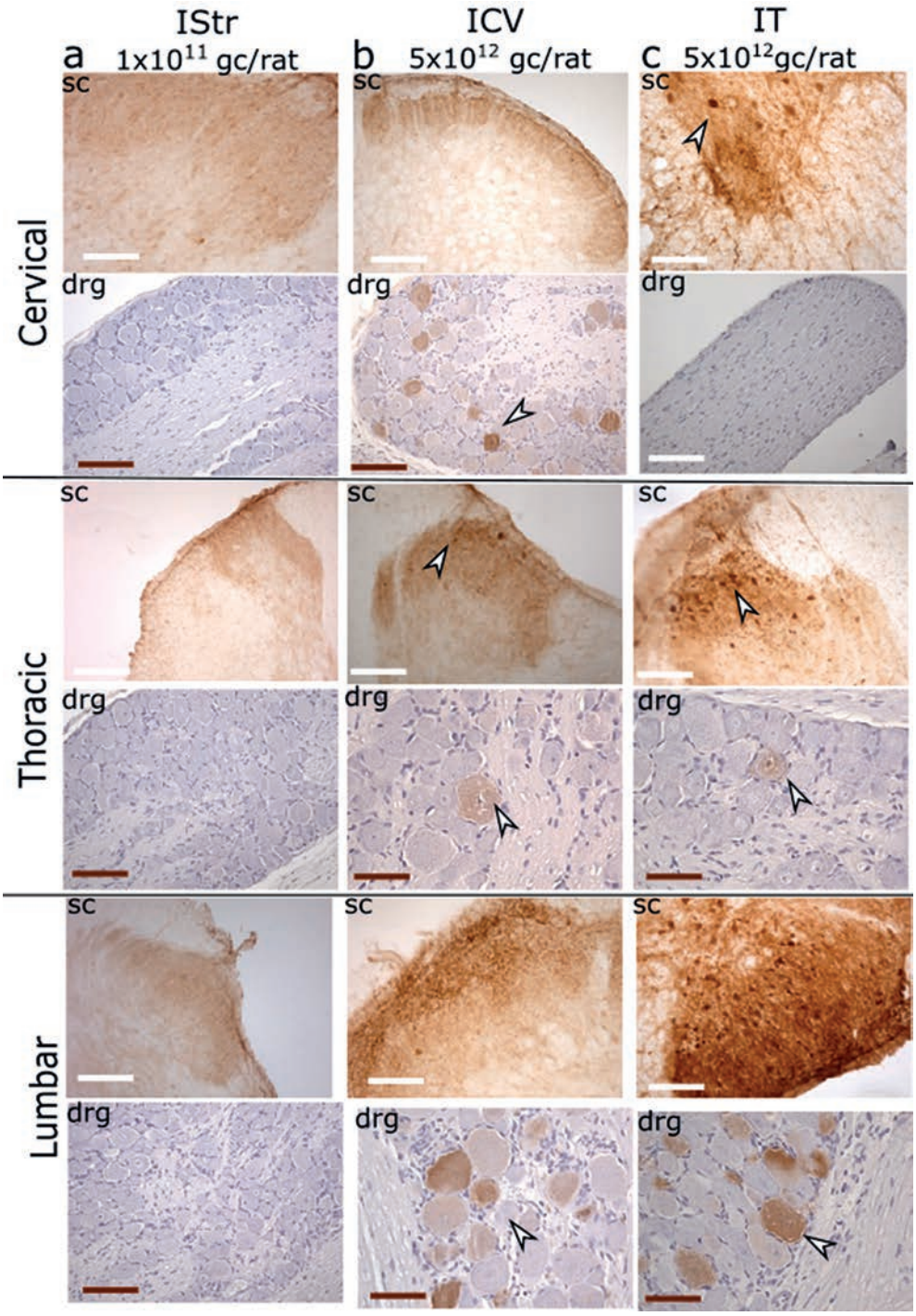
IStr
ICV
IT
a 1x10^11 gc/rat
b 5x10^12 gc/rat
c 5x10^12gc/rat
Cervical
Thoracic
Lumbar
sc
drg

an afferent projection to the mammillary body which could explain the positive cells observed in this region. Based on the transduction pattern it seems that ICV-based-AAV5 transduction of the brain is a mixture of transependymal CSF flow of structures close to the ventricles and subsequent axonal transport to deeper areas. The transependymal CSF flow describes the progress of CSF across the ependymal layer that surrounds the ventricles into the brain parenchyma and adjacent structures. This flow is pushed by a pressure gradient which is driven by the production of CSF in the lateral ventricles. CSF flows in the direction of the venous sinuses into which it is eventually absorbed [15].

Lumbar IT delivery of AAV5-GFP resulted in GFP-positive cells in SC & DRG. Some GFP-positive neurons were also observed in the cerebrum, the cerebellum and frontal brain. There are indications that after IT administration AAV9 and AAVrh10 transduce the parenchyma via perivascular transport of CSF [13, 16]. Guo et *al*., 2014 [26] observed distinct GFP patches in the vicinity of vascular cavities in rat brains following IT administration of AAVrh10 [26] and double staining with aquaporin 4, a marker for perivascular space, showed colocalization with GFP expression. We did not observe an obvious pattern of colocalization of vascular cavities and GFP staining. Both AAV9 and AAVrh10 are known to cross the blood-brain barrier after IV administration, while AAV5 does not [9], indicating that AAV5 employs a different method to cross pia mater.

Even though in both IT and ICV the same amount of vector is administered to the CSF, a different expression pattern was observed that could be explained by the flow of CSF. ICV-administered vector moves with the natural flow of the fluid, from the lateral ventricle, where it is produced, to ventricles beyond. AAV5 injected into the lumbar subarachnoid space has to populate and transduce the tissue against the flow and has no gradient push towards the parenchyma of the cerebrum. The GFP-positive areas observed in the cerebrum after IT administration are most likely due to axonal transport and not transport of the vector via the CSF.

Surprisingly, ITH- and ICV-administered vector was observed outside the CNS, however this did not result in GFP-RNA expression. Possibly, the CAG promoter was not active in rats in these organs. In a study using the CAG promoter in a non-human primate (NHP) vector, the distribution in the periphery also did not lead to expression in the spleen, kidney and liver [17]. Surprisingly, the CAG promoter is active in mouse liver [18], pointing towards species specificity of the promoter in peripheral organs. Presence of vector copies in unwanted locations may lead to side effects. Our results indicate that ICV delivery is promising when a CNS-specific promoter is used.

Figure 7. GFP staining in the spinal cord and the dorsal root ganglion of intrastriatal (IS), intracerebroventricular (ICV) or intrathecal (IT) administered AAV5 rats. a) No staining was observed throughout the spinal cord (SC) and Dorsal Root Ganglia (DRG) of IS-administered rats. b) ICV-administered rats showed staining of cervical DRG, thoracic and lumbar SC and DRG. c) IT-administered rats show GFP positive cells and matter in lumbar and thoracic SC&DRG. GFP stained cells marked by Arrow. White bar represents 100μm and brown bar 50 μm for scale.

On the other hand, the delivery methods targeting all tissues equally are advantageous for lysosomal diseases such as Mucopolysaccharidoses IIA, where both the organs of the periphery and the CNS are affected. Both IT-and ICV-delivery routes can be considered for the treatment of such diseases that need a widespread transduction. Furthermore, lysosomal enzymes are capable of cross-correction as they are secreted to the extracellular space and taken up by neighboring cells which were not transduced, and have the capacity to travel across axonal projections [19]. Due to these properties, the IT- and ICV-induced transduction to distal areas may give a therapeutic effect.

To allow translation to humans, the delivery methods should be tested in larger animal models. IStr administration of AAV5 has been tested in numerous NHP studies [6, 8, 20]. IT delivery of AAV5 was tested in NHP at the same dose as in the current study and a similar transduction pattern was observed [8]. Of the delivery methods, ICV is the least tested in larger animal models, but in dogs resulted in efficient transduction of the brain and spinal cord, and, importantly, no adverse effects were seen [21]. In a more recent study, ICV administration to the lateral ventricle of dogs resulted in encephalitis in one animal [25]. As ventriculostomy is a common procedure in humans, one would not suspect the procedure to be high risk. However, both represent small studies and more research on large-animal pre-clinical models for ICV administration is necessary to carefully assess this delivery method and compare it to alternative methods.

Based on our current data and data from others, IStr and ITH could be used for gene-delivery therapy for more localized diseases such as PD and HD. ICV could be employed for a disease like AD targeting the hippocampus and due to its broader reach also AAV5-based therapy for lysosomal storage disease could be developed using ICV delivery. Both ICV and IT could be used for diseases where the cerebellum is the main target, although the transgene expression levels are relatively low. Moreover, IT delivery of AAV5-mediated therapy transduces the complete spinal cord and most of the cortical area, and could thus be used for diseases affecting the spinal cord.

This study was performed in rodents and therefore the delivery methods need to be studied in larger animal models prior to application in the clinic. Ongoing studies in both wild-type and transgenic HD minipigs show promising results for IStr- and/or ITH-administration to HD-patients [22]. Especially when degeneration of the striatum is advanced, thalamic infusion may be an attractive alternate option. Our current data constitute a solid base for further development of AAV5-based gene therapy for neurological diseases.

Material and methods

Production of vectors

Vectors were produced using uniQure's patented insect cell-based system as previously described [23]. Briefly, Spodoptera Frugiperda (SF) + cells were infected with recombinant baculovirus encoding for the capsid AAV5, REP gene and insert. The expression cassette of the insert consisted of the nucleotides encoding for CAG promoter, a combination

of the cytomegalovirus (CMV) early enhancer element and chicken beta-actin promoter. The transgene GFP is preceded by a Kozak sequence and followed by the bovine growth hormone polyadenylation (BGHpA) signal. At 72 hours post infection, cells were lysed and clarified lysate was purified on the AKTA explorer (FPLC chromatography system, GE healthcare) using AVB sepharose (GE healthcare). The vectors were titrated by Sybergreen Q-PCR using a primer pair binding to the promoter region (forward primer; GAG CCG CAG CCA TTG C, reverse primer; CAC AGA TTT GGG ACA AAG GAA GT) expressed as genome copies per ml (GC/ml).

Animal study

All animal studies described were approved by the local animal experimentation ethical committee. Female Wistar rats (Janvier labs) were used for all experiments. Rats were anesthetized before surgery, by intramuscular administration of Hypnorm/Dormicum. A small hole is drilled in the skull, and the striatum or lateral ventricle are stereotactically approached. Coordinates for intrastriatal infusion were A/P 1.3, L +/- 2.5 and D 3.5; for intrathalamic A/P -2.5, +/- 3 and D 4.5; for intracerebroventricular A/P -1.5, L 2.5 and D 3.5. For the intrathecal administration, an incision was made in the skin on the back of the animal, muscle layers are split and a laminectomy performed at the lumbar vertebral level L3. The animal is placed into the spinal cord fixator and using a pulled glass needle the vector is infused. Volumes and dosage are described in table 1. After surgery, animals are given Temgesic for pain relief and returned to their cage. Depending on experiment, 4 or 6 weeks after experiments animals were sacrificed by decapitation under isoflurane anesthesia. Organs used for distribution analysis were snap frozen in liquid nitrogen and stored at -80 °C until analysis. Brains used for histology were fixed in 4% paraformaldehyde for 24-48 hours.

Vector distribution and GFP expression

Organs were retrieved from -80 °C and pulverized to a powder using the Cryoprep system (Covaris, Woburn, MA, USA), from ±10 mg powder DNA was extracted using the DNeasy 96 Blood and Tissue kit (QIAGEN, Germany). Vector DNA was detected by

Table 1. Overview of volume and dosages used in study

Study	Injection route	Volume (µl)	Total dose(gc/rat)	Titer (gc/ml)
Injection routes 1st study	IStr	2 (per hemisphere)	$5x10^{10}$	$1.25x10^{13}$
	ITH	2 (per hemisphere)		
	ICV	40	$5x10^{11}$	$1.25x10^{13}$
Injection routes 2nd study	IStr	1 (per hemisphere)	$1x10^{11}$	$1x10^{14}$
	ICV	50	$5x10^{12}$	$1x10^{14}$
	IT	50	$5x10^{12}$	$1x10^{14}$

Q-PCR using TaqMan primers and probe binding to CAG promoter (forward primer: GAG CCG CAG CCA TTG C, reverse primer: CAC AGA TTT GGG ACA AAG GAA GT, probe: ATG GTA ATC GTG CGA GAG GGC GC). Vector DNA gc per µg DNA were quantified by interpolating from a standard line prepared from the plasmid of the expression cassette. RNA was isolated from powder using the RNeasy kit from Qiagen. Total RNA was reverse transcribed to cDNA using Maxima strand kit. RNA expression was quantified by using primers binding to GFP (forward primer: AGC AAA GAC CCC AAC GAG AA, reverse primer: GCG GCG GTC ACG AAC TC probe: CGC GAT CAC ATG GTC CTG CT) and GAPDH (Taqman expression array from Thermo Fisher) as housekeeping gene for reference. RNA expression was calculated using the ΔCT method normalized to the housekeeping gene.

Histology

24-48 hours after immersion fixation in 4% paraformaldehyde brains were embedded in 10% gelatin (Difco) in PBS as described previously [24]. Embedded tissue was sectioned on a vibratome. Coronal sections were collected in PBS in series at a thickness of 50 µM. Immunohistochemistry was performed on free-floating sections. Endogenous peroxidase block was performed by incubating sections for 1 hour in 1% H2O2/30% ethanol in PBS. Sections were washed 3 times with washing buffer (PBS/0,05% tween). A-specific blocking was performed by incubating sections for 1 hour in PBS supplemented with 4% BSA (Bovine Serum Albumin) and 5% Normal Goat Serum (NGS). Subsequently, sections were incubated overnight with primary antibody against GFP (Abcam ab290), diluted 1:1000 in PBS/1%BSA/1.25%NGS/0,5% Tween and incubated for one hour with horse radish peroxidase (HRP)-conjugated anti-rabbit before detection with 3,3'-Diaminobenzidine (DAB) according to manufacturer's instructions (Dako envision kit K4009). Sections of the spinal cord were counterstained with haematoxylin and eosin stain (H&E). Subsequently, they were dehydrated through ethanol series, Xylene and embedded in Entellan before microscopical analysis.

References

1. Leone P, Shera D, McPhee S, et al (2012) Long-Term Follow-Up After Gene Therapy for Canavan Disease. Sci Transl Med 4:165ra163-165ra163. https://doi.org/10.1126/scitranslmed.3003454
2. Boutin S, Monteilhet V, Veron P, et al (2010) Prevalence of Serum IgG and Neutralizing Factors Against Adeno-Associated Virus (AAV) Types 1, 2, 5, 6, 8, and 9 in the Healthy Population: Implications for Gene Therapy Using AAV Vectors. Human Gene Therapy 21:704–712. https://doi.org/10.1089/hum.2009.182
3. Aschauer DF, Kreuz S, Rumpel S (2013) Analysis of transduction efficiency, tropism and axonal transport of AAV serotypes 1, 2, 5, 6, 8 and 9 in the mouse brain. PloS one 8:e76310. https://doi.org/10.1371/journal.pone.0076310
4. Lisowski L, Tay S, Alexander I (2015) Adeno-associated virus serotypes for gene therapeutics. Curr Opin Pharmacol 24:59–67. https://doi.org/10.1016/j.coph.2015.07.006
5. Paterna J-C, Feldon J, Büeler H (2004) Transduction Profiles of Recombinant Adeno-Associated Virus Vectors Derived from Serotypes 2 and 5 in the Nigrostriatal System of Rats. J Virol 78:6808-6817. https://doi.org/10.1128/jvi.78.13.6808-6817.2004
6. Dodiya HB, Bjorklund T, Ill J, et al (2010) Differential Transduction Following Basal Ganglia Administration of Distinct Pseudotyped AAV Capsid Serotypes in Nonhuman Primates. Molecular Therapy 18:579–587. https://doi.org/10.1038/mt.2009.216
7. Markakis EA, Vives KP, Bober J, et al (2010) Comparative Transduction Efficiency of AAV Vector Serotypes 1–6 in the Substantia Nigra and Striatum of the Primate Brain. Molecular Therapy 18:588–593. https://doi.org/10.1038/mt.2009.286
8. Samaranch L, Blits B, Sebastian SW, et al (2017) MR-guided parenchymal delivery of adeno-associated viral vector serotype 5 in non-human primate brain. Gene Therapy 24:253–261. https://doi.org/10.1038/gt.2017.14
9. Schuster DJ, Belur LR, Riedl MS, et al (2014) Supraspinal gene transfer by intrathecal adeno-associated virus serotype 5. Frontiers in Neuroanatomy 8:66. https://doi.org/10.3389/fnana.2014.00066
10. Schapira A, Chiasserini D, Beccari T, Parnetti L (2016) Glucocerebrosidase in Parkinson's disease: Insights into pathogenesis and prospects for treatment. Movement Disorders 31:830–835. https://doi.org/10.1002/mds.26616
11. Reiner A, Dragatsis I, Dietrich P (2011) International Review of Neurobiology. 98:325–372. https://doi.org/10.1016/b978-0-12-381328-2.00014-6
12. Salegio E, Samaranch L, Kells A, et al (2012) Axonal transport of adeno-associated viral vectors is serotype-dependent. Gene Therapy 20:gt201227. https://doi.org/10.1038/gt.2012.27
13. Schuster DJ, Dykstra JA, Riedl MS, et al (2014) Biodistribution of adeno-associated virus serotype 9 (AAV9) vector after intrathecal and intravenous delivery in mouse. Frontiers in Neuroanatomy 8:42. https://doi.org/10.3389/fnana.2014.00042
14. Tardieu M, Zérah M, Gougeon M-L, et al (2017) Intracerebral gene therapy in children with mucopolysaccharidosis type IIIB syndrome: an uncontrolled phase 1/2 clinical trial. The Lancet Neurology. https://doi.org/10.1016/s1474-4422(17)30169-2
15. Casaca-Carreira J, Temel Y, Hescham S-A, Jahanshahi A (2018) Transependymal Cerebrospinal Fluid Flow: Opportunity for Drug Delivery? Molecular Neurobiology 55:2780–2788. https://doi.org/10.1007/s12035-017-0501-y
16. Guo Y, Wang D, Qiao T, et al (2016) A Single Injection of Recombinant Adeno-Associated Virus into the Lumbar Cistern Delivers Transgene Expression Throughout the Whole Spinal Cord. Molecular Neurobiology 53:3235–3248. https://doi.org/10.1007/s12035-015-9223-1
17. Meyer K, Ferraiuolo L, Schmelzer L, et al (2015) Improving Single Injection

CSF Delivery of AAV9-mediated Gene Therapy for SMA: A Dose–response Study in Mice and Nonhuman Primates. Molecular Therapy 23:477–487. https://doi.org/10.1038/mt.2014.210
18. Chen B, He C, Chen X, et al (2015) Targeting transgene to the heart and liver with AAV9 by different promoters. Clinical and Experimental Pharmacology and Physiology 42:1108–1117. https://doi.org/10.1111/1440-1681.12453
19. Cearley CN, Wolfe JH (2006) Transduction characteristics of adeno-associated virus vectors expressing cap serotypes 7, 8, 9, and Rh10 in the mouse brain. Molecular Therapy 13:528–537. https://doi.org/10.1016/j.ymthe.2005.11.015
20. Emborg ME, Hurley SA, Joers V, et al (2014) Titer and Product Affect the Distribution of Gene Expression after Intraputaminal Convection-Enhanced Delivery. Stereotactic and Functional Neurosurgery 92:182–194. https://doi.org/10.1159/000360584
21. Haurigot V, Marcó S, Ribera A, et al (2013) Whole body correction of mucopolysaccharidosis IIIA by intracerebrospinal fluid gene therapy. Journal of Clinical Investigation 123:3254-3271. https://doi.org/10.1172/JCI66778
22. Evers MM, Miniarikova J, Juhas S, et al (2018) AAV5-miHTT gene therapy demonstrates broad distribution and strong human mutant huntingtin lowering in a Huntington disease minipig model. https://doi.org/10.1016/j.ymthe.2018.06.021
23. Bosma B, du Plessis F, Ehlert E, et al (2018) Optimization of viral protein ratios for production of rAAV serotype 5 in the baculovirus system. Gene Therapy 1–10. https://doi.org/10.1038/s41434-018-0034-7
24. Oudega M, Varon S, Hagg T (1994) Regeneration of Adult Rat Sensory Axons into Intraspinal Nerve Grafts: Promoting Effects of Conditioning Lesion and Graft Predegeneration. Exp Neurol 129:194–206. https://doi.org/10.1006/exnr.1994.1161

Chapter 6

In-depth characterization of a Mifepristone regulated expression system for AAV5-mediated gene therapy in the liver

Jolanda M. Liefhebber[1], Raygene Martier[1,2], Tom Van der Zon[1], Sonay Keskin[1], Angelina Huseinovic[1,3], Jacek Lubelski[1], Bas Blits[1], Harald Petry[1], Pavlina Konstantinova[1#]

[1] Department of Research & Development, uniQure N.V., Amsterdam, The Netherlands;
[2] Department of Gastroenterology and Hepatology, Leiden University Medical Center, Leiden, The Netherlands;
[3] Amsterdam UMC, The Netherlands

Mol. Ther. Methods & Clinical Development. (2019); 13: 512-525

Abstract

Gene therapy is being developed for the treatment of inherited diseases, whereby a therapeutic gene is continuously expressed in patients after delivery via viral vectors such as Adeno-associated virus (AAV). Depending on the transgene there could be a limited therapeutic window and regulating timing and levels of transgene expression is advantageous. To control transgene transcription, the regulatory system GeneSwitch was evaluated in detail both *in vitro* and *in vivo*. The classical two plasmid mifepristone (MFP)-inducible GeneSwitch system was put into one plasmid or a single AAV5 vector. Our data demonstrate inducibility of multiple transgenes and the importance of promoter and regulatory elements within the GeneSwitch system. Mice injected with AAV5 containing the GeneSwitch system transiently expressed mRNA and protein after MFP induction. The inducer MFP could be measured in plasma and liver tissue, and assessment of MFP and its metabolites showed rapid clearance from murine plasma. In a head-to-head comparison, our single vector outclassed the classical two vector GeneSwitch system. Finally, we show repeated inducibility of the transgene that also translated into a dynamic phenotypic change in mice. Taken together, this in-depth analysis of the GeneSwitch system shows its applicability for regulated gene therapy.

Keywords

Regulated gene expression, mifepristone inducible GeneSwitch system,
AAV5 gene therapy

Introduction

Several metabolic and inherited diseases are clinically targeted using gene therapeutic approaches[1,2], which offer the prospect of a long-term causal correction of diseases that currently only have supportive treatments. One of the main gene therapy challenges is reaching sufficient concentrations of the therapeutic gene to correct disease symptoms, and for approaches based on growth factors or master regulators, fine-tuning of the protein expression is essential. Inducible protein expression also may improve the safety of approaches that have limited therapeutic windows, or that require temporal protein expression.

An efficient inducible system should be able to switch a gene on by delivering a clinically approved and safe small molecule and should switch off upon withdrawal of the drug, without any background expression. The inducer drug should be easy to deliver and have rapid on-off dynamics. Several regulatory systems have been engineered to control gene transcription, for example Tet-on/off and GeneSwitch. Both systems are based on binding of a transactivator protein to a specific DNA sequence in the promoter of the transgene and on ligand dependent activation of the system. In the presence of a small molecule-inducing compound the transactivator protein is activated and can subsequently bind to sequences in the promoter of the transgene, which is then being transcribed.

The well-known Tet-on/off system gene transcription is modulated through the transactivator-protein (rtTA) which is sensitive to doxycycline. Although the Tet-system has been optimized for usage at doxycycline concentrations acceptable in the clinic[3], long-term use of antibiotics is not preferred. Moreover the rtTA is potentially immunogenic[4], because it contains domains of bacterial origin. This would limit the clinical use of the Tet-system to immune privileged areas such as the brain.

The GeneSwitch system, addresses several limitations of the Tet-on/off system, because it is of mainly human origin and activated by the synthetic steroidal anti-progesterone drug, mifepristone (MFP), a clinically approved drug. MFP acts as an agonist to activate gene transcription by binding to a subunit of the GeneSwitch protein, this interaction has been described by others previously.[5–8] GeneSwitch, can induce regulated gene expression in rat brain at an MFP concentration that is in range of clinical use[9]. The GeneSwitch system has been successfully used in an animal model for Parkinson's disease, where Glial cell-derived neurotrophic factor (GDNF) was regulated in rat brain and had neuroprotective and neurorestorative effects[10,11]. Moreover, the GeneSwitch system was able to modulate interferon (IFN) in the periphery, however in that study a CMV promoter was used which could elicit an immune response due to expression in antigen presenting cells[12–14]. Besides, in the periphery IFN has been modulated, however in that study GeneSwitch was behind a CMV promoter which could elicit an immune response due to expression in antigen presenting cells[12–14].

The GeneSwitch system consists of two expression cassettes: one constitutively expressing the GeneSwitch protein, the chimeric trans-activator protein. The other cassette

contains a transgene transcribed from an inducible promoter. GeneSwitch is a fusion protein of two human domains and a 97 amino acid yeast-derived sequence. The N-terminal domain is the DNA-binding domain of yeast transcription factor Gal4 that binds to a 17 nucleotide long sequence in the regulatable promoter of the transgene. GeneSwitch binds to this sequence after dimerization, which is triggered by a conformational change of the ligand binding domain (LBD) in the presence of MFP. The LBD is a domain from the human progesterone receptor, hence that MFP is an inducer. The C-terminal part of GeneSwitch is the activation domain of NFkappaB p65 and is responsible for the initiation of transgene transcription (Figure 1).

In the current study we performed an in-depth optimization of the GeneSwitch system for AAV gene therapy in the liver. Different promoters and regulatory elements were tested. A detailed head-to-head comparison of a single- and two-vector system were performed both *in vitro* and *in vivo*. Moreover, the kinetics of the GeneSwitch system transgene induction was investigated systematically. The inducer MFP and its metabolites were measured *in vivo* to gain insight in plasma kinetics and liver tissue concentrations. Insulin-like growth factor (IGF) and erythropoietin (EPO) were chosen as transgenes, due to the easy plasma read out and having a suitable size to fit into AAV vectors in combination with the GeneSwitch system. By using several transgenes, proof of concept and wide applicability of the single GeneSwitch system for AAV gene therapy in the liver was explored. Besides expression of the transgenes IGF and EPO upon MFP treatment, we have demonstrated that the single GeneSwitch-EPO vector induction translates into a reversible increase in hematocrit levels; a hallmark phenotypic effect of EPO expression.

Results

Mifepristone induces a dose dependent regulation of luciferase expression by a single vector GeneSwitch system

In our initial experiments to develop regulated gene therapy, the expression of the GeneSwitch protein was placed under the control of the cytomegalovirus (CMV)-promoter and firefly-luciferase was used as read-out reporter transgene for MFP inducibility. The two expression cassettes containing GeneSwitch (GS) and firefly-luciferase (FL) were cloned in a single vector in the head-to-tail configuration (CMV-GS-FL), as shown in Figure 2a.

This plasmid CMV-GS-FL and a control plasmid expressing GFP from a CMV promoter (CMV-GFP) were transfected into HEK293T cells. Cells introduced with CMV-GFP showed GFP expression indicating successful transfection (data not shown). Exposure of cells transfected with CMV-GS-FL to MFP caused a concentration-dependent increase of luminescence, indicating MFP-dependent GeneSwitch activation (Figure 2b).

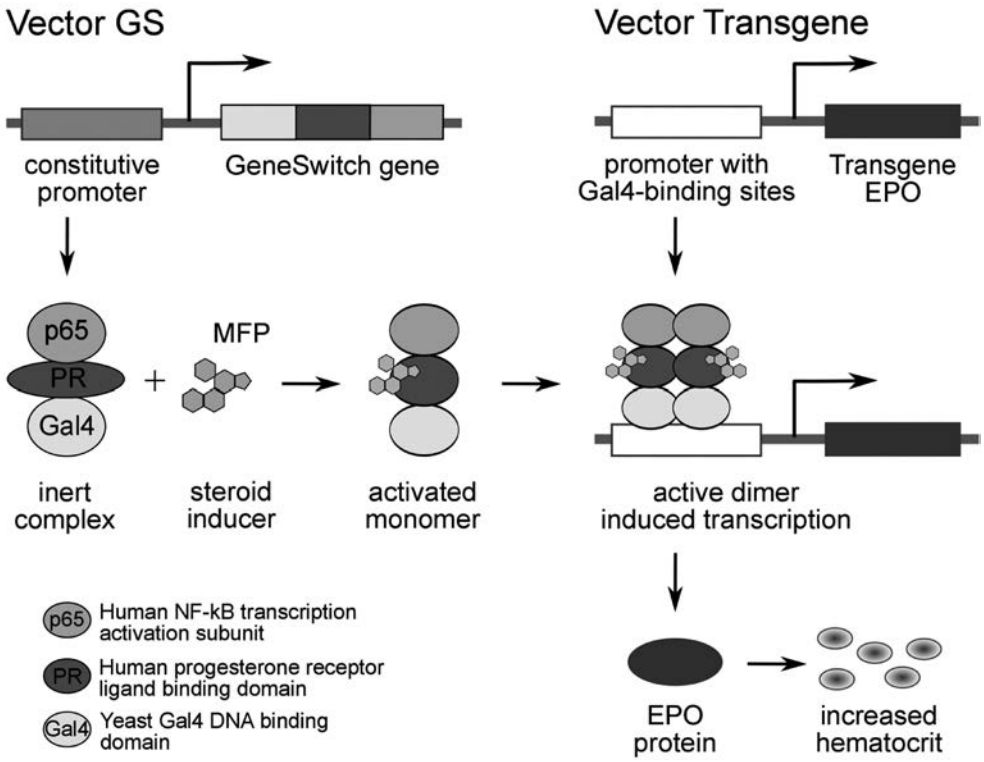

Figure 1. Schematic for the regulation of transgene expression by mifepristone inducible GeneSwitch system. Within the GeneSwitch system there are two protein expression cassettes, one for the inducible transgene of interest and another for GeneSwitch protein. The regulatory vector (Vector GS) contains the GeneSwitch gene and a promoter that is driving constant expression of GeneSwitch protein. In this example the promoter is a liver specific promoter, which is only active in hepatic tissue. GeneSwitch protein is a fusion protein of three domains: human NF-kB transcription activation subunit named p65, human progesterone receptor ligand binding domain (PR) and yeast Gal4 DNA binding domain (Gal4). After binding of the steroid inducer mifepristone (MFP) to the PR domain, GeneSwitch protein gets activated and changes conformation. An active dimer is formed that can bind via the Gal4 domain to the four Gal4 binding sites within the inducible promoter of the transgene vector. Then the p65 subunit of GeneSwitch protein facilitates the start of transcription of the regulated transgene (here EPO). EPO protein on its turn stimulates production of erythrocytes, resulting in increased hematocrit levels.

Induction rate of the single vector GeneSwitch system is promoter dependent

For many clinical indications it is preferred to restrict therapeutic gene expression to a single organ by using tissue specific promoters. To investigate the influence of different promoters on the GeneSwitch system for liver application, the universal CMV-promoter was compared with the liver specific human alpha1-antitrypsin (AAT)-promoter. Rat

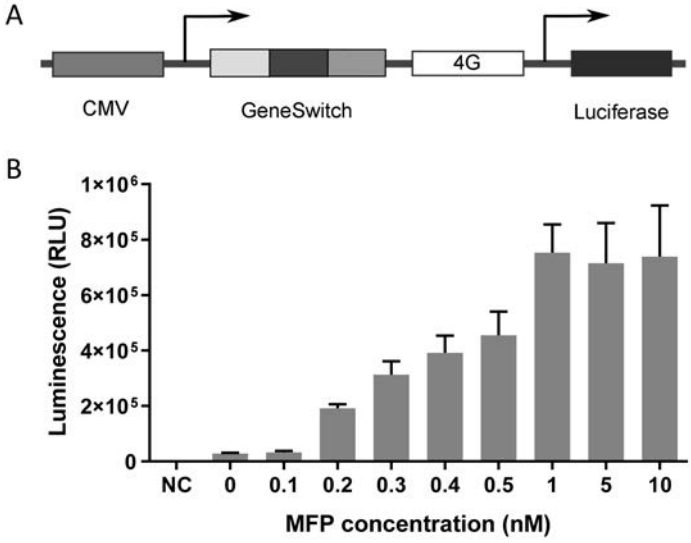

Figure 2. Mifepristone dose dependent expression of luciferase by a single-vector GeneSwitch system. A. Schematic of the two expression cassettes of the GeneSwitch system within a single vector. The cassettes are put into a tail to head configuration, where transcription is in the same direction. GeneSwitch protein expression is driven by a CMV-promoter and the inducible promoter of luciferase contains four Gal4 binding sites (4G). B. HEK293T cells were transfected with the CMV-GS-Luc plasmid shown in A or a control plasmid (N.C.). The next day cells were incubated with different concentrations of MFP ranging from 0 to 10nM for 48h. Firefly luciferase activity was measured from three independent samples and averages are shown.

insulin like growth factor-1 (IGF1) was used as a transgene, as it is an endocrine hormone mainly produced by hepatocytes. Plasmids with GS-IGF1 were cloned under control of the AAT-promoter and the CMV-promoter, respectively, in front of GeneSwitch (Figure 3a). The expression cassettes of GeneSwitch and IGF1 were in opposite transcription directions based on results from Szymanski et al[12]. and in order to avoid close proximity of the promoters to the AAV inverted terminal repeats.

MFP induced expression of IGF1 by the hepatocyte cell line Huh7 transfected with the AAT- or CMV-driven plasmids. The AAT promoter construct resulted in much higher IGF1 protein induction than the CMV promoter, 1,6 and 12 times over baseline respectively (Figure 3b). In the non-induced state, cells with the AAT-promoter plasmid secreted only 6 ng/ml IGF1 in contrast to 28 ng/ml IGF1 with the CMV-promoter, revealing low basal expression of the AAT-promoter compared to the high background expression of the CMV promoter. The difference in IGF1 basal expression levels between the AAT- and CMV-promoters was unexpected as both promoters are strong and have been widely used to drive gene expression in hepatocellular cells. Additionally, the MFP-induced IGF1 expression was higher with the AAT-promoter (76 ng/ml IGF1) than with the CMV promoter (45 ng/ml IGF1). Consequently, the AAT promoter resulted in low

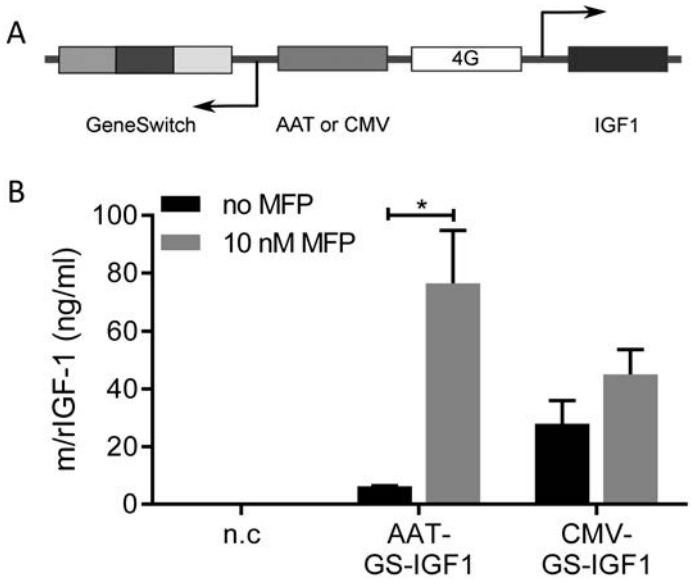

Figure 3. Single-vector GeneSwitch system promoter optimization and applicability to different transgenes. A. Configuration of head-to-head single vector GeneSwitch system in which the transgene is insulin like growth factor 1(IGF1) and the promoter in the GeneSwitch expression cassette is either CMV or AAT. B. Huh7 cells were mock transfected (negative control, n.c) or transfected with AAT-GS-IGF1 or CMV-GS-IGF1. The next day culture medium was replenished by medium without (no MFP, black bars) or with 10nM MFP (gray bars). After 48h, IGF1 secretion into the culture supernatant was measured by ELISA. Data were evaluated using student's t test for the treatment with MFP versus without MFP. The significant difference of $p < 0.05$ between the AAT-GS-IGF1 groups is indicated with (*). There was only a positive trend for the difference between no MFP and 10 nM MFP of the CMV promotor containing construct.

background expression and a high dynamic range of MFP-dependent induction. Because of the superior characteristics of the AAT-promoter it was selected for further testing *in vivo*.

In vitro expression kinetics of the single vector GeneSwitch system

We next investigated the expression kinetics of the GeneSwitch system *in vitro*, using EPO as a reporter, to gain more insight into the GeneSwitch system. A single vector (GS-EPO) was constructed containing the AAT-promoter in front of GeneSwitch and an EPO expression cassette with the inducible promoter in opposite direction (Figure 4a).

Huh7 cells were transfected with GS-EPO, incubated with 0, 1 or 10nM MFP and harvested 6, 16, 24 or 48 hours after induction. EPO mRNA levels were measured by RT-qPCR and ELISA was performed to determine EPO protein concentrations in the culture supernatant. Both EPO mRNA and protein levels increased in the presence of MFP (Figure 4b and 4c). EPO mRNA levels increased to reach a maximum at 16h, followed by

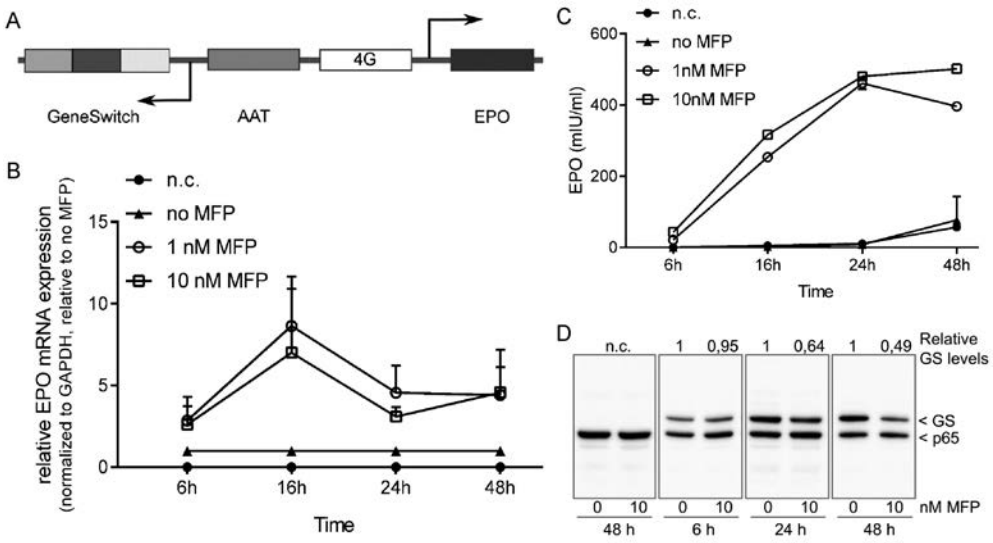

Figure 4. *In vitro* expression kinetics of EPO mRNA, protein and GeneSwitch protein after MFP induction of the single-vector GeneSwitch system. A. Configuration of head-to-head single vector GS-EPO in which the transgene is erythropoietin (EPO) and with the AAT-promoter in the GeneSwitch expression cassette. B. EPO mRNA kinetics. Huh7 cells were transfected with single vector GS-EPO or no plasmid (n.c.). The next day they were incubated with 0 to 10nM MFP for 6 to 48h hours. Then EPO mRNA expression in the cells was determined by reverse transcription qPCR. Data were analyzed with a two-way ANOVA and the most significant induction rate was at 16h after 1nM and 10 nM MFP ($p < 0.0001$). At 24 and 48h induction was also significant ($p < 0.05$). Full statistical analysis can be found in supplemental table 1. C. EPO protein kinetics. EPO protein expression and secretion into the culture medium was measured by ELISA. Two-way ANOVA at 6h revealed $p < 0.05$ for no MFP versus 1 nm MFP and $p < 0.0001$ for no MFP versus 10 nm MFP. At 16, 24, and 48h, p values were < 0.0001 for no MFP versus both 1 nM and 10 nM MFP. D. Detection of GeneSwitch protein. Presence of GeneSwitch protein in cells was assessed by SDS-PAGE followed by western blotting using a p65-antibody. Arrows indicate endogenous p65 and GeneSwitch protein. Relative GeneSwitch protein levels were quantified by normalizing the GeneSwitch protein signal to endogenous p65 signal and set relative to 0nM MFP of each timepoint. The values are indicated above each lane.

protein expression that reached its maximum at 24h to 48h. GeneSwitch protein kinetics were monitored by western blot using an antibody against its p65-domain and quantified relative to endogenous NF-kappaB p65 signal. In the absence of MFP, the amount of GeneSwitch protein increases from 6h to 48h, due to constitutive production of GeneSwitch from the AAT-promoter (Figure 4d). After addition of 10nM MFP the signal for GeneSwitch protein on the western blot was constant. However, in comparison to non-induced cells GeneSwitch protein declined over time, to two-thirds the amount at 24h and half the amount at 48h post MFP. This difference could either be due to lack of antibody recognition, as activated GeneSwitch changes conformation to form a dimer, or due to degradation of GeneSwitch after activation. Hence, induction by MFP results in

transgene mRNA expression followed by protein expression, after which all components including the GeneSwitch protein reach an equilibrium from 24 hours to at least 48h.

In vitro induction and comparison of the single- and two-vector GeneSwitch system

The original GeneSwitch system is based on two plasmids, but we have put all GeneSwitch components into a single plasmid and kept within the maximal packaging capacity of the AAV vector. We compared the characteristics of the single and two-vector GeneSwitch system *in vitro* and *in vivo* using four constructs (Figure 5a). In addition to the single vector GS-EPO, described in the previous section, two combinations of the two vector system were designed: A two vector system containing GeneSwitch on one plasmid (GS) and the EPO transgene together with the regulated promoter having either four or eight Gal4 binding sites (GS-EPO, 4G-EPO or 8G-EPO) on the second plasmid. GS-EPO, GS together with 4G-EPO and GS with 8G-EPO were investigated for inducibility and the effect of the number of GeneSwitch protein binding sites on (basal) expression levels.

The hepatocyte cell lines Huh7 and Hepa1-6 were transfected with these plasmids and after two days of incubation with MFP, EPO was measured in the culture supernatant. In both cell lines, addition of MFP induced the expression of EPO from the single and two vector systems (Figure 5b and c). In Huh7 cells induction rates for all three conditions tested were just above 6 times (6,2 times for GS and 4G-EPO; 6,4 times for GS and 8G-EPO and 6,3 times for GS-EPO), indicating that in these cells the single and two vector GeneSwitch systems perform similarly (Figure 5b). The measured induction levels were higher and more distinctive in Hepa1-6 cells than in Huh7 cells (Figure 5b and c), mostly because in Huh7 cells the constructs have to overcome endogenous EPO expression. In Hepa1-6 cells the single vector outperformed the two-vector system. Whereas the induction ratio in cells transfected with GS and 4G-EPO was 4 times and 14 times using GS and 8G-EPO, with the GS-EPO construct this was more than 500-fold (Figure 5c). These Induction differences were in large part due to the different levels of background expression of the GeneSwitch systems tested. With the single vector GS-EPO expression of EPO was not detectable without MFP. This was in contrast to the two-vector systems which triggered EPO expression in the absence of MFP. A higher leakiness was observed with the 4G-EPO plasmid compared to the 8G-EPO plasmid, but only in Hepa1-6 cells and not in Huh7 cells. These results showed an impact of the number of Gal4-binding sites on the activity of the inducible promotor and indicated that an increased number of those sites could result in less background expression.

Measurement of Mifepristone concentrations in biological matrices such as plasma and liver tissue

Because the GeneSwitch system is regulated by MFP, it is important to know the MFP concentrations necessary for gene induction in plasma and in liver. MFP is metabolized

and then excreted from the body, hence its pharmacokinetics are important for the timing of GeneSwitch activation.

In rats, maximal MFP plasma levels are reached one to two hours after MFP administration[15]. Mice were injected intraperitoneally during four consecutive days with 20mg/kg MFP and sacrificed 2h after the last injection. MFP was extracted from plasma and liver tissue and measured quantitatively by HPLC followed by quadrupole time of flight-mass spectrometry. In Figure 6a a positive and negative chromatogram are shown. A peak with a retention time consistent with MFP (2,73 min) was exclusively present in the plasma sample from the MFP injected mice. Applying the same method MFP levels could also be measured in liver tissue (Table in Figure 6b). The average concentration of MFP from six mice was 677 ng/ml in the plasma and 3835 ng/g in the liver. Hence, MFP seems to be a suitable inducer for liver-directed gene therapy.

MFP can be C-hydroxylated, mono- and di-demethylated and in the liver. These MFP metabolites retain binding affinity to the human progesterone receptor and could induce the GeneSwich system[16,17] . To follow MFP and MFP metabolite concentrations in plasma in time, mice were injected three consecutive days with MFP and plasma was recovered at 1h, 4h, 8h, 16h and 24h post last MFP injection. Each MFP metabolite has a different retention time and to compare MFP to its metabolite concentrations deuterated MFP was used as an internal standard. MFP, mono- and di-demethylated MFP levels peaked at 1h post last MFP injection in the plasma samples, while hydroxylated MFP reached a maximum at 4h (Figure 6c). Mono-demethylated MFP was more prevalent than di-demethylated MFP in plasma, as the demethylations occur successively. At 16h post MFP the concentration of each compound reached the detection limit of 10ng/ml and at 24h post injection no MFP or metabolite could be detected. The half-lives were calculated to be around 3,5h for MFP and hydroxylated MFP, 1h for mono-demethylated MFP and 2,5h for di-demethylated MFP. Although the half-life of MFP measured in mice was slightly longer than the 2 hours reported previously in rats[15] , MFP and its metabolites are rapidly cleared in rodents.

In vivo expression kinetics of the single vector GeneSwitch system

For testing kinetic expression of the components of the GeneSwitch system in mice, the single vector construct GS-IGF1 and constitutive expression construct IGF1 both with the AAT-promoter were encapsulated into AAV5 (AAV5-GS-IGF1 and AAV5-IGF1). IGF1 was chosen as transgene, because protein-bound IGF1 has a longer half-life than EPO[18], and the rat IGF1 sequence was used, to distinguish between endogenous murine IGF1 and vector-expressed IGF1.

The AAV5-vectors were injected intravenously at a dose of 10e13 genome copies (gc) per animal. One group of mice received the constitutive expression vector AAV5-IGF1 (Figure 7a). The other groups were transduced with AAV5-GS-IGF1 and 4 weeks later injected with MFP for three consecutive days. Blood was drawn at 1h, 4h, 8h, 16h or

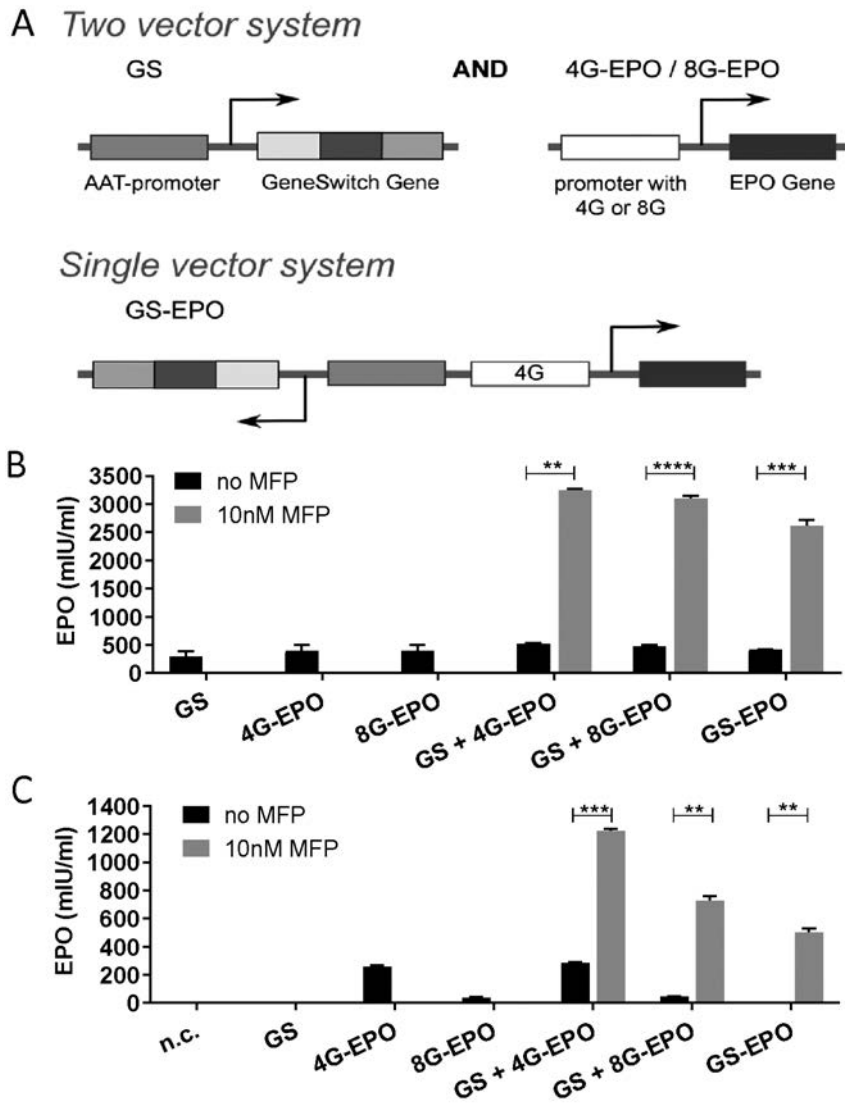

Figure 5. Mifepristone inducible expression of EPO by single- and two-vector GeneSwitch system *in vitro.* A. Within the two-vector system the GeneSwitch protein expression cassette is in one vector (GS) and the transgene expression cassette with EPO is in the second vector. The latter contains either four Gal4 (4G-EPO) or eight Gal4 (8G-EPO) binding sites in their inducible promoter. The single-vector system comprises both the GeneSwitch protein and erythropoietin (EPO) expression cassettes in one vector (GS-EPO), here in tail-to-tail orientation with transcription in opposing directions. B. The different plasmids illustrated in A. were transfected into Huh7 cells. The next day, they were incubated with 0 or 10nM MFP for 48h. Then ELISA was performed on culture supernatant, to measure the concentration of secreted EPO. C. Same as B, except in Hepa1-6 cells. Mock transfected cells are indicated with negative control (n.c.). In the GS-EPO treated cells, the background levels of EPO without MFP were too low to visualize in the graph. Data were evaluated using student's t test to compare with MFP versus without MFP. MFP treatment significantly induced EPO expression in both cell lines. (**$p < 0.01$; ***$p < 0.001$; ****$p < 0.0001$)

24h after each MFP injection (Figure 7a). Following the third MFP injection the mice were sacrificed and vector DNA and rat IGF1 mRNA levels were quantitated in the liver. The average transduction efficiency of the AAV5-vector was similar for the groups, however there was high variance within each group (Figure 7a and b). Four animals seemed to have been miss-injected and had very low liver vector DNA levels (less than 10e6 gc/ug DNA), were excluded from the subsequent mRNA and protein analyses.

Rat IGF1 mRNA levels were quantified using rat specific IGF1 primers and compared to the AAV5-GS-IGF group that did not receive MFP. AAV5-IGF1 injected animals constitutively express IGF1 and around 60 times over the non-induced AAV5-GS-IGF1 transduced animals. After induction of the AAV5-GS-IGF1 groups, IGF1 mRNA concentrations increased up to 4 hours after administration MFP, and subsequently gradually decreased to non-induced levels at 24h post MFP. Concordantly, a time dependent increase in IGF1 mRNA levels after induction with MFP using the GeneSwitch system was detected *in vivo* (Figure 7c).

Finally, IGF1 protein levels were determined in murine plasma upon MFP induction at three consecutive days. The plasma concentrations of IGF1 varied between 100 and 400 ng/ml for all groups over these three days (Supplemental Figure 1). Higher steady state IGF1 levels were detected in mice injected with the constitutive AAV5-IGF1 vector compared to the uninduced AAV5-GS-IGF1 injected group. IGF1 protein induction was determined at 1, 4, 8, 16 and 24h after the last induction. A clear time-dependent increase was observed in all animals (Fig7D), demonstrating a tight regulation of the transgene expression over time. Taken together these results indicate MFP and time dependent regulated transgene mRNA and protein expression by the GeneSwitch system *in vivo*.

In vivo induction and comparison of the single- and two-vector GeneSwitch system

After evaluating the kinetics of MFP and the GeneSwitch system in mice, we compared the characteristics of the single and the two vector GeneSwitch system encapsulated in AAV5. Instead of IGF1, EPO was as the reporter gene because it can be easily measured in blood and increases hematocrit, providing a simple measurable functional effect.

Mice were transduced with 10e12 gc of the constitutive expressing AAV5-EPO or the single vector virus AAV5-GS-EPO. In addition, two groups of mice were injected intravenously with AAV5-GS either in combination with AAV5-4G-EPO or AAV5-8G-EPO, each virus at 10e12 gc per animal (Table in Figure 8a). To investigate repeated inducibility of the GeneSwitch system, the mice received two rounds of MFP at 4- and 8-weeks post transduction. Blood was taken regularly from the mice to measure EPO plasma concentrations and hematocrit (Figure 8b).

After the second round of MFP injections the mice were sacrificed and vector DNA was measured with EPO or GeneSwitch specific primers (Table in Figure 8a). The liver-

specific transduction of the different AAV5-delivered constructs was similar for all groups (Figure 8c).

AAV5-EPO caused continuous transgene expression resulting in plasma EPO levels of approximately 600 mIU/ml (Figure 8d, panel i). This caused a high hematocrit and after a month it was decided to sacrifice the mice. (Figure 8e). The groups injected with either the single or the two vector GeneSwitch system, all had increased EPO plasma levels after induction with MFP. The EPO levels dropped to background at four days post last MFP injection (data not shown) and remained at basal levels till the week before the next MFP-induction round (Figure 8d, panels ii, iii, iv). The induction ratio of the single vector was more than 200 times, while the ratios with two-vector system with 4G-EPO or 8G-EPO were 60 and 20 times, respectively. The difference of the induction ratios was mainly a consequence of the low background expression levels and not the amplitude of expression observed with the single vector system. Although the two-vector system GS and 4G-EPO showed high levels of EPO after induction, they were considerably more basal expression than the single vector system. As had been observed *in vitro*, the addition of four additional Gal4 binding sites, to a total of eight, reduced background levels as well as the induced expression levels, resulting in a lower induction ratio. The induced EPO production in mice injected with the single-vector system had functional effects and increased red blood cell volume (Figure 8e). Hematocrit levels were above normal in mice injected with either of the two-vector systems in the absence of MFP, due to background EPO expression. In summary, *in vivo* the single vector GeneSwitch system had low background expression and a high induction rate, two requirements that are essential for developing regulated AAV gene therapy. Mice injected with the single vector system had a normal hematocrit in the non-induced state, and hemoglobin levels increased upon MFP injection, returning to baseline in the absence of the inducer (Figure 8f). Hence, the GeneSwitch system can be adapted to cause background free repeated induction of a therapeutic transgene, resulting in an inducible phenotype.

Discussion

Gene therapy offers the potential of a long-term solution for many chronic diseases, whereby the transgene is continuously expressed following a single vector administration. However, in some cases it would be desirable to regulate transgene expression within a well-defined therapeutic window in time, or to regulate the rate of expression of a therapeutic transgene. The present report describes a series of *in vitro* and *in vivo* proof-of-concept studies to explore the MFP-inducible GeneSwitch system in regard of timing and transgene expression levels and carrying out an in depth characterization of the regulated gene expression system. Our data support the rationale that the GeneSwitch system could be applied in future clinical development programs.

The classical GeneSwitch system consists of two vectors with separate GeneSwitch and transgene expression cassettes. We chose to develop a single vector system, because

A

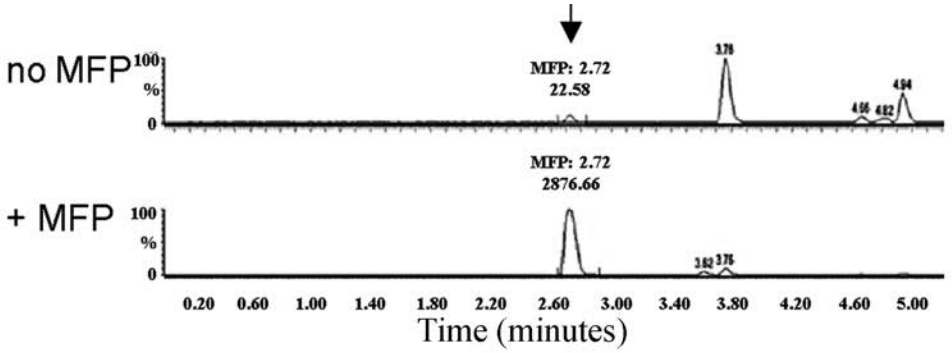

B

MFP concentration	regime	plasma	liver
with MFP	4days IP 20 mg/kg	677 ng/ml (+/- 86)	3853 ng/g (+/-717)
without MFP	-	1,8 ng/ml (+/- 0,9)	0,3 ng/g (+/- 0,7)

C

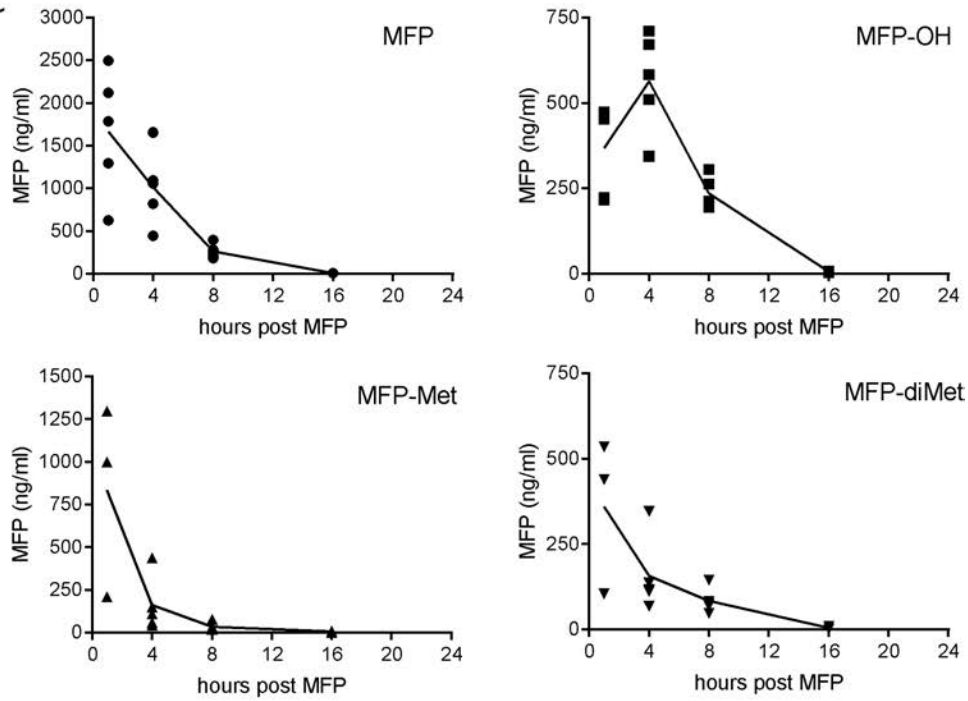

Figure 6. Assay development for detection of mifepristone and its metabolites in biological matrices. A. Mice received intraperitoneal MFP injections (20mg/kg) for four consecutive days. Then plasma and liver samples were taken 2 hours after the last MFP injection and measured by UPLC-QTOF-MS. Mass spectrometry chromatograms for mifepristone at 2.73 min in murine plasma samples from mice without (no MFP) or with MFP injections (+MFP) are shown in A. The table in B. contains the average MFP concentration in plasma and liver samples of six mice. The standard deviation is

in brackets. C. Mice were treated with MFP for three consecutive days, blood samples on the third day were taken at indicated hours post injection, followed by measurement on UPLC MSMS to determine concentrations of MFP (i) and three MFP metabolites C-hydroxylated MFP (ii), mono-demethylated MFP (iii) and di-demethylated MFP (iv).

it circumvents the hurdle of delivery of both cassettes at a predefined ratio in the same target cell *in vivo*. Furthermore, a single product would simplify AAV manufacturing. Based on the relative large size of GeneSwitch (2,5kb), the additional cargo size is limited to approximately 2 kb to not exceed the AAV packaging limit of approximately 4,7kb. With suitable sized transgenes such as luciferase, EPO and IGF we were able to show inducibility of the single vector system for all three genes. Albeit in a different expression cassette orientation, others have used a single vector AAV with transgenes GFP, GDNF and IFN[9,10,12] . Collectively, this demonstrates wide applicability of the single vector GeneSwitch system to multiple transgenes. Besides transgene size, other discriminating points in the development of a single vector are the orientation of both expression cassettes and the promoter for the GeneSwitch protein, as described by Szymanski et al[12]. In addition, we showed that the promoter can affect the inducibility of the system, as the use of the AAT-promoter improved induction ratios compared to the CMV-promoter because it has lower non-induced expression and higher transgene expression after MFP addition. The use of the liver specific AAT-promoter adds additional value to the GS system because expression will be limited to hepatocytes, hence increase the safety of the approach.

The GS system is designed to be silent in a non-induced state and active after the addition of MFP. The advantage of a positively induced system is that it requires the administration of the inducer MFP only when necessary, increasing the safety profile of the regulated expression system. The need-on-demand principle for MFP would allow discontinuation of therapy in case of adverse effects or when treatment is no longer required, by simply stop taking the inducer drug. In mice we observed a rapid (16-24 hour) clearance of MFP and metabolites after the last injection with the inducer. Moreover, transgene levels increased at first and then decreased, showing that the GeneSwitch system can be switched off by the removal of MFP. It should be noted that the half-life of MFP in humans is around 25 to 30 hours, and it therefore is expected that the induced transgene expression in humans would last longer than in rodents[19] .

One requirement for a regulated expression planned for clinical use would be to turn it on and off repeatedly. Previous data showed effective usage of the GeneSwitch system in a murine model of experimental allergic encephalomyelitis, with one plasmid containing the inducible system that regulated interferon expression[20]. This single vector system was packaged into AAV1 and injected intramuscularly into mice and interferon was induced over nearly a year[20]. We carried out a similar *in vivo* study using AAV5 to target hepatocytes in the liver. The Gene switch system was induced twice with MFP resulting both times in high EPO plasma levels with a meaningful impact on hematocrit levels

A

Group	Virus name	MFP	sampling post MFP	transduction efficiency average (gc/ug DNA)
1	AAV5-IGF	no	n.a.	2,48E+07
2	AAV5-GS-IGF	no	n.a.	1,04E+07
3	AAV5-GS-IGF	yes	1h	5,95E+07
4	AAV5-GS-IGF	yes	4h	7,53E+07
5	AAV5-GS-IGF	yes	8h	7,50E+07
6	AAV5-GS-IGF	yes	16h	3,27E+07
7	AAV5-GS-IGF	yes	24h	1,41E+07

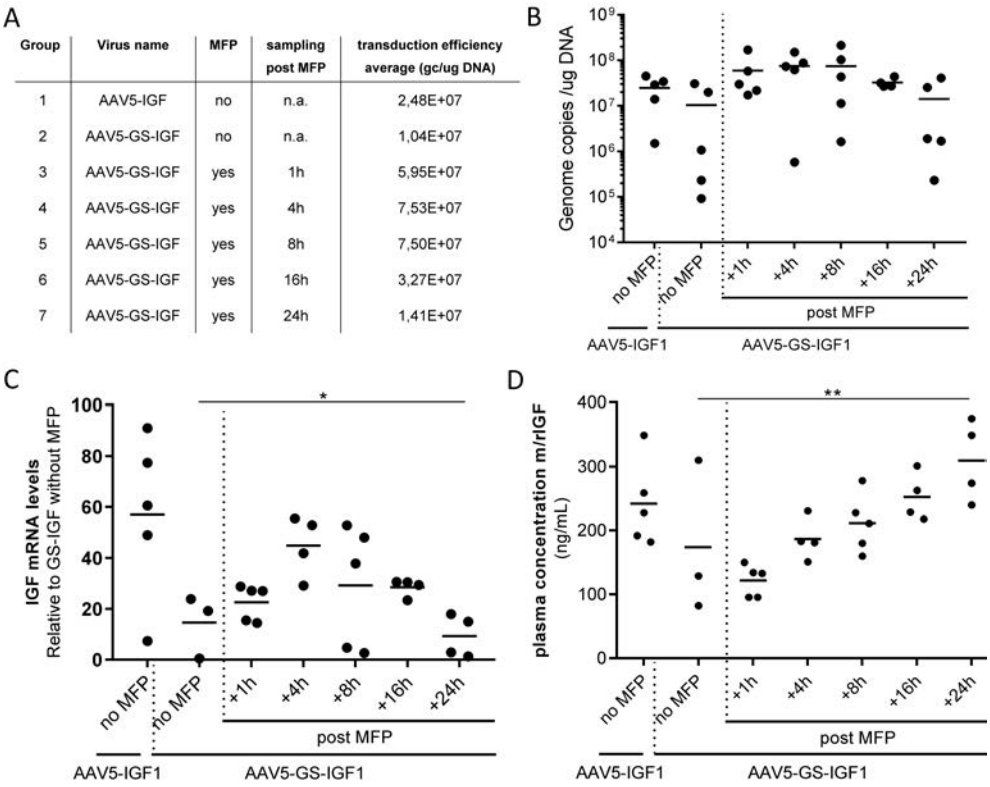

Figure7. ***In vivo*** **expression kinetics of IGF mRNA and protein after MFP induction in murine liver by the single-vector GeneSwitch system.** Mice were transduced with AAV5 expressing rat IGF constitutively (AAV5-IGF, group 1) or regulated through the GeneSwitch system (AAV5-GS-IGF, group 2 to 7). Four weeks later, groups 3 to 7 were given MFP on three consecutive days and blood was taken at the indicated hours after each injection (+1h, +4h, etc). Group 1 and group 2 did not receive MFP (no MFP). On the third day the animals were sacrificed, and the livers dissected. One animal of the 16h group died before MFP injections for unknown reasons. A. Table indicates with which AAV5 the groups were injected, treatment of MFP and time post MFP for blood sampling. The average transduction efficiency of vector DNA was determined in liver tissue 5 weeks after virus injection by qPCR. B. Transduction efficiency of vector DNA of each mouse from each group. The small lines indicate the average per group. Four animals seemed to be miss-injected and had below 10e6 genome copies per ug DNA, they were excluded from the subsequent mRNA and protein analyses. C. Liver samples were analyzed for rat IGF mRNA levels by reverse transcription and qPCR. Levels were normalized to GAPDH and put relative to mRNA levels in mice transduced with GS-IGF without induction (group 2). A one-way ANOVA revealed a significant change in IGF mRNA levels over time post MFP induction. Full statistical analysis can be found in supplemental table 1. D. IGF plasma concentrations were determined in the blood samples after three days of MFP injections by ELISA against mouse and rat IGF. There was a significant increase in plasma concentration post MFP induction (one-way ANOVA).

that increased temporarily. Both studies demonstrate the broad and robust versatility of the Gene Switch system.

A critical feature in optimizing a regulation system for gene expression is to avoid background expression of the system. Our study has identified several factors that are involved in non-induced transgene expression: promoter choice, regulatory elements and the application as a single or two-vector system. The use of the liver-specific AAT promoter in conjunction with GeneSwitch resulted in a higher induction ratio, mainly due to low basal transgene expression in the absence of MFP. Increasing the number of Gal4-binding sites from four to eight to more tightly regulate transcription, also resulted in reduced basal expression levels. However, whilst this approach reduced background expression, both *in vitro* and *in vivo*, it also lowered maximal expression, resulting in a lower induction ratio in mice. The lowest background expression levels were observed using a single vector system: Mice transduced with the single vector GS-EPO and not injected with MFP had EPO plasma levels that were similar to the control group. Therefore, the single vector with the AAT-promoter meets the safety criteria of reducing basal expression levels of the transgene.

The transgene induction rate provides an estimate of the dynamic range of protein expression using the GeneSwitch system. *In vivo* with the single vector AAV5-GS-EPO a more than 200 times increased transgene expression was observed compared to the basal state in the presence of MFP, indicating a two-log range regulated EPO expression. To compare the induction rate of GeneSwitch to other inducible systems *in vivo,* multiple variables need to be taken into account, including the promoter, vector architecture, the transgene, a single or two-vector, the target cell and the inducer. We preferred the AAT-promoter over the CMV-promoter, with a 7,5-times induction rate difference and with the additional benefit of restricting transgene expression to the liver. It has been reported that the transthyretin promoter can drive GeneSwitch protein to regulate IL12 expression. Mice injected with the inducible adenoviral vector showed two to three log increased IL12 levels, depending on viral load and MFP dose[21]. Other tissue specific promoters that were used in combination with the GeneSwitch system were selective for brain and muscle and had 24 and 500 times induction ratios respectively[10,22]. Hence, the performance of the AAT-promoter as part of the GeneSwitch system is comparable to the previously reported results.

The single vector architecture of the GeneSwitch system as well as the type of transgene, can make a difference for inducibility[12]. The orientation of the expression cassettes determined the induction rates for SEAP between 4 to 900 times, while the rates from vectors with EPO were between 19 and 34 times, which is significantly lower than the AAV5-GS-EPO we have tested. The Tet-on system has been incorporated into a single AAV vector with a liver specific albumin promoter and expressing luciferase as transgene[23]. Injection of the vector into mice, gave similarly to the AAV5-GS-EPO vector, a dynamic range of 250 times. In contrast, an *in vivo* study using the Tet-on

A

Group	name virus 1	name virus 2	gc injected per animal virus 1	gc injected per animal virus 2	MFP	transduction efficiency (gc/ug DNA) virus 1	transduction efficiency (gc/ug DNA) virus 2
1	- (Ctrl)	-	-	-	no	-	-
2	AAV5-EPO	-	1,0E+12	-	no	1,5E+05	-
3	AAV5-GS-EPO	-	1,0E+12	-	no	8,0E+04	-
4	AAV5-GS-EPO	-	1,0E+12	-	yes	1,0E+05	-
5	AAV5-GS	AAV5-4G-EPO	1,0E+12	1,0E+12	no	1,8E+05	2,5E+05
6	AAV5-GS	AAV5-4G-EPO	1,0E+12	1,0E+12	yes	2,2E+05	3,0E+05
7	AAV5-GS	AAV5-8G-EPO	1,0E+12	1,0E+12	no	8,7E+04	1,1E+05
8	AAV5-GS	AAV5-8G-EPO	1,0E+12	1,0E+12	yes	1,1E+05	2,1E+05

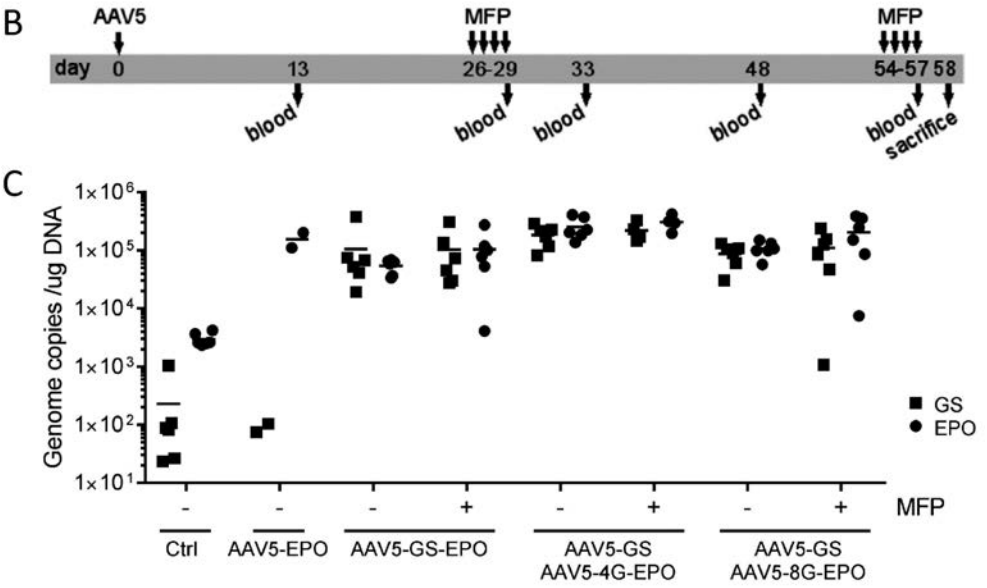

Figure 8. Mifepristone inducible expression of EPO in murine liver by the single- and two-vector GeneSwitch system. A. Table indicating the groups, the name and concentration of the AAV5 injected and the MFP treatment. The average vector DNA level of each vector per group determined in murine liver tissue using qPCR. B. Illustration of experimental set up. Arrows above timeline indicate the day of AAV5 transduction and the days of intraperitoneal injections with MFP. Arrows below the timeline specify when blood samples were taken and at day 58 when the animals were sacrificed. C. Individual values of vector DNA levels in liver tissue of each AAV5, determined in mice 9 weeks post vector injection using qPCR. Specific primers were used to quantify GeneSwitch sequences (GS, squares) and EPO sequences (EPO, circles). D. EPO concentrations in the plasma of mice injected with different AAV5 vectors. In panel i animals were transduced with AAV5-EPO and EPO plasma concentration was measured at day 13, 29 and 33. The mice of panel ii received the single vector AAV5-GS-EPO. In panel iii and iv the animals were co-injected with AAV5-GS and AAV5-4G-EPO or AAV5_8G-EPO. EPO plasma levels were measured at day 13, 29, 48 and 57. Animals subjected to two rounds of four days of MFP injections are indicated with circles, the non-MFP injected animals with triangles. Each panel contains the EPO plasma concentration of animals without vector and MFP injections (Ctrl). Data were evaluated using student's t test to determine the significance between groups treated with and without MFP. Some measurements are also indicated with n.s to show they are not significantly different. E. All ghemoloups were subjected to hematocrit measurement ▸

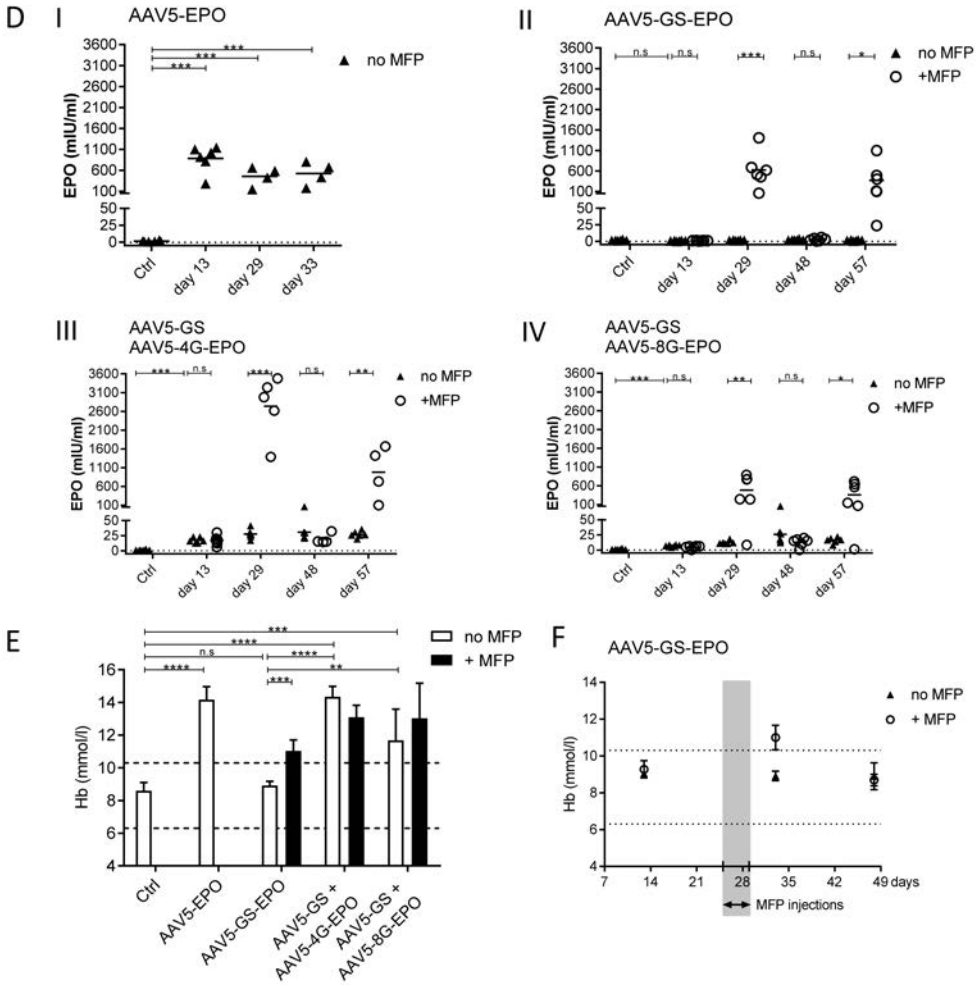

at day 33. The hematocrit levels between the dotted lines at 6,3 and 10,3 mmol/l are considered normal or healthy. Basal expression levels between groups were analyzed by a two-way ANOVA (see table S1). A second comparison was done with a t-test to determine the effect of MFP on Hb levels. F. Average hematocrit levels from animals transduced with the single vector AAV5-GS-EPO at day 13, 33 and 48. Triangles represent the mice without MFP and circles is the group injected with MFP. Gray bar indicates when MFP was injected and dotted lines are the borders of normal hematocrit levels. (*p < 0.05; **p < 0.01; ***p < 0.001; ****p < 0.0001).

system, controlling EPO expression in a single vector with both cassettes facing inward the induction rate reported was 15 times above baselines. This relatively low increase after administration of doxycycline was mainly due to the high basal expression levels that already were sufficient to increase the hematocrit in mice[24] . In contrast, a two-vector AAV Rapamycin system expressing EPO did not elevate hematocrit levels in the absence of the inducer, and similar to our experiments, rapamycin administration resulted in an induction rate of 200 times[25,26]. A main advantage of the two-vector rapamycin system is its tight regulation compared to other systems[27] . We here report that using a single vector, a similar tight control of gene regulation and predictable repeated induction, leading to an induced phenotype, can be achieved.

The kinetics and orchestration of transgene expression has not been studied extensively for GeneSwitch, nor for other regulated gene expression systems, and was therefore investigated by us *in vitro* and *in vivo*. *In vivo* we observed that the highest plasma levels of MFP and metabolites were measured at 1 to 4 hours post injection, followed by a peak expression of mRNA at 4 to 8 hours. Transgene protein levels could be measured the same day and the next day; a timeframe confirmed with our two vector system and by others[21,22]. The rise of transgene mRNA followed by increasing levels of protein correlated with the *in vitro* results. We also managed to detect GeneSwitch protein by western blot in liver tissue, albeit weakly, showing that after MFP induction GeneSwitch protein decreased, confirming our *in vitro* data (data not shown). We´d expect similar kinetics for other regulated gene expression systems, however how long it takes before expression can be switched off will depend on the pharmacodynamics of the inducer and the stability of the mRNA and protein. Here we used EPO as transgene, which has a half-life of around 5 hours and could not be measured four days post the last MFP injection (data not shown). On the other hand, using GDNF as transgene with a half-life of 37 hours resulted in longer expression, as GDNF was still detectable one week post MFP injections[10]. Doxycycline is cleared from the body in 15-25 hours, which is shorter than MFP (25-30 hours), but is around twice as long for rapamycin (60 hours). Expression from the GeneSwitch system might therefore, due to MFP inducibility, be switched off relatively quickly.

One of the advantages of using MFP as an inducer in the GeneSwitch system is the fact that it is licensed for clinical use. The GeneSwitch inducer MFP and its safety has been studied only short term and in females. However, the drug is currently investigated for long term use in psychiatric disorders with male and female participants[28]. Moreover, the MFP concentration inducing expression in our *in vivo* experiments has been safely tested in psychiatric patients[29–31]. Besides progesterone-antagonizing effects MFP has anti-glucocorticoid properties. Although, the IC50 of the latter effects is a 100-fold lower, and low-dose MFP is not expected to have an effect on the glucocorticoid receptor. In the current experiments, using a single vector GeneSwitch system MFP induced the transgene at a concentration between 0,2 nM and 1 nM. This is as low as

demonstrated previously[32]. Alternative regulated systems use rapamycin or tetracyclins as inducer. Rapamycin is an immunosuppressant and clinical application would require development of non-toxic rapamycin orthologs. Tetracyclins have short-term side effects and long-term use of tetracyclins could increase antibiotic resistance in microorganisms. Recently, a Tet-on system was optimized to be inducible at low enough concentrations to have the potential to not invoke resistance[3].

Gene therapy should be restricted to the organ where the gene product is required. The delivery to the target organ is achieved by the choice of the AAV variant, by the route of administration and by a promoter that is restricting the expression to the area of choice. In case of a regulated gene expression system it is also necessary to ensure that the inducer is reaching the target cells. We found that sufficient concentrations of MFP reach the liver *in vivo*. Rapamycin and doxycyclin have difficulty reaching the brain and CSF levels are 30% and 25% of the plasma concentration, respectively[33,34] . MFP does cross the blood brain barrier, and the GeneSwitch system has been successfully utilized in rat brain[9]. Additionally, it is possible to induce expression from the GeneSwitch system which is injected in mice muscle or when expressed in lung cells[22,35] . Hence, the Gene Switch system is applicable to multiple organs and can be controlled by tissue-specific promoters.

The ongoing successes for clinical trials for hemophilia A and hemophilia B have led to increasing enthusiasm for AAV gene therapy targeting liver diseases[36]. Preclinical studies in animal models have demonstrated proof of concept for several other types of liver disorders[36]. Many of these disorders such as glycogen storage disease type Ia, citrullinemia type I, ornithine transcarbamylase deficiency, phenylketonuria, Wilson disease, methylmalonic acideamia and Crigler-Najjar syndrome are currently under investigation by several pharmaceutical companies[36,37]. As more disease indications for the liver are moving closer to the clinic, inducible systems will inevitable be needed in the future to allow a more controlled regulation of transgenes that may induce transgene-specific immune responses or cause other unwanted effect at sustained expression and/or high doses. The data presented in this study supports the applicability of regulatable GeneSwitch system delivered by AAV for future clinical application in the liver.

Material and Methods

Plasmid construction

Erythropoietin (EPO) coding sequence is from M18189.1, Insulin like growth factor 1 (IGF1) coding sequence from M15480.1 (rat) and human growth hormone polyA tail (pA) sequence from NM_022560, these were synthesized and digested from shuttle vectors prepared by BaseClear (Leiden, The Netherlands). The alpha1 anti-trypsin promoter combined with the mouse albumin gene enhancer (AAT-promoter) was taken from a plasmid described before[38] . pIF1683 (Inovio, San Diego, CA) contained minimal pol II

promoter with four upstream activation elements (4xGal4) and IVS8 that was cloned in front of the transgene. The GeneSwitch sequence (GS) was from pGS1694 (Inovio, San Diego, CA). The specific order of elements within the expression cassettes designed in this study will be summed up here: CMV-GS-luciferase has CMV-GS-pA-4xGal4-IVS8-luciferase-pA, CMV-GS-IGF has pA-IGF-IVS8-4xGal4-CMV-IVS8-GS-pA, AAT-GS-IGF has pA-IGF-IVS8-4xGal4-AAT-IVS8-GS-pA, EPO has AAT-EPO-pA, GS has 4xGal4-AAT-IVS8-GS-pA, 4G-EPO has 4xGal4-IVS8-EPO-pA, 8G-EPO has 4xGal4-4xGal4-IVS8-EPO-pA and GS-EPO has pA-EPO-4xGal4-AAT-IVS8-GS-pA.

Cell culture, transfection and MFP induction

Huh7, Hepa1-6 and HEK293 cells were cultured in DMEM medium (Gibco), supplemented with 10% fetal bovine serum with or without penicillin/streptomycin at 37C, 5% CO2. Trypsin 0,25% EDTA (Gibco) was utilized for cell detachment and cells were seeded one day prior to transfection. HEK293 cells were transfected using Lipofectamine 2000, according to manufacturer's protocol. Lipofectamine 3000 at a ratio of 1: 0,75 for P3000: Lipofectamine 3000 was used to transfect Huh7 and Hepa1-6 cells. The following day culture supernatant was replaced by medium with the appropriate MFP concentration. MFP was diluted from a 1mM MFP-ethanol stock solution into medium.

Luciferase assay

To measure luciferase activity, culture medium was removed and cells were washed ones in PBS, followed by lysis with 1x passive lysis buffer (Promega). Plates were incubated on an orbit-shaker at 450 rpm at room temperature for 20 min. Firefly luciferase activity of 10ul samples was measured with the dual-luciferase reporter assay system (Promega) according to manufacturer's protocol. An average of luciferase counts was taken from triplicate transfections.

ELISA

For EPO and IGF1 ELISA murine plasma or cell culture supernatant was collected. The samples were diluted in specimen diluent buffer for EPO measurements and in calibrator diluent buffer for IGF1 measurements to range within the standard curve values. After that manufacturer's protocol was followed (R&D systems; DEP00 and MG100). EPO or IGF1 concentrations were calculated using a trend line derived from the standard curve samples in Excel.

RNA and DNA isolation, cDNA synthesis and qPCR

Genomic DNA (gDNA) was isolated from murine liver using the DNeasy Blood & Tissue Kit (QIAGEN Inc., Chatsworth, CA) according to the manufacturer's protocol. Total RNA was isolated from liver sections or from Huh7 cells using Trizol (Invitrogen, Carlsbad, CA)

according to the manufacturer's protocol. gDNA was removed by double stranded DNase treatment using engineered shrimp DNase (Thermo Scientific, EN0771). First strand cDNA was reverse transcribed using random hexamer primers with DyNAmo cDNA synthesis kit (Thermo Scientific, F-470L) and 500 ng of total RNA.

Real time PCR amplification was performed with 10 time diluted cDNA or 250 ng gDNA, Fast SYBR Green Master Mix (Thermo Scientific, 4385612) and primers specific for EPO (ATATCACCGTCCCAGACACC and CAGGACAGCTTCTGAGAGCA), IGF (TCACAGGGATGCCAAGAT and GTCAACATGAGCGCACC), GeneSwitch (AGCATGCGATATTTGCCGAC and AGAGTAGCGACACTCCCAGT), AAT (AGGCCAACTTGTCTACGTTTAGTATG and CAGCGTCCTGTGTCCAAGGT), beta-Actin (ACGGCCAGGTCATCACTATTG and CAAGAAGGAAGGCTGGAAAAGA) and/or GAPDH (TCCACCCATGGCAAATTCC and GGGATTTCCATTGATGACAAGCT). PCR reaction conditions were: 95°C for 20 sec, followed by 40 cycles of 3 sec at 95°C and 30 sec at 60°C. The assays were performed on ABI 7500 Fast (Applied Biosystems, Foster City, CA). EPO and IGF mRNA expression levels were normalized to GAPDH or beta-Actin and the relative gene expression $2^{-DeltaDeltaCt}$ method was used for analysis of PCR data. AAV5 titers were determined using a standard curve, made with plasmid containing the AAT-promoter and EPO coding sequence.

SDS-PAGE, transfer and western blot

Cells were washed in PBS and lysed in 1x NuPAGE LDS Sample Buffer (Life Technologies). NuPAGE Reducing Agent was added to the samples prior to heating at 95C. Proteins were separated on a NuPAGE Novex Tris-bis, 4-12% gel in a Biorad system with MOPS SDS Running buffer (Life Technologies). To transfer proteins from the gel onto Immun-Blot PVDF Membrane (Biorad) a wet blotting system (Biorad) was used with NuPAGE transfer buffer containing 10% methanol. The membrane was blocked with 5% semiskimmed milk (Sigma), 0,1% Tween-20 (Calbiochem) in PBS (Gibco). This was followed by incubation with the primary antibody against NF-kappaB p65 (abcam ab7970) in blocking buffer. After washing the membrane, the antibody swine-anti-rabbit with HRP conjugate (Dako) was added. Subsequent to washing the membrane, HRP was visualized by ECL Lumilight plus (Roche) and the signal was captured with the ImageQuant LAS4000 (GE Healthcare). Quantification of the protein bands in the images was done with ImageJ Fiji.

AAV5 vector production

AAV5 vectors used in this study were produced by a baculovirus-based AAV production system. Briefly, the expression cassettes of interest were cloned into a uniQure transfer plasmid in order to generate an entry plasmid. The presence of the two inverted terminal repeats (ITRs) was confirmed. The ITR-expression cassette was inserted in a recombinant baculovirus vector by homologous recombination in Sf9 cells and clones were selected by plaque purification. The recombinant baculoviruses containing the ITR-expression cassette

were further amplified and screened for the best production and stability by PCR and qPCR. To generate AAV5, cells were infected with recombinant baculoviruses expressing the ITRs-expression cassette, the replicon enzyme and the capsid protein. The cells were lysed and crude lysate was treated with Benzonase (50U/ml) (Merck, Darmstadt, Germany) for 1 hour at 37 °C. AAV5 was purified on an AVB Sepharose column (GE Healthcare, Little Chalfont, UK) using an AKTA purification system (GE Healthcare) and the final concentration was determined by quantitative PCR.

In vivo

C57BL6 mice were maintained under a 12-hour light: 12-hour dark cycle in a clean facility with free access to food and water. Experiments were performed with the approval of the Animal Ethics Committee (DEC) in the Netherlands. Three-month-old animals were intravenously injected with AAV5; EPO expressing viruses at 1e12 and IGF expressing viruses at 1e13 vector genome copies per animal. Four weeks after, mice injected with AAV5-GS-IGF were treated with 20mg/kg MFP three days in a row, except for the non-induced group of mice. In the experiment concerning EPO expression, four- and eight-weeks post-transduction several groups of mice were injected intraperitoneally with 20mg/kg MFP for four consecutive days. Blood was taken at the indicated days of the experiment; in general before transduction, before and after induction with MFP. All blood samples were collected in tubes with heparin and after centrifugation at 1500rpm for 15min plasma was stored at -80C and used for ELISA or MFP measurement at a later stage. Hematocrit was analyzed in a HemoCue 201+ (HemoCue AB, Ängelholm, Sweden) with a drop of blood immediately collected on a microcuvette. When the animals were sacrificed their liver was dissected.

MFP quantification

MFP was quantified at Eurofins | PROXY Laboratories the Netherlands according to company's SOPs. In brief, after addition of internal standard D3-Mifepristone, MFP was extracted from 50ul of plasma or approximately 10 mg of liver tissue. The MFP standard curve was prepared in the appropriate matrix. Chromatographic separation of the samples was performed on a UPLC (Ultra Performance Liquid Chromatography) column, followed by positive electrospray ionization at QTOF-MS (Quadrupole Time of Flight-Mass Spectrometry). Then MFP concentrations were calculated from the recorded chromatograms.

Statistical Analysis

Data were analyzed using either the one-way ANOVA, two-way ANOVA or Student's t-test with a predefined significance level of α=0.05 to determine statistically significances between two groups. The p values are represented by the following number of asterisks:

*p < 0.05; **p < 0.01; ***p < 0.001; ****p < 0.0001. Table S1 shows the full statistical analysis for the one-way ANOVA and two-way ANOVA.

Acknowledgements

We'd like to thank Richard van Logtenstein, Cynthia Brouwers and Stephan Pouw for their technical support during the animal experiments. Kimberley Pietersz and Jolanda Snapper are appreciated for their help in acquiring several of the research tools.

The authors declare no conflict of interest. The researchers are or were employed by uniQure N.V. and the research project was partly funded by the European grant Eurostar project E!7900: ESTAR13113 Regulated gene expression for Huntington's disease therapy.

Author contributions

Conceptualization: H.P., P.K and J.M.L. Investigation: J.M.L., R.M., T.Z., S.K. and A.H. Recourses: J.Lu. and B.B. Supervision, formal analysis, visualization and writing - initial draft: J.M.L. Project Administration and Writing – review and editing: P.K. and H.P. Funding acquisition: P.K.

References

1. Boudes, PF (2014). Gene therapy as a new treatment option for inherited monogenic diseases. *Eur. J. Intern. Med.* 25: 31–36.
2. Dunbar, CE, High, KA, Joung, JK, Kohn, DB, Ozawa, K and Sadelain, M (2018). Gene therapy comes of age. *Science (80-.).* 359: eaan4672.
3. Chtarto, A, Humbert-Claude, M, Bockstael, O, Das, AT, Boutry, S, Breger, LS, *et al.* (2016). A regulatable AAV vector mediating GDNF biological effects at clinically-approved sub-antimicrobial doxycycline doses. *Mol. Ther. - Methods Clin. Dev.* 3: 16027.
4. Guiner, C, Stieger, K, Snyder, R, Rolling, F and Moullier, P (2007). Immune Responses to Gene Product of Inducible Promoters. *Curr. Gene Ther.* 7: 334–346.
5. Wang, Y, Xu, J, Pierson, T, O'Malley, BW and Tsai, SY (1997). Positive and negative regulation of gene expression in eukaryotic cells with an inducible transcriptional regulator. *Gene Ther.* doi:10.1038/sj.gt.3300402.
6. Vegeto, E, Allan, GF, Schrader, WT, Tsai, MJ, McDonnell, DP and O'Malley, BW (1992). The mechanism of RU486 antagonism is dependent on the conformation of the carboxy-terminal tail of the human progesterone receptor. *Cell*doi:10.1016/0092-8674(92)90234-4.
7. Marmorstein, R, Carey, M, Ptashne, M and Harrison, SC (1992). DNA recognition by GAL4: structure of a protein-DNA complex. *Nature*doi:10.1038/356408a0.
8. Raaijmakers, HCA, Versteegh, JE and Ultdehaag, JCM (2009). The X-ray structure of RU486 bound to the progesterone receptor in a destabilized agonistic conformation. *J. Biol. Chem.*doi:10.1074/jbc.M109.007872.
9. Maddalena, A, Tereshchenko, J, Bähr, M and Kügler, S (2013). Adeno-associated virus-mediated, mifepristone-regulated transgene expression in the brain. *Mol. Ther. - Nucleic Acids* 2: e106.
10. Tereshchenko, J, Maddalena, A, Bähr, M and Kügler, S (2014). Pharmacologically controlled, discontinuous GDNF gene therapy restores motor function in a rat model of Parkinson's disease. *Neurobiol. Dis.* 65: 35–42.
11. Cheng, S, Tereshchenko, J, Zimmer, V, Vachey, G, Pythoud, C, Rey, M, *et al.* (2018). Therapeutic efficacy of regulable GDNF expression for Huntington's and Parkinson's disease by a high-induction, background-free "GeneSwitch" vector. *Exp. Neurol.* 309: 79–90.
12. Szymanski, P, Kretschmer, PJ, Bauzon, M, Jin, F, Qian, HS, Rubanyi, GM, *et al.* (2007). Development and validation of a robust and versatile one-plasmid regulated gene expression system. *Mol. Ther.* 15: 1340–1347.
13. Weeratna, RD, Wu, T, Efler, SM, Zhang, L and Davis, HL (2001). Designing gene therapy vectors: Avoiding immune responses by using tissue-specific promoters. *Gene Ther.* 8: 1872–1878.
14. De Geest, BR, Van Linthout, SA and Collen, D (2003). Humoral immune response in mice against a circulating antigen induced by adenoviral transfer is strictly dependent on expression in antigen-presenting cells. *Blood* 101: 2551–2556.
15. Heikinheimo, O, Pesonen, U, Huupponen, R, Koulu, M and Lähteenmäki, P (1994). Hepatic metabolism and distribution of mifepristone and its metabolites in rats. *Hum. Reprod.* 9: 40–46.
16. Oskari, H, Kimmo, K, Horacio, C, Irving, S, Tapani, L and Pekka, L (1987). Plasma concentrations and receptor binding of RU 486 and its metabolites in humans. *J. Steroid Biochem.* 26: 279–284.
17. Shi, Y en, Ye, Z hou, He, C hai, Zhang, G qing, Xu, J qiu, Van Look, PFA, *et al.* (1993). Pharmacokinetic study of RU 486 and its metabolites after oral administration of single doses to pregnant and non-pregnant women. *Contraception* 48: 133–149.
18. Guler, HP, Zapf, J, Schmid, C and Froesch, ER (1989). Insulin-like growth factors I and II in healthy man. Estimations of half-lives and production rates. *Acta Endocrinol. (Copenh).* 121: 753–758.

19. Heikinheimo, O (1997). Clinical pharmacokinetics of mifepristone. *Clin. Pharmacokinet.* 33: 7–17.
20. Harkins, RN, Szymanski, P, Petry, H, Brooks, A, Qian, HS, Schaefer, C, *et al.* (2008). Regulated expression of the interferon-β gene in mice. *Gene Ther.* 15: 1–11.
21. Wang, L, Hernández-Alcoceba, R, Shankar, V, Zabala, M, Kochanek, S, Sangro, B, *et al.* (2004). Prolonged and Inducible Transgene Expression in the Liver Using Gutless Adenovirus: A Potential Therapy for Liver Cancer. *Gastroenterology* 126: 278–289.
22. Nordstrom, JL (2003). The antiprogestin-dependent GeneSwitch® system for regulated gene therapy. *Steroids* 68: pp 1085–1094.
23. Vanrell, L, Di Scala, M, Blanco, L, Otano, I, Gil-Farina, I, Baldim, V, *et al.* (2011). Development of a liver-specific tet-on inducible system for AAV vectors and its application in the treatment of liver cancer. *Mol. Ther.* 19: 1245–1253.
24. Bohl, D, Salvetti, A, Moullier, P and Heard, JM (1998). Control of erythropoietin delivery by doxycycline in mice after intramuscular injection of adeno-associated vector. *Blood* 92: 1512–7.
25. Ye, X, Rivera, VM, Zoltick, P, Cerasoli, F, Schnell, MA, Gao, GP, *et al.* (1999). Regulated delivery of therapeutic proteins after in vivo somatic cell gene transfer. *Science (80-.).* 283: 88–91.
26. Rivera, VM, Gao, GP, Grant, RL, Schnell, MA, Zoltick, PW, Rozamus, LW, *et al.* (2005). Long-term pharmacologically regulated expression of erythropoietin in primates following AAV-mediated gene transfer. *Blood* 105: 1424–1430.
27. Xu, ZL, Mizuguchi, H, Mayumi, T and Hayakawa, T (2003). Regulated gene expression from adenovirus vectors: A systematic comparison of various inducible systems. *Gene* 309: 145–151.
28. Howland, RH (2013). A "Glucose Eater" Drug as a Therapeutic Agent in Psychiatry. *J. Psychosoc. Nurs. Ment. Health Serv.* 51: 13–16.
29. Block, T, Petrides, G, Kushner, H, Kalin, N, Belanoff, J and Schatzberg, A (2017). Mifepristone Plasma Level and Glucocorticoid Receptor Antagonism Associated with Response in Patients with Psychotic Depression. *J. Clin. Psychopharmacol.* 37: 505–511.
30. Gallagher, P, Watson, S, Elizabeth Dye, C, Young, AH and Nicol Ferrier, I (2008). Persistent effects of mifepristone (RU-486) on cortisol levels in bipolar disorder and schizophrenia. *J. Psychiatr. Res.* 42: 1037–1041.
31. Watson, S, Gallagher, P, Porter, RJ, Smith, MS, Herron, LJ, Bulmer, S, *et al.* (2012). A randomized trial to examine the effect of mifepristone on neuropsychological performance and mood in patients with bipolar depression. *Biol. Psychiatry* 72: 943–949.
32. Oligino, T, Poliani, PL, Wang, Y, Tsai, SY, O'Malley, BW, Fink, DJ, *et al.* (1998). Drug inducible transgene expression in brain using a herpes simplex virus vector. *Gene Ther.* 5: 491–496.
33. Meikle, L, Pollizzi, K, Egnor, A, Kramvis, I, Lane, H, Sahin, M, *et al.* (2008). Response of a Neuronal Model of Tuberous Sclerosis to Mammalian Target of Rapamycin (mTOR) Inhibitors: Effects on mTORC1 and Akt Signaling Lead to Improved Survival and Function. *J. Neurosci.* 28: 5422–5432.
34. Yim, CW, Flynn, NM and Fitzgerald, FT (1985). Penetration of oral doxycycline into the cerebrospinal fluid of patients with latent or neurosyphilis. *Antimicrob. Agents Chemother.* 28: 347–348.
35. Dong, A, Hu, J, Zhao, L, Xu, H and Liu, X (2007). Regulation and pharmacokinetics of inducible recombinant TRAIL expression. *Cancer Biol. Ther.* 6: 1978–1985.
36. Baruteau, J, Waddington, SN, Alexander, IE and Gissen, P (2017). Gene therapy for monogenic liver diseases: clinical successes, current challenges and future prospects. *J. Inherit. Metab. Dis.* doi:10.1007/s10545-017-0053-3.
37. Kattenhorn, LM, Tipper, CH, Stoica, L, Geraghty, DS, Wright, TL, Clark, KR, *et al.* (2016). Adeno-Associated Virus Gene Therapy for Liver Disease. *Hum. Gene Ther.* doi:10.1089/hum.2016.160.
38. Salido, E, Rodriguez-Pena, M, Santana, A, Beattie, SG, Petry, H and Torres, A (2011).

Phenotypic correction of a mouse model for primary hyperoxaluria with adeno-associated virus gene transfer. *Mol. Ther.* 19: 870–875.

Supplemental data

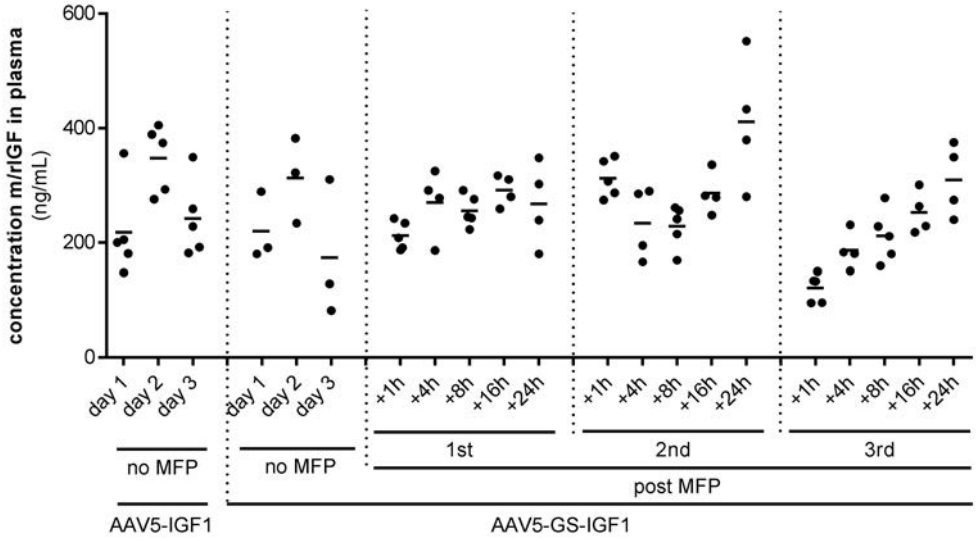

Supplemental figure 1. ***In vivo*** **expression of IGF protein after MFP induction in murine liver by the single-vector GeneSwitch system.** Mice were transduced with AAV5 expressing rat IGF constitutively (AAV5-IGF) or regulated through the GeneSwitch system (AAV5-GS-IGF). Four weeks later, MFP was given three consecutive days (1st, 2nd, 3rd) and blood was taken at the indicated hours after each injection (+1h, +4h, etc). One group of the AAV5-GS-IGF injected mice and the AAV5-IGF1 group did not receive MFP (no MFP), from them blood was collected at a convenient time on day 1, 2 and 3 when the other groups received MFP. The IGF plasma concentrations were determined by ELISA against mouse and rat IGF.

Supplemental Table 1. Statistical analysis using either the one-way or two-way ANOVA. Statistical analysis was performed using Graphpad Prism 8.0.0.

Figure	Test	Alpha	Source of Variation	% of total variation	P value	P value summary	F (DFn, DFd)
4b	Two-way ANOVA, Dunnett's multiple comparisons test	0.05	Interaction:	11.36	0.0671	ns	F (9, 40) = 1,984
			Time:	9.693	0.0045	**	F (3, 40) = 5.076
			MFP treatment	49.33	<0.0001	****	F (3, 40) = 25.83
4c	Two-way ANOVA, Dunnett's multiple comparisons test	0.05	Interaction	14,86	<0,0001	****	Yes
			Time	37,92	<0,0001	****	Yes
			MFP treatment	47,17	<0,0001	****	Yes
7c	One-way ANOVA	0.05	NA	NA	0.0246	*	F (5, 19) = 3,347
7d	One-way ANOVA	0.05	NA	NA	0,0019	**	F (5, 19) = 5,907
8e	Two-way ANOVA, Bonferroni's multiple comparisons test	0.05	Interaction	5,688	0,0098	**	Yes
			MFP treatment	0,7851	0,1548	ns	No
			AAV5 vector	74,25	<0,0001	****	Yes

Chapter 7

General discussion and future perspectives

Main findings of this thesis

In this thesis we demonstrated the development and characterization of miRNA-based gene therapies for two common neurogenerative diseases, ALS and SCA3, each with a different pathology. We used the novel miQURE™ silencing technology developed by uniQure to design several therapeutic miRNAs to target different regions in *C9orf72* and *ATXN3* gene. The miRNAs were incorporated in AAV5 and evaluated for efficacy and safety using several *in vitro* and *in vivo* model systems. The main goal was to reduce the gain of toxicity caused by mutations in these genes. In addition, we studied two key aspect for a successful gene therapy which is the route of delivery to reach the affected cells in the CNS and regulation of transgene expression using an inducible system.

Therapeutic approaches for *C9orf72*-ALS/FTD: unanswered questions and the road ahead

Targeting *C9orf72* RNA

An efficient way to reduce the negative effects caused by both the repeat-containing transcripts and DPR proteins is by therapeutically targeting the RNA transcripts containing the mutation. The two most common approaches that have been extensively studied in preclinical studies are based on RNAi and ASOs. Several targeting methods have been tested herein and each have their own advantages and disadvantages. Targeting the coding region of the *C9orf72* gene is highly efficient and specific and we confirmed with RNAseq data (chapter 1) that the exons are well conserved between patients. However, this approach would further reduce *C9orf72* expression in patients. Targeting the G_4C_2 repeat directly would spare the "healthy" transcripts but the probability to bind to off-target genes is high, as GC rich sequences are widespread within the human genome. In addition, sequence variations have been found between patients in the region around the repeat and screening of patients may be required if non-conserved regions are targeted.[1] The presence of sense and antisense transcripts adds to the complexity and two products would be needed to target both strands. Thus, an important unanswered question remains what the roles of the sense versus the antisense strand of *C9orf72* are, and what is their individual contribution to the disease pathology.

Liu et al reported on a C9BAC mouse model for *C9orf72* ALS/FTD with decreased survival, paralysis, muscle denervation, motor neuron loss, anxiety-like behavior, and cortical and hippocampal neurodegeneration.[2] Interestingly, they reported that antisense transcripts were upregulated in these mice and mainly expressed in regions that tend to degenerate such as in spinal interneurons. The authors suggested that the antisense transcripts and/or the corresponding antisense DPR proteins may be critical drivers of the disease.[2] Attempts to determine expression of the sense and antisense transcripts in patient-derived iPSC-neurons and brain tissue have yielded controversial data, with some studies reporting a trend towards upregulated antisense transcripts or its corresponding

DPRs, while others observed more sense transcript products.[2–6] Some data suggest that targeting only one of the two strands could potentially rescue G_4C_2 repeat-related cellular defects. ASOs targeting the repeat-containing sense transcripts significantly reduced the accumulation of sense RNA foci and its DPR proteins in a C9BAC mouse model.[7] In addition, the development of behavioral deficits was also significantly attenuated.[8] Consistently, mislocalization of proteins was rescued in motor neurons treated with ASOs against either the sense or antisense transcripts (Hayes et al, unpublished results presented at AAN2018). Thus, it seems that targeting either the sense or antisense transcripts of *C9orf72*, may reduce motor neuron toxicity in ALS. These findings suggest that accumulation of both sense and antisense repeat-containing transcripts could have a combined threshold at which they become toxic. Reducing either one of these strands could sufficiently decrease the threshold at which they become toxic. We demonstrated in chapters 1 and 2 the design of miRNAs to target the sense and/or antisense transcripts of *C9orf72*. Two candidates that are targeting coding regions for a total knockdown of *C9orf72* were selected for a proof of concept *in vivo* study. A total knockdown approach was preferred in this study because currently the repeat-containing transcripts are poorly characterized, and little is known about their sequence conservation among patients. We demonstrated significant reduction of *C9orf72* and its repeat-containing sense transcripts and sense RNA foci in a C9BAC mouse model. Thus, despite that the antisense transcripts were not targeted, targeting coding regions can contribute in reduction of the toxicity threshold.

Another aspect to consider is the tolerability of *C9orf72* silencing. *C9orf72* expression is already reduced in patients due to repressive epigenetic marks, such as DNA hypermethylation within CpG islands in the G_4C_2 repeat. Therefore, it is arguable whether further reduction of *C9orf72* is safe for the patients. RNAi or ASOs can be designed to selectively target the mutant allele or to target both healthy and mutant allele. An allele specific targeting approach is theoretically attractive, but difficult to implement, as the therapeutic molecule should bind to the poorly conserved GC sequences. On the other hand, a total silencing approach can be highly specific, but will result in further reduction of the *C9orf72* protein in patients.

There is currently no *in vivo* evidence to link *C9orf72* reduction to the pathology seen in patients. Complete reduction of *C9orf72* in mice was not linked to neurodegeneration but these mice developed immune-related problems, most likely due to *C9orf72* depletion in the peripheral organs.[9] Heterozygous mice with 50% less *C9orf72* expression compared to wildtype mice are healthy. Notably, reduction of *C9orf72* levels due to DNA hypermethylation of the G_4C_2 repeat seems to occur in at least ~30% patients and this has been reported to have neuroprotective properties due the decrease of repeat-containing *C9orf72* transcripts.[10–14] This suggests that therapeutic silencing of *C9orf72* transcription may have neuroprotective benefits in patients. Taken together, we believe that both selective and non-selective approaches with either RNAi or ASOs could have the potential to modify the course of the disease as long as the G_4C_2 repeat-containing transcripts

are being reduced. Both approaches would not only target the RNA-mediated toxicity but will also reduce DPRs as less transcripts are available to undergo RAN translation. The advantage of our AAV-based miRNA approach is that a single administration would be enough for a long-lived silencing of *C9orf72* without the need for re-administration. Currently, a phase I clinical trial run by Biogen and IONIS is ongoing using ASOs targeting only the sense transcript. The outcome of this study could provide better understanding whether targeting only one of the toxic strands is indeed beneficial to the patients.

Targeting DPRs

The repeat-containing transcripts of *C9orf72* are translated into five DPR proteins through an unconventional translation, known as RAN translation.[15–21] DPR proteins are considered typical pathological hallmark in *C9orf72*-ALS/FTD patients and form cytoplasmic aggregates.[22,23] While most current therapeutic strategies are targeting the RNA, it is assumable that targeting RAN translation or DPRs directly could also lower the toxicity threshold of the *C9orf72* expansion.

Although our understanding on the occurrence of RAN translation from the *C9orf72* repeat-containing transcripts is poor, some crucial evidence were found suggesting that they follow a canonical mechanism of translation.[24] Canonical translation of mRNAs requires several complex processes and recruitment of numerous eukaryotic initiation factors. These factors can form complex with the 40S ribosomal subunit, which subsequently binds to the 5′ cap of a mRNA to start scanning for a start codon. The translation regulation in eukaryotes almost always initiates at a methionine (AUG) start codon that once recognized by the 40S ribosomal subunit is decoded by the methionyl-tRNA.[25] The production of DPR proteins from the G_4C_2 repeat-containing transcripts also requires a 5′ cap insertion and follow a 5′ to 3′ canonical scanning mechanism to start translation at a near-cognate CUG codon.[24] Interestingly, it was demonstrated that ASOs targeting the region immediately upstream of the repeats can block the ribosomal scanning and prevent RAN translation, resulting in efficient reduction of DPR proteins without inducing RNAse-H-dependent RNA degradation.[24] Thus, blocking the ribosomal scanning mechanism could be considered a therapeutic intervention. The advantage of this approach is that the healthy *C9orf72* transcripts are not affected. However, the specificity and therapeutic efficacy was not addressed in this study.

Another promising method to achieve reduction of DPR protein is by immunotherapy. For example, Anti-GA antibodies showed efficient reduction of poly-GA DPR protein levels and prevented aggregate formation in cell lines over-expressing DPR proteins.[26] Currently, Neurimmune in collaboration with three other research institutes (University of Florida, University of Zurich and Massachusetts General Hospital) won the target discovery and development funding for the development immunotherapies targeting DPR proteins in ALS and FTD. Preliminary data was presented during the 2019 Gordon Research Conference on CAG Triplet Repeat Disorders, showing that targeting only the poly-GA

from all 5 DPR proteins is sufficient to improve gait and cage behavior and increase survival in the progressive C9BAC ALS mouse model (Ranum et al, data unpublished). Their findings support our earlier mentioned hypothesis that by removing only one component from the bulk of toxic products could be enough to lower the toxicity threshold and improve symptoms. Ultimately targeting more pathways could lead in better reverse of the disease phenotype.

One advantage of our AAV-based miRNA approach is that besides targeting RNA toxicity, it is likely to also reduce DPR proteins because less transcripts will be available to undergo RAN translation. Crucial evidence for this was shown by another group using ASOs targeting either intronic or coding regions of *C9orf72*.[8] Both strategies led to a significant reduction of RNA toxicity and DPR-mediated toxicity *in vitro* and *in vivo*.

Targeting nucleocytoplasmic transport in *C9orf72*-ALS/FTD

It was recently discovered that nucleocytoplasmic transport pathways are highly affected in *C9orf72*-ALS/FTD.[27–29] For example, cytoplasmic mislocalization and aggregation of TDP-43 is observed in nearly all *C9orf72* related ALS and FTD cases and is also often seen in other ALS cases caused by other mutations. Other proteins that are less commonly found mislocalized in the cytoplasm are the RNA-binding proteins FUS and hnRNPs.[30,31] Cytoplasmic mislocalization of proteins results in depletion of these proteins in the nucleus, leading to loss of function and accumulation of cytoplasmic aggregates leads to gain of toxicity in the cytoplasm.

As disruption of nucleocytoplasmic trafficking plays a critical role in the pathogenesis of *C9orf72*-ALS/FTD, some attention has turned on strategies to restore nucleocytoplasmic trafficking function. Using a forward genetic screen of putative G_4C_2 repeat RNA-binding proteins in Drosophila, RanGAP (RanGTPase activating protein A) was found to be a major regulator of nucleocytoplasmic trafficking.[27,32] RanGAP is an nuclear pore protein that is normally localized on the cytoplasmic surface of the nuclear pore complex that stimulates the hydrolysis of RanGTPase in the cytoplasm and plays a key role in importin-mediated nuclear import of proteins. It has been found in Drosophila models and in patients derived iPSC-neurons that the G_4C_2 repeat of *C9orf72* inhibits RanGAP, leading to mislocalization of proteins to the cytoplasm.[27] Consistently, overexpression of RanGAP or a single copy of a gain of function allele of RanGAP (RanGAP[SD]) significantly suppressed neurodegeneration and rescued certain phenotypic traits due to the G_4C_2 repeat in flies.[27] Thus, RanGAP is considered an effective suppressor of the G_4C_2 repeat mediated toxicity by preventing mislocalization of proteins in the cytoplasm and is an interesting target for therapeutics.

There has been also some interest in compounds that block nuclear export to prevent cytoplasmic mislocalization of nuclear proteins. Karyopharm Therapeutics developed several selective inhibitors of nuclear export (SINE) compounds that specifically inhibit exportin-1 (XPO1) aiming to treat different types of cancer. These compounds have been

also tested in preclinical studies for several neurodegenerative diseases such as ALS and HD and showed neuroprotective features. in *C9orf72*-related ALS/FTD, the efficacies of these compounds are still unclear as increased toxicity was observed in some preclinical models, while mitigated toxicity was observed in others.[27,28,33] Interestingly, neuron survival and motor neuron function was improved in rats overexpressing TDP-43 when treated with SINE compounds.[34] The SINE compound Selinexor (KPT-330), has been tested in clinical trials for different types of cancers and some studies reported promising results.[35] Biogen has acquired KPT-350 in 2018 and is planned to initiate a phase I trial for *C9orf72*-ALS using this compound.[36] Overall, it seems that SINE compounds could have mild neuroprotective properties but several challenges remain to be solved. Completely blocking nuclear export with SINE compounds have been linked to significant neurotoxicity and finding the right balance seems challenging. In preclinical studies, these compounds were often not effective at low doses that are considered safe to humans.[34] A main advantage of our RNAi approach over SINE compounds is that no safety concerns was observed thus far in preclinical studies and multiple toxicity pathways can be targeted, increasing the probability for therapeutic efficacy.

Current advances and therapeutic strategies for SCA3: implications for AAV5-miATXN3 gene therapy

Gene silencing in SCA3

RNAi and ASOs can be designed to selectively target the mutant *ATXN3* transcripts or to non-selectively silence both mutant and healthy alleles. Both strategies have been tested in preclinical studies and resulted into successful reduction of the mutant *ATXN3* transcripts and protein. In chapter 4 we described a non-selective approach to target both healthy and mutant *ATXN3* using miRNAs delivered by AAV5. The advantage of our approach is that it is highly specific because we are targeting a well conserved coding region. Besides, our approach can treat the whole SCA3 patient population and several crucial steps has been taken to ensure minimal risk for off-target effects. Despite that our approach led to a reduction of the healthy ataxin-3 protein in mice, this was well tolerable without major alterations in gene expression. A very similar approach was performed by Rodríguez-Lebrón et al.[37] Their strategy was to silence mutant *ATXN3* expression using miRNA mimics designed to target the 3'UTR region of human *ATXN3*. The lead miRNA mimic was tested *in vivo* by delivery in the DCN using rAAV1. They demonstrated clearance of mutant ataxin-3 from neuronal nuclei and improved phenotype in the cerebellum of a SCA3/MJD84.2 transgenic mice expressing the full human *ATXN3* disease gene. Rodríguez-Lebrón et al also hypothesized that targeting the 3'UTR of *ATXN3* could be more efficient because this region could be more accessible for the RNAi machinery due to limited translational activity in this region of the transcript. They further argued that targeting the 3'UTR of *ATXN3* would guide AGO2-mediated cleavage of

most *ATXN3* isoforms leading to a robust reduction in ataxin-3 levels. We have shown that targeting coding regions using artificial miRNA can achieve similar silencing efficacy, thus both the coding region and the 3'-UTR can be effective targets. More importantly, we believe that a proper miRNA design would ensure targeting of all transcript isoform. One important question remains whether the silencing specificity is the same when targeting 3'UTRs or coding regions of mRNAs. Interestingly, one study investigated this using siRNA with introduced mismatches to target 3'UTR and coding regions of reporter genes.[38] it was found that the silencing activity of siRNA on mismatched sites was universally much higher in the 3'-UTR compared to the silencing in mismatched coding region. On perfectly-matches sites, the potency was only slightly better in the 3'-UTR. They further tested the effect on AGO2 ablation on the silencing activity of siRNA on matched and mismatched sites placed in the 3'-UTR and coding regions. The absence of AGO2 resulted in only a slight decrease in silencing potency of siRNA targeting both matched and mismatched sites in the 3'-UTR. In contrast, the activity of siRNAs targeting matched and mismatches sites of coding regions were greatly diminished in AGO2 knock-down cells. Thus, clearly suggesting the existence of an AGO2 independent translational repression activity in the 3'-UTR. Another aspect to consider is that sequence variation in 3'-UTRs between patients is common.[39] Taken together, these finding may implicate that targeting 3'UTR is less specific and although this approach still seems promising in the study of Rodríguez-Lebrón et al., it may be less suitable in allele-specific RNAi approaches to discriminate SNPs from wildtype alleles. Nevertheless, targeting 3'UTRs could be useful to facilitate the design of RNAi approaches that would target multiple genes in a large gene family.

Non-allele-specific targeting of *ATXN3* using ASOs also proofed promising in different preclinical studies.[40] A study conducted by Alves et al. showed that silencing wildtype *ATXN3* do not increase SCA3/MJD pathology, and silencing both wildtype and mutant allele mitigated neuropathology in a rat model of SCA3/MJD.[41] All together the studies performed by us and others strongly suggest that an non-allele-specific therapy is probably safe and as effective as allele-specific approaches to treat SCA3/MJD. Ataxin-3 is a deubiquitinating enzyme and other deubiquitinating enzymes might compensate for the loss of normal ataxin-3 function.[42]

The RNAi approach investigated by us rely on delivery to the CNS using viral vectors. Conceiçao et al investigated the delivery of siRNA targeting the mutant *ATXN3* allele using nucleic acid lipid particles (SNALPs) aiming to a systemic administration. They demonstrated that intravenous administration of SNALPs can successfully cross the BBB and reduce mutant ataxin-3 levels, resulting in alleviation of motor performance defects and improved striatal and cerebellar-associated neuropathology in a lentiviral SCA3 mouse model. This RNAi-delivery strategy is less invasive and overcomes the main disadvantages of other non-viral approaches, such as electrostatic interaction leading to inflammatory toxicity. One major concern of this approach is that *ATXN3*-lowering is not restricted to the CNS. In fact, they found high siRNA expression in the brain, heart, lungs, liver, spleen

and kidney. Thus, expression of gene silencing molecules in these organs and their off-target effects should be carefully investigated. Allele specific silencing of mutant *ATXN3* has been widely studied by different other groups. For example, siRNA targeting SNPs resulted in silencing of only the mutant *ATXN3* and not the wildtype *ATXN3*.[43] Similar results was obtained with shRNAs targeting SNPs.[44,45] Evers et al demonstrated that ASO-mediated exon skipping targeting exon 9 and 10 of *ATXN3* can also efficiently reduce the mutant *ATXN3* while maintaining normal *ATXN3* function.[46]

Notably, despite the extensive preclinical studies on *ATXN3* gene silencing for nearly 2 decades, none of these studies have reached clinical trial yet. This is expected to change in the coming years as more gene silencing approaches for other neurodegenerative diseases is entering human trials and the safety concerns of these therapeutic approaches are being tackled. Our RNAi approach for SCA3 have been designed based on several years of experience gained by the HD program that is currently moving to clinical trial. The strong lowering of mutant *ATNX3* observed in cell and mouse model increases our confidence to continue investigating this program for clinical applications.

Clearance of mutant ataxin-3 by inducing autophagy

The autophagy and the ubiquitin–proteasome system (UPS) are crucial for the degradation of misfolded, oligomerized, and aggregated mutant proteins in cells. Therefore, enhancing autophagy using therapeutic compounds or by long term fasting is proposed to have beneficial effects. In SCA3 patients, autophagy dysfunction is regarded to be one of the mechanisms involved in the SCA3 phenotype and reversing this dysfunction could be therapeutically relevant.[47,48] A common classical method to induce autophagy in mammalian cells is by inhibition of the mammalian target of rapamycin (mTOR) pathway. This can be achieved by administration of rapamycin, a macrolide compound known to cross the BBB and a well-known inducer of autophagy.[49] Indeed, preclinical studies in SCA3 cell models and in SCA3 transgenic mice showed that rapamycin and a rapamycin ester can induce clearance of mutant ataxin-3 and reduce its toxicity.[50,51] Several compounds to induce autophagy in a mTOR-independent manner have also been tested in SCA3 models, some showing clearance of mutant ataxin-3 and others showing only limited effect.[52–58] Thus, it seems uncertain whether induction of autophagy could reduce toxic mutant ataxin-3 to therapeutically relevant levels. The advantage is that most of these compounds can be administered orally without complicated delivery methods. However, it is important to bear in mind that autophagy dysfunction is only one aspect of the disease within the bulk of cellular disturbances that was described earlier in chapter 1. Other dysfunctional pathways that are caused for instance by RNA toxicity is not being targeted. Thus, whether enhancing autophagy alone is sufficient to modify the course of the disease in patients is yet to be discovered in clinical trials. Alternatively, combination therapies to rescue normal function of multiple dysfunction pathways in SCA3 could be more potent.

Clearance of mutant ataxin-3 by targeting proteolytic cleavage

Ataxin-3 can be cleaved by proteolytic enzymes such as caspases and calcium-dependent calpains, yielding short ataxin-3 fragments containing the polyQ stretch. These short ataxin-3 fragments have increased toxicity profile and are prone to accumulate nuclear aggregates as they lack the N-terminal nuclear export signal (NES).[59–64] inhibition of proteolytic cleavage have been proposed to reduce the formation of the toxic ataxin-3 short fragments and could potentially have therapeutic benefit for treatment of SCA3 patients. Indeed several inhibitors of caspases and calpains have been tested in preclinical models for SCA3 and showed attenuation of the short ataxin-3 fragments, reduced levels of nuclear ataxin-3 levels and reduction of its aggregates.[48,60–62,65,66] In a lentiviral SCA3 mouse model of SCA3/MJD, inhibition of calpain resulted in improvement of neuropathology and alleviation of motor deficits.[66] Thus, inhibition of proteolytic enzymes could potentially be considered as a therapeutic intervention. However, the side effects due to inhibition of caspases and calpains should be carefully investigated as these enzymes play key roles in several crucial cellular processes including apoptosis, synaptic plasticity, dendritic development, and learning ability.[48,63,67,68] Thus, inhibition of their normal functions is less favorable. An alternative approach that are currently being investigated is removal and/or modification of cleavage sites for caspases and calpains on mutant ataxin-3. This approach could be safer because it does not interfere with the activity of proteolytic enzymes.

7.4 Safety and delivery of RNAi gene therapy in ALS and SCA3 patients

The use of AAV vectors as transgene delivery has become one of the safest and most reliable method to obtain sustained expression of a therapeutic transgene. Non-viral delivery methods using nanoparticles or ASOs can also deliver therapeutic agents but the need for recurrent injections can become overwhelming and increase the risk for infections in patients. Nevertheless, ASOs have shown to be efficient and safe in animal models and have led to the initiation of several clinical trials for SOD1-ALS, *C9orf72*-ALS and SMN2 for SMA.[69–71]

The delivery of RNAi to the affected cells in ALS and SCA3 patients is currently a challenge that is still not completely answered in this thesis. We demonstrated the potential of different routes of administration for AAV5 in rodent models and studies in larger animal models is still required to see how our findings in rodent models translate to larger animal models. Several studies have implicated that the utility of AAV vectors for gene transfer is mainly determined by the capsid. We believe that this statement is partly true as the capsid is involved in several key cell entry steps. However, in chapter 5 we also showed crucial evidence that the route of administration is equally important as capsids behave differently upon different administration routes due to different

microenvironments. For example, we demonstrated that intraparenchymal injection of AAV5 resulted in high transduction of the rat brain. This finding was later confirmed by us in a transgenic minipig model showing successful transduction at the injection site (striatum) and its surrounding area.[72] In addition, both anterograde (e.g., to caudate) and retrograde (to cortex) AAV5 viral transport was observed, suggesting that the vector can travel along axons and transduce distance areas. While this route is promising for diseases with a more localized pathology, such as HD, it is unlikely to be sufficient in multifocal neurological pathologies such as in ALS because anterograde and retrograde transport to cerebellum, brain stem and spinal cord was not observed. Intrathecal administration led to a more even distribution of the vector within the CNS and is potentially more relevant in ALS and potentially also SCA3. The feasibility to deliver therapeutically relevant dose still needs to be addressed in larger animal models. Another crucial aspect for AAV delivered RNAi is safety. Especially, due to the irreversible nature of current gene therapies, evaluation of short term and long-term toxicity is critical. Other crucial parameters that needs to be addressed during preclinical studies are prediction of on- and off-target effects, immunogenicity, dose finding, timing of treatment and the ability to modulate gene expression.

Prediction of safety, on- and off-target effect

The most important aspects for drug development are safety and tolerability in patients. In the case of RNAi-based gene therapies, both RNAi and the delivery vector could lead to toxicity. Several clinical studies have demonstrated that administration of AAV in human CNS is safe, but immune responses should still be investigated during preclinical and clinical studies. The RNAi products that are delivered could induce on- and off-target effects. Prediction of these unwanted side effects can be evaluated early in preclinical studies using the currently available tools such as iPSC-technology, animal models and bioinformatics to increase safety and tolerability in patients.

Timing of treatment

The success of RNAi based gene therapy is likely to be determined by the timing. Most of the adult onset neurodegenerative diseases have a pre-symptomatic stage and it may take several years to gradually progress into a severe state with progressive neuronal death. While neuronal death cannot be reversed, emerging evidence suggests that neurons in atrophic state can regenerated their normal functions.[73] Thus, early treatment before neuron death occur is likely to provide better protection and could decelerate neuronal death. Currently all gene therapy clinical trials are performed during the manifest state in patient while treatment during pre-manifest could be more beneficial. With the current knowledge and technologies, neurodegenerative diseases with a family history can be diagnosed prenatal or later in life during the pre-symptomatic phase using genetic screening. The discovery and characterization of more clinically validated biomarkers that

correlate with disease progression will also contribute to early diagnosis of both familial and sporadic neurodegenerative diseases. Biomarkers that track disease progression and correlate predictably in response to a therapeutic intervention can also greatly support future clinical trials by reducing the duration of the studies and number of patients that need to be followed. This is especially important in pre-manifest subjects when no clinical measures of disease progression can be applied. Another good predictor of disease onset could be the brain volume. For example, in HD, changes in striatal and brain volume seems to occur more than 10 years prior symptom onset. [74] However due to the lack of effective treatments, diagnoses during premanifest also raises many ethical concerns and even patients at high risk to develop these diseases are fearful to do a genetic screening. Patients who test positive are currently faced with difficult decisions that can have mayor psychological and financial impacts on the patients themselves and their families. For example, a positive genetic test could have implications on the daily life of the persons, on their health insurance, on their ability to find a job and on making decisions in their lives that may affect their family.[75,76] Ultimately, a positive genetic test may have consequences on the ability of the person to get a mortgage and integrate into society.[77] This is a phenomenon known as "*genetic discrimination*" and needs further attention. The success of new therapeutics will hopefully extend to trials in premanifest carriers and could make it easier for patients at risk to make the decision to do a genetic screening.

7

Modulation of gene expression

Besides from constitutively active promotors to drive transgene expression, the ability to "turn on" expression of a therapeutic molecule when it is needed and to "turn off" its expression in case of unwanted effects would also add considerably to the safety profile of any genetic therapy. In chapter 6 we demonstrated the feasibility of the GeneSwitch inducible transgene expression system to use in combination with gene therapy. Furthermore, we optimize this system to fit into a single vector with enhanced inducibility and less leakage compared to the classical duo vector system. The incorporation of this system to regulated RNAi gene therapy would add to the safety by preventing accumulation of high RNAi concentrations that could result in a gene knockdown outside the therapeutic window or adjustments on individual basis. For example, for the ALS and SCA3, we are aiming for approximately 50% endogenous knockdown of the mRNA for in case they are still needed to maintain normal cellular processes. The GeneSwitch system would make it possible to modulate expression of our therapeutic genes. A second example is the long-term shRNA-mediated apolipoprotein B100 knockdown that resulted in a dramatic cholesterol decrease in mice associated with fat accumulation in the liver as a side effect.[78] In such cases a inducible transgene expression system would be highly desired. However, there are still room for improvement to make inducible systems suitable for clinical applications. One drawback is the basal activity of these systems in the "off-state". Especially small transgenes such as non-coding RNAs tend to be leaky when using

inducible systems and further optimizations are needed. Another aspect that needs more attention is to obtain sufficient expression of the transgene once in the on-state. Especially for CNS diseases, the inducer drug needs to efficiently cross the BBB and reach the target tissue at concentrations that are high enough for therapeutically relevant expression of the transgene. Possible immune responses to element inherent to the GeneSwitch system and side effects of the inducer drug should also be considered for clinical development. The co-development of two different products (GeneSwitch and transgene) in either a single or duo vector also add more parameters to the safety concerns of gene therapies, but these systems also offer notable advantages. Being able to modulate transgene expression will at least reduce safety concerns of the permanency expressed transgene. Thus, making further investigation and optimization of these systems highly attractive for application in gene therapy.

Future perspectives

Gene therapy holds great promise to deliver therapeutic genes to treat neurological disorders. AAV vectors are currently considered one of safest vehicles to deliver therapeutic genes to treat CNS disorders. Several serotypes are available and as the potential of gene therapy is becoming more recognized, there is emerging need for new AAV serotypes. for multi-focal neurological disorders, there is an enormous desire for new AAV vectors with improved transduction profile and better distribution in the target organs upon less invasive administration routes. Although direct administration of AAV vectors into the parenchyma is invasive, the advantages over injections into the venous system or other fluid-filled compartments are clear. Intra-parenchymal administration provides high concentration of the transgene in the target cells, high local transduction, less distribution to other organs and lower risk for immune responses or toxicities due to AAV particles or ectopic expression of the transgene. There is also much room for improvement at the transgene level. For example, generation of new tissue-specific promotors and efficient transgene design could improve efficacy in the desired cell populations and restrict unwanted transgene expression in other cell types. In chapter 1, several clinical trials on AAV-based gene therapies for CNS disorders was discusses. Although all studies showed that AAV is safe and well tolerable in the human CNS, few of these studies have been efficacious in demonstrating therapeutic outcomes. Too low transduction of the target organs could have played important role but one of the major problems is the lack of good predictive animal models for better translation of favorable preclinical outcomes to the clinic. another important aspect that are often overlooked is the potential of immune responses, both against the vector and expressed transgene, as the CNS is considered immune privileged. Recent studies have demonstrated that neutralizing antibodies against some capsids can be generated in the CNS, and transduction of antigen-presenting cells can trigger neurotoxic immune response.[79,80] Addressing these concerns early during preclinical studies could increase the success of next generation CNS gene therapy clinical

trials. Furthermore, the discovery of biomarkers for early detection of the diseases will be important to identify new patients and to better predict clinical outcome. More importantly, delivering therapies prior to onset of neurodegeneration will be key to improving efficacy of gene therapies for neurodegenerative diseases. Finally, we should also acknowledge and give credit to all the efforts ongoing using different cell and animal models to better understand the pathways leading to neurodegenerative diseases. Good understanding of the genetic factors and mechanisms involved in neurodegenerative diseases is crucial to develop new and effective therapies. A better understanding of factors leading to these diseases will also allow development of better pre-clinical models to better predict clinical success. uniQure is preparing to initiate the first ever gene therapy trial using the miQure technology with AMT-130 for the treatment of early-stage HD patients. Investigational New Drug Application (IND) has been accepted by FDA in January 2019. This trial will provide uniQure with additional knowledge and experience and a better understanding of the translation from preclinical to clinical studies. Such knowledge is critical to improve study designs for better vector and transgene design, more effective dose setting, more rational patient-selecting criteria and more directed clinical measurements. Accordingly, these lessons will be highly valuable to apply on other programs in the pipeline such as SCA3, ALS and other neurodegenerative diseases.

References

1. Nordin, A. *et al.* Sequence variations in *C9orf72* downstream of the hexanucleotide repeat region and its effect on repeat-primed PCR interpretation: a large multinational screening study. *Amyotroph. Lateral Scler. Front. Degener.* 18, 256–264 (2017).
2. Liu, Y. *et al. C9orf72* BAC Mouse Model with Motor Deficits and Neurodegenerative Features of ALS/FTD. *Neuron* 90, 521–534 (2016).
3. Wagoner, N. Van *et al.* Genome-Encoded Cytoplasmic Double-Stranded RNAs, Found in *C9orf72* ALS-FTD Brain, Provoke Propagated Neuronal Death. *BioRxiv* (2018). doi:10.1101/248328
4. Mizielinska, S. *et al. C9orf72* frontotemporal lobar degeneration is characterised by frequent neuronal sense and antisense RNA foci. *Acta Neuropathol.* (2013). doi:10.1007/s00401-013-1200-z
5. Mizielinska, S. *et al. C9orf72* repeat expansions cause neurodegeneration in Drosophila through arginine-rich proteins. *Science (80-.).* 345, 1192–1194 (2014).
6. Wen, X. *et al.* Antisense proline-arginine RAN dipeptides linked to *C9orf72*-ALS/FTD form toxic nuclear aggregates that initiate invitro and invivo neuronal death. *Neuron* (2014). doi:10.1016/j.neuron.2014.12.010
7. O'Rourke, J. G. *et al. C9orf72* BAC Transgenic Mice Display Typical Pathologic Features of ALS/FTD. *Neuron* 88, 892–901 (2015).
8. Jiang, J. *et al.* Gain of Toxicity from ALS/FTD-Linked Repeat Expansions in *C9orf72* Is Alleviated by Antisense Oligonucleotides Targeting GGGGCC-Containing RNAs. *Neuron* 90, 535–550 (2016).
9. O'Rourke, J. G. *et al. C9orf72* is required for proper macrophage and microglial function in mice. *Science (80-.).* 351, 1324–1329 (2016).
10. Belzil, V. V. *et al.* Characterization of DNA hypermethylation in the cerebellum of c9FTD/ALS patients. *Brain Res.* (2014). doi:10.1016/j.brainres.2014.02.015
11. Xi, Z. *et al.* Hypermethylation of the CpG-island near the *C9orf72* G 4 C 2 -repeat expansion in FTLD patients. *Hum. Mol. Genet.* (2014). doi:10.1093/hmg/ddu279
12. Xi, Z. *et al.* Hypermethylation of the CpG island near the G 4 C 2 repeat in ALS with a *C9orf72* expansion. *Am. J. Hum. Genet.* (2013). doi:10.1016/j.ajhg.2013.04.017
13. Liu, E. Y. *et al. C9orf72* hypermethylation protects against repeat expansion-associated pathology in ALS/FTD. *Acta Neuropathol.* 128, 525–541 (2014).
14. McMillan, C. T. *et al. C9orf72* promoter hypermethylation is neuroprotective: Neuroimaging and neuropathologic evidence. *Neurology* (2015). doi:10.1212/wnl.0000000000001495
15. Zu, T. *et al.* Non-ATG– initiated translation directed by microsatellite expansions. *Proc. Natl. Acad. Sci.* (2011). doi:10.1073/pnas.1013343108/-/DCSupplemental. www.pnas.org/cgi/doi/10.1073/pnas.1013343108
16. Cleary, J. D. & Ranum, L. P. New developments in RAN translation: insights from multiple diseases. *Current Opinion in Genetics and Development* (2017). doi:10.1016/j.gde.2017.03.006
17. Zu, T. *et al.* RAN proteins and RNA foci from antisense transcripts in *C9orf72* ALS and frontotemporal dementia. *Proc. Natl. Acad. Sci.* 110, E4968–E4977 (2013).
18. Zu, T. *et al.* RAN Translation Regulated by Muscleblind Proteins in Myotonic Dystrophy Type 2. *Neuron* (2017). doi:10.1016/j.neuron.2017.08.039
19. Mori, K. *et al.* Bidirectional transcripts of the expanded *C9orf72* hexanucleotide repeat are translated into aggregating dipeptide repeat proteins. *Acta Neuropathol.* 126, 881–893 (2013).
20. Ash, P. E. A. *et al.* Unconventional Translation of *C9orf72* GGGGCC Expansion Generates Insoluble Polypeptides Specific to c9FTD/ALS. *Neuron* 77, 639–646 (2013).
21. Gendron, T. F. *et al.* Antisense transcripts of the expanded *C9orf72* hexanucleotide repeat form nuclear RNA foci and undergo repeat-

associated non-ATG translation in c9FTD/ALS. *Acta Neuropathol.* 126, 829–844 (2013).
22. Mahoney, C. J. *et al.* Frontotemporal dementia with the *C9orf72* hexanucleotide repeat expansion: Clinical, neuroanatomical and neuropathological features. *Brain* (2012). doi:10.1093/brain/awr361
23. MacKenzie, I. R. *et al.* Dipeptide repeat protein pathology in *C9orf72* mutation cases: Clinico-pathological correlations. *Acta Neuropathol.* (2013). doi:10.1007/s00401-013-1181-y
24. Tabet, R. *et al.* CUG initiation and frameshifting enable production of dipeptide repeat proteins from ALS/FTD *C9orf72* transcripts. *Nat. Commun.* (2018). doi:10.1038/s41467-017-02643-5
25. Hinnebusch, A. G., Ivanov, I. P. & Sonenberg, N. Translational control by 5′-untranslated regions of eukaryotic mRNAs. *Science* (2016). doi:10.1126/science.aad9868
26. Zhou, Q. *et al.* Antibodies inhibit transmission and aggregation of *C9orf72* poly-GA dipeptide repeat proteins . *EMBO Mol. Med.* (2017). doi:10.15252/emmm.201607054
27. Zhang, K. *et al.* The *C9orf72* repeat expansion disrupts nucleocytoplasmic transport. *Nature* 525, 56–61 (2015).
28. Freibaum, B. D. *et al.* GGGGCC repeat expansion in *C9orf72* compromises nucleocytoplasmic transport. *Nature* 525, 129–133 (2015).
29. Jovičič, A. *et al.* Modifiers of *C9orf72* dipeptide repeat toxicity connect nucleocytoplasmic transport defects to FTD/ALS. *Nat. Neurosci.* 19, 1226–1229 (2015).
30. Kwiatkowski, T. J. *et al.* Mutations in the FUS/TLS gene on chromosome 16 cause familial amyotrophic lateral sclerosis. *Science (80-.).* (2009). doi:10.1126/science.1166066
31. Kim, H. J. *et al.* Mutations in prion-like domains in hnRNPA2B1 and hnRNPA1 cause multisystem proteinopathy and ALS. *Nature* (2013). doi:10.1038/nature11922
32. Donnelly, C. J. *et al.* RNA Toxicity from the ALS/FTD *C9orf72* Expansion Is Mitigated by Antisense Intervention. *Neuron* 80, 415–428 (2013).
33. Boeynaems, S. *et al.* Drosophila screen connects nuclear transport genes to DPR pathology in c9ALS/FTD. *Sci. Rep.* (2016). doi:10.1038/srep20877
34. Archbold, H. C. *et al.* TDP43 nuclear export and neurodegeneration in models of amyotrophic lateral sclerosis and frontotemporal dementia. *Sci. Rep.* (2018). doi:10.1038/s41598-018-22858-w
35. Chen, C. *et al.* Safety and efficacy of selinexor in relapsed or refractory multiple myeloma and Waldenstrom macroglobulinemia. *Blood* (2018). doi:10.1182/blood-2017-08-797886
36. Dolgin, E. To halt brain diseases, drugs take aim at protein traffic jams that kill neurons. *Science (80-.).* (2019). doi:10.1126/science.aaw6864
37. Rodríguez-Lebrón, E. *et al.* Silencing mutant *ATXN3* expression resolves molecular phenotypes in SCA3 transgenic mice. *Mol. Ther.* 21, 1909–1918 (2013).
38. Wei, N. *et al.* siRNA Has Greatly Elevated Mismatch Tolerance at 3′-UTR Sites. *PLoS One* (2012). doi:10.1371/journal.pone.0049309
39. Devanna, P. *et al.* Next-gen sequencing identifies non-coding variation disrupting miRNA-binding sites in neurological disorders. *Mol. Psychiatry* (2018). doi:10.1038/mp.2017.30
40. Moore, L. R. *et al.* Evaluation of Antisense Oligonucleotides Targeting *ATXN3* in SCA3 Mouse Models. *Mol. Ther. Nucleic Acids* (2017). doi:10.1016/j.omtn.2017.04.005
41. Alves, S. *et al.* Silencing ataxin-3 mitigates degeneration in a rat model of Machado-Joseph disease: No role for wild-type ataxin-3? *Hum. Mol. Genet.* 19, 2380–2394 (2010).
42. Nijman, S. M. B. *et al.* A genomic and functional inventory of deubiquitinating enzymes. *Cell* (2005). doi:10.1016/j.cell.2005.11.007
43. Miller, V. M. *et al.* Allele-specific silencing of dominant disease genes. *Proc. Natl. Acad. Sci.* (2003). doi:10.1073/pnas.1231012100

44. Alves, S. *et al.* Allele-specific RNA silencing of mutant ataxin-3 mediates neuroprotection in a rat model of Machado-Joseph disease. *PLoS One* 3, (2008).
45. Nóbrega, C. *et al.* RNA interference mitigates motor and neuropathological deficits in a cerebellar mouse model of Machado-Joseph disease. *PLoS One* (2014). doi:10.1371/journal.pone.0100086
46. Evers, M. M. *et al.* Ataxin-3 protein modification as a treatment strategy for spinocerebellar ataxia type 3: Removal of the CAG containing exon. *Neurobiol. Dis.* (2013). doi:10.1016/j.nbd.2013.04.019
47. Onofre, I. *et al.* Fibroblasts of Machado Joseph Disease patients reveal autophagy impairment. *Sci. Rep.* (2016). doi:10.1038/srep28220
48. Wang, Z. Experimental and Clinical Strategies for Treating Spinocerebellar Ataxia Type 3. *Neuroscience* (2018). doi:10.1016/j.neuroscience.2017.11.051
49. Ravikumar, B. *et al.* Inhibition of mTOR induces autophagy and reduces toxicity of polyglutamine expansions in fly and mouse models of Huntington disease. *Nat. Genet.* (2004). doi:10.1038/ng1362
50. Berger, Z. *et al.* Rapamycin alleviates toxicity of different aggregate-prone proteins. *Hum. Mol. Genet.* (2006). doi:10.1093/hmg/ddi458
51. Menzies, F. M. *et al.* Autophagy induction reduces mutant ataxin-3 levels and toxicity in a mouse model of spinocerebellar ataxia type 3. *Brain* (2010). doi:10.1093/brain/awp292
52. Sarkar, S. *et al.* Lithium induces autophagy by inhibiting inositol monophosphatase. *J. Cell Biol.* (2005). doi:10.1083/jcb.200504035
53. Jia, D. D. *et al.* Lithium chloride alleviates neurodegeneration partly by inhibiting activity of GSK3â in a SCA3 drosophila model. *Cerebellum* (2013). doi:10.1007/s12311-013-0498-3
54. Duarte-Silva, S. *et al.* Lithium Chloride Therapy Fails to Improve Motor Function in a Transgenic Mouse Model of Machado-Joseph Disease. *Cerebellum* (2014). doi:10.1007/s12311-014-0589-9
55. Sarkar, S., Davies, J. E., Huang, Z., Tunnacliffe, A. & Rubinsztein, D. C. Trehalose, a novel mTOR-independent autophagy enhancer, accelerates the clearance of mutant huntingtin and α-synuclein. *J. Biol. Chem.* (2007). doi:10.1074/jbc.M609532200
56. Lin, C.-H. *et al.* Novel Lactulose and Melibiose Targeting Autophagy to Reduce PolyQ Aggregation in Cell Models of Spinocerebellar Ataxia 3. *CNS Neurol. Disord. Drug Targets* (2016).
57. Pollitt, S. K. *et al.* A rapid cellular FRET assay of polyglutamine aggregation identifies a novel inhibitor. *Neuron* (2003). doi:10.1016/S0896-6273(03)00697-4
58. Cunha-Santos, J. *et al.* Caloric restriction blocks neuropathology and motor deficits in Machado-Joseph disease mouse models through SIRT1 pathway. *Nat. Commun.* (2016). doi:10.1038/ncomms11445
59. Goti, D. A Mutant Ataxin-3 Putative-Cleavage Fragment in Brains of Machado-Joseph Disease Patients and Transgenic Mice Is Cytotoxic above a Critical Concentration. *J. Neurosci.* (2004). doi:10.1523/jneurosci.2734-04.2004
60. Berke, S. J. S., Schmied, F. A. F., Brunt, E. R., Ellerby, L. M. & Paulson, H. L. Caspase-mediated proteolysis of the polyglutamine disease protein ataxin-3. *J. Neurochem.* 89, 908–918 (2004).
61. Haacke, A., Hartl, F. U. & Breuer, P. Calpain inhibition is sufficient to suppress aggregation of polyglutamine-expanded ataxin-3. *J. Biol. Chem.* (2007). doi:10.1074/jbc.M611914200
62. Jung, J., Xu, K., Lessing, D. & Bonini, N. M. Preventing Ataxin-3 protein cleavage mitigates degeneration in a Drosophila model of SCA3. *Hum. Mol. Genet.* (2009). doi:10.1093/hmg/ddp456
63. Evers, M. M., Toonen, L. J. A. & Van Roon-Mom, W. M. C. Ataxin-3 protein and RNA toxicity in spinocerebellar ataxia type 3: Current insights and emerging therapeutic strategies. *Molecular Neurobiology* 49, 1513–1531 (2014).
64. Hübener, J. *et al.* Calpain-mediated ataxin-3 cleavage in the molecular pathogenesis of spinocerebellar ataxia

type 3 (SCA3). *Hum. Mol. Genet.* (2013). doi:10.1093/hmg/dds449
65. Koch, P. *et al.* Excitation-induced ataxin-3 aggregation in neurons from patients with Machado-Joseph disease. *Nature* (2011). doi:10.1038/nature10671
66. Simões, A. T., Gonçalves, N., Nobre, R. J., Duarte, C. B. & Pereira de Almeida, L. Calpain inhibition reduces ataxin-3 cleavage alleviating neuropathology and motor impairments in mouse models of machado-Joseph disease. *Hum. Mol. Genet.* (2014). doi:10.1093/hmg/ddu209
67. Troy, C. M. & Salvesen, G. S. Caspases on the brain. *Journal of Neuroscience Research* (2002). doi:10.1002/jnr.10294
68. Li, Z. & Sheng, M. Caspases in synaptic plasticity. *Molecular Brain* (2012). doi:10.1186/1756-6606-5-15
69. Meyer, K. *et al.* Improving single injection CSF delivery of AAV9-mediated gene therapy for SMA: A dose-response study in mice and nonhuman primates. *Mol. Ther.* (2015). doi:10.1038/mt.2014.210
70. Sproule, D. *et al.* AVXS-101 phase 1 gene therapy clinical trial in SMA Type 1: end-of-Study event free survival and achievement of developmental milestones. *Neuromuscul. Disord.* (2017). doi:10.1016/j.nmd.2017.06.412
71. Miller, T. *et al.* A Phase I, Randomised, First-in-Human Study of an Antisense Oligonucleotide Directed Against SOD1 Delivered Intrathecally in SOD1-Familial ALS Patients. *Lancet Neurol* (2013). doi:10.1016/S1474-4422(13)70061-9
72. Evers, M. M. *et al.* AAV5-miHTT Gene Therapy Demonstrates Broad Distribution and Strong Human Mutant Huntingtin Lowering in a Huntington's Disease Minipig Model. *Mol. Ther.* 26, 2163–2177 (2018).
73. John M. Petitto, G. K. H. Reversal of Neuronal Atrophy: Role of Cellular Immunity in Neuroplasticity and Aging. *J. Neurol. Disord.* (2014). doi:10.4172/2329-6895.1000170
74. Tabrizi, S. J. *et al.* Predictors of phenotypic progression and disease onset in premanifest and early-stage Huntington's disease in the TRACK-HD study: Analysis of 36-month observational data. *Lancet Neurol.* (2013). doi:10.1016/S1474-4422(13)70088-7
75. Cozaru, G. C., Aschie, M., Mitroi, A. F., Poinareanu, I. & Gorduza, E. V. ETHICAL AND GENETIC ASPECTS REGARDING PRESYMPTOMATIC TESTING FOR NEURODEGENERATIVE DISEASES. *Rev. Med. Chir. Soc. Med. Nat. Iasi* 120, 15–22 (2016).
76. Uhlmann, W. R. & Roberts, J. S. Ethical issues in neurogenetics. in *Handbook of Clinical Neurology* (2018). doi:10.1016/B978-0-444-63233-3.00003-8
77. Wauters, A. & Van Hoyweghen, I. Concerns about Genetic Discrimination after Regulation: A Qualitative Study of the Situation Regarding BRCA and Huntington's Disease in Belgium. *Laws* (2018). doi:10.3390/laws7020017
78. Maczuga, P. *et al.* Therapeutic expression of hairpins targeting apolipoprotein B100 induces phenotypic and transcriptome changes in murine liver. *Gene Ther.* 21, 60–70 (2014).
79. Samaranch, L. *et al.* AAV9-mediated expression of a non-self protein in nonhuman primate central nervous system triggers widespread neuroinflammation driven by antigen-presenting cell transduction. *Mol. Ther.* (2014). doi:10.1038/mt.2013.266
80. Ciesielska, A. *et al.* Cerebral infusion of AAV9 vector-encoding non-self proteins can elicit cell-mediated immune responses. *Mol. Ther.* (2013). doi:10.1038/mt.2012.167

Addendum

&

English Summary

Nederlandse samenvatting

Resúmen na Papiamentu

List of abbreviations

List of publications

Acknowledgements

English Summary

Neurodegenerative diseases are a group of disorders caused by degeneration of nerve cells (also called neurons) in the central nervous system (CNS). The occurrence of these diseases is increasing while no effective treatments are available. It is well established that some neurodegenerative disorders such as amyotrophic lateral sclerosis (ALS) and spinocerebellar ataxia type 3 (SCA3) are caused by genetic mutations leading to a toxic gain of function. Artificial microRNAs designed to reduce the expression of these defective genes are a promising therapeutic strategy to slow down the toxicity caused by these genes. microRNAs are small non-coding RNAs that can bind to complementary sequences of mRNAs, leading to mRNA degradation and/or supress the translation of mRNA into protein (gene silencing). For therapeutic applications, gene therapy can be used to deliver therapeutic microRNAs to the target cells in patients and silence the genes responsible for the diseases. This can be done by packaging a transgene (in this case, the precursor microRNA) into recombinant adeno-associated virus (AAV) vectors for delivery to the affected cells. Once inside the cell, the AAV vector is unpackaged to deliver the precursor microRNA to the cell. The precursor microRNA remains in the cell for life and uses the cell's own RNA interference (RNAi) machinery for further processing into a mature microRNA molecule that can bind and silence the expression of the defective target gene to provide long-lived benefit to the patient.

This thesis describes the development of microRNA-based gene therapies for ALS and SCA3. Other aspects of a successful gene therapy including the administration routes to reach the target organs and regulation of the transgene expression were also investigated. Due to the permanent nature of gene therapy, a method to modulate the transgene expression is desirable.

Chapter 1 is a general introduction reviewing the past, current and future perspectives of gene therapy for neurodegenerative diseases. The mechanisms leading to the pathology of ALS and SCA3 are discussed as well as the therapeutic strategies that are currently being investigated. The challenges facing the currently available preclinical models are discussed and an overview is provided on the outcome of gene therapy clinical trials for neurodegenerative diseases. In chapter 2 we describe the design, characterization and selection of therapeutic microRNAs targeting the *C9orf72* gene. A GGGGCC repeat expansion in this gene is responsible for most ALS cases. Based on several *in vitro* experiments, we demonstrated the feasibility to silence different types of *C9orf72* transcripts in both nucleus and cytoplasm of cells. In chapter 3 we further investigated the potential of AAV5-delivered microRNAs targeting *C9orf72* (AAV5-miC) in neurons derived from human induced pluripotent stem cells (iPSC) and in an *C9orf72*-ALS mouse model. We showed that *C9orf72* silencing results in reduction of toxic nuclear RNA foci in the brain of ALS-mice. These RNA foci are one of the contributors to the ALS disease pathology. This study demonstrated a functional efficacy of AAV5-miC to reduce toxicity caused by the mutated *C9orf72* gene. In chapter 4 we applied our microRNA technology

and designed microRNAs to target the *ATXN3* gene (AAV5-mi*ATXN3*). A polyglutamine expansion in the *ATXN3* gene is responsible for SCA3. We showed efficient silencing of *ATXN3 in vitro* on human-derived iPSC-neurons and *in vivo* in the SCA3 mouse model. In addition, different routes of delivery were investigated to target the affected brain regions. We found therapeutically relevant reduction of the mutant ataxin-3 protein in the brain stem and cerebellum after a single injection with AAV5-mi*ATXN3* in the cisterna magna. These brain regions are also the most affected in SCA3 patients. Using a minipig model, the transduction of these brain regions was confirmed in a model with a larger brain size. This proof of concept study shows the potential of our approach to reduce toxicity by the mutant ataxin-3 protein in the affected brain regions of SCA3 patients. In chapter 5 we further investigated the administration of AAV-based gene therapy in rodents for delivery of therapeutic transgenes in neurodegenerative diseases. We demonstrated that local injection of AAV to the brain leads to efficient transduction of neuronal cell bodies of the deeper brain structures and is promising for diseases with a localized pathology such as Huntington's disease. Intrathecal administration led to a more even distribution within the CNS and is potentially more relevant in diseases with a spread pathology throughout the CNS such as ALS. In chapter 6, the feasibility to modulate the expression of gene therapy using the mifepristone-inducible GeneSwitch system was investigated *in vitro* and *in vivo*. We showed repeated inducibility of the transgene that also translated into a dynamic phenotypic change in mice. Chapter 7 Is a general discussion about our findings compared to others. Different target strategies are described and compared to our AAV-microRNA strategy. We further discuss the safety preclinical measures and future perspectives for a successful gene therapy to treat neurodegeneratative diseases.

Nederlandse samenvatting

Neurodegeneratieve ziektes behoren tot een groep aandoeningen die veroorzaakt wordt door degeneratie van zenuwcellen (ook wel bekend als neuronen). Hoewel deze ziektes steeds vaker voorkomen, is er nog geen effectieve behandeling voor gevonden. Het is bekend dat sommige neurodegeneratieve aandoendingen zoals amyotrofische laterale sclerose (ALS) en spinocerebellaire ataxie type 3 (SCA3) veroorzaakt worden door een mutatie in bepaalde genen dat leidt tot een toxische functie. Een veelbelovende therapeutische strategie is om de expressie van deze defecte genen te reduceren door middel van artificiële microRNAs om de bijbehorende toxische effecten van deze genen te verminderen. MicroRNAs zijn korte niet-coderende RNA moleculen die aan complementaire stuk messenger RNA (mRNA) kan binden om vervolgens de mRNA te degraderen en/of om de translatie tot eiwit stop te zetten (ofwel uitschakelen van een gen). Door middel van gentherapie kan therapeutische microRNAs aan de cellen van patiënten worden geleverd om zo de expressie van de genen die betrokken zijn bij de ziektes uit te schakelen. Dit wordt gedaan door een transgen (in dit geval de voorloper van de microRNA (ofwel microRNA precursor)) te verpakken in een recombinant virus genaamd "adeno-associated virus" (AAV). Eenmaal in de cel, wordt de AAV uitgepakt en de precursor microRNA geleverd aan de cel. De precursor microRNA kan gedurende een hele leven stabiel blijven in de cel en wordt verder verwerkt door de cellulaire RNA interferentie (RNAi) mechanisme tot een gematureerde microRNA molecuul. De gematureerde microRNA molecuul kan vervolgens binden aan een complementair stukje mRNA en zo blijft de expressie van de defecte gen langdurig uitgeschakeld in de patiënt.

Dit proefschrift beschrijft de ontwikkeling van een microRNA gentherapie voor ALS en SCA3. Andere cruciale aspecten voor een succesvolle gentherapie komen ook ter sprake, zoals de methodes waarop de gentherapie toegediend kan worden en een methode om gentherapie naar eigen wens te moduleren. Omdat de huidige gentherapieen permanent en omkeerbaar zijn, is een methode die expressie van de transgen kan moduleren zeer gewenst.

Hoofdstuk 1 is een algemene introductie waar onder andere de huidige en toekomstige perspectieven van gentherapie wordt samengevat. Daarnaast worden de ziekte veroorzakende mechanismen, die leiden tot ALS en SCA3 beschreven. Ook komen de behandelingsstrategieën die tot nu werden onderzocht aan orde. Verder worden de uitdagingen van de huidige preklinische modellen, en de toepassing van gentherapie in klinische studies voor neurodegeneratieve ziekten beschreven. In hoofdstuk 2 wordt het ontwerp, karakterisering en selectie van microRNAs beschreven die resulteren in het uitschakelen van het *C9orf72* gen. Een expansie bestaande uit GGGGC nucleotides in deze gen is de meest voorkomende oorzaak van ALS. Door middel van verschillende *in vitro* experimenten lieten we zien dat het mogelijk is om de expressie van verschillende types *C9orf72* mRNA moleculen zowel in de celkern als in het cytoplasma te verlagen.

In hoofdstuk 3 hebben we de microRNAs tegen *C9orf72* in AAV verpakt (AAV5-mic) en vervolgens getest in een ALS muismodel en op humane neuronen gedifferentieerd vanuit geïnduceerde pluripotente stamcellen (iPS-cellen). Dit resulteerde tot een sterke vermindering van een soort toxische precipitaat genaamd RNA-foci in de brein van de ALS muismodel. Deze RNA foci worden geproduceerd door de mutante *C9orf72* mRNA en zijn deels verantwoordelijk voor de ALS-pathologie. Onze bevindingen dienen als een mechanistische bewijs dat AAV5-miC de toxische effecten van de mutante *C9orf72* gen kan verminderen in het brein van een ALS-muismodel. In hoofdstuk 4 hebben we onze microRNA technologie toegepast voor de ontwikkeling van een gentherapie die de *ATXN3* gen kan uitschakelen (AAV5-mi*ATXN3*). SCA3 wordt veroorzaakt door een zogenaamde polyglutamine expansie in de *ATXN3* gen. We hebben een sterke reductie van de *ATXN3* mRNA aangetoond na behandeling met AAV5-mi*ATXN3*, zowel *in vitro* op iPS-neuronen en *in vivo* in een SCA3 muismodel. Daarnaast hebben we uitgebreid onderzocht op welke manieren onze AAV5-mi*ATXN3* toegediend kan worden om de aangetaste gebieden in de hersenen te bereiken. Het beste methode van toediening was door te injecteren in de cisterna magna. Eén enkele injectie in de cisterna manga leidde tot een sterke vermindering van de mutante ataxin-3 eiwit in de cerebellum en hersenstam van de muizen. Deze gebieden zijn ook het meest aangetast in SCA3 patiënten. Vervolgens lieten we zien dat deze gebieden van de hersenen ook bereikt kunnen worden in een varkensmodel met een veel grotere hersensvolume. Deze proof-of-concept studie liet zien dat onze strategie mogelijk tot reductie van de mutante ataxin-3 eiwit kan leiden in SCA3 patiënten. In hoofdstuk 5 werd de verschillende type methodes om gentherapie toe te dienen uitgebreid onderzocht in ratten. Lokale injectie van AAV in de hersenen, bijvoorbeeld in de striatum leidde tot efficiënte transductie van neuronen in de diepere structuren van de brein. Dus, deze methode is vooral interessant voor ziektes waar de pathologie op een bepaalde gebied van de hersenen is geconcentreerd, bijvoorbeeld de ziekte van Huntington. Intrathecale toediening resulteerde in een meer verspreide transductie in de CNS en kan een uitkomst bieden voor ziektes waar de pathologie verspreid ligt tussen meerdere gebieden in de CNS, bijvoorbeeld in ALS. In hoofdstuk 6 wordt een zogenaamd mifrepristone-induceerbare GeneSwitch systeem beschreven om de expressie van gentherapieën te moduleren. Door deze systeem toe te passen in gentherapie kan de expressie van de transgen aan- of uitgezet worden door wel of niet toedienen van de medicijn mifrepristone. We lieten zowel in celculturen en in muizen zien dat dit systeem gebruikt kan worden om expressie van de transgen te moduleren. Tot slot, in hoofdstuk 7 wordt onze AAV-microRNA strategie vergeleken met andere therapeutische strategieën die momenteel worden onderzocht voor behandeling van ALS en SCA3. Verder worden veschillende parameters besproken die belangrijk zijn om te onderzoeken om zo de veiligheid en succes van gentherapie voor neurodegeneratieve ziektes te garanderen.

Resúmen na Papiamentu

Enfermedat neurodegenerativo ta un grupo di trastorno kousá pa degenerashon di sèl di sistema nèrvioso (konosí tambe komo neurona). E enfermedatnan akí ta birando mas frekuente i ainda no tin tratamentu efektivo pa nan. Ta bon konosí ku sierto enfermedat neurodegenerativo, manera por ehèmpel sklerósis lateral amiotrófiko (abreviá na ingles komo ALS) i ataksia spinoserebeloso tipo 3 (SCA3) ta surgi debí na sierto mutashon genétiko ku ta okashoná toksisidat. Un strategia terapéutiko prometedor pa baha e toksisidat okashoná pa e gènnan akí ta mikroRNA artifisial diseñá pa limitá ekspreshon di e gènnan defektuoso. MikroRNA ta un tipo di RNA chikitu ku no ta kontené kódigo di proteina i ku por mara na un sekuensia di RNA mensahero (mRNA) komplementario pa asina silensiá e gèn dor di degradá e mRNA i/òf blòkia e proseso di traha proteina a base di e mRNA. Por usa terapia di gèn pa hiba mikroRNA na e sèlnan konserní di un pashènt i silensiá e gènnan ku ta okashoná e enfermedat. Pa hasi esaki, ta paketá e transgèn (den e kaso akí, e prekursor di e mikroRNA) den un vírùs rekombinante di e tipo "adeno-asosiá" (abreviá na ingles komo AAV) pa e vírùs hiba e mikroRNA prekursor na e sèlnan afektá. Unabes den e sèl, e AAV ta wordu desempaketá i e mikroRNA prekursor ta ser entregá na e sèl. E mikroRNA prekursor por keda stabil den e sèl permanentemente i usa e sèl su mekanismo di interferensia di RNA (RNAi) mes pa sigui madurá i bira un molékula di mikroRNA ku por mara na e gèn defektuoso i silensi'é, di e manera ei silensiando e gèn defektuoso di e pashènt pa bida largu.

E tesina akí ta deskribí desaroyo di un terapia genétiko basá riba mikroRNA pa ALS i SCA3. A investigá tambe algun otro aspekto krusial pa éksito di un terapia genétiko, entre otro, ki método ta usa pa atministrá e terapia genétiko i kon por regulá e terapia. Debí ku terapia genétiko ta di karakter permanente, un método pa regulá ekspreshon di e transgèn ta algu sumamente deseabel.

Kapítulo 1 ta sirbi komo un introdukshon general. E ta resumí e perspektivanan di terapia genétiko aktual i pa futuro pa enfermedat neurodegenerativo. E kapítulo akí ta papia tambe riba e mekanismonan ku ta okashoná e patologia di ALS i SCA3, i e strategianan terapéutiko ku ta siendo studiá te asina leu. Ta menshoná e desafionan relashoná ku e modelonan preklíniko ku tin disponibel aktualmente i ta duna un resúmen di e resultadonan di terapia genétiko optení den tèst klíniko pa enfermedat neurodegenerativo. Na Kapítulo 2, nos ta splika diseño, karakterisashon i selekshon di mikroRNA terapéutiko pa silensiá e gèn *C9orf72*. Mayoria di kaso di ALS ta debí na un ekspanshon di nukleotido GGGGCC den e gèn akí. A base di diferente eksperimento *in vitro*, nos a demostrá ku ta faktibel pa redusí ekspreshon di diferente tipo di *C9orf72* tantu den núkleo komo den sitoplasma di sèl. Den Kapítulo 3, nos a sigui investigá uso di mikroRNA ku ta silensiá *C9orf72,* empaketá den AAV (AAV5-miC). A tèst esaki riba neurona derivá for di sèl mama (stamcel) humano pluripotente indusí (iPSC) i tambe riba raton ku ta sirbi komo modelo pa studia ALS. E resultado tabata un redukshon supstansial di e presipitashon tóksiko konosí komo RNA-foci den serebro di e raton ku ALS. RNA-foci

ta ser produsí pa *C9orf72* mRNA mutante i ta un di e faktornan ku ta kontribuí na patologia di e enfermedat ALS. E investigashon akí a demostrá efektividat funshonal di AAV5-miC pa redusí e toksisidat kousá pa gèn *C9orf72* mutante. Na Kapítulo 4, nos a pone nos teknologia di mikroRNA na práktika i a diseñá un terapia genétiko (AAV5-miATXN3) pa silensiá e gèn *ATXN3*. Un ekspanshon di poliglutamina den e gèn *ATXN3* ta loke ta okashoná SCA3. Nos a silensiá *ATXN3* supstansialmente, tantu *in vitro* den neurona iPSC derivá di tehido humano, komo *in vivo* serka raton ku ta sirbi komo modelo pa studia SCA3. Ademas, nos a investigá diferente manera pa atministrá e terapia pa trata e regionnan afektá di serebro. E mihó método di atministrashon a resultá di ta via inyekshon den *cisterna magna.* Serka raton, nos a konstatá un redukshon supstansial di e proteina ataksina-3 mutante den tronkon di serebro i den serebro chikitu despues di un solo inyekshon di AAV5-miATXN3 den *cisterna magna.* E regionnan akí di serebro ta tambe esunnan mas afektá serka pashènt di SCA3. A usa un porko miniatura komo modelo, konfirmando di e manera ei ku serka modelo ku serebro mas grandi tambe e terapia por alkansá e regionnan ei di serebro. E estudio akí ta un 'proof of concept' ku ta demostrá e potensial di nos strategia pa redusí nivel di e proteina ataksina-3 mutante serka pashènt di SCA3. Den Kapítulo 5, nos ta sigui investigá diferente método pa atministrá terapia genétiko serka djaka. A base di e estudio aki por concluí ku inyekshon lokal di AAV den serebro ta produsí transdukshon efisiente di neurona den e strukturanan mas profundo di serebro, loke ta hasié un método di inyekshon prometedor, prinsipalmente pa enfermedat kaminda e patologia ta konsentrá den sierto area di serebro, manera enfermedat di Huntington. Via angua den wes'i lomba, tabatin transdukshon den un área mas amplio di sistema nèrvioso sentral, loke ta nifiká ku esaki por ta un bon opshon ora ta trata di enfermedat kaminda e patologia ta plama den diferente region di e sistema nèrvioso sentral, por ehèmpel ALS. Kapítulo 6 ta deskribí kon por usa e sistema 'mifepristone-inducible GeneSwitch' pa regulá ekspreshon di terapia genétiko. Ku e sistema akí, por sea aktivá òf desaktivá ekspreshon di e transgèn. Pa hasi esei, ta sea atministrá òf keda sin atministrá e remedi mifrepristona. Nos a demostrá tantu *in vitro* komo serka raton bibu ku por usa e sistema akí pa regulá ekspreshon di e transgèn. Finalmente, na Kapítulo 7 nos ta kompará nos strategia di AAV-mikroRNA ku algun otro strategia terapéutiko ku ta siendo studiá aktualmente komo tratamentu pa ALS i SCA3. Ademas, nos ta papia riba diferente parameter ku ta importante pa investigá, pa garantisá ku tratamentu di enfermedat neurodegenerativo por ta eksitoso i tambe safe.

List of abbreviations

AAT	alpha1-antitrypsin
AAV	adeno-associated virus
AD	Alzheimer's disease
AGO	argonaute
ALS	amyotrophic lateral sclerosis
ASOs	antisense oligonucleotides
ATXN	ataxin gene
BAC	bacterial artificial chromosome
BBB	blood brain barrier
C9orf72	chromosome 9 open reading frame 72
CA	Cornu Ammonis
CAG	cytomegalovirus immediate-early enhancer fused to chicken β-actin promoter
Cas9	CRISPR-associated system 9
CMV	cytomegalovirus
CRISPR	clustered regulatory interspaced short palindromic repeats
CSF	cerebrospinal fluid
DCN	deep cerebellar nuclei
DG	Dentate Gyrus
DM1	myotonic dystrophy type 1
DMD	Duchenne muscular dystrophy
DPRs	dipeptide repeat proteins
DRG	dorsal Root Ganglia
DSBs	DNA double strand breaks
EPO	erythropoietin
FISH	fluorescence in situ hybridization
FTD	frontotemporal dementia
FUS	fused in sarcoma
GA	glycine-alanine
gc	genome copies
GDNF	glial cell-derived neurotrophic factor
GFP	green fluorescent protein
GP	glycine-proline
GR	glycine-arginine
GS	GeneSwitch
HD	Huntington's disease
HDR	homology-directed repair
HP1α	heterochromatin protein 1α
HSV	herpes simplex virus

HTT	huntingtin gene
ICV	intracerebroventricular
IFN	interferon
IGF	Insulin-like growth factor
iPSC	induced-pluripotent stem cells
Istr	Intrastriatal
IT	intrathecal
ITH	intrathalamic
ITRs	inverted terminal repeats
IV	intravenously
Kb	kilobase
Luc	luciferase
MBNL1	muscleblind-like 1
MFP	mifepristone
mi*ATXN3*	*ATXN3* targeting microRNA
miC	*C9orf72* targeting microRNA
miR-451a or miR-451	microRNA-451a
miRNA	microRNA
MJD	Machado-Joseph disease
mRNA	messenger RNA
NGS	next generation sequencing
NHEJ	nonhomologous end-joining
NHP	nonhuman primate
Nt	nucleotide
PA	proline-alanine
PARN	poly(A)-specific ribonuclease
PD	Parkinson's disease
piRNAs	piwi-interacting RNAs
polyA	polyalanine
PolyQ	polyglutamine
PR	proline-arginine
pre-miRNA	precursor microRNA
pri-miRNA	primary microRNA
rAAV	recombinant adeno-associated virus
RAN	translation repeat-associated non-ATG translation
RISC	RNAi-induced silencing complex
RNAi	RNA interference
RNAse H	ribonuclease H
RT-PCR	real-time polymerase chain reaction
RT-qPCR	quantitative real-time polymerase chain reaction

rtTA	transactivator-protein
SCA	spinocerebellar ataxia
shRNA	short hairpin RNA
siRNA	small interfering RNA
SMA	spinal muscular atrophy
SMN	survival motor neuron
SN	substantia nigra
SNP	single nucleotide polymorphism
SNpc	SN pars compacta
SNrc	pars recticulata
SOD1	superoxide dismutase1
TALENs	transcription activator-like effector nucleases
TARDBP	transactive response DNA-binding protein of 43 kDa
TDP-43	transactive response DNA-binding protein 43
UIM	ubiquitin-interacting motifs
UTR	untranslated region
VTA	Ventral Tegmental Area
ZFNs	zinc-finger nucleases

List of publications

Martier R, Sogorb Gonzalez M, Stricker-Shaver J, Hübener-Schmid J, Keskin S, Witjas J, van Deventer SJ, Konstantinova P, Phuc Nguyen H, Evers MM. (2019). Development of an AAV-based microRNA gene therapy to treat Machado-Joseph disease. Mol. Ther. Methods & Clinical Development Acids. 15: 343-358

Pietersz KL, **Martier R**, Baatje SM, Liefhebber JM, Brouwers CC, Pouw SM, Fokkert L, Lubelski J, Petry H, Martens GJM, van Deventer SJ, Konstantinova P, Blits B. (2020). Transduction patterns in the CNS following various routes of AAV-5-mediated gene delivery. Gene Ther. Accepted, March 2020

Liefhebber, J., **Martier, R**., Van der Zon, T., Keskin, S., Huseinovic, A., Lubelski, J., Blits, B., Petry, H., Konstantinova, P. (2019) In depth characterization of a Mifepristone regulated expression system for AAV5-mediated gene therapy in the liver. Mol. Ther. Methods & Clinical Development.13: 512-525

Martier R, Liefhebber JM, Garcia-Osta A, Miniarikova J, Cuadrado-Tejedor M, Espelosin M, Konstantinova P. (2019). Targeting RNA-Mediated toxicity in C9orf72 ALS and/or FTD by RNAi-Based gene Therapy. Mol. Ther. Nucleic. Acids.16: 26-37

Martier R, Liefhebber JM, Miniarikova J, van der Zon T, Snapper J, Kolder I, Konstantinova P. (2019). Artificial MicroRNAs Targeting C9orf72 Can Reduce Accumulation of Intranuclear Transcripts in ALS and FTD Patients. Mol. Ther. Nucleic. Acids.14: 593-608

Miniarikova J, Zimmer V, **Martier R**, Brouwers C. C, Pythoud C, Richetin K, Konstantinova P. (2017). AAV5-miHTT gene therapy demonstrates suppression of mutant huntingtin aggregation and neuronal dysfunction in a rat model of Huntington's disease. Gene Ther. 24: 630-639

Miniarikova J, Zanella I, Huseinovic A, van der Zon T, Hanemaaijer E, **Martier R**, Konstantinova P. (2016). Design, Characterization, and Lead Selection of Therapeutic miRNAs Targeting Huntingtin for Development of Gene Therapy for Huntington's Disease. Mol. Ther. Nucleic Acids: e297

MacZuga P, Verheij J, Van Der Loos C, Van Logtenstein R, Hooijer G, **Martier R**, Konstantinova P. (2014). Therapeutic expression of hairpins targeting apolipoprotein B100 induces phenotypic and transcriptome changes in murine liver. Gene. Ther. 21: 60-70

Staszewski O, Baker RE, Ucher AJ, **Martier R**, Stavnezer J, Guikema JEJ. (2011). Activation-Induced Cytidine Deaminase Induces Reproducible DNA Breaks at Many Non-Ig Loci in Activated B Cells. Molecular Cell. 41(2): 232-242

Curriculum Vitae

Raygene Martier was born on 11-02-1987 in Willemstad, Curaçao. In 2005 he graduated from high school Maria Immaculata Lyceum, Curaçao with a focus on natural sciences. After his graduation, he moved to the Netherlands and started the Bachelor study Biotechnology at Van Hall Larenstein en Noordelijke Hoge School Leeuwarden. During his Bachelor studies he did two different internships. The first internship was under supervision of Dr. Johanna (Hannie) Westra at the University Medical Center Groningen, department of Rheumatology and Clinical Immunology where he studied the role of Hypoxia Inducible Factor-1α in patients with rheumatoid arthritis. The second internship was under supervision of Dr. Jeroen Guikema at the University of Massachusetts Medical School, Department of Molecular Genetics and Microbiology (USA) where he studied the role of the DNA repair protein Ataxia Telangiestacta Mutated Kinase in intrachromosomal recombination of the immunoglobulin heavy chain genes. In the second half year of this internship he also studied the function of the enzyme Activation Induced Cytidine Deaminase. He obtained his bachelor degree in 2009 with a major in Biomedical Sciences.

In 2011 he enrolled in the master program Biomolecular Sciences at VU University (Vrije Universiteit) Amsterdam where he also did two internships. The first master internship was under supervision of Prof. Ewa Snaar-Jagalska at the Institute of Biology Leiden (IBL), department of Molecular cell Biology. Here he studied the immune response of ewing sarcoma implants/engrafts in zebrafish and also gained experience in generation of zebrafish transgenic lines. His last internship was at Crucell (Johnson & Johnson) in Leiden where he worked on the development of Hepatitis A virus micro neutralization assay under supervision of Dr. Amanda Versteilen. He obtained his master degree in 2013 with majors in Molecular Biology and Biological Chemistry.

In 2013, he joined uniQure as a Research Technician in the New Therapeutic Target Discovery department under supervision of Dr. Pavlina Konstantinova. He worked on the development of regulated gene expression systems for gene therapy. He also had a supporting role in various other preclinical studies within the company, focusing on the development of microRNA-based and gene replacement gene therapies to treat genetic disorders. In 2015, he started his PhD at Leiden University. The work described in his thesis was performed at uniQure under daily supervision of Dr. Pavlina Konstantinova and his promoter Prof. Sander van Deventer. Besides his scientific work, he had the opportunity to work closely together with uniQure's IP department where he became fascinated about the importance of a strong IP portfolio for the economic value of the company. In January 2019, he started as Junior Scientist and IP support at uniQure and in October 2019 he joined Vereenigde Octrooibureaux (V.O) as trainee patent attorney in the section life sciences.

Acknowledgements

This PhD track has been a life-changing experience for me and the work presented in this thesis would not have been possible without the help, support and guidance that I received from many people. Firstly, I would like to express my sincere gratitude to my mentor, daily supervisor and Co-promoter **Dr. Pavlina Konstantinova**. I am very grateful for all the opportunities that you provided to me. You allowed me to learn, grow and shape my career path in the way I wanted. Thank you for the continuous support, for your patience, dedication, and good advices. I would also like to thank my promoter **Prof. Sander van Deventer**. Your critical mindset and insightful comments always encouraged me to think further and broaden by knowledge from various perspectives. **Dr. Harald Petry**, thank you for your support during the first two years of my PhD and for allowing me to perform my work at uniQure. Dear **Kimberly**, we have been friends in better and difficult times. Part of my achievements are also yours. Thank you so much for your support and advises. Dear **Tom**, a lot of the data provided in this thesis would not have been possible without your help in the lab. I am extremely grateful for your dedication and hard work. Dear **Melvin**. I have learned a great deal from you. You taught me how to manage my projects and solve problems on a daily basis. Thank you for always finding time to meet and discuss with me. Dear **Jolanda L**, your critical way of looking at results and figures were always so helpful. You are somebody I could always reach to whenever I needed an advice. Dear **Andrew**, I am glad to have met you in the final phases of my PhD track. Thank you very much for being a mentor to me. Dear **Ellen**, I am so grateful that you gave me the opportunity to join the IP department. Thank you for all your advices. Dear **Vanessa**, thank you for your help and support and for being a good friend and colleague. Dear **Jana**, I am going to miss our discussions, your positive attitude and advices. Many thanks for your help and support. Dear **Marina**, you are one of the most positive persons I have ever met and I am going to miss our discussions. Thank you for all your help and support. Dear **Sumiati**, I am very grateful for your help with all the *in vivo* and histology experiments. Dear **Sonay**, thanks a lot for your support. You are one of the few persons who offers help without being asked. Your jokes always bring laughter to the lab. Dear **Jolanda S**, thank you very much for your help input on the ALS project and for keeping everything organized. Dear **Ying Poi**, I always admire your hard work and dedication to the R&D department. After discussing with you, I was always left with new ideas to explore. Dear **Astrid**, thank you very much for your support and advice. Also a special thanks to the in vivo team, **Bas Blits, Stefan** and **Richard** for the tremendous help with all the *in vivo* experiments. Dear **Lisa van den Haak**, thank you for your role in keeping everything organized. Dear **Jorien**, I was lucky to have you as a student. Thank you for your hard work and dedication on the SCA3 project. Dear **Bas Bosma**, thank you for sharing your knowledge whenever I needed it. I would also like to thank **Erich** and the PD department for the AAV productions, **Valerie** and **Jacek** for your scientific input

and advices, **Olivier** for your help with the patent applications and **Eileen**, for critically reviewing all manuscripts presented in this thesis.

I would also like to thank my fellow (ex) colleagues for the great help, support and for providing a nice work environment: **Cynthia, Huining, Piotr, Karin, Hendrina, Lieke, Fanny, Wim, Anouk, Carlos, Josse, Nikki, Lukas, Betty, Rudy, Lodewijk, Anna, Ismael, Roberto, Maroeska, Mark, Tamar, Lisa Spronck, Francois, Frank, Frans, Martin.** A special thanks to **Dennis**, **Christian** and **Pascal** from the IT department for the great support.

This thesis could not be completed without good collaborations. I would like to thank **Ana**, **Mar**, **Maria** and **Susana** from the Center for Applied Medical Research in Pamplona, Spain for the breeding of the *C9orf72* ALS mice, to perform surgeries and tissue collection. I am also extremely thankful to my collaborators in Tubingen Germany; **Hoa**, **Jeannette**, **Janice** and **Eva** for providing the SCA3 mouse model, perform the surgeries and perform the TR-FRET assay.

Tot slot zou ik graag mijn familie en vrienden willen bedanken. **Mijn ouders** die mij altijd ondersteunde in mijn beslissingen. Zonder jullie hulp was ik nooit zo ver gekomen Mijn broertje **Raygendy** en zusje **Rayenne**, bedankt voor jullie onvoorwaardelijke ondersteuning. Mijn **Oma** en **Opa**, jullie zijn inmiddels niet meer tussen ons maar blijven altijd in onze harten voortbestaan. Hartelijk bedankt voor jullie steun en adviezen. Lieve **Ciyaeda**, mijn leven is in een positieve zin veranderd sinds ik jouw papa ben geworden. Jouw vrolijke en positieve energie wil ik geen enkele dag missen. Lieve **Lisa**, sinds ik jou heb leren kennen ben je er altijd voor mij geweest. Je gaf me het mooiste wat er is in het leven, onze lieve dochter Ciyaeda. Bedankt om er altijd voor mij te zijn. Ik wil de rest van mijn familie bedanken, mijn **tantes**, **ooms**, **neven** en **nichten**. **Anja** en **Theo**, toen in naar Nederland verhuisde was het een totaal andere wereld als wat ik gewend was. Jullie hebben mij geholpen om mij hier thuis te laten voelen. Ontzettend bedankt daarvoor. Mijn maatjes, **Adson**, **Liandro**, **Hanslin**, **Gurine**, **Sherwin** en overige vrienden in Curaçao en Nederland. Bedankt voor jullie vriendschap en gezelligheid.